Influence of impurities on the H2/H2O/Ni/YSZ electrode

Høgh, Jens Valdemar Thorvald

Publication date:
2005

Document Version
Publisher's PDF, also known as Version of record

Citation (APA):
Høgh, J. V. T. (2005). *Influence of impurities on the H_2/H_2O/Ni/YSZ electrode*. Technical University of Denmark. Risø-PhD No. 22(EN)

Risø-PhD-22 (EN)

Influence of impurities on the H_2/H_2O/Ni/YSZ electrode

Jens Høgh

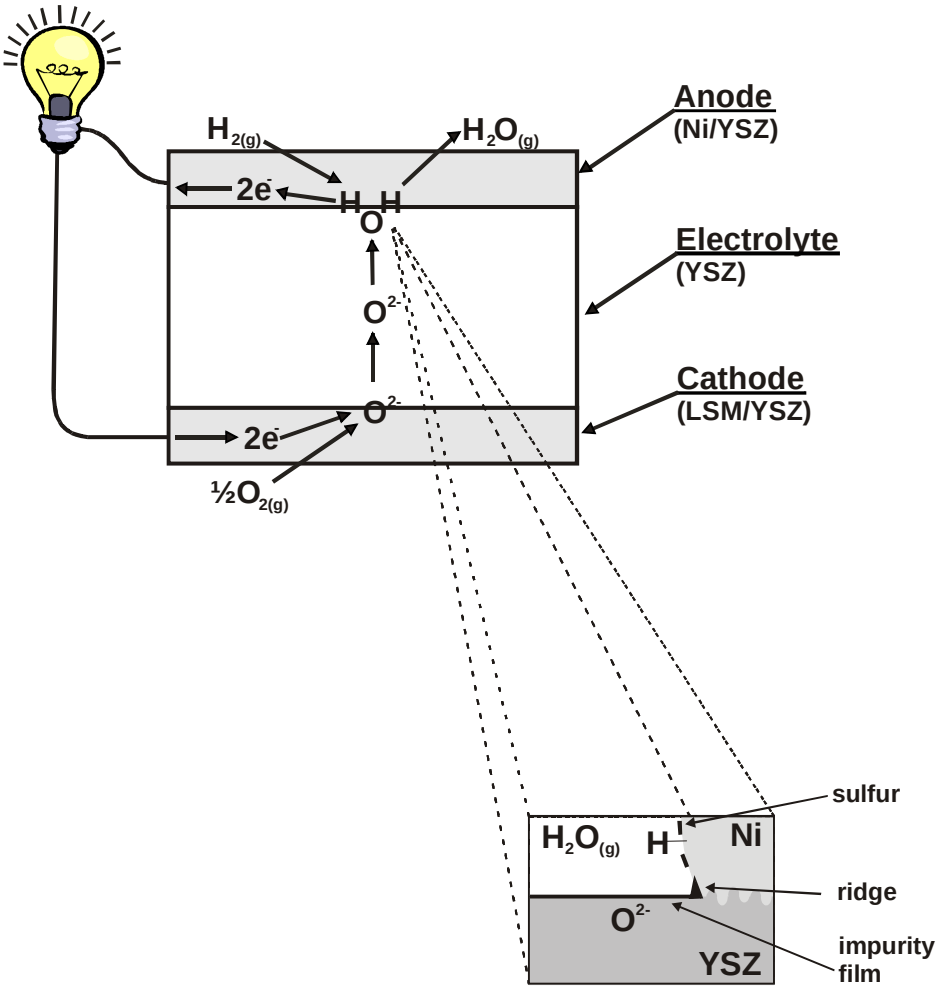

Risø National Laboratory
Roskilde
Denmark
May 2005

Author: Jens Høgh
Title: Influence of impurities on the H_2/H_2O/Ni/YSZ electrode
Department: Materials research department

This thesis is submitted in partial fulfilment of the requirements for the Ph.D. degree at the Technical University of Denmark

Abstract :
The kinetics of the SOFC anode or more specific the H_2/H_2O/Ni/SZ electrode (SZ=stabilized zirconia) is widely investigated, but there are large disagreements about the kinetics and mechanisms in the literature. It is reported that impurities from the electrode materials (Ni/SZ) segregate to the surface/interface/TPB (TPB=three phase boundary) and that these impurities have a negative influence on the kinetics. These impurities may be the explanation for the disagreements found in the literature. The purpose of this study is therefore to perform electrochemical measurements in a very clean system to avoid the effects of impurities. This is attempted by using high purity materials, lowering the operation temperature to prevent fast segregation of impurities and by limiting impurities from the environment. A simplified geometry of the real SOFC anode, which is a porous Ni/SZ composite, was studied. The simplified anode was made by pressing a Ni wire against a single crystal of stabilized zirconia.
In spite of the efforts of making electrochemical measurements in a very clean system, impurities were still found on the surface of the electrode materials (Ni and SZ) after an electrochemical experiment. The impurities found on the SZ are believed to segregate from the bulk of SZ to the surface. Sulfur was found on the surface of the Ni, but its origin is unclear. A higher impurity level was detected on the surface of the Ni and SZ outside the contact area (between the Ni and YSZ) than inside the contact area. The initial smooth surface of the SZ had developed a hill and valley structure in the contact area after a heat treatment. Also, a ridge around the contact area on the SZ was seen.
The polarization resistance at open circuit voltage (500°C, 3% H_20/H_2) increased by a factor of 5-19 over 10-20 days before leveling out. The increase in polarization resistance is believed to be caused by: 1) Segregated impurities, 2) The built up of a ridge around the contact area and 3) The sulfur adsorption on the Ni wire.
An increasing water content in the atmosphere was seen to lower the polarization resistance at OCV and at anodic overpotentials, but it had no effect at cathodic overpotentials. It was hypothesized that water changes the properties of the impurities and hereby promote the electrode reaction at OCV and anodic overpotentials.
A strong cathodic polarization <-2000 mV vs. air at 700°C was seen to lower the polarization resistance by a factor of 5-60. It was hypothesized that the strong cathodic polarization reduces or partly reduces the impurities from oxide to metal. Hence, the blocking influence of impurities would be diminished.

Risø-PhD-22 (EN)
May 2005

ISBN 87-550-3502-7 (Internet)

Group's own reg. no.:
1625049-10

Sponsorship:
This Ph.D. project is a part of the larger project "Towards a hydrogen based society" which is sponsored by the Danish Technical Research Council (STVF)

Cover :
Sketch of a solid oxide fuel cell (SOFC)

Risø National Laboratory
Information Service Department
P.O.Box 49
DK-4000 Roskilde
Denmark
Telephone +45 46774004
bibl@risoe.dk
Fax +45 46774013
www.risoe.dk

May 2005

Influence of impurities on the H_2/H_2O/Ni/YSZ electrode

Jens Høgh

Ph.D. Thesis

Risø National Laboratory, Materials Research Department

The Technical University of Denmark, Department of Chemistry

Preface

This thesis is submitted in partial fulfilment of the requirements for the Ph.D. degree at the Technical University of Denmark. The present work is carried out in the period June 2002 to June 2005 at Materials Research Department, Risø National Laboratory. This Ph.D. project is a part of the larger project "Towards a hydrogen based society" which is sponsored by the Danish Technical Research Council (STVF). The title of the Ph.D. project is "Influence of impurities on the H_2/H_2O/Ni/YSZ electrode", hence the project is closely related to The Danish DK-SOFC program where Risø National Laboratory is a participant.

I would like to thank my supervisors:

Torben Jacobsen, Department of Chemistry, Technical University of Denmark, for educational discussions and guiding regarding electrochemistry.
Ib Chorkendorff, Department of Chemical Engineering, Technical University of Denmark, for educational discussions and guiding regarding surface science.
Mogens Mogensen, Materials Research Department, Risø National Laboratory, for daily discussions and guiding regarding the project.
Karin Vels Hansen, Materials Research Department, Risø National Laboratory, for daily discussions and guiding regarding the project.

A special acknowledgement goes to the following persons and their respective departments for their extraordinary help:

John Larsen, Department of Chemical Engineering, Technical University of Denmark, for help with XPS and AES measurements.
Jørgen Poulsen, Materials Research Department, Risø National Laboratory, for help with various electrical problems.
Nikolaos Bonanos, Materials Research Department, Risø National Laboratory, for help with impedance measurements.
Kion Norrman, Danish Polymer Centre, Risø National Laboratory, for help with TOF-SIMS measurements.
Lene Hubert, Danish Polymer Centre, Risø National Laboratory, for help with XPS and AFM measurements.
Noemi Rozlosnik, Danish Polymer Centre, Risø National Laboratory, for help with AFM measurement.

Also, I would like to thanks the whole SOFC group at Risø National Laboratory for the help and for creating a good working environment.

Jens Høgh
Roskilde, May 31st, 2005

Dansk resume

Der er udført talrige undersøgelser af SOFC (fast-oxid-brændselscelle) anode kinetikken for H_2/H_2O/Ni/SZ elektroden (SZ= stabiliseret zirconia), men der er stadig stor uenighed om kinetikken og reaktionsmekanismerne. I de seneste år er det vist at elektrodereaktionen hindres ved at urenheder, der kommer fra elektrodematerialerne (Ni og SZ), segregerer til overfladen, grænsefladen mellem Ni og SZ, og TPB (trefase-grænsen). Måske kan disse urenheder være forklaringen på de store forskelle, der observeres vedrørende kinetik og reaktionsmekanismer. Formålet med dette studie er på denne baggrund at fortage elektrokemiske målinger i et rent system, for at undgå effekten af urenhederne. Dette er forsøgt ved at bruge materialer af høj renhed, sænke temperaturen hvorved de elektrokemiske målinger foretages for at undgå en hurtig segregering af urenheder, samt at begrænse kontakten med urenhedskilder fra omgivelserne. Den rigtige SOFC anode er en kompositelektrode bestående af Ni og SZ. I dette studie er målt på en geometrisk simplificeret anode, der blev fremstillet ved at presse en Ni tråd mod en enkrystal af SZ.
Selvom anstrengelserne for at udføre målinger på et rent system var store, blev der fundet urenheder på overfladen af elektrodematerialerne (Ni og SZ) efter de elektrokemiske forsøg. Urenhederne, der blev fundet på overfladen af SZ, menes at segregere fra bulken af SZ til overfladen. Det er uvist om det svovl, der blev fundet på overfladen af Ni tråden, stammer fra omgivelserne eller stammer fra urenheder i Ni bulk materialet. En større mængde af urenheder blev detekteret på overfladen af Ni og SZ uden for kontaktområdet mellem Ni og SZ end i kontaktområdet. Det kunne ses at overfladen af SZ, der før elektrode eksperimentet var jævn, havde udviklet en såkaldt ”hill and valley” struktur i Ni/SZ kontaktområdet efter et elektrodeeksperiment. Ydermere var der udviklet en forhøjning af materiale langs omkredsen af kontaktområdet.
En øgning i polarisationsmodstanden ved OCV på en faktor 5-19 (500°C, 3% H_20/H_2) blev observeret over en periode på 10-20 dage hvorefter polarisationsmodstand blev stabil. Det menes, at øgningen i polarisationsmodstanden skyldes: 1) Segregerede urenheder, 2) En forhøjning af materiale langs TPB samt 3) Adsorbering af svovl på Ni tråden.
En øgning af vandindholdet i atmosfæren medførte en lavere polarisationsmodstand ved OCV og ved anodiske overpotentialer, mens ingen ændring ved katodiske overpotentialer blev observeret. Det menes, at et stigende vandindhold ændrer egenskaberne af urenhederne på overfladen, hvilket øger hastigheden af elektrodereaktionen ved OCV og anodiske overpotentialer.
Polarisationsmodstanden faldt med en faktor 5-60 ved at polarisere elektroden stærkt katodisk (<-2000 mV vs. air ved 700°C). En hypotese for denne mindskning af polarisationsmodstanden er, at urenhederne reduceres fra oxid til metal, hvilket medfører muligheden for elektrontransport. Dette svarer til en udvidelse af TPB.

Contents

1 Introduction

This chapter gives an introduction to the Solid Oxide Fuel Cell (SOFC) with focus on the anode, which is the subject of this thesis.
A fuel cell is an electrochemical cell that converts chemical energy directly into electricity, like in a battery. The difference between a battery and a fuel cell is that the reactants (oxidation and reduction agents) are continuously added to the fuel cell, whereas in a battery the reactants are consumed until they are used up. In the last ten years fuel cell research has been increasing. One of the reasons for this is that fuel cells have the potential of producing electricity more effectively than a conventional power plant as fuel cells are not restricted to the Carnot cycle.
In general, fuel cells are divided into high and low temperature fuel cells. The high temperature fuel cells have a higher efficiency and are more tolerant to the choice of fuel. High temperature fuel cells are suitable for continuous power and heat production and low temperature fuel cells are suitable for mobile applications (car, mobile phone, laptops etc.). The main focus on high temperature fuel cells has been on Solid Oxide Fuel Cell and Molten Carbonate Fuel Cell (MCFC). Based on the pros and cons for the different fuel cells the Danish Department of Energy decided to found a national program concerning SOFC: The Danish DK-SOFC program [1]. This Ph.D. project is closely related to this program.

1.1 Principles of SOFC operation

A SOFC fuel cell consists of two electrodes, one on each side of the electrolyte. The electrode where the oxidation (liberation of electrons) occurs is referred to as the anode and the electrode where the reduction (acceptance of electrons) occurs are referred to as the cathode. Figure 1 shows how hydrogen and oxygen (air) react to form water and produce electricity. Other fuels than hydrogen has the potential for being used in the SOFC e.g. natural gas, diesel, ammonia and methanol.

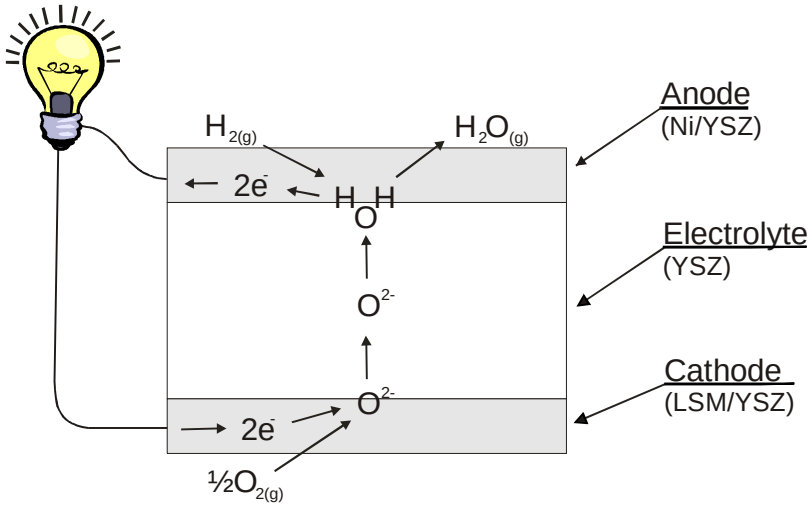

Figure 1. Sketch of a solid oxide fuel cell. YSZ= yttria stabilized zirconia. LSM= strontium doped lanthanum manganite.

The standard materials (for electrochemical oxidation of hydrogen) used in a SOFC are Ni/YSZ (anode), YSZ (electrolyte) and LSM/YSZ (cathode). The electrodes consist of a porous structure, which allows gas transport to and from the electrolyte. The anode is a cermet consisting of Ni and YSZ particles. The electrolyte is a dense oxide ion conductor of yttria stabilized zirconia (YSZ, $(ZrO_2)_{1-x}(Y_2O_3)_x$). The cathode is a composite consisting of strontium doped lanthanum manganite (LSM, $La_{1-x}Sr_xMn_yO_{3\pm\delta}$) and YSZ.

The electrochemical oxidation of hydrogen is an electrochemically reversible process. If electricity is supplied to the cell it works as an electrolyzer cell (SOEC, solid oxide electrolyzer cell) where water is split into hydrogen and oxygen. Note that when the cell is operated in electrolyzer mode the anode and cathode are reversed so that reduction takes place at the Ni/YSZ electrode (cathode) and vice versa, see Table 1.

Table 1. Polarity of the SOFC electrodes in fuel cell mode and in electrolyzer mode.

Type of cell	Electrode	Function	Polarity
Fuel cell mode	Ni/YSZ	Anode/Oxidation	-
	LSM/YSZ	Cathode/Reduction	+
Electrolysis mode	LSM/YSZ	Anode/Oxidation	+
	Ni/YSZ	Cathode/Reduction	-

The operation temperature of SOFC's has been relatively high (~1000°C) in order to achieve an attractive efficiency i.e. a low internal resistance. The high temperature operation sets high demands on the choice of material. By lowering the operation temperature (550-650°C) less costly materials can be used. Lowering of the temperature will cause an increase in the internal resistance so this has to be lowered as well in order to maintain a high efficiency.

A single SOFC cell produces ~1 V. In order to obtain a higher voltage the cells are series connected (stacked) by use of an interconnect material. The function of the interconnect material is to conduct electrons and separate the fuel gas from the air. An important argument for lowering the operation temperature is that metal can be used as interconnect material, which will lower the cost of the fuel cell stack.

1.2 Electrical efficiency

The internal resistance (R_i) of a fuel cell is an important parameter as it determines the electrical efficiency as seen by

$$E = Emf - R_i \cdot j \tag{1}$$

or

$$P = Emf \cdot j - R_i \cdot j^2, \tag{2}$$

where E is the electrode potential, EMF is the electro motive force, P is the power output and j is the current density. The internal resistance of a cell can be divided into a series resistance or electrolyte resistance (R_s), a cathodic polarization resistance ($R_{p,c}$) and a anodic polarization resistance ($R_{p,a}$),

$$R_i = R_s + R_{p,c} + R_{p,a}. \tag{3}$$

Again, the polarization resistance at each electrode can be split into a charge transfer or activation resistance (R_{ct}), a diffusion resistance (R_{diff}) and a chemical reaction resistance (R_{chem}),

$$R_{p,i} = R_{ct} + R_{diff} + R_{chem}. \quad (4)$$

Another term for the losses is overpotentials (η) which are related to the resistance through equation (5). Note that the series resistance is referred to as potential drop across the electrolyte and not overpotential.

$$R_{p,i} = \frac{d\eta_i}{dj} \quad (5)$$

Equation (4) can hereby be rewritten to

$$\eta_i = \eta_{ct} + \eta_{diff} + \eta_{chem} \quad (6)$$

The diffusion loss and the chemical reaction loss are often referred to as the mass transport loss ($\eta_{mass\ transfer}$). A schematic of the various losses is shown Figure 2.

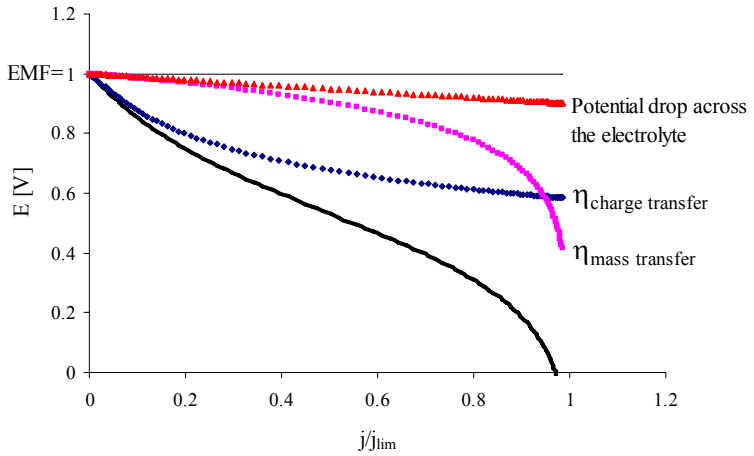

Figure 2. Schematic presentation of a current/voltage-curve (j/V-curve) for a fuel cell. EMF=1 V.

The potential drop across the electrolyte is a ohmic loss due to conduction of oxygen ions through the electrolyte. The oxygen ions are transported over a potential barrier which results in lattice vibrations i.e. dissipation of heat.

The loss due to charge transfer is similar to the loss mechanism of oxygen ion transfer, as a charged particle has to overcome a potential barrier. In this case the resistance decreases as the overpotential increases due to the fact that the barrier decreases when the overpotential increases. The charge transfer loss is also called activation polarization and is described by the Butler-Volmer equation.

The losses due to diffusion arise when the reaction products are removed slower than they are produced or the reactants are supplied more slowly than they are consumed. This is similar to the loss of a chemical reaction where the reaction rate is so slow that the reactants are not consumed rapidly enough. The reactants and products may be intermediate reactants and intermediate products. The diffusion and chemical reaction overpotentials are denoted as mass transfer overpotential or concentration overpotential.

A more detailed description of the polarization resistance and electrode kinetics can be found elsewhere [2,3,4].

1.3 Impurities and the Ni/YSZ electrode

Recently it was shown that segregation of impurities to the interfaces has a negative influence on the kinetics of the $H_{2(g)}/H_2O_{(g)}/Ni_{(s)}/YSZ_{(s)}$ electrode, resulting in a more ineffective electrode [5,6].
Also, segregated impurities at the interface may be the reason for the disagreements about the kinetics in literature [7], which has been accounted for elsewhere [8].
A TEM (transmission electron microscopy) study of the Ni/YSZ cermet anode after long term testing at 850°C showed an accumulation of impurities at the Ni/YSZ interface [9]. The impurity phase was characterized as a silicate glass with an amorphous structure. The composition of the glass phase was ~90 mol% SiO_2 and a few percent of Na_2O, CaO, ZrO_2, V_2O_3 etc. The raw materials used where 99.92 wt.% $(ZrO_2)_{0.92}(Y_2O_3)_{0.08}$ and 99.6 wt.% NiO.

Vels Jensen [10] studied the Ni/YSZ interface by placing a bent Ni wire on top of a polycrystalline YSZ crystal, which hereafter are referred to as a point electrode. Two different purities of Ni wires were used, 99.8 wt% Ni and 99.995 wt%. The YSZ was made from 99.92 wt.% $(ZrO_2)_{0.92}(Y_2O_3)_{0.08}$ powder. It was found that impurities both from the Ni and YSZ segregate to the Ni/YSZ interface, surface of YSZ and the three-phase boundary (TPB). The TPB is where the Ni, YSZ and fuel gas meet. A ridge of impurities was seen along the TPB and was characterised as a alkali silicate (glassy) phase. The polarisation resistance of the 99.995 wt.% Ni electrode was 10-100 times lower than that of the 99.8 wt.% Ni electrode. Also it was found that the Ni/YSZ interface is dynamic at elevated temperatures i.e. the initial smooth YSZ surface showed a topographic structure after a heat treatment. Both the ridge and the dynamic interface is also seen for the Pt/YSZ [11] point electrode.

1.4 Scope of this thesis

The purpose of this study is to perform electrochemical measurements in a very clean system to avoid the effects of impurities. This is attempted by using high purity materials, lowering the operation temperature to prevent fast segregation of impurities and by limiting impurities from the environment. Figure 3 illustrates the objective of this project, which is to study a pure Ni/YSZ electrode. When a clean and pure system is mentioned is this project, the classification by Stoneham [12] should be born in mind:

1	Uncleaned surface	≡Dirty surface	
2	Cleaned surface	≡Probably dirty surface	Experiment
3	Vacuum cleaned surface	≡Possibly clean surface	
4	Relaxed* surface	≡Model of real surface	Theory
5	Unrelaxed* surface	≡Science fiction	

Relaxed surface=decrease in spacing of the outer two atomic planes

This means that the system studied in this work is classified to level 2.
Mogensen *et al*. [8] made an extrapolation of the polarization resistance for the hydrogen electrode in a aqueous electrolyte from room temperature up to 1000°C. The extrapolation showed that the polarization resistance was a factor of 10-100 lower than the polarization resistance for the hydrogen reaction at the Ni/YSZ electrode at 1000°C [13]. There are many differences between the aqueous and gaseous electrode so the comparison is not straightforward, but if just some of the large difference is caused by segregated impurities there is a promising potential for improving the Ni/YSZ electrode.

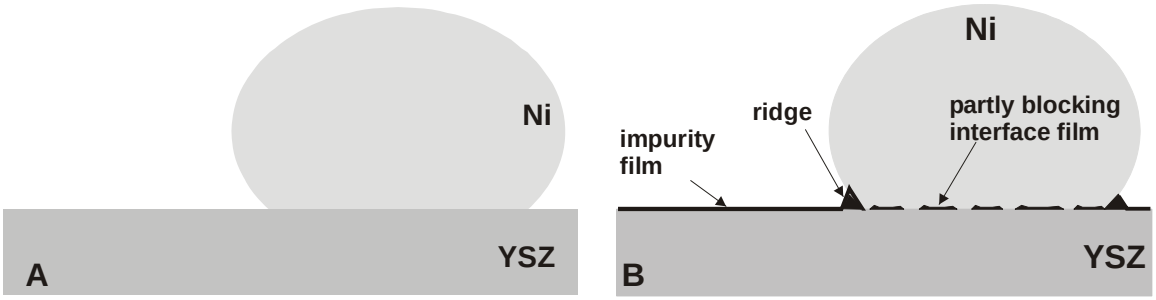

Figure 3. Schematic presentation of Ni/YSZ electrode. A) Illustration of the clean electrode we want to study. B) Illustration of the electrodes that have been studied so far. The sketch is from Vels Jensen [10].

The real SOFC anode is a porous Ni/YSZ composite in order to optimize mass transport and charge transfer near or at the TPB. A point electrode is used in this study as a model system because: 1) It provides a well defined length of the TPB and 2) the easiness of investigating the Ni/YSZ interface after an electrochemical experiment and 3) to obtain a more well defined electrode potential compared to the cermet anode. In a cermet anode the reaction takes place over a distance of ~10 μm from the electrolyte. This causes a gradual potential drop through the cermet anode due to the resistance of the YSZ cermet network. This means that the electrochemical reaction takes place at different potentials at the same time, which makes it more difficult to analyze kinetic data. Electrochemical measurements are performed at 400-700°C to test the performance of the Ni/YSZ electrode. An essential part of the project is to characterize the surfaces of Ni and YSZ both structurally and chemically before and after an electrochemical measurement to detect differences.

The performance of the electrode is tested using impedance spectroscopy and potential sweeps. The morphology of the surfaces is investigated using optical microscope, SEM (scanning electron microscopy) and AFM (atomic force microscopy). The chemical analyses are performed with XPS (X-ray photoelectron spectroscopy), AES (Auger electron spectroscopy), EDS (energy dispersive analysis) and TOF-SIMS (time of flight secondary ion mass spectroscopy).

1.5 Thesis layout

Besides the introduction, this thesis begins with a general description of the electrochemical setup (chapter 2). After this, some introductory experiments that were necessary prior to performing the electrochemical measurements are described (chapter 3). Chapter 4 to 7 are describing the electrochemical experiments together with the surface analysis performed on the electrodes. These chapters are built up as articles. This means that some of the experimental description is repeated in these chapters. In chapter 8 is described some trends in the surface analysis of the Ni and YSZ. Chapter 9 are describing possible ways of removing trace impurities from YSZ. An overall discussion and an overall conclusion for the thesis are given in chapter 10 and 11, respectively. Finally, a suggestion to future work is given in chapter 12.

2 Experimental

This chapter describes: 1) the preparation of the Ni wires and the electrolytes, 2) the setup in which the electrochemical measurements are performed and 3) the measurement equipment used to perform the electrochemical measurements. The other experimental apparatus used in this work are described separately in the relevant chapters. The terminology used throughout this thesis regarding the electrode materials are: 1) Electrode=Ni wire in contact with an zirconia electrolyte, 2) Electrolyte=Stabilized zirconia crystals and 3) Ni= Ni wire.

2.1 Materials and preparation

2.1.1 Electrolytes

The single crystals of stabilized zirconia used as electrolytes in the electrochemical experiments are listed in Table 2.

Table 2. The composition of the electrolytes.

Composition	Code
$(ZrO_2)_{0.9}(Y_2O_3)_{0.1}$ $Zr_{0.82}Y_{0.18}O_{1.91}$	ZY10
$(ZrO_2)_{0.87}(Y_2O_3)_{0.13}$ $Zr_{0.77}Y_{0.23}O_{1.87}$	ZY13
$(ZrO_2)_{0.82}(Y_2O_3)_{0.18}$ $Zr_{0.70}Y_{0.30}O_{1.85}$	ZY18
$(ZrO_2)_{0.9}(Y_2O_3)_{0.04}(Sc_2O_3)_{0.06}$ $Zr_{0.82}Y_{0.07}Sc_{0.11}O_{1.91}$	ZSc6Y4

The notation $(ZrO_2)_{0.9}(Y_2O_3)_{0.1}$ is equivalent to 90 mol% ZrO_2 and 10 mol% Y_2O_3. The other notation used: $Zr_{0.82}Y_{0.18}O_{1.91}$ is based on the fluorite structure were the summation of the cations is one. YSZ will be used when referring to the crystals that are solely stabilized with yttria and SZ will be used when referring to the crystals that is stabilized with yttria and yttria+scandia.

The crystals ZY10 (1 piece), ZY18 (1 piece) and ZSc6Y4 (2 pieces) were provided by Dr. Sergey Shkerin and professor Perfilliev, Institute of High-temperature Electrochemistry, RAS, 20 S. Kovalevskaya Str., 620219 Ekaterinburg, Russia. The surface orientations of the samples are unknown.

The ZY13 crystals were purchased at MTI Corporation (www.mticrystal.com). According to the certificate the Y_2O_3 content is 8 mol% but XPS, AES and EDS measurements show that the content is 13 mol%. The purity is stated as 99.99% and the surface orientation is [100]. Five pieces of this crystal was purchased.

All electrolytes were polished with 6, 3, 1 and ¼ μm diamond suspension. For the final polishing an acidic suspension of alumina particles (0.02 μm) was used. The electrolytes were only polished for 30 seconds with the acidic suspension (OP-AA suspension, Struers) as longer polishing time results in an attack of the electrolyte surface. The polishing cloths were used for the electrolytes only in order to avoid contamination. After each step the samples were cleaned in an ultrasonic bath with ethanol and rubbed with lens paper to avoid mixing between particles from the different suspensions used.

Figure 4 illustrates the need for manual rubbing with lens paper. The optical micrograph shows an electrolyte surface after polishing with ¼ μm diamond suspension and ultrasonic cleaning in ethanol for 20 minutes. The ultrasonic cleaning is insufficient as traces of droplets from the polishing suspension can be seen. After manual rubbing with lens paper the droplet traces disappear.

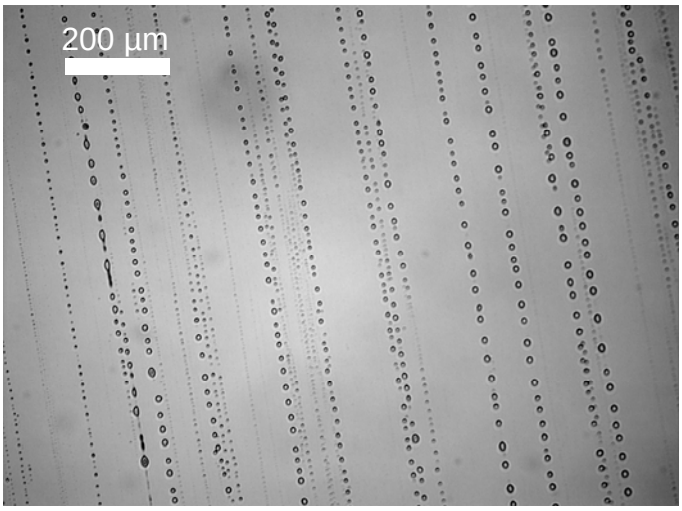

Figure 4. Optical micrograph of an electrolyte surface after polishing with ¼ μm diamond suspension and ultrasonic cleaning in ethanol for 20 minutes.

For the electrochemical measurements a counter and a reference electrode were applied on the back of the electrolyte, see chapter 4.3. The back was ground with SiC-320 paper (particle size: 32 – 37 μm) in order to obtain a high surface area, and thereby a low polarization resistance of the two electrodes.

2.1.2 The nickel wire

A nickel wire with a diameter of 0.5 mm was purchased at Alfa Aesar (Puratronic®, www.matthey.com). The stated purity is 99.999% (metal basis). The chemical analysis is shown in Table 3.

Table 3. Certificate of analysis for the Ni wire provided by Alfa Aesar (values given in ppm).

Ag	0.7	Al	0.005	As	<0.05	Au	<0.05
B	<0.005	Ba	<0.05	Be	<0.005	Bi	<0.01
Br	<0.05	Ca	<0.05	Cd	<0.1	Ce	<0.05
Cl	2.1	Co	1.2	Cr	0.01	Cs	<0.01
Cu	0.15	Dy	<0.01	Er	<0.01	Eu	<0.01
F	<0.05	Fe	0.15	Ga	<0.05	Gd	<0.01
Ge	<0.05	Hf	<0.01	Hg	<0.05	Ho	<0.01
I	<0.01	In	<0.05	Ir	<0.05	K	<0.05
La	<0.005	Li	<0.005	Lu	<0.01	Mg	0.02
Mn	<0.005	Mo	<0.05	Na	0.85	Nb	<0.01
Nd	<0.01	Os	<0.05	P	<0.005	Pb	0.9
Pd	<0.05	Pr	<0.01	Pt	<0.05	Rb	<0.05
Re	0.05	Rh	<0.1	Ru	<0.5	S	0.06
Sb	<0.01	Sc	<0.001	Se	<0.05	Si	0.2
Sm	<0.01	Sn	0.04	Sr	<0.05	Ta	<1
Tb	<0.01	Te	<0.05	Th	<0.001	Ti	0.2
Tl	<0.01	Tm	<0.01	U	<0.001	V	<0.001
W	<0.05	Y	<0.05	Yb	<0.01	Zn	0.2
Zr	<0.05						

Stock number: 43761, Lot number: G19M28
Elements are determined by GD-MS (Glow Discharge Mass Spectrometry)

The Ni wire was heat treated in 3% H_2O/9% H_2/N_2 (1000°C, 7 days) and electro polished before use. Electro polishing was performed with Pt as the cathode and Ni wire as the anode. The electrolyte used for electro polishing is given in Table 4. The electrolyte was cooled to between -5 and -10°C.

Table 4. Electrolyte used for electro polishing of the Ni wire.

Compound	Quantity
Water, H_2O	120 ml
Ethanol, CH_3CH_2OH	700 ml
2- butoxy ethanol, $CH_3CH_2CH_2CH_2OCH_2CH_2OH$	100 ml
Perchloric acid, $HClO_4$	78 ml

A voltage of 10 V was applied between the Ni wire and the Pt plate which resulted in a current of 0.2-0.3 A. The Ni wire was electro polished for ~3 minutes. A sketch of the system for electro polishing is shown in Figure 5.

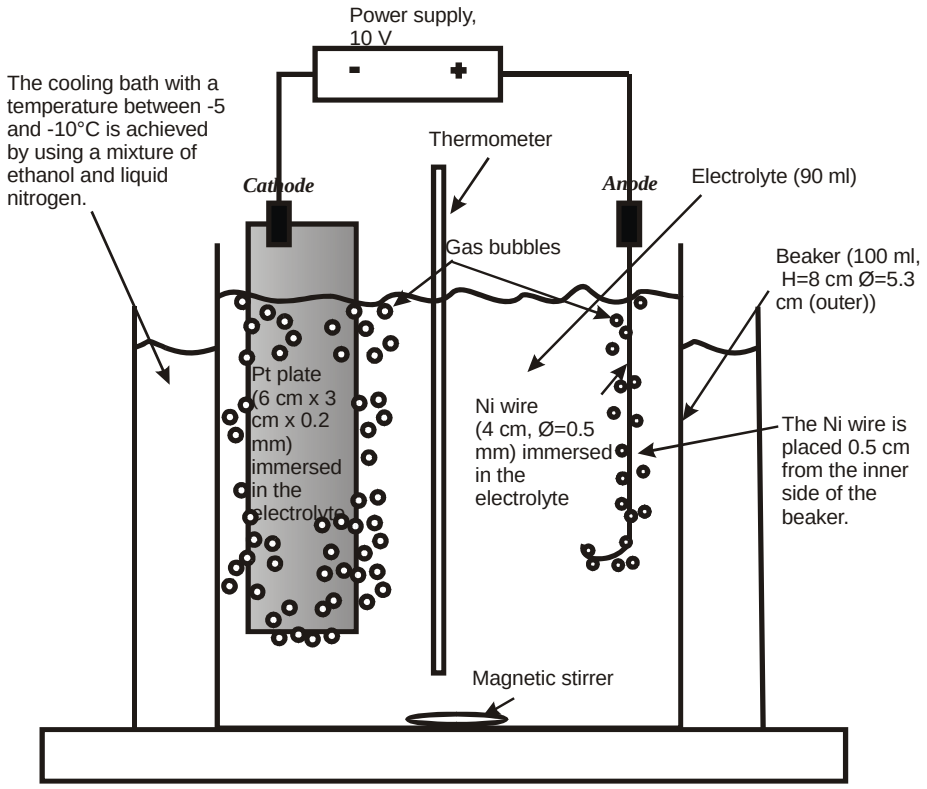

Figure 5. Sketch of setup for electro polishing.

Gas development at both the Ni wire and Pt plate occurs during the electro polishing. Some possible reactions that occur during electro polishing are listed in Table 5.

Table 5. Possible reactions during electro polishing of the Ni wire.

Anode, Ni	1) $Ni \rightarrow Ni^{2+} + 2e^-$
	2) $2H_2O \rightarrow O_{2(g)} + 4H^+ + 4e^-$
	3) $ClO_4^- \rightarrow \frac{1}{2}Cl_{2(g)} + 2O_{2(g)} + e^-$
Cathode, Pt	1) $H^+ + e^- \rightarrow \frac{1}{2}H_{2(g)}$

The gas development at the anode makes it difficult to calculate the amount of dissolved Ni as an unknown amount of current is used for oxidation of water and/or perchlorate. When prolonged electro polishing was performed there was no doubt that Ni was dissolved as the wire becomes thinner and the electrolyte was colored green. After electro polishing the Ni wire was shining. Finally, the Ni wire was ultrasonically cleaned in ethanol for 20 minutes.

2.2 Equipment used for the electrochemical measurements

Two electronic setups were used to perform the electrochemical measurements: 1) Solartron 1260 and 2) Solartron 1255b in combination with Solartron 1287, which hereafter will be referred to as Solartron 1255b+1287. The Solartron 1260 and 1255b are frequency response analyzers and the Solartron 1287 works as a potentiostat. The software Elchemea [14] was used for controlling the Solartron 1260. The software Z-plot [15] was used to control the Solartron 1255b+1287. The software Z-view [15] was used to fit the impedance

spectra using equivalent circuits. An ac amplitude of 30 mV and 5 points per frequency decade was used to perform the impedance spectra unless other is stated.

2.3 Setup for electrochemical characterization

A 3-electrode setup (4-wires, one atmosphere) was used for the electrochemical characterization. Three electrodes are in principle necessary to characterize only one electrode. The three electrodes are referred to as the working electrode (WE), the reference electrode (RE) and the counter electrode (CE). The electrode under investigation is the WE, which in this study is the Ni/YSZ electrode.
Figure 6 shows a photo of the rig that was used for the electrochemical measurements. Weights of copper (OFHC= oxygen free high conductivity quality) are used to press the Ni wire against the electrolyte. The gas inlet to the furnace tube is in the bottom of the rig. This ensures that the copper sits downstream from the samples and a possible contamination from the copper is minimized. The alumina parts used for the setup had a purity of 99.8%.

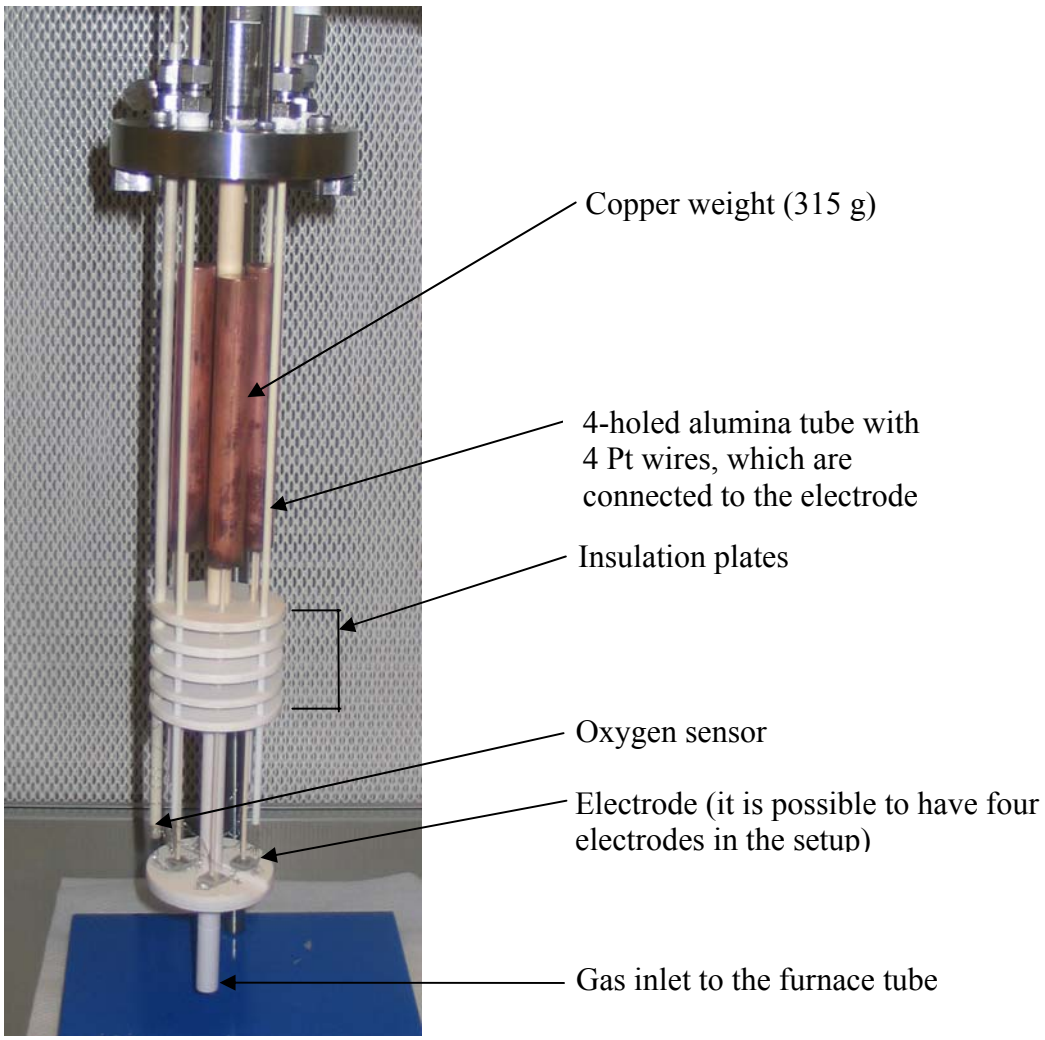

Figure 6. Photo of the rig used for electrochemical measurements.

After preparation of the zirconia electrolytes and the Ni wires they were transported in closed containers to a laminar air flow system. The electrodes were mounted in a laminar air flow system (see Figure 7), gloves, mask and hairnet was used to avoid contamination. After mounting of the electrodes the rig was inserted into the furnace tube, which protects

against direct exposure to the atmosphere. Finally, it was transported to the furnace where the electrochemical experiments were conducted. After the electrochemical experiments the handling procedure was reversed. The electrolytes and Ni wires from the electrode were kept in closed containers, in which they also were transported to the surface analysis apparatus. The laminar air flow system (from Holten, Denmark) is equipped with a HEPA (High Efficiency Particulate Air) filter with a efficiency of > 99.999% against particles of 0.3 μm.

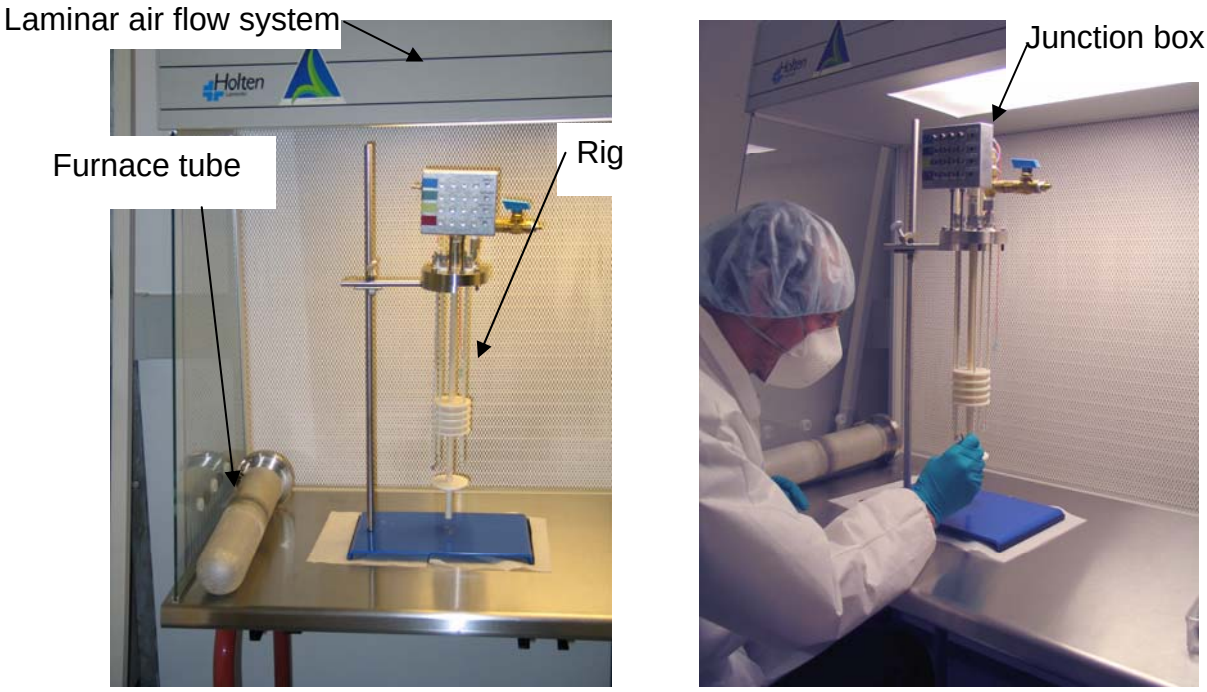

Figure 7. Photos of the laminar air flow system, the furnace tube and the electrochemical rig where the junction box is located in the top.

The rig can contain four electrodes. Each electrode are connected to four Pt wires that runs through 4-holed alumina tubes to the junction box. Leads are used to connect the junction box to the Solartron. Measurements were performed at one electrode at the time and manual change of the leads was necessary to perform measurements between the electrodes.
A sketch of the outer system is shown in
Figure 8. The setup was constructed during the project and approved by the hydrogen safety committee at Risø National Laboratory (Materials Research Department). In this connection a safety report regarding the use of hydrogen was worked out. The report is filed at the Materials Research Department, Risø National Laboratory. The outer system can supply pure H_2 and mixture of H_2 and an inert gas (N_2, He, Ar). The gasses can be lead directly to the electrodes or they can be humidified or partial humidified in ion-exchanged water. The water temperature can be controlled from 2-60°C, which corresponds to a water content of 0.7-20 vol. %. The water content is easily lowered by only humidify a part of the gas, i.e. by only leading a part of the gas through the water. The safety arrangement in the outer setup makes it possible to perform measurements below the self-ignition temperature (~570°C) for mixture of H_2 and air. Measurements at low temperature are essential in this project as it lowers the segregation rate of impurities from the electrode materials to the surface.

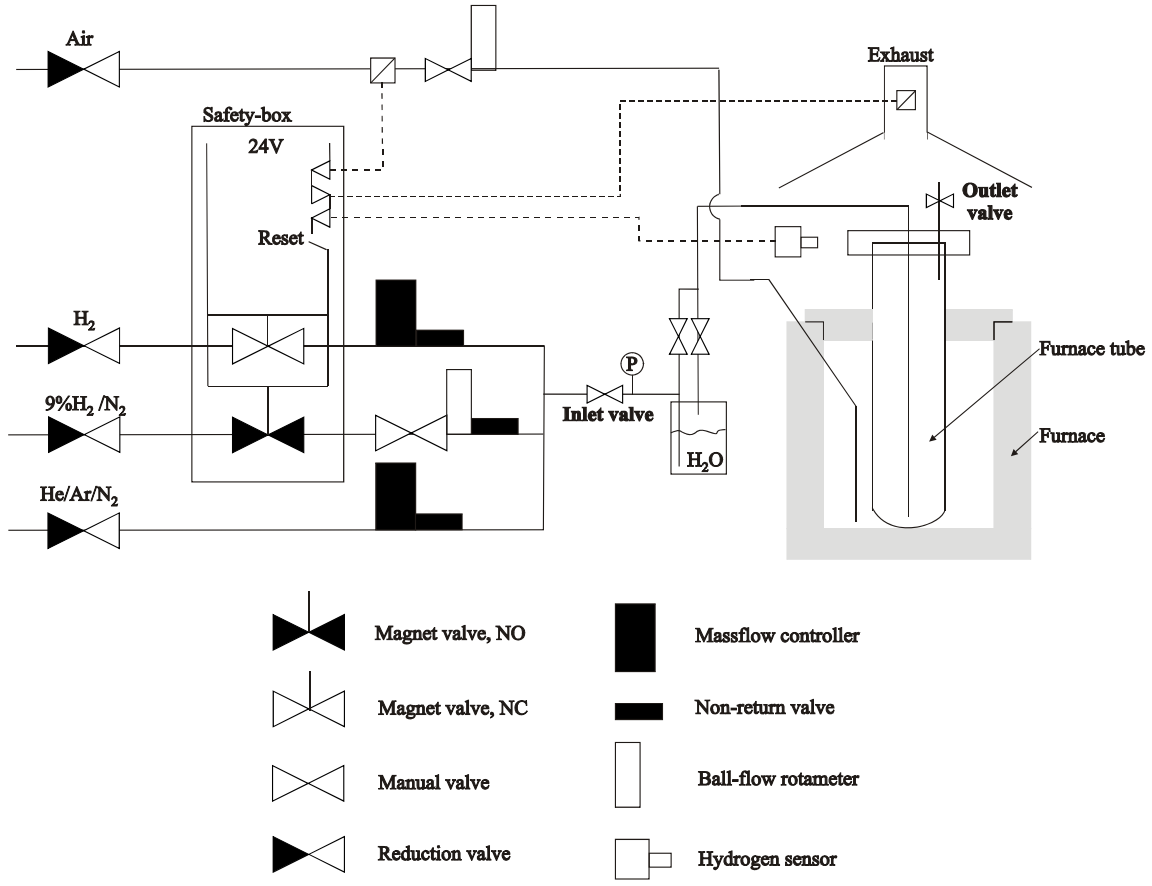

Figure 8. Schematic view of the outer system. NO=normally open. NC= normally closed.

The electrochemical rig that was built in this project was only used for the Ni/SZ electrodes in order to prevent contamination from other usage. The setup (rig + furnace tube) was heat treated before it was used for electrochemical measurements in order to remove volatile material. Two heat treatments at 1000°C (7 days each) were performed; first it was heated in air (technical air, 21 mol% O_2 and 79 mol% N_2) and then in 3% H_2O/H_2. The gas flow was in each case 100 ml/min (1 atm, 25°). The technical air was only temporarily connected to the setup.

3 Introductory experiments

This chapter describes some introductory experiments, which among other things deal with the difficulties of performing measurements on high impedance samples and the difficulties to obtain a well defined contact area.

3.1 Copper contamination

To test if the copper weights would contaminate the electrode a sample of copper and YSZ was heat treated in a gas stream of 9% H_2/3% H_2O/N_2 at 1000°C for 7 days. The YSZ was placed 1 cm downstream of the copper sample. XPS was performed on the YSZ sample after the heat treatment and no traces of copper were found. This indicates that the copper is not likely to contaminate the electrode.

3.2 Contact area of the Ni wire

Heat treatment of the Ni wire at 1000°C prior to an electrochemical experiment was performed in order to obtain a homogeneous contact area between the Ni wire and the SZ single crystal. A homogeneous contact area is important in order to achieve a well defined length of the TPB and a well defined contact area. Figure 9 shows two Ni wires after they were used as point electrodes at 650°C. Only the wire marked B has been heat treated prior to the experiment. It is seen that a more homogeneous contact area is achieved when a heat treatment prior to the experiment is performed. In Figure 9B the area outside the contact area is partly covered with islands of irregularities. These irregularities turn up after electro polishing of the heat treated Ni wire. The islands are not homogeneously distributed on the Ni wire and in some cases no islands are seen near the contact area. An AES analysis of an island is shown in Figure 25.

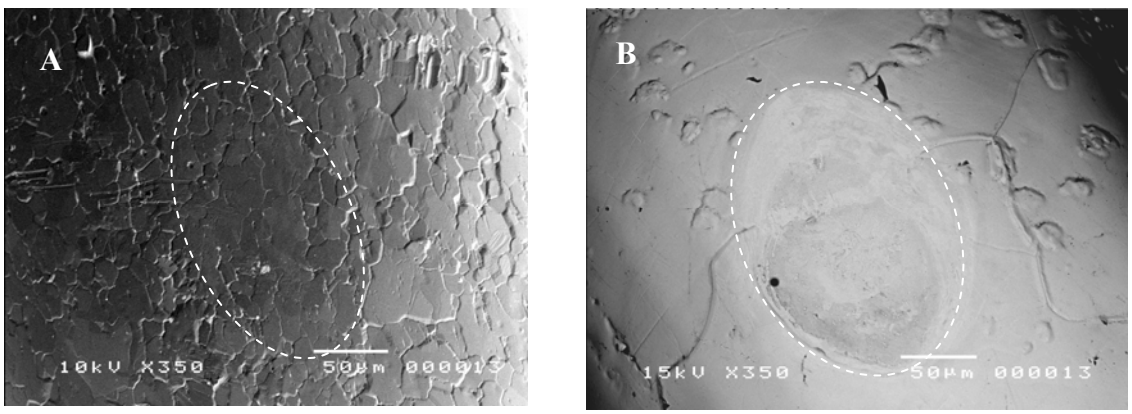

Figure 9. Two Ni wires after point electrode experiments at 650°C. The ellipse marked by a white dashed line shows the contact area. A) This Ni wire was not heat treated prior to the experiment. B) This Ni wire was heat treated (1000°C, 7 days) in reducing atmosphere prior to the experiment.

3.3 Vibrations and general improvements

In a preliminary point electrode experiment performed in another setup (described in Vels Jensen [10]) it was seen that the electrochemical measurements were sensitive to vibrations. Figure 10 shows that the value of R_s (series resistance) increases after a vibration, which was caused by mounting/dismounting of leads to the junction box. R_s scales with the

contact area i.e. the higher the resistance the smaller the contact area. The sudden increase in R_s after the 1st and 2nd vibration is followed by a slow decrease due to creep of the Ni wire as it probably is forming a new contact area. It would be expected that R_p (polarization resistance) increases when the contact area decreases. This is, however, only the case after the 2nd vibration, see Figure 10. This information indicates that the polarization resistance is dependent on other factors than the size of the contact area.
Several improvements were made to the setup that was constructed during the beginning of this project compared to the setup described in Vels Jensen [10] in order to make it less sensitive for vibrations from the surroundings: 1) Usage of heavier weights (76 → 315 g), 2) Mounting of the Ni wire directly on the alumina tube which carries the weight, 3) Stabilization of the furnace tube and 4) Vibration damping material (SB-XL-feet, www.holfi.dk) was placed between the rig and the base.

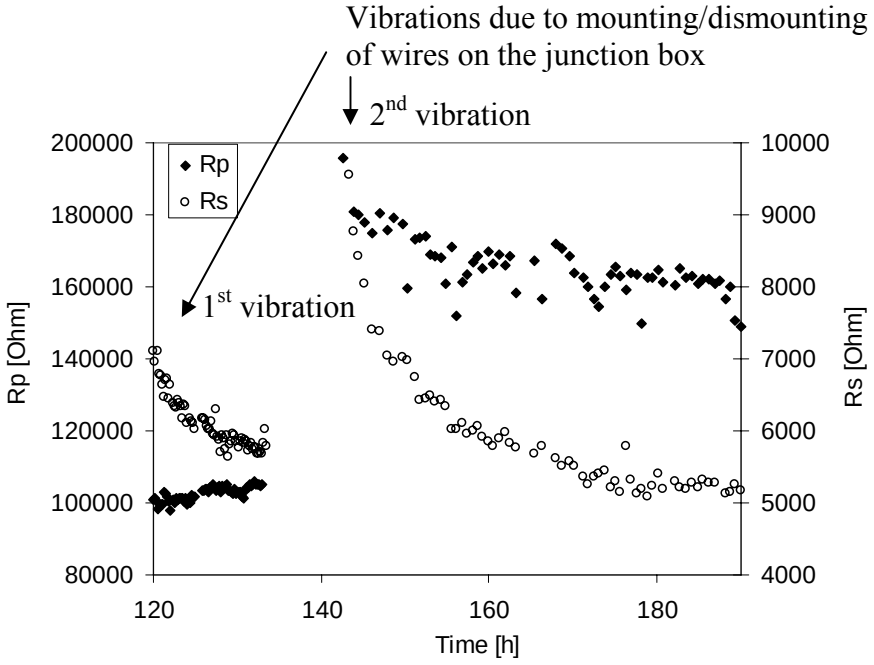

Figure 10. Effect of vibrations on R_s and R_p. The point electrode experiment was conducted at 650°C in 3% H_2O/H_2 in the setup described by Vels Jensen [10].

3.4 Capacitance of the setup

Impedance measurements were performed with no samples in the electrochemical rig to determine the impedance of the setup. The obtained impedance spectra could be fitted well to an RC-circuit. The resistance was too high to influence the impedance measurements but the capacitance (~$2.5 \cdot 10^{-11}$ F) is likely to influence the impedance spectra. This capacitance is hereafter called the stray capacitance (C_{stray}).
In the following it is shown that the stray capacitance may be important when fitting to an equivalent circuit. The equivalent circuit (model) used for fitting is shown in Figure 11. The symbols in the equivalent circuit are: R_s is the electrolyte resistance, R_t is the resistance due to charge transfer, C_{stray} is the stray capacitance, C_{dl} is the double layer capacitance and the R_1Q_1 refers to a chemical reaction. Except for the stray capacitance the symbols are not proven to have the physical meaning that they refer to but are simply adopted directly from [16]. The polarization resistance is here the sum of R_t and R_1. Figure 12 and Figure 13 show a common impedance spectrum of a Ni/YSZ point electrode at 500°C in 3% H_2O/H_2

and two fits. One fit is performed without the stray capacitance (fit 1) and in the other fit the stray capacitance is excluded (fit 2).

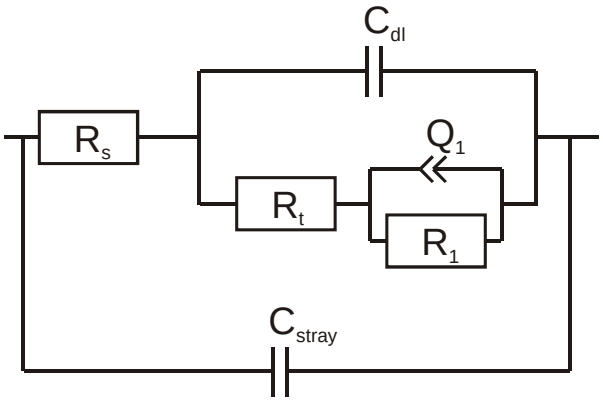

Figure 11. The model used for fitting. R_s is the electrolyte resistance, R_t is the resistance due to charge transfer, C_{stray} is the stray capacitance, C_{dl} is the double layer capacitance and the R_1Q_1 refers to a chemical reaction.

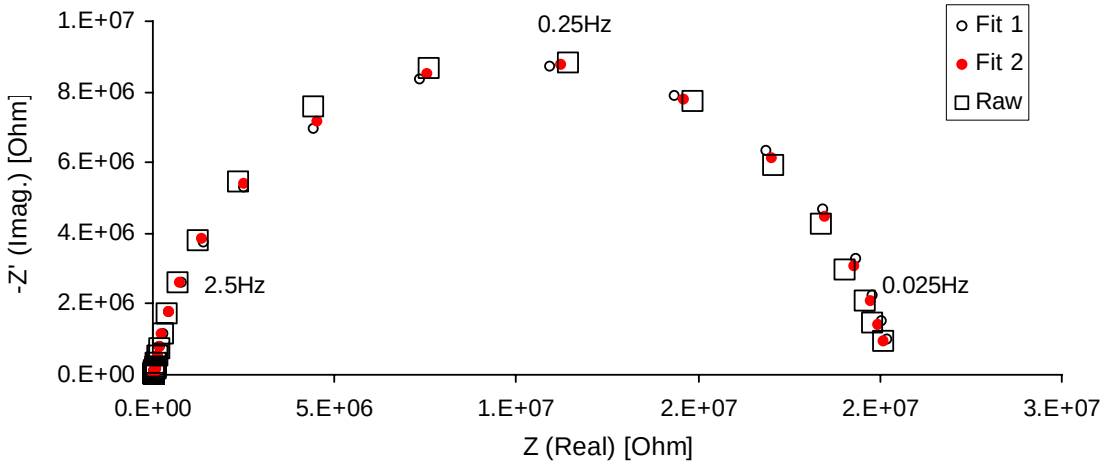

Figure 12. Impedance spectrum of a Ni/YSZ point electrode at 500°C in 3% H_2O/H_2 and two fits. Fit 1 is modeled according to the circuit shown in Figure 11 with the C_{stray} excluded. Fit 2 is modeled according to the circuit shown in Figure 11. The fitted parameters are listed in Table 6.

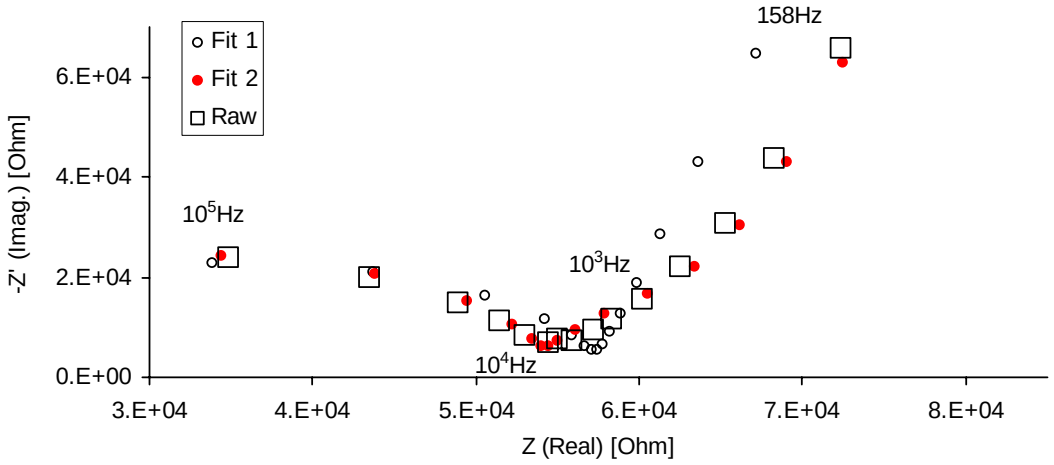

Figure 13. The high frequency part of an impedance spectrum for a Ni/YSZ point electrode at 500°C in 3% H_2O/H_2 and two fits. Fit 1 is modeled according to the circuit shown in Figure 11 without the C_{stray}. Fit 2 is modeled according to the circuit shown in Figure 11. The fitted parameters are listed in Table 6.

The fit where the stray capacitance is included explains the high frequency part better. The fitted parameters are listed in Table 6. Notice that the polarization resistance (R_p) is $R_t + R_1$. A main description of the parameters is: R_1Q_1 dominates the low frequency part (0.1 – 100 Hz). C_{dl} and R_t are significant in the range 100 – 10^4 Hz and C_{stray} dominates the range from 10^4 – 10^5 Hz. R_s is important in the high frequency part. In the case where C_{stray} omitted from the fit it is seen that C_{dl} changes towards a value of C_{stray} in order to fit the high frequency part.

Table 6. Fitted parameters for impedance spectra shown in Figure 12 and Figure 13.

R_s [kΩ]	R_t [kΩ]	C_{dl} [F]	R_1 [Ω]	Q_1 [F/(1/s)$^{n-1}$]	n_1	C_{stray} [F]	χ^2
50	35	$6.9\cdot10^{-9}$	$2.0\cdot10^{7}$	$2.2\cdot10^{-8}$	0.88	$2.6\cdot10^{-11}$	$8\cdot10^{-4}$
66	46	$3.6\cdot10^{-11}$	$2.0\cdot10^{7}$	$3.0\cdot10^{-8}$	0.90	-	$4\cdot10^{-3}$

The fitted stray capacitance ($2.6\cdot10^{-11}$ F) correlates very well with the measured capacitance of the setup (~$2.5\cdot10^{-11}$ F).
The following calculation shows that the stray capacitance most likely originates from the Pt wires that are connecting the electrodes to the junction box. The Pt wires (Ø=0.3 mm) that are located in an alumina tube (length=45 cm). The two Pt wires are separated by ~1 mm alumina. Using a model for a plate capacitor (7), where C is the capacitance, ε_r is the relative permittivity, ε_0 is the permittivity of vacuum, A is the area of the plate and d is the distance between the plates. Setting ε_r=10 (alumina) the capacitance for the Pt/alumina was calculated to $1.2\cdot10^{-11}$ F.

$$C = \frac{\varepsilon_r \cdot \varepsilon_0 \cdot A}{d} = \frac{10 \cdot 8.85 \cdot 10^{-12} \frac{C^2}{J \cdot m} \cdot \left(45 \cdot 10^{-2}\, m \cdot 0.3 \cdot 10^{-3}\, m\right)}{1 \cdot 10^{-3}\, m} = 1.2 \cdot 10^{-11}\, F \qquad (7)$$

This capacitance is approximately a factor of two lower than the measured and fitted values. As edge effects are not included in the simple plate capacitor model a higher

capacitance is expected from the measurement than the calculation. Hence, it is likely that stray capacitance can be ascribed to the Pt wires in the alumina tube.
In general the R_s values are much smaller than R_p. This means that the uncertainty in determining R_s does not influence the R_p value. R_s is still important, as it is an indicator of the size of the contact area as described in section 3.3.

3.5 Measurement equipment/dummy cell

A concern when measuring impedance spectra using a 3-electrode setup is that the impedance of the reference electrode is low compared to the input impedance of the measurement equipment. This problem is treated in appendix A for a reference electrode with the highest impedance used in this work. It was found that erroneous measurements occurred when using the Solartron 1260 but satisfactory measurements was achieved when using the Solartron 1255b+1287, which have a higher input impedance than the Solartron 1260. When performing measurement with the Solartron 1260 it was controlled that the impedance of the reference electrode was low enough that satisfactory measurements were achieved.

A dummy cell with high impedance was made in order to test the validity of the Solartron's used. Impedance spectra and potential sweeps for the dummy cell are shown in appendix B. It was found that the Solartron 1255b+1287 was better than the Solartron 1260 to measure high impedance samples i.e. small currents. In the potential sweeps performed for the dummy cell small zero points offsets were seen. These small offsets were corrected for the sweeps shown in this report. They did not influence the analysis of the sweeps.

4 Reproducibility of the H_2/H_2O/Ni/YSZ point electrode at 700°C

4.1 Abstract

Nickel point electrodes on YSZ (yttria stabilized zirconia) are often used as model electrodes for the SOFC anode. The reproducibility with respect to the electrochemical performance using the polarization resistance as a characteristic parameter is poor [10]. Reproducibility is the first step in characterization of a system. In this study the performance of four identical point electrodes is investigated. It is attempted to control the factors that are believed to cause the poor reproducibility e.g. impurities, microstructure (interfacial roughness), atmosphere and history of polarization. Bent Ni wires (99.999 %) were pressed against polished single crystals of YSZ, thereby forming point electrodes. Four single crystals with the composition $(ZrO_2)_{0.87}(Y_2O_3)_{0.13}$ were used as electrolytes. The polarization resistances (R_p) at OCV (open circuit voltage) were measured from 550-750°C in mixtures of H_2/H_2O over 7 days. The R_p for the electrodes varied by a factor of 2.6, which are considered as low when studying the literature. The Ni wires and single crystals were analyzed before and after the electrochemical experiment using SEM (scanning electron microscopy) to study morphology, XPS (X-ray photoelectron spectroscopy) to determination the chemical composition of the YSZ surface and AES (Auger electron spectroscopy) to determination the chemical composition of the Ni surface. After the electrochemical experiment, impurities were found on the Ni the YSZ surfaces.

4.2 Introduction

Previously large variations (factor ~200) in point electrode performance using pure Ni (99.995 wt.%) and polycrystalline YSZ has been observed [10]. The poor reproducibility of electrode measurements is in general a problem and is not completely understood. The object of this experiment is to reproduce the performance of four identical electrodes. Single crystals were used instead of polycrystalline YSZ in order to get a more well defined electrode. The surfaces of Ni and YSZ were carefully polished and cleaned. A secondary purpose of this study is to perform electrochemical measurements on high purity electrodes in order to avoid the effects of impurities, which are known to increase the polarization resistance [5,6]. It was attempted to make high purity electrodes by using high purity materials, lowering the operation temperature from 1000°C to 700°C in order to prevent fast segregation of impurities, and by limiting impurities from the environment.

The reactions under investigation at the Ni/YSZ electrode are the oxidation of hydrogen and the reduction of water, see (8) and (9) respectively.

$$H_{2(g)} + O^{2-}_{(SZ)} \rightarrow H_2O_{(g)} + 2e^-_{(Ni)} \qquad \text{(Anodic current)} \qquad (8)$$

$$H_2O_{(g)} + 2e^-_{(Ni)} \rightarrow H_{2(g)} + O^{2-}_{(SZ)} \qquad \text{(Cathodic current)} \qquad (9)$$

Reactions (8) and (9) dominate when the cell is operated as a fuel cell (SOFC) and as an electrolyzer cell (SOEC, solid oxide electrolyzer cell), respectively. Note that since this is a one-atmosphere setup it is the opposite reactions that occur at the WE and the CE, in that way there is no overall usages of hydrogen or water. By convention anodic current and overpotential is positive and cathodic current and overpotential is negative [2].

The real SOFC anode is a porous Ni/YSZ composite in order to optimize mass transport and charge transfer near or at the three phase boundary (TPB) where the Ni, YSZ and fuel gas (e.g. $H_{2(g)}$) meet. A point electrode is used here as a model system because: 1) It provides a well defined length of the TPB and 2) the easiness of investigating the Ni/YSZ interface after an electrochemical experiment and 3) to obtain a more well defined electrode potential compared to the cermet anode. In a composite anode the reaction takes place over a distance of ~10 μm from the electrolyte. This causes a gradual potential drop through the cermet anode due to the resistance of the YSZ cermet network. This means that the reactions in (8) and (9) take place at different potentials at the same time, which makes it more difficult to analyze kinetic data.

4.3 Experimental

4.3.1 Electrochemical setup

A 3-electrode setup (4-wires, one atmosphere) and impedance spectroscopy were used to measure R_p at OCV using a 30 mV signal. A frequency response analyzer (Solartron 1260) was used for the impedance measurements at OCV. For polarization measurements a frequency response analyzer (Solartron 1255b) in combination with a potentiostat (Solartron 1287) were used. Two gas compositions ~3% H_2O/H_2 and ~0.7% H_2O/H_2 were used. Figure 14 shows a sketch of the electrochemical 3-electrode setup. On top of the alumina tube a weight of copper (315 g) is arranged to press the Ni wire against the electrolyte. Prior to the electrochemical experiment the setup, which consists mainly of alumina, was heat treated twice to remove volatile material; first in air (technical air, 21 mol% O_2 and 79 mol% N_2) and then in humidified hydrogen (3% H_2O/H_2). The heat treatments were conducted at 1000°C for 7 days.

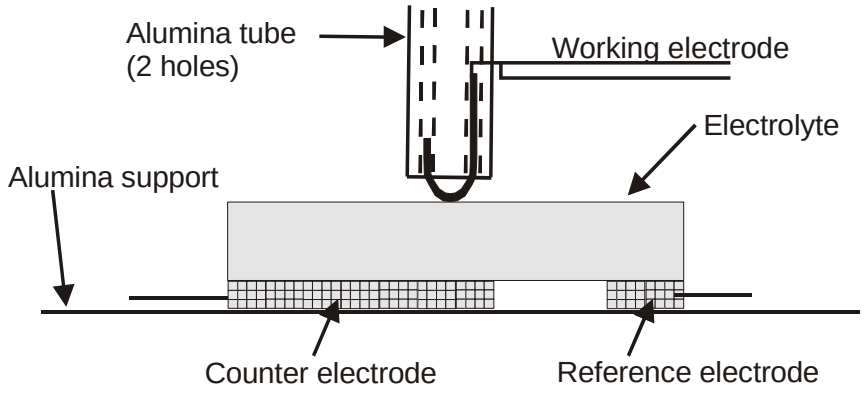

Figure 14. Sketch of the 3-electrode setup. Two leads are connected to the working electrode (Ni wire). Pt is used as counter and reference electrodes. Two Pt meshes collect the current and allow for gas transport to the counter and reference electrodes.

The four electrodes were operated for 8 days as illustrated in Figure 15. The saturation temperature refers to the temperature of the water in which the hydrogen was saturated. The electrodes were numbered 1, 2, 3 and 4, respectively.

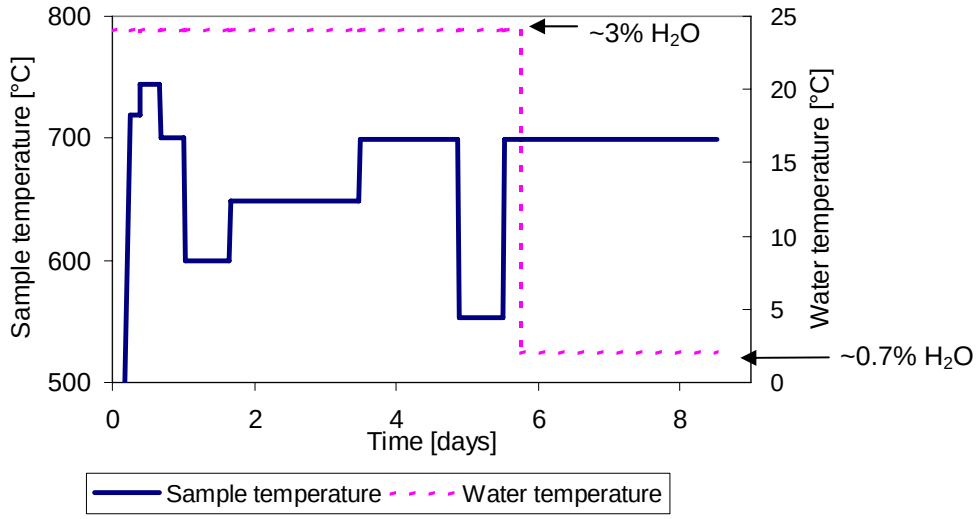

Figure 15. Sample and water temperature throughout the experiment.

4.3.2 Materials and sample preparation

A nickel wire (Ø=0.5 mm) from Alfa Aesar (Puratronic®) was used as working electrode. The stated purity was 99.999 % (metal basis). Prior to the electrochemical experiment the Ni wires were annealed in 3% H_2O/9% H_2/N_2 (1000°C, 7 days) and electro polished.
Four single crystals with the composition $(ZrO_2)_{0.87}(Y_2O_3)_{0.13}$ were used as electrolytes. The single crystals were purchased at MTI Corporation (www.mticrystal.com). The purity is stated as 99.99 % and the surface orientation is [100]. The electrolytes were polished with 6, 3, 1 and ¼ µm diamond suspension. For the final polishing an acidic suspension of alumina particles (0.02 µm, OP-AA suspension, Struers) was used. After polishing and cleaning of both the Ni wire and the electrolyte in an ultrasonic bath with ethanol, they were handled in a laminar air flow system while wearing gloves, mask and hairnet.
Platinum was used as counter and reference electrodes and were painted on the electrolyte using Pt-paste (Degussa, 308A). As current collector for the counter and the reference electrodes Pt meshes were used in order to allow gas transport to the electrodes. A mesh consists of 0.1 mm Pt wires with a mask size of 0.5x0.5 mm. The thickness of the mesh is 0.3 mm.

4.3.3 Surface characterization techniques

Several surface techniques were used to characterize the Ni wires and the single crystals before and after the electrochemical measurements.
SEM (scanning electron microscopy) was performed using a Jeol JSM-5310LV. SEM images were used to determine the Ni/YSZ contact areas from the Ni wires. Backscattered electrons were used to produce the images.
XPS (X-ray photoelectron spectroscopy) was performed using a Sage 100 from SPECS with a non-monochromated Mg-Kα X-ray source and a take-off angle of 90°. From the full spectrum elements in the sample determined using a step size of 0.5 eV and a detector pass energy of 100 eV. Narrow scans with a step size 0.2 eV and a detector pass energy of 23 eV were performed to get a better resolution. An electron floodgun was used to limit charging. XPS was used for analysis of the electrolyte surfaces.
AES (Auger electron spectroscopy) was performed using a Phi 550/590 spectrometer from Perkin Elmer. The electron gun was set to 5 keV. The step size was 1 eV. Depth profiling

was performed using an ion gun with 2 keV Ar^+ and a current of 45 μA/cm^2, the angle of incident was 54° to the surface. AES was used for elemental surface analysis of the Ni wire. XPS and AES probe a depth of 10-40 Å.

4.4 Results

4.4.1 Surface analysis

Figure 16 shows an SEM image of the Ni wire before it was used in the electrode experiment (sample 3). SEM images of the other Ni wires looked similar to the one used for sample 3.

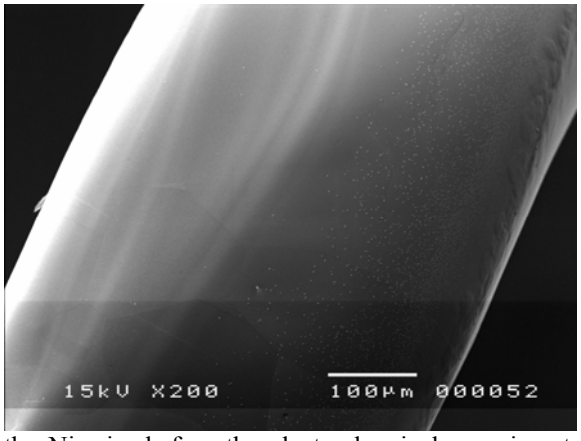

Figure 16. SEM image of the Ni wire before the electrochemical experiment. This Ni wire was used in electrode 3.

The elliptic contact areas on the Ni wires after the electrochemical experiment were investigated using SEM images. The long (2α) and short axis (2β) of the contact area, the size of contact area (A) and the perimeter (p) of the contact area are listed in the figure text, see Figure 17 - Figure 19. The particles seen in Figure 17 and Figure 18 are believed to originate from the surroundings e.g. during mounting of the sample in the SEM. The origin of the scratches and holes seen in Figure 18 and Figure 20 respectively are unknown. Smooth and homogenous contact areas were only observed from the Ni wires from electrode 1 and 3, see Figure 17 and Figure 19 respectively.

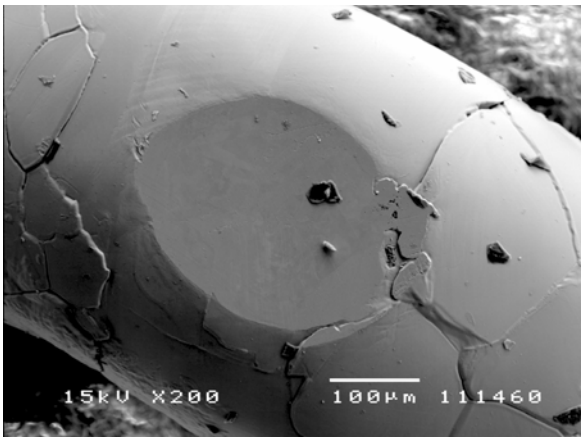

Figure 17. Ni wire from electrode 1 after the electrochemical experiment. α=155 μm, β=119 μm, A=0.0579 mm^2 and p=0.868 mm.

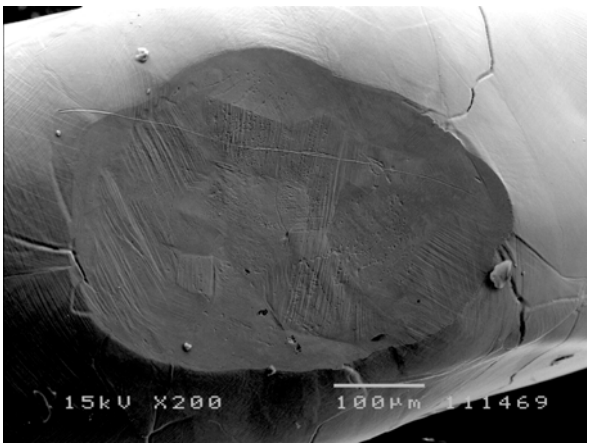

Figure 18. Ni wire from electrode 2 after the electrochemical experiment. α=238 μm, β=168 μm, A=0.125 mm^2 and p=1.293 mm.

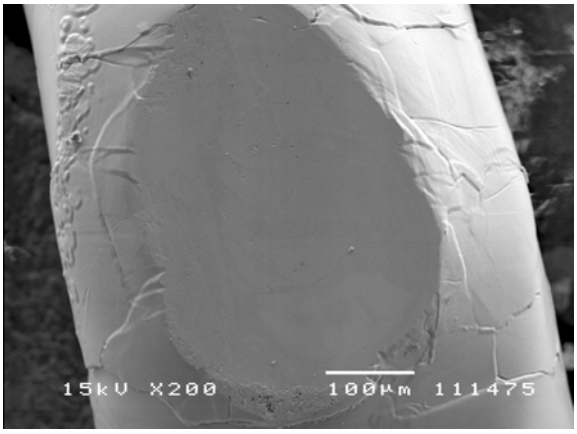

Figure 19. Ni wire from electrode 3 after the electrochemical experiment. α=238 µm, β=156 µm, A=0.117 mm^2 and p=1.262 mm.

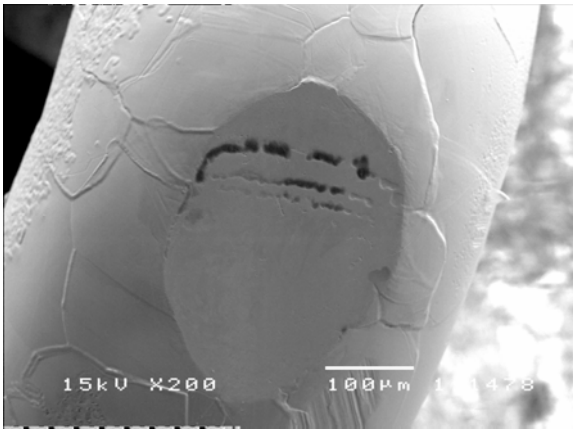

Figure 20. Ni wire from electrode 4 after the electrochemical experiment. α=184 µm, β=127 µm, A=0.0732 mm^2 and p=0.992 mm.

An XPS measurement was performed on a polished single crystal (reference sample). The only impurity that was detected was carbon. When a sample has been exposed to the atmosphere carbon is always present due to adsorption of organic species. After the electrochemical experiment the single crystal from electrode 1 was investigated with XPS. The detected impurities was Si and Na in the following ratios: Si/Zr = 0.16 and Na/Zr=0.23. An AES depth profile of a Ni wire (reference sample) that was heat treated in reducing atmosphere, electro polished and ultrasonically cleaned in ethanol for 20 min is shown in Figure 21.

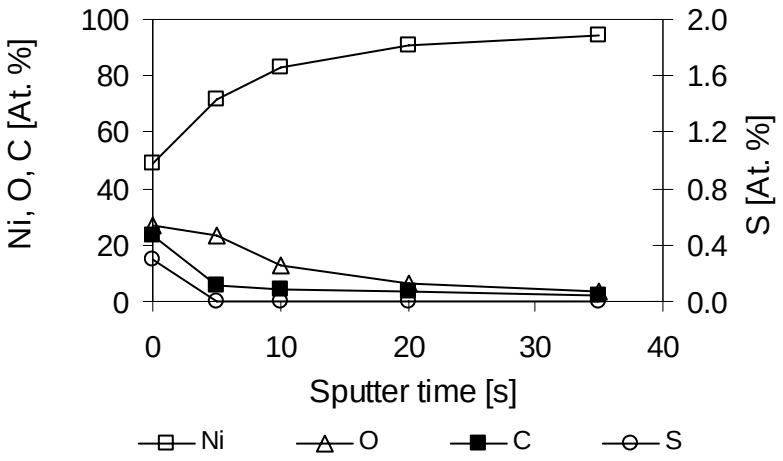

Figure 21. Depth profiling with AES on a Ni wire (reference sample) before the electrochemical experiment. The Ni wire was heat treated for 7 days in 3% H_2O/9% H_2/N_2 at 1000°C, electro polished and ultrasonically cleaned in ethanol for 20 min. Sputtering was performed using 2 keV Ar^+ (45 µA/cm^2).

AES depth profiles were also performed on the Ni wire from electrode 1 after the electrochemical experiment. Depth profiles were performed in four points as seen in Figure 22. Point 1 is in the contact area, point 2 and 4 are from irregularities on the Ni wire (from electro polishing) outside the contact area and point 3 is from homogenous area outside the contact area on the Ni wire.

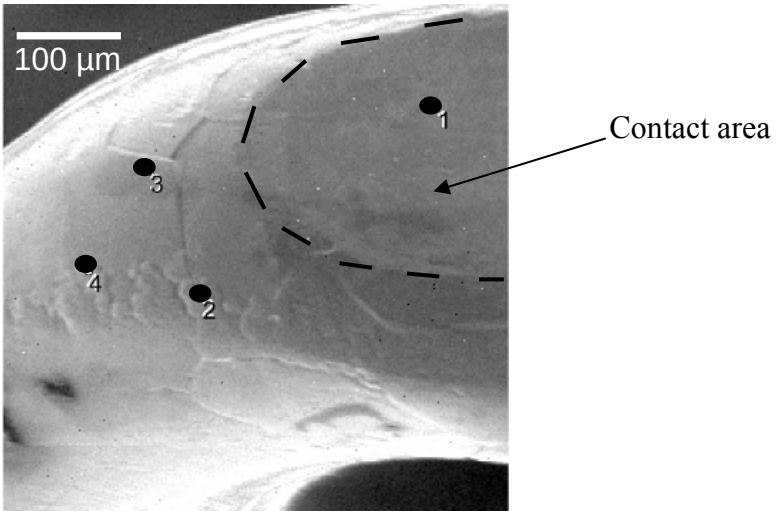

Figure 22. Ni wire from electrode 1 after the electrochemical experiment. The numbers refer to where the AES depth profiles were performed.

AES sputter profile from point 1 and 3 are shown in Figure 23 and Figure 24 respectively. The O, C and Ni depth profiles are similar for the two profiles, but a higher sulfur content is seen point 3. Traces of Si were seen in point 1.

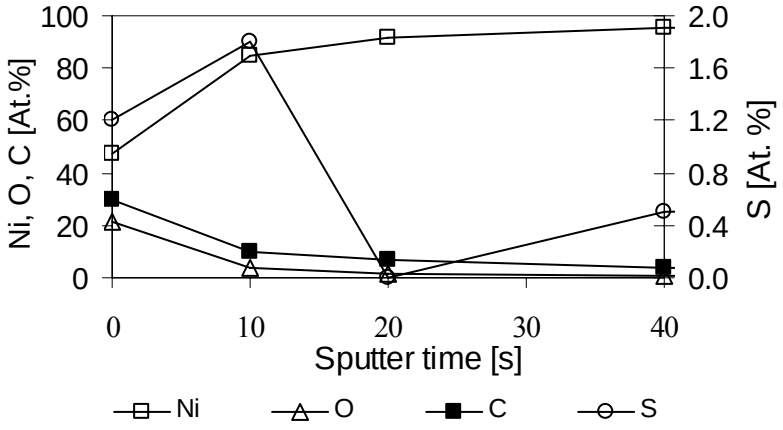

Figure 23. AES depth profile (point 1) of the Ni wire from electrode 1 after the electrochemical experiment. The profile is from the contact area. Sputtering was performed using 2 keV Ar^+ (45 µA/cm^2).

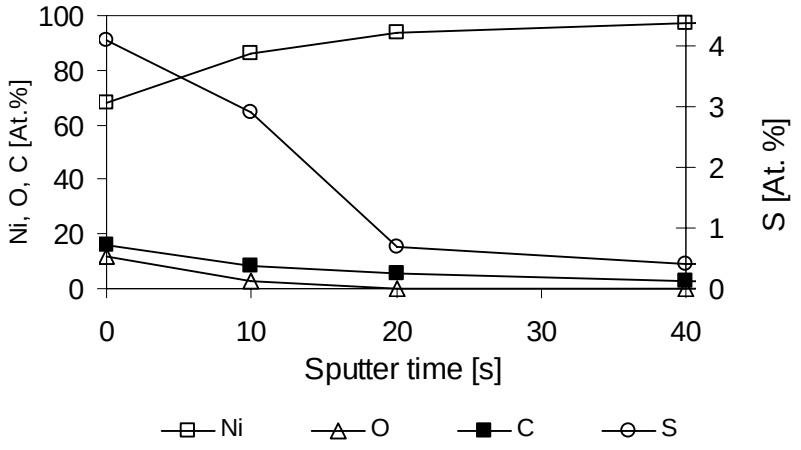

Figure 24. AES depth profile (point 3) of the Ni wire from electrode 1 after the electrochemical experiment. The profile is from outside the contact area. Sputtering was performed using 2 keV Ar^+ (45 μA/cm^2).

The sputter profile from point 2 and 4 differ a lot from point 1 and 3. A sputter profile from point 2 is shown in Figure 25. It is seen that the concentrations of O,C and S do not approach 0 %, hence Ni do not approach 100 %. Even after 10 minutes of sputtering the composition remains almost unchanged. This is seen both for point 2 and 4. Traces of Si are also seen in point 2.

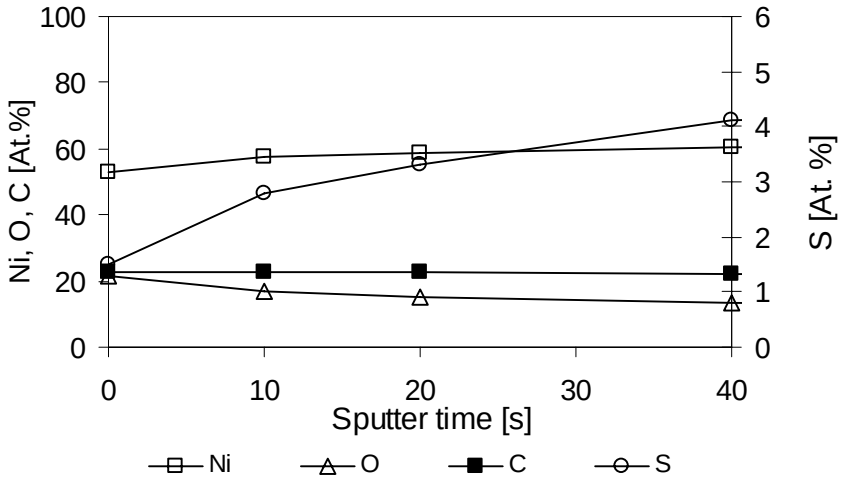

Figure 25. AES depth profile (point 2) of the Ni wire from electrode 1 after the electrochemical experiment. The profile is from outside the contact area on an irregularity that appears after electro polishing. Sputtering was performed using 2 keV Ar^+ (45 μA/cm^2).

4.4.2 Electrochemistry

4.4.2.1 Impedance spectra

R_p and R_s were found from impedance spectroscopy. The area specific resistance ($ASR \equiv R_p \cdot A$) was calculated for comparison between samples with different contact areas (A). The contact area were determined from SEM pictures of the Ni wires after the

electrochemically experiment, see Figure 17 - Figure 19. In Figure 26 are shown impedance spectra of the four electrodes at 745°C (3% H_2O/H_2).

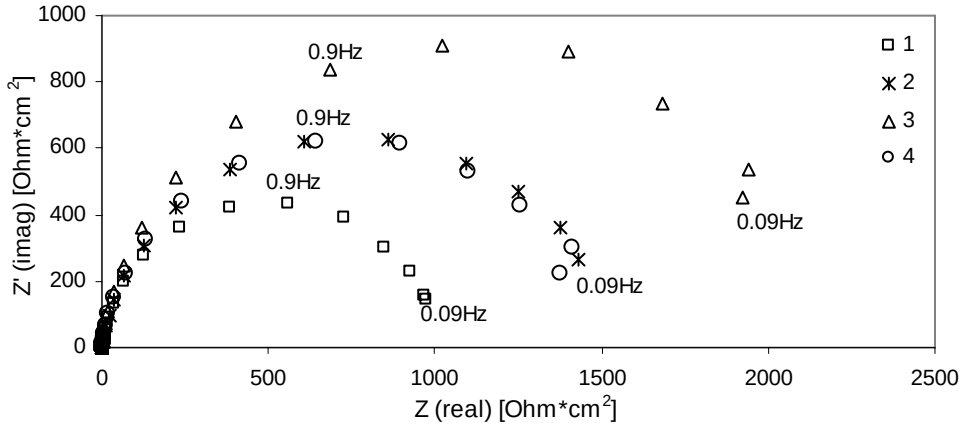

Figure 26. Impedance spectra for the 4 electrodes at 745°C (3%H_2O/H_2).

4.4.2.2 Temperature variation

The variation of R_s with temperature is shown in Figure 27. The activation energies for electrode 1, 2, 3 and 4 were 0.95±0.03, 0.94±0.03, 1.00±0.03 and 0.94±0.03 eV, respectively.

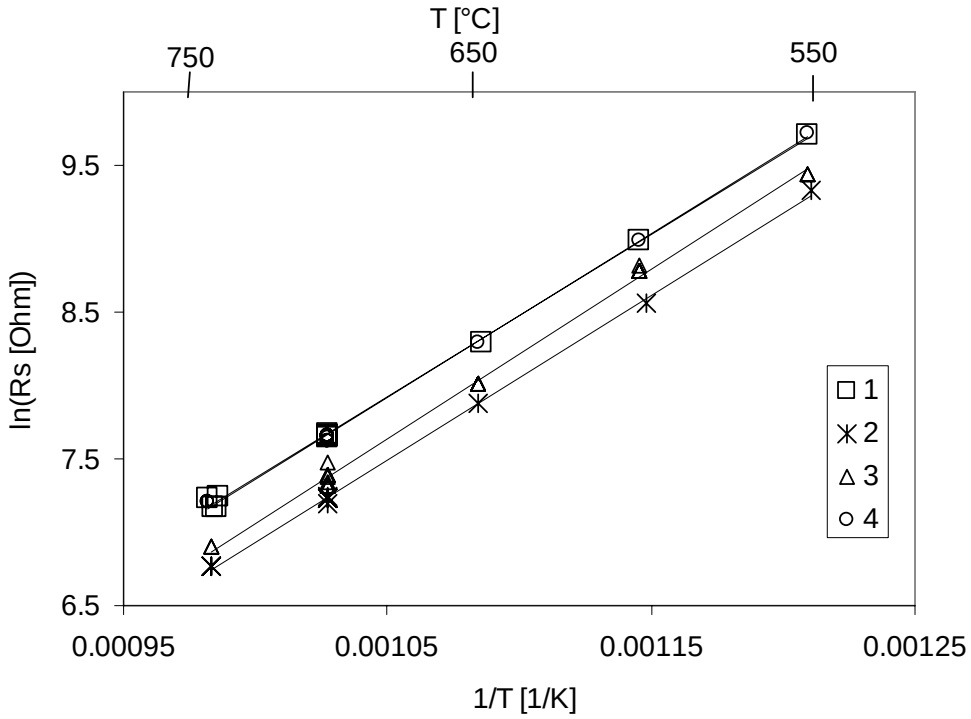

Figure 27. Arrhenius plot for R_s for the four electrodes.

The temperature variation of R_p in 3% H_2O/H_2 for electrode 3 is shown in Figure 28. The activation energy was 0.9 eV. Most measurements were performed on electrode 3. Only few measurements were performed at each temperature on the three other samples. Looking at the variation of R_p in Figure 28 at each temperature it does not seem reasonable to derive

an activation energy if only one measurements are performed at each temperature, hence only the activation energy for sample 3 is derived.

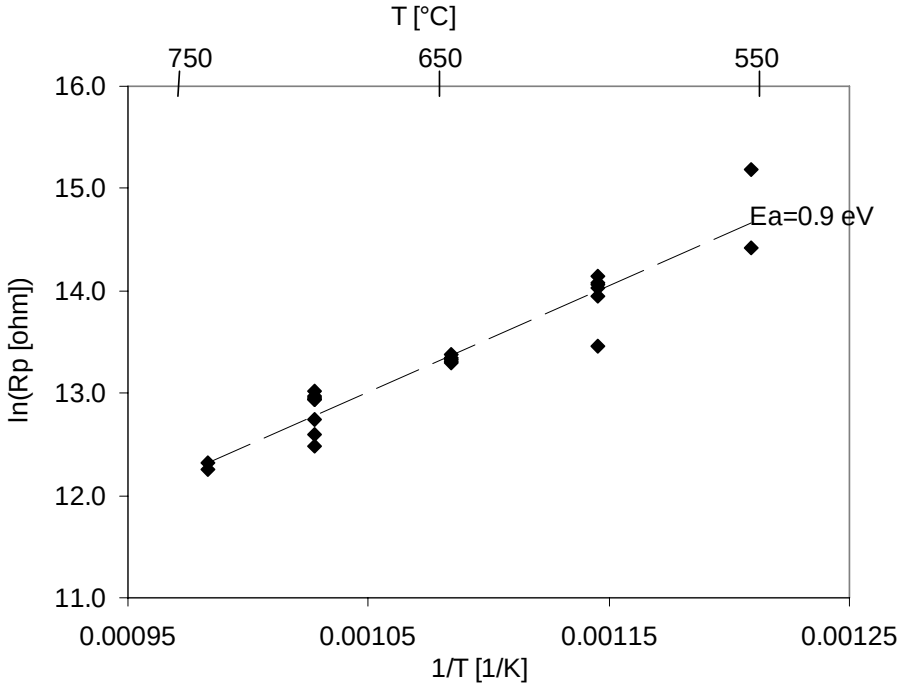

Figure 28. Arrhenius plot for R_p for electrode 3 in 3% H_2O/H_2.

4.4.2.3 Polarization resistance at 700°C

The variations in R_p and R_s for the four electrodes at 700°C are shown in Figure 28 - Figure 32. Measurements were performed in 3% H_2O/H_2 and 0.7% H_2O/H_2. An increase in R_p was seen when changing the atmosphere from 3% H_2O/H_2 to 0.7% H_2O/H_2 while R_s remained constant. In general R_s showed a decreasing tendency with time while no tendency was found on R_p, except for the atmosphere variation.

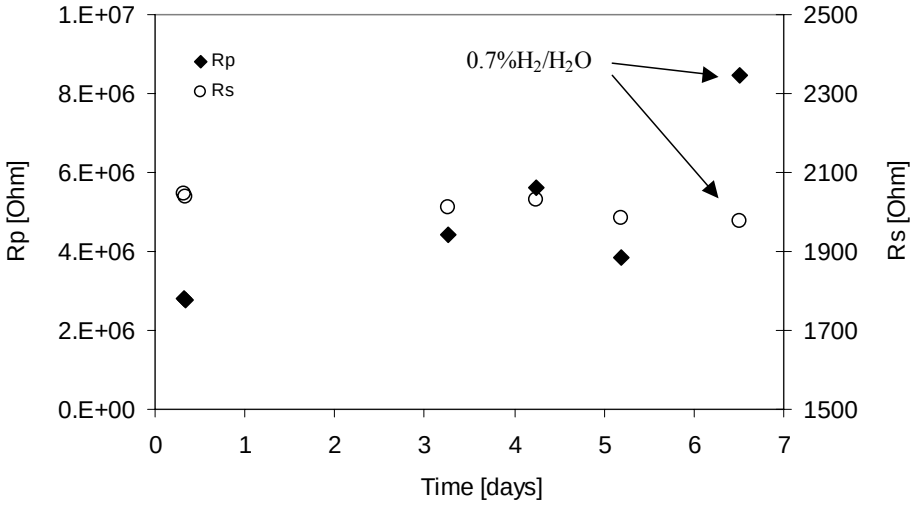

Figure 29. R_p (OCV) and R_s versus time for electrode 1. The measurements were performed in 3% H_2O/H_2 and 0.7% H_2O/H_2.

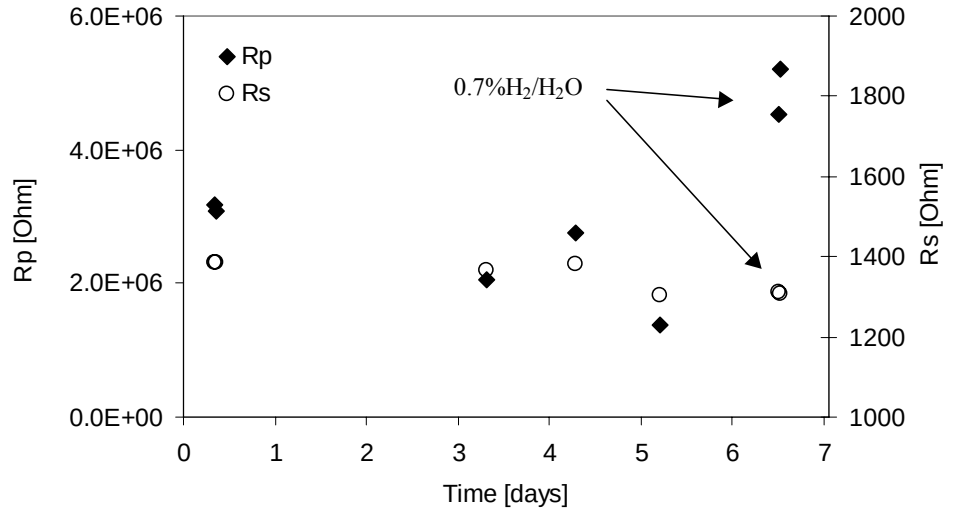

Figure 30. R_p (OCV) and R_s versus time for electrode 2. The measurements were performed in 3% H_2O/H_2 and 0.7% H_2O/H_2.

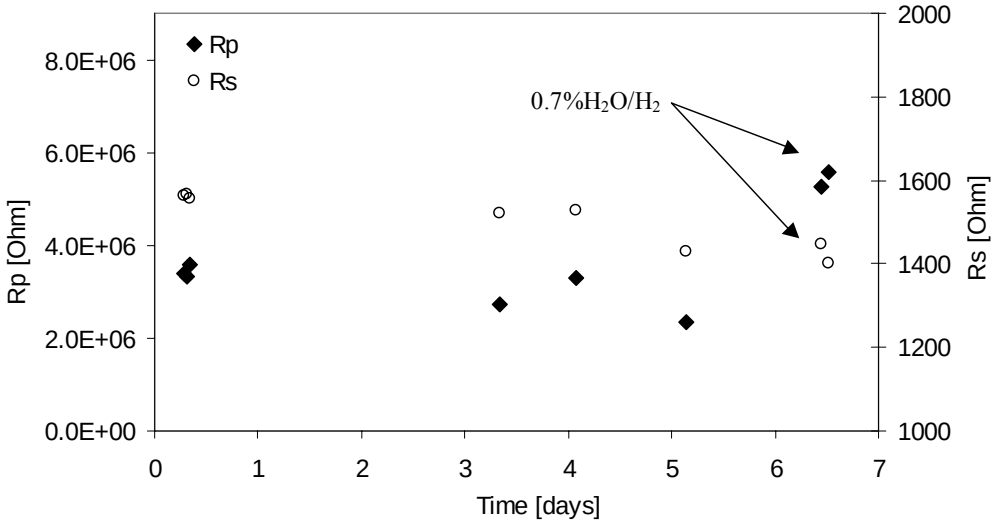

Figure 31. R_p (OCV) and R_s versus time for electrode 3. The measurements were performed in 3% H_2O/H_2 and 0.7% H_2O/H_2. One measurement was also performed under 100 mV anodic polarization.

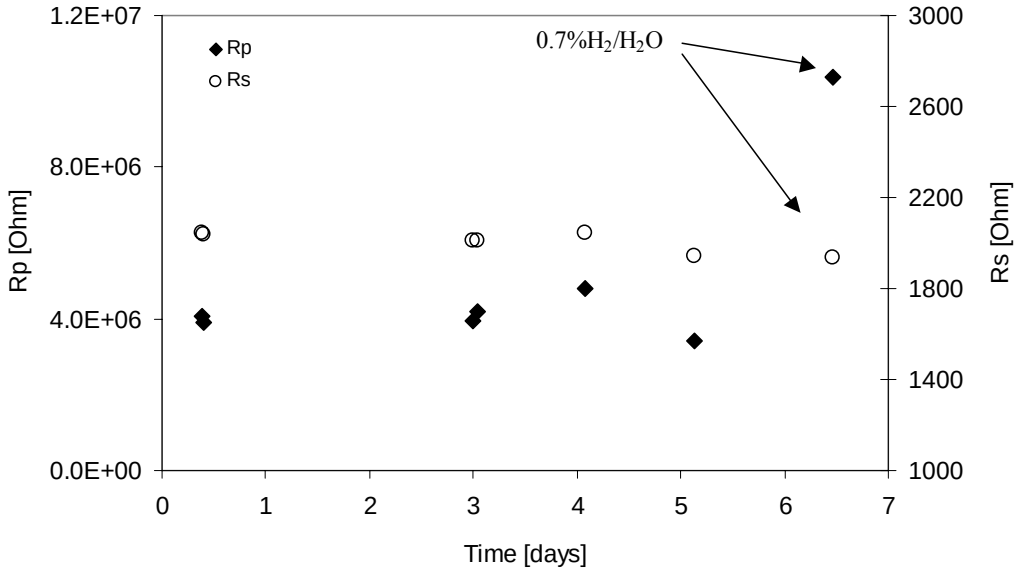

Figure 32. R_p (OCV) and R_s versus time for electrode 4. The measurements were performed in 3% H_2O/H_2 and 0.7% H_2O/H_2.

Data for the four electrodes tested at 700°C are listed in Table 7. The maximum and minimum polarizations resistances for each electrode are listed, hence the maximum and minimum LSR and ASR values are also shown. The length specific resistances (LSR) were calculated by multiplying R_p with the length of the perimeter from the contact area for comparison with the ASR. The area varies a factor ~2 between electrode 1 and 3, this means that the perimeter only changes with the square root of two. Hence different trends could be expected if the polarization resistance is related the length of the TPB (perimeter) or the contact area.

Table 7. Data for the four electrodes at 700°C in 3% H_2O/H_2.

	Electrode 1	Electrode 2	Electrode 3	Electrode 4
Area [mm^2]	0.0579	0.125	0.117	0.0732
Perimeter [mm]	0.868	1.293	1.262	0.992
$R_{p,min}$ [MOhm]	2.8	1.4	2.3	3.4
$R_{p,max}$[MOhm]	5.6	3.1	3.6	4.8
ASR_{min} [kOhm·cm^2]	1.6	2.2	2.7	2.5
ASR_{max} [kOhm·cm^2]	3.2	4.0	4.2	3.5
LSR_{min} [kOhm·cm]	243	181	290	337
LSR_{max} [kOhm·cm]	486	401	454	476
$R_{s,min}$ [Ohm]	1983	1302	1429	1945
$R_{s,max}$ [Ohm]	2046	1387	1568	2046

4.5 Discussion

4.5.1 Surface analysis

4.5.1.1 SEM images of the Ni wire

The Ni wires used for the electrodes appeared equally smooth on the surface before the electrochemistry experiment (see Figure 16). After the electrochemical experiment the Ni

wires from sample 2 and 4 showed structure while the Ni wires from electrode 1 and 3 were smooth and uniform as attempted. Though the Ni wires from electrode 2 and 4 did not have a well defined and uniform smooth contact area the polarization resistance did not deviate more than between electrode 1 and 3, see Table 7. It is not clear why the different structures in the Ni contact area for sample 2 and 4 are formed.

4.5.1.2 XPS on the electrolyte

After removal of the Ni wire from the electrolyte XPS was performed on the electrolyte. The XPS analyzes an area of ~1cm^2. This means that the signals from the contact area (~0.1 mm^2), which might have a different chemical composition, are negligible, i.e. the chemical composition outside the contact area is determined. The Si and Na that where detected on the YSZ single crystal are known to segregate to the surface from the bulk [17,18]. It is believed that the chemical composition of the other electrolytes is similar to the electrolyte from electrode 1.

4.5.1.3 AES on the Ni wire

Prior to the electrochemical experiment only the expected impurity elements (oxygen, carbon and sulfur) could be detected on a heat treated and electro polished Ni wire (reference sample). A small amount of sulfur (0.06 ppm, see Table 6) is present in the Ni wire but it is under the detection limit for the AES unless it is segregated to the surface. The expected impurities are present in the atmosphere and are adsorbed onto the Ni wire while exposed to the atmosphere. The expected impurities are also seen for the electrochemically tested Ni wires as they are exposed to the atmosphere while transporting them to the AES apparatus. A noteworthy difference is that the sulfur content outside the contact area is higher on the Ni wire after the electrochemical experiment i.e. sulfur is either segregating from the Ni or is present in the gas phase. A poisoning effect of sulfur is known to increase the polarization resistance [1]. The chemical composition of the irregularities does not change after long time (10 min) of sputtering. The reason for this might be that the irregularities are porous and have a higher surface roughness. This is known to give shadow affect which limits the depth resolution [19]. The traces of Si seen in the contact area can be cross over contamination from the electrolyte. The traces of Si seen on the irregularities are more difficult to explain as Si is not seen on the area outside the contact area were the irregularities are located.

4.5.2 Electrochemistry

4.5.2.1 Reproducibility of measurements

As most measurements were performed at 700°C (3% H_2O/H_2) the reproducibility is evaluated at these conditions. R_s decreases slightly for all four samples during the experiment due to creep of the Ni wire. R_s is related to the size of the contact area through: $R_S = \frac{1}{4 \cdot \sigma \cdot r}$, where r is the radius of the contact area and σ is the conductivity of the electrolyte. The change in R_s is small compared to the change of R_p and is therefore not the explanation for the variation in ARS. The variation $\left(\frac{ASR_{max}}{ASR_{min}} \right)$ in ASR for electrode 1, 2, 3 and 4 are 2.0, 1.8, 1.5 and 1.4 respectively. The maximum variation between the electrodes (electrode 1 and 3) was 2.6. This variation is low compared to that accounted for in the literature, which is up to factor of ~200. The reason for the better reproducibility might be the high purity materials used for the electrodes and the effort on polishing and

cleaning the YSZ and Ni. Also, the fact that single crystals were used instead of polycrystalline electrolytes might be important for the reproducibility.
When comparing the ASR and LSR no trend was evident, i.e. it is not obvious if the polarizations resistance relates to the area or the length of the perimeter (TPB). In pattern electrode experiment where it is possible to change the ratio between area and length orders of magnitude is has been argued that the resistances correlates to the length of the TPB [20]. In the presence point electrode experiments the variation of the ratio between the area and perimeter is little. This means that this relation drown in the variation seen on the polarization resistance. That is to say that it does not matter if the LSR or ASR values are used for comparison the same trends will be observed.

4.5.2.2 Variation in atmosphere and polarization

For all four electrodes the polarization resistance increased when the water content was lowered from 3 to 0.7 %. The increase for electrode 1, 2, 3 and 4 was a factor of ~4, ~3, ~3 and ~3 respectively. This water effect is known from the literature [1].

4.6 Conclusion

The chemical analysis of the YSZ and Ni surfaces showed an increase of the amount of impurities after the electrochemical experiment. The Si and Na detected on the YSZ surface are probably segregated from bulk. An increase in the S content on the Ni surface was detected. It is not known whether the S originates from the Ni or the surroundings. The reproducibility of the point electrode measurements was within a factor 2.6 using the polarization resistance at OCV as a characteristic parameter. This variation is small compared to values in the literature. The small variation might be due to the effort of controlling the impurities and polishing and cleaning of the Ni and YSZ.

5 Atmosphere variations at the H_2/H_2O/Ni/YSZ point electrode at 700°C[1]

5.1 Abstract

Impedance measurements and potential sweeps were performed on a model system of the SOFC anode. The measurements were performed in various gas mixtures of H_2, H_2O and N_2 at 700°C over a period of ~40 days. The electrode was made by pressing a bent Ni wire against a single crystal of YSZ ($(ZrO_2)_{0.87}(Y_2O_3)_{0.13}$), which here after is referred to as a point electrode.
The polarization resistance at OCV decreased with increasing water content in the region 0.08-3% H_2O. In the region 3-20% H_2O no dependence was seen. No dependence on the hydrogen pressure or electrode potential was evident in the investigated atmospheres. From the potential sweeps a higher anodic current was seen when the water content was increased even though the hydrogen content was decreased.
After the electrochemical experiment SEM (scanning electron microscopy) images of the Ni wire was performed to determine the size and morphology of the contact area on the Ni side. XPS (X-ray photoelectron spectroscopy) was performed on the YSZ single crystals, which showed that the surface was contaminated with Si, Al and Na after the electrochemical experiment.

5.2 Introduction

It is of interest to know how the hydrogen partial pressure, water partial pressure and electrode potential influence the kinetics of the H_2/H_2O/Ni/YSZ electrode as this can provide information that can lead to improvement of the electrode. The reactions under investigation at the Ni/YSZ electrode are the oxidation of hydrogen and the reduction of water, see (10) and (11) respectively.

$$H_{2(g)} + O^{2-}_{(YSZ)} \rightarrow H_2O_{(g)} + 2e^-_{(Ni)} \qquad (Anodic\ current) \qquad (10)$$

$$H_2O_{(g)} + 2e^-_{(Ni)} \rightarrow H_{2(g)} + O^{2-}_{(YSZ)} \qquad (Cathodic\ current) \qquad (11)$$

Reaction (10) and (11) dominate when the cell is operated as a fuel cell (SOFC) and as an electrolyzer cell (SOEC, solid oxide electrolyzer cell), respectively.

The real SOFC anode is a porous Ni/YSZ composite in order to optimize mass transport and charge transfer near or at the three phase boundary (TPB) where the Ni, YSZ and fuel gas (e.g. $H_{2(g)}$) meet. A point electrode is used here as a model system because: 1) It provides a well defined length of the TPB and 2) the easiness of investigating the Ni/YSZ interface after an electrochemical experiment and 3) to obtain a more well defined electrode potential compared to the composite anode. In a cermet anode the reaction takes place over a distance of ~10 µm from the electrolyte. This causes a gradual potential drop through the cermet anode due to the resistance of the YSZ composite network. This means that the

[1]Helge Danneskiold-Samsøe from the Technical University of Denmark participated in the measurements presented in this chapter. The work is a part of Helge Danneskiold-Samsøe's midterm project. The measurements were performed in January 2004.

reactions in (10) and (11) take place at different potentials at the same time, which makes it more difficult to analyze kinetic data.

5.3 Experimental

5.3.1 Materials and sample preparation

As the working electrode a nickel wire (Ø=0.5 mm) from Alfa Aesar (Puratronic®) was used. The stated purity was 99.999 % (metal basis). Prior to the electrochemical experiment the Ni wire was annealed in 3% H_2O/9% H_2/N_2 (1000°C, 7 days) and electro polished.
A single crystal of YSZ $(ZrO_2)_{0.87}(Y_2O_3)_{0.13}$ with the dimensions 10x10x3 mm^3 was used as electrolyte. The single crystal was purchased at MTI Corporation (www.mticrystal.com). The purity is stated as 99.99 % and the surface orientation is [100]. The single crystal was polished with 6, 3, 1 and ¼ µm diamond suspension. For the final polishing an acidic suspension of alumina particles (0.02 µm, OP-AA suspension, Struers) was used. After polishing and cleaning of both the Ni wire and the electrolyte in an ultrasonic bath with ethanol, they were handled in a laminar air flow system while wearing gloves, mask and hairnet.
Platinum was used as counter and reference electrodes and were painted on the electrolyte using Pt-paste (Degussa, 308A). As current collector for the counter and the reference electrodes Pt meshes were used in order to allow gas transport to the electrodes. A mesh consists of 0.1 mm Pt wires with a mask size of 0.5x0.5 mm, the thickness of the mesh is 0.3 mm.

5.3.2 Electrochemical setup

A frequency response analyzer (Solartron 1255b) in combination with a potentiostat (Solartron 1287) were used to measure the impedance spectra and the potential sweeps in a 3-electrode setup (4-wires, one atmosphere). The impedance spectra were performed using a 30 mV signal at OCV.
Figure 33 shows a sketch of the 3-electrode setup and a photo of the Ni wire on top of the electrolyte. On top of the alumina tube a weight of copper (315 g) is arranged to press the Ni wire against the electrolyte.

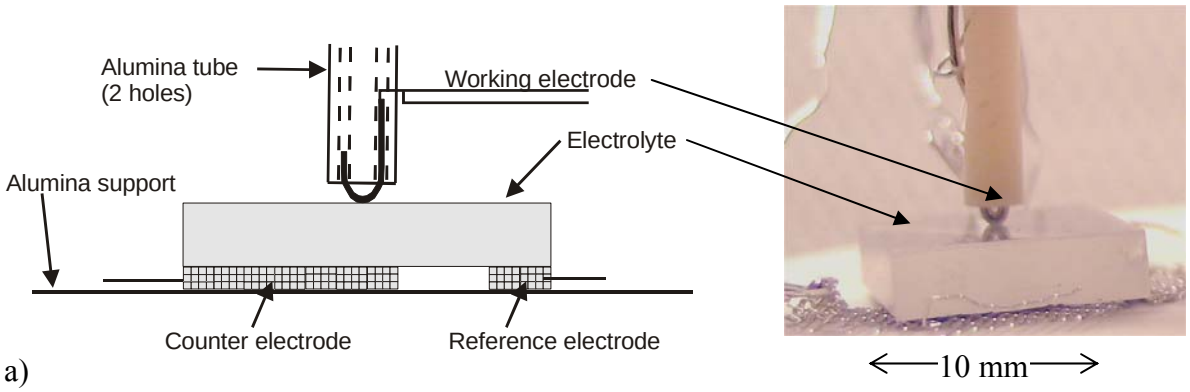

Figure 33. a) Sketch of the 3-electrode setup. Two leads are connected to the working electrode (Ni wire). Pt is used as counter and reference electrodes. Two Pt meshes collect the current and allow for gas transport to the electrodes. b) Photo of the electrode used in this work.

The electrode was operated for ~40 days in various gas compositions. The gas compositions used are listed in the order that they were used in Table 8. The pressure in the system was 1 atm at all times. The gas compositions are given in volume percent. The gas

compositions were balanced with nitrogen. Measurement was performed 2-3 days at each gas composition.

Table 8. Gas compositions used for the electrochemical measurements and the corresponding EMF vs. air at 700°C. The compositions are numbered in the order that they were used. The gas compositions were balanced with nitrogen.

No.	H_2 [%]	H_2O [%]	EMF vs. air at 700°C
1	96.9	3.1	1117
2	8.7	2.9	1019
3	97.1	2.9	1119
4	2.4	2.9	965
5	2.5	0.75	1023
6	8.9	0.7	1080
7	2.5	0.08	1120
8	99.9	0.1	1259
9	99.3	0.72	1179
10	96.9	3.1	1117
11	2.0	19.7	876
12	84.8	15.2	1045
13	7.6	15.2	943
14	89.5	10.5	1063
15	92.3	7.7	1077
16	51.0	7.3	1054

An overview of the gas mixtures used and the corresponding EMF are given in Figure 34.

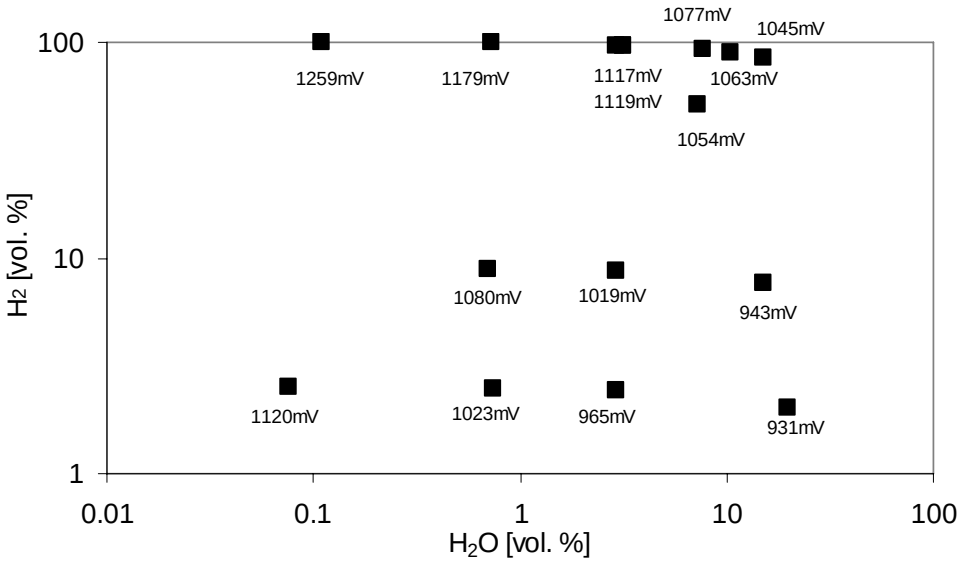

Figure 34. Gas compositions and the corresponding EMF vs. air at 700°C. The total pressure is 1 atm. The gas compositions are balanced with nitrogen.

The gas compositions were made by mixing H_2 and N_2 and humidify or partially humidify the mixture in water. The EMF was measured using an oxygen sensor. The sensor was not working during the entire experiment, but the first and last gas mixture were measured and they were in good agreement with the expected values, i.e. the system was gas tight. The

EMF values are calculated from the water and hydrogen pressures. The water pressure is known from the saturation temperature and is calculated from (12)

$$p_{H_2O(g)} = 10^{A-\left(\frac{B}{T+C}\right)}, \tag{12}$$

where T is the saturation temperature in Kelvin and $P_{H2O(g)}$ is the vapor pressure of water in bar. The relevant constants for (12) are given in Table 9.

Table 9. Constants for calculating the vapor pressure of water [21].

Temperature [K]	Temperature [°C]	A	B	C
273-303	0-30	5.40221	1838.675	-31.737
304-333	31-60	5.20389	1733.926	-39.485
334-363	32-90	5.07680	1659.793	-45.854

From the pH_2O/pH_2 ratio and the equilibrium shown in (13) the partial pressure of oxygen can be calculated. The equilibrium constant for (13) is given in (14) [22].

$$H_{2(g)} + {}^{1}\!/_{2} O_{2(g)} \Leftrightarrow H_2O_{(g)} \tag{13}$$

$$K = \frac{pH_2O_{(g)}}{pH_{2(g)} \cdot \sqrt{pO_{2(g)}}} = 10^{-\left(2.958-\frac{13022}{T}\right)} \tag{14}$$

The temperature T is in Kelvin.
Using the Nernst equation for an oxygen concentration cell the EMF can be calculated from

$$EMF = \frac{R \cdot T}{n \cdot F} \cdot ln\left(\frac{pO_{2,anode}}{pO_{2,cathode}}\right), \tag{15}$$

where n= 4, R is the gas constant, T is the temperature in Kelvin and F is Faradays constant. Air is used as reference gas, i.e. $pO_{2,cathode}$=0.21 atm. In the following all EMF values refer to air and a temperature of 700°C.

5.3.3 Surface characterization techniques

SEM was performed using a Jeol JSM-5310LV. An SEM image was used to determine the Ni/YSZ contact area from the Ni wire. Backscattered electrons were used to produce the images.
XPS was performed using a Sage 100 from SPECS with a non-monochromated Mg-Kα X-ray source and a take-off angle of 90°. Elements in the sample were determined from the full spectrum using a step size of 0.5 eV and a detector pass energy of 100 eV. Narrow scans with a step size 0.2 eV and a detector pass energy of 23 eV were performed to get a better resolution. An electron floodgun was used to limit charging. XPS was used for analysis of the electrolyte surface.

5.4 Results

5.4.1 Surface analysis

An XPS measurement was performed on a polished YSZ reference sample identical to the one used in the electrochemical measurements. The XPS spectra showed carbon as the only impurity. When a sample has been exposed to the atmosphere carbon is always seen due adsorption of organic species. After the electrochemical experiment the following impurities were found, Si/Zr=0.16, Al/Zr=0.02 and Na/Zr=0.05. Carbon was also detected on the electrolyte surface after the electrochemical experiment as the sample is exposed to the atmosphere when transporting it to the XPS apparatus.

SEM images of the Ni wire before and after the electrochemical experiment are shown in Figure 35. The contact area after the electrochemical experiment is elliptic.

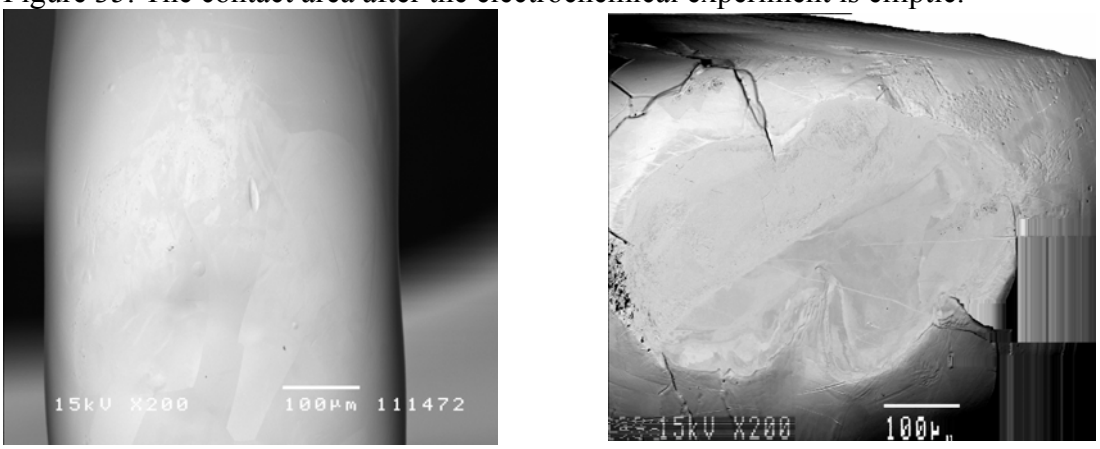

Figure 35. a) SEM image of the Ni wire before the electrochemical experiment. b) SEM image of the elliptic contact area on the Ni wire after the electrochemical experiment. α=285 µm, β=158 µm, area=0.141 mm^2, perimeter=1.42 mm, where 2α and 2β are the length of the long and short axis of the elliptic contact area.

5.4.2 Electrochemistry

5.4.2.1 Impedance spectra

Impedance spectra for the gas composition that showed the highest (H_2=2.5% and H_2O=0.08%) and lowest (H_2=2.4% and H_2O=2.9%) polarization resistance are shown in Figure 36. The highest polarization resistance is seen for the gas composition with the lowest water content.

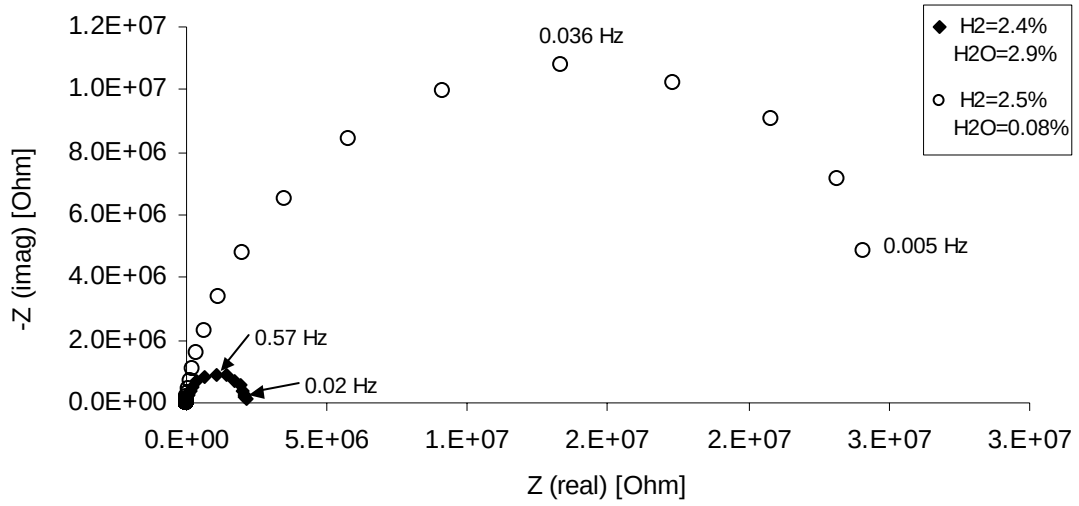

Figure 36. Impedance spectra at 700°C in the gas compositions that showed the highest (H_2=2.5% and H_2O=0.08%) and lowest (H_2=2.4% and H_2O=2.9%) polarization resistance.

5.4.2.2 Atmosphere dependence on R_p

In Figure 37 the area specific resistances at the various atmospheres are shown. The measurements are performed in the order in which they are shown. Several measurements were performed at each atmosphere and the average value was used in the plot. The contact area between the Ni and YSZ wire increases during the experiment due to creep of the Ni wire, this is seen as a decrease in the R_s value. The R_s value is related to the radius of the contact area through[2]

$$R_S = \frac{1}{4 \cdot \sigma \cdot r}, \tag{16}$$

where σ is the ionic conductivity and r is the radius of a circle. In our case the contact area is elliptic and an equivalent radius is used, i.e. $r = \sqrt{\alpha \cdot \beta}$, where 2α and 2β are the length of the long and short axis of the elliptic contact area. The area specific resistance (ASR) is calculated ($ASR \equiv R_p \cdot A$) for comparison between the measurements as the contact area (A) increases during the experiment. The contact area after the electrochemical experiment is determined by SEM. As this contact area corresponds to the R_s value from the end of the experiment the area throughout the experiment is calibrated according to this. The increase in contact area during the experiment was ~40%.

[2] In this relation an infinitely thick electrolyte and a circular area is assumed. A relation [23] which matches our samples (not infinitely thick and elliptic contact area) deviates less than 5 % from (19) and as 5 % is a small value in this context the simple approximation is used due to the ease of computation.

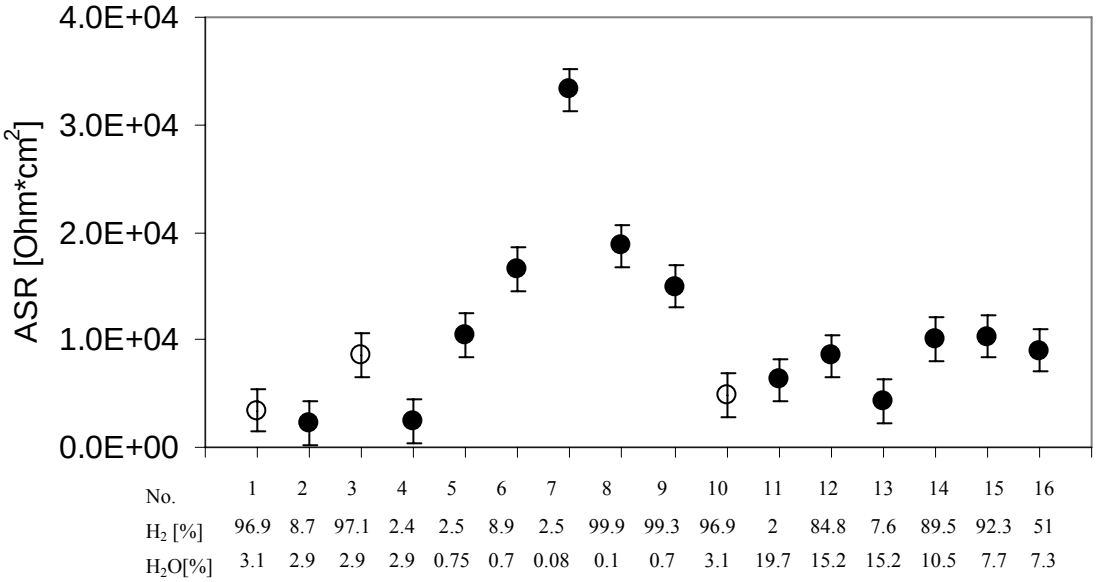

Figure 37. ASR for the series of measurement at 700°C. The measurements were performed in the order in which they are numbered.

The open symbols represent the same atmosphere (3% H_2O/H_2). Three measurements were performed in this atmosphere at different stages in the measurements series in order to test the reproducibility. The error bars are determined from these three measurements so that the three measurements are within the error bars.

ASR as a function of the water content is plotted in Figure 38.

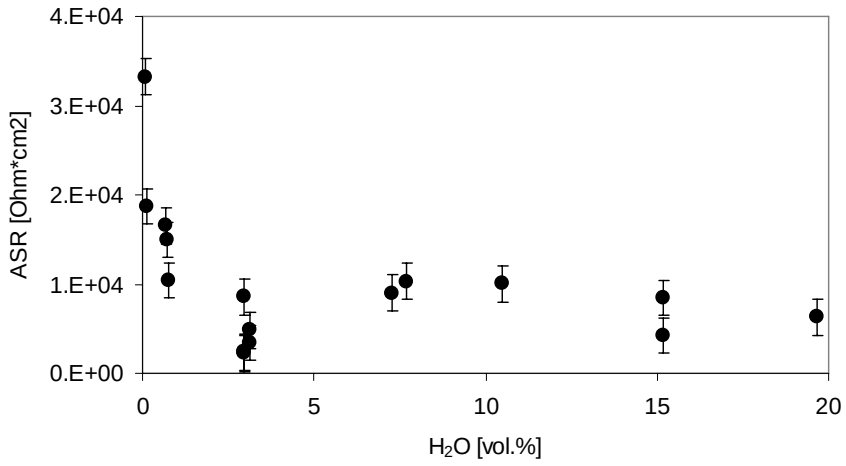

Figure 38. ASR as a function of the water content at 700°C.

ASR as a function of the hydrogen content and EMF are plotted in Figure 39 and Figure 40, respectively. As the water content has an obvious effect on ASR the measurements with the same water content have the same symbols in the figures.

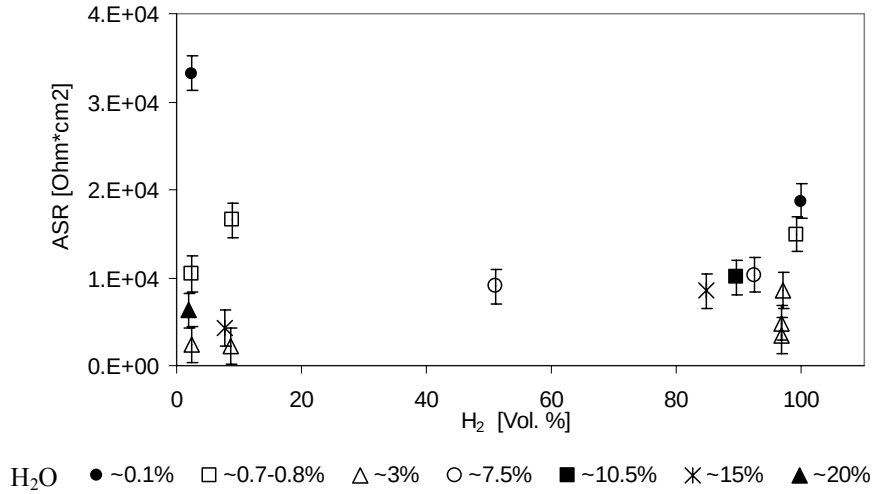

Figure 39. ASR as a function of the hydrogen content at 700°C.

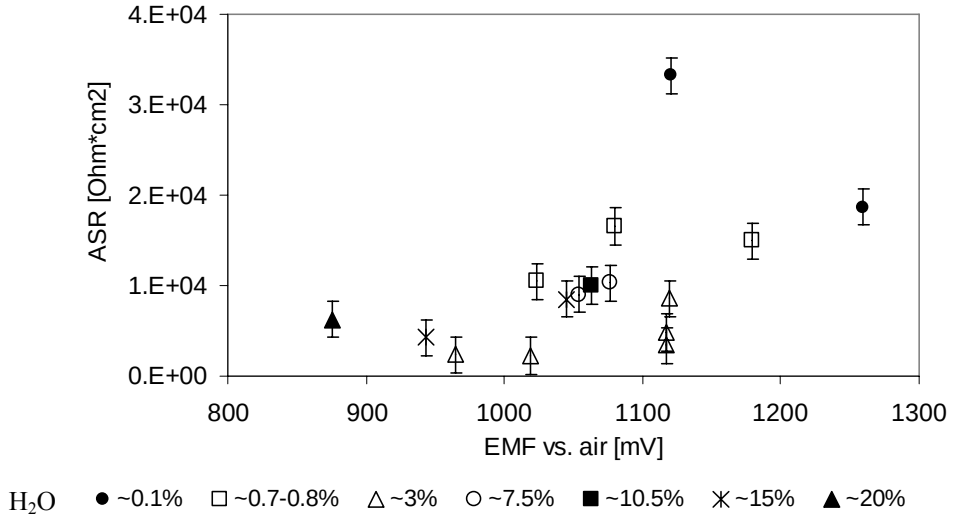

Figure 40. ASR as a function of the EMF vs. air at 700°C.

5.4.2.3 Potential sweeps

Potential sweeps were performed at selected atmospheres. The sweeps are corrected for the series resistance, which was found from the impedance measurements. The three following sweeps shows that there is a large difference between the anodic reaction (oxidation of hydrogen) and cathodic reaction (reduction of water). Also, reduction of other species than water is seen at about -1200 mV. According to the thermodynamics Ni start to oxidize at about –760 mV vs. air at 700°C, but no special features were seen when crossing this limit.

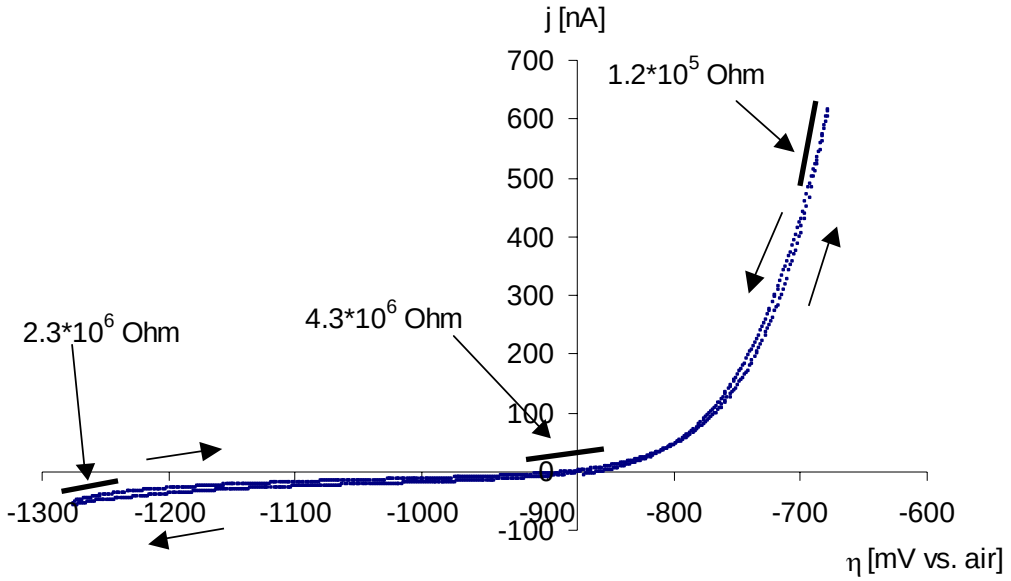

Figure 41. Potential sweep (5 mV/s) at 700°C (H_2 = 2%, H_2O= 19.7%, EMF=-876 mV vs. air). Sweep direction: -876 → -1276 → -676 → -876 mV vs. air. The solid lines in the figure are representing the polarization resistance (=the reciprocal slope).

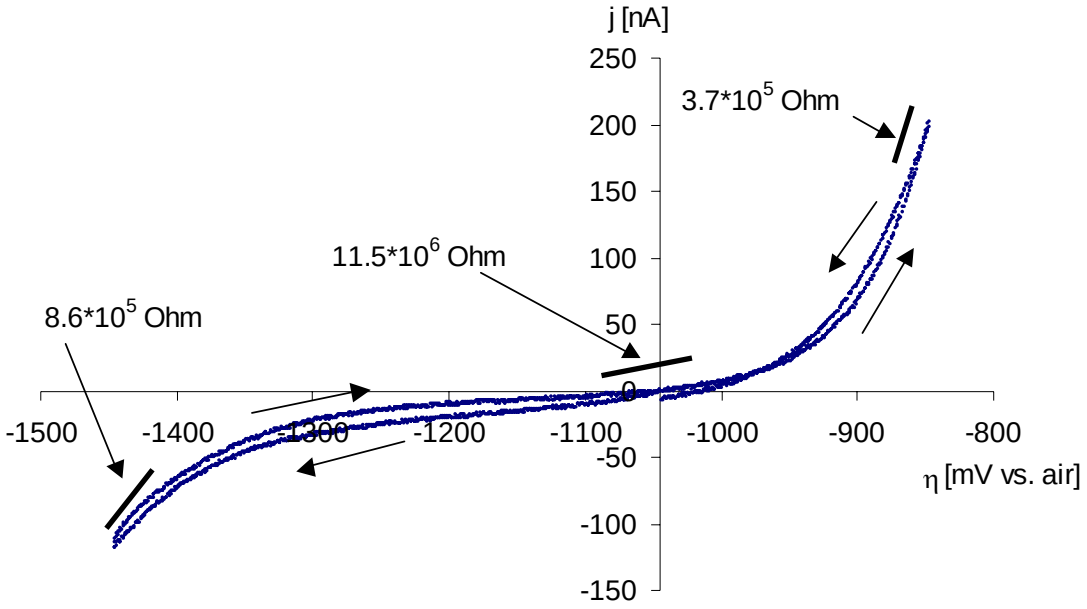

Figure 42. Potential sweep (5 mV/s) at 700°C (H_2= 84.8%, H_2O= 15.2%, EFM=-1045 mV vs. air). Sweep direction: -1045 → -1445 → -845 → -1045 mV vs. air. The solid lines in the figure are representing the polarization resistance (=the reciprocal slope).

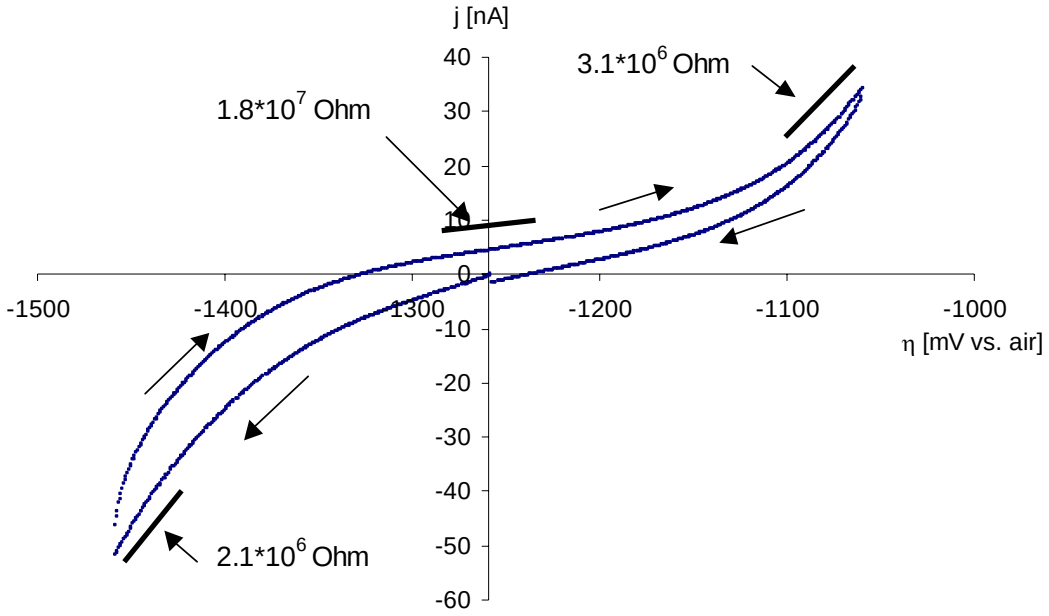

Figure 43. Potential sweep (5 mV/s) at 700°C (H_2= 99.9%, H_2O= 0.1%, EMF=-1259 mV vs. air). Sweep direction: -1259 → -1459 → -1059 → -1259 mV vs. air. The solid lines in the figure are representing the polarization resistance (=the reciprocal slope).

5.5 Discussion

5.5.1 Surface analysis

After removal of the Ni wire from the electrolyte XPS was performed on the electrolyte. The XPS analyzes an area of ~1cm^2. This means that the signals from the contact area (~0.1 mm^2) are negligible, i.e. the chemical composition outside the contact area is determined. The elements (Si, Al and Na) that were detected on the electrolyte are known to segregate to the surface from the bulk of YSZ [17,18].
The contact area on the Ni side was smooth as intended in order to obtain a well defined contact area. The smoothness was evaluated from the SEM images.

5.5.2 Electrochemistry

5.5.2.1 Impedance spectra

For gas composition 2 and 4 the spectra can be fitted well to one depressed semicircle if the capacitance of the setup is disregarded (see section 3.4). For the other atmospheres two or three depressed semicircles is needed to produce a good fit. One semicircle indicates that there may be only one significant rate determining step etc.

5.5.2.2 Atmosphere dependence

The ASR decreases with increasing water content in the region from 0.08 to 3% after which no evident dependence is observed. The strong dependence below 3% H_2O is in agreement with the literature [24]. From the measurements at the lowest water content in Figure 39 and Figure 40 it looks like that there is a hydrogen or EMF dependence. This dependence is however ascribed to the small different in water content of 0.08 and 0.11% H_2O as the dependence is very strong at such low water partial pressures. No evident dependence on hydrogen content or EMF was observed.

The three measurements that where performed in the same atmosphere (H_2=~97% and H_2O=~3%) at different stages in the measurement series is an indicator of the reproducibility of the electrode measurement (R_p). The deviation between the smallest and largest value was a factor of ~2.5.

5.5.2.3 Potential sweeps

The resistance derived from the potential sweeps at OCV should be the same as R_p derived from the impedance measurements for the same atmosphere. The R_p derived from potential sweeps and impedance spectroscopy are listed in Table 10. The deviation is given as the ratio between the largest and lowest R_p.

Table 10. Overview of the potential sweep data and comparison between the Rp derived from impedance spectroscopy and potential sweep at OCV.

Gas	11	12	8
H_2 [%]	2	85	99.9
H_2O [%]	19.7	15.2	0.1
EMF vs. air [mV]	-876	-1045	-1259
$R_{p,OCV\ (impedance)}$	$5.2 \cdot 10^6$	$6.8 \cdot 10^6$	$15.7 \cdot 10^6$
$R_{p,OCV\ (potential\ sweep)}$	$4.3 \cdot 10^6$	$11.5 \cdot 10^6$	$18.4 \cdot 10^6$
Ratio ($R_{p,max}/R_{p,min}$)	1.2	1.7	1.2
I at η=+200 mV [$\mu A/cm^2$]	425	142	25

The deviation between R_p derived from potential sweeps and impedance are within the reproducibility found in chapter 4, i.e. the variation is to be expected.
At anodic overpotentials the anodic current are increasing non-linearly. From Table 10 it is seen that the current at η=+200 mV increases with the water content even though the hydrogen content decreases. The water effect at η=+200 mV is obvious in the range 0.1 – 20 %, whereas the water effect seen at OCV (Figure 38) only is visible from 0.08 – 3 % H_2O. The sweep performed in Figure 41 crosses the thermodynamic potential for oxidation of Ni, which is about –760 mV. No characteristics are seen in the sweep at the Ni/NiO potential. An explanation for this can be that a sweep rate of 5 mV/s is too fast for the oxidation to give a considerable contribution to the anodic current or that the oxidation currents drowns in the oxidation current of hydrogen.
At cathodic overpotential there seems to be two trends. When the overpotential is between OCV and -1200 mV a limiting current less than $|-35\ \mu A/cm^2|$ is observed. The limiting current did not depend on the water concentration. At cathodic overpotentials lover than ~ -1200 mV the cathodic current starts to increase non-linearly. It is believed that at ~ -1200 mV the reduction of YSZ and/or impurities begins. From thermodynamic data the reduction of YSZ should start at ~ -2000 mV but electrochemical reduction is observed at as high as ~-700 mV [25]. In chapter 7 it is shown that a strong cathodic overpotential lowers the polarization resistance remarkably. This is presumably due to reduction of YSZ/impurities. The lowering in polarization resistance is not seen here presumably because the amount of current, in coulombs, used for reduction was 3 orders of magnitude lower than the experiment described in chapter 7. The number of coulombs reduced were in all cases $\sim 10^{-3} C/cm^2$. If the zirconia is completely reduced to zirconium this would correspond to a depth of $\sim 10^{-10}$ m of zirconium metal under the Ni wire. This indicates that not more than one atomic layer would be reduced and that might be too little to obtain a lowering of the polarization resistance.

5.6 Conclusion

Segregated impurities (Si, Al and Na) were detected on the surface of the YSZ after the electrochemical experiment. The polarization resistance at OCV decreases with increasing water content in the range from ~0.1-3% H_2O. No evident dependence on H_2 and electrode potential was observed. The anodic reaction (oxidation of hydrogen) increases non-linearly as a function of the anodic overpotential. Also, an increasing water content enhances the anodic current in the whole range tested (0.1-20% H_2O). The cathodic reaction seems to have a limiting current independent of the water content. It is believed that the reduction of YSZ and/or impurities are seen at ~ -1200 mV.

6 High purity H_2/H_2O/Ni/SZ electrodes at 500°C[3]

6.1 Abstract

Segregated impurities seem to be detrimental for the performance of a SOFC (solid oxide fuel cell) anode. In this study the performance of a model system of the SOFC anode was measured. It is sought to minimize the segregation of impurities by using high purity materials at relatively low temperature to prevent fast segregation. Bent Ni wires (99.999 %) were pressed against polished single crystals of stabilized zirconia (SZ), thereby forming point electrodes. Four single crystals stabilized with: 10, 13 and 18 mol% yttria and one stabilized with 6 mol% scandia and 4 mol% yttria were used as electrolytes. The polarization resistances (R_p) at OCV (open circuit voltage) of the electrodes were measured from 400-500°C in mixtures of H_2/H_2O over 46 days. The R_p for all electrodes increased significantly during the first 10-20 days at 500°C after which they became relatively constant. An effect on the R_p of the different electrolytes was not evident. The Ni wires and single crystals were analyzed before and after the electrochemical experiment using SEM (scanning electron microscopy) to study morphology, and surface sensitive techniques for determination of composition and distribution of elements. After the electrochemical experiment the analysis showed segregation of impurities to the surfaces/interfaces, which means that a pure model system was not achieved even though high purity materials were used at a relatively low temperature. These impurities are believed to impede the electrode processes and hence to cause the increase in R_p.

6.2 Introduction

Recently it was shown that segregation of impurities to the interfaces has a negative influence on the kinetics of the $H_{2(g)}/H_2O_{(g)}/Ni_{(s)}/SZ_{(s)}$ electrode, resulting in a more ineffective electrode [5,6]. Also, segregated impurities at the interface may be the reason for the disagreements about the kinetics in literature, which has been accounted for elsewhere [8].

The purpose of our study is to perform electrochemical measurements in a very clean system to avoid the effects of impurities. This is attempted by using high purity materials, lowering the operation temperature to prevent fast segregation of impurities, and by limiting impurities from the environment.

The reactions under investigation at the Ni/SZ electrode are the oxidation of hydrogen and the reduction of water, see (17) and (18) respectively.

$$H_{2(g)} + O^{2-}_{(SZ)} \rightarrow H_2O_{(g)} + 2e^-_{(Ni)} \qquad \text{(Anodic current)} \qquad (17)$$

$$H_2O_{(g)} + 2e^-_{(Ni)} \rightarrow H_{2(g)} + O^{2-}_{(SZ)} \qquad \text{(Cathodic current)} \qquad (18)$$

Reactions (17) and (18) dominate when the cell is operated as a fuel cell (SOFC) and as an electrolyzer cell (SOEC, solid oxide electrolyzer cell), respectively.

The real SOFC anode is a porous Ni/SZ composite in order to optimize mass transport and charge transfer near or at the three phase boundary (TPB) where the Ni, SZ and fuel gas meet. A point electrode is used here as a model system because: 1) It provides a well

[3] An extract from this chapter was published as: J.Høgh, K. Vels Hansen, I. Chorkendorff, T. Jacobsen, K. Norrman and M. Mogensen, "High purity H_2/H_2O/nickel/stabilized zirconia electrolytes at 500°C ", Proceedings of the 29th International Conference on advanced Ceramics and Composites, The American Ceramic Society, Jan 2005. (the publication is shown in appendix C)

defined length of the TPB and 2) the easiness of investigating the Ni/SZ interface after an electrochemical experiment.

6.3 Experimental

6.3.1 Materials and sample preparation

As the working electrodes a nickel wire (Ø=0.5 mm) from Alfa Aesar (Puratronic®) was used. The stated purity was 99.999 % (metal basis). Prior to the electrochemical experiment the Ni wires were annealed in 3% H_2O/9% H_2/N_2 (1000°C, 7 days) and electro polished.
Four different electrolyte compositions of single crystals were used: $(ZrO_2)_{0.9}(Y_2O_3)_{0.1}$, $(ZrO_2)_{0.87}(Y_2O_3)_{0.13}$, $(ZrO_2)_{0.82}(Y_2O_3)_{0.18}$ and $(ZrO_2)_{0.9}(Sc_2O_3)_{0.06}(Y_2O_3)_{0.04}$. They were coded ZY10, ZY13, ZY18 and ZSc6Y4, respectively. The crystals ZY10, ZY18 and ZSc6Y4 were provided by Dr. Sergey Shkerin and professor Perfilliev, Institute of High-Temperature Electrochemistry, RAS, 20 S. Kovalevskaya Str., 620219 Ekaterinburg, Russia. The surface orientations of the samples are unknown. The ZY13 electrolyte was purchased at MTI Corporation (www.mticrystal.com). The purity is stated as 99.99 % and the surface orientation is [100]. All electrolytes were polished with 6, 3, 1 and ¼ μm diamond suspension. For the final polishing an acidic suspension of alumina particles (0.02 μm, OP-AA suspension, Struers) was used. After polishing and cleaning of both electrodes and electrolytes in an ultrasonic bath with ethanol, they were handled with gloves using mask and hairnet in a laminar air flow system.
Platinum was used as counter and reference electrodes and were painted on the electrolyte using Pt-paste (Degussa, 308A). As current collector for the counter and the reference electrodes Pt meshes were used in order to allow gas transport to the electrodes (Figure 44). A mesh consists of 0.1 mm Pt wires with a mask size of 0.5x0.5 mm, the thickness of the mesh is 0.3 mm.

6.3.2 Electrochemical setup

A 3-electrode setup (4-wires, one atmosphere) and impedance spectroscopy were used to measure R_p at OCV using a 30 mV signal. A frequency response analyzer (Solartron 1255b) in combination with a potentiostat (Solartron 1287) were used for the electrochemical measurements. Two gas compositions ~3% H_2O/H_2 and ~0.7% H_2O/H_2 were used and a YSZ based oxygen sensor with atmospheric air as the reference gas indicated oxygen pressures of $1.5 \cdot 10^{-31}$ atm (EMF=-1156 mV) and $9.5 \cdot 10^{-33}$ atm (EMF=-1202 mV) at 500°C, respectively. Figure 44 shows a sketch of the electrochemical 3-electrode setup. On top of the alumina tube a weight of copper (315 g) is arranged to press the Ni wire against the electrolyte. Prior to the electrochemical experiment the setup, which consists mainly of alumina, was heat treated twice to remove volatile material; first in air (technical air, 21 mol% O_2 and 79 mol% N_2) and then in humidified hydrogen (3% H_2O/H_2). The heat treatments were conducted at 1000°C for 7 days.

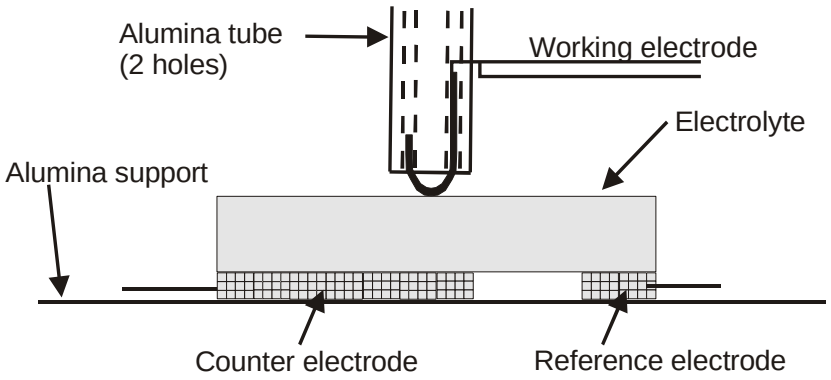

Figure 44. Sketch of the 3-electrode setup. Two leads are connected to the working electrode (Ni wire). Pt is used as counter and reference electrodes. Two Pt meshes collect the current and allow for gas transport to the electrodes.

It was found that 2-electrode measurements had a higher signal to noise ratio compared to 3-electrode measurements, hence fewer cycles (less time) were necessary for each impedance measurement using the 2-electrode mode. The area of the counter electrode is around 1000 times larger than the area of the working electrode (Ni wire), hence a negligible contribution from the counter electrode is expected on the total R_p. Also, the series resistance (R_s) should not be affected, as this resistance mainly originates from the current constriction at the point electrode. 3-electrode measurements were performed to confirm the results from 2-electrode measurements and they were in good agreement.
The four electrodes were operated for 46 days. The samples were heated from room temperature to 400°C over 4 h and kept at this temperature for 15 h. Next the temperature was increased to 450°C over 30 min and kept at this temperature for 7 h. Finally, the temperature was increased to 500°C over 30 min and kept at this temperature for 38 days before cooling down. Measurements were performed at 450 and 400°C before cooling to room temperature. The heating and cooling sequences will be referred to as the heating run and the cooling run.

6.3.3 Surface characterization techniques

Several surface techniques were used to characterize the Ni wires and the single crystals before and after the electrochemical measurements.
SEM (scanning electron microscopy) was performed using a Jeol JSM-5310LV. SEM images were used to determine the Ni/SZ contact areas from the Ni wires. Backscattered electrons were used to produce the images. Elemental analysis was performed using energy dispersive X-ray spectroscopy (EDS, Noran). EDS probes a volume of ~1 μm^3. EDS was used to verify the bulk composition of the electrolytes.
XPS (X-ray photoelectron spectroscopy) was performed using a Sage 100 from SPECS with a non-monochromated Mg-Kα X-ray source and a take-off angle of 90°. From the full spectrum elements were determined using a step size of 0.5 eV and a detector pass energy of 100 eV. Narrow scans with a step size 0.2 eV and a detector pass energy of 23 eV were performed to get a better resolution. An electron floodgun was used to limit charging. XPS was used for analysis of the electrolyte surfaces.
AES (Auger electron spectroscopy) was performed using a Phi 550/590 spectrometer from Perkin Elmer. The electron gun was set to 5 keV. The step size was 1 eV. Depth profiling was performed using an ion gun with 2 keV Ar^+ and a current of 45 $\mu A/cm^2$, the angle of incident was 54° to the surface. AES was used for elemental surface analysis of the Ni wire. XPS and AES probe a depth of 10-40 Å. AES was used for elemental surface analysis after the electrochemical experiment of the Ni wire placed on ZY10. An AES analysis was also

performed on a Ni wire (reference sample) that were annealed in 3% H_2O/9% H_2/N_2 (1000°C, 7 days) and electro polished. XPS and AES probe a depth of 10-40 Å.
TOF-SIMS (Time of flight secondary ion mass spectrometry) was performed on the electrolytes with a TOF-SIMS IV from ION-TOF GmbH. At first scans were performed to produce images of the elemental distribution. Depth profiles were subsequently performed. Xe^+ (3 keV, 3-16 nA, 300x300 μm^2) was used as coarse sputtering and Ga^+ (25 keV, 1 pA, 100x100 μm^2) was used for analysis. The total sputter time was 250-1000 s. The procedure for the depth profiling was: 0.5-2 s sputter → 0.5-1 s pause → ~1 s analysis (1/20kHz). The pause was inserted to limit charging even though an electron floodgun was used. The sputter rate on similar materials (ZY8, polycrystalline) was estimated elsewhere [26] to 1-10 Å per 100 s using Xe^+ (3 keV, 3 nA, 300x300 μm^2). TOF-SIMS images and depth profiling of all samples were performed after the electrochemical measurements. In the case of ZY13 and ZSc6Y4, two polished reference samples (not heat treated) were additionally examined. For each sample two depth profiles were performed outside the contact area and one inside the contact area. Two depth profiles were performed on each of the reference samples.

6.4 Results

6.4.1 Surface analysis

XPS measurements showed only carbon as an impurity on the polished electrolytes. When the samples have been exposed to the atmosphere carbon is always seen due adsorption of organic species. After the electrochemical experiment, Si/Zr ratios of 0.06, 0.05, 0.02 and 0.07 were observed on ZY10, ZY13, ZY18 and ZSc6Y4, respectively. Note that the Zr content is not the same in the crystals.
AES depth profiles of the Ni wire before and after the electrochemical experiment are shown in Figure 45.

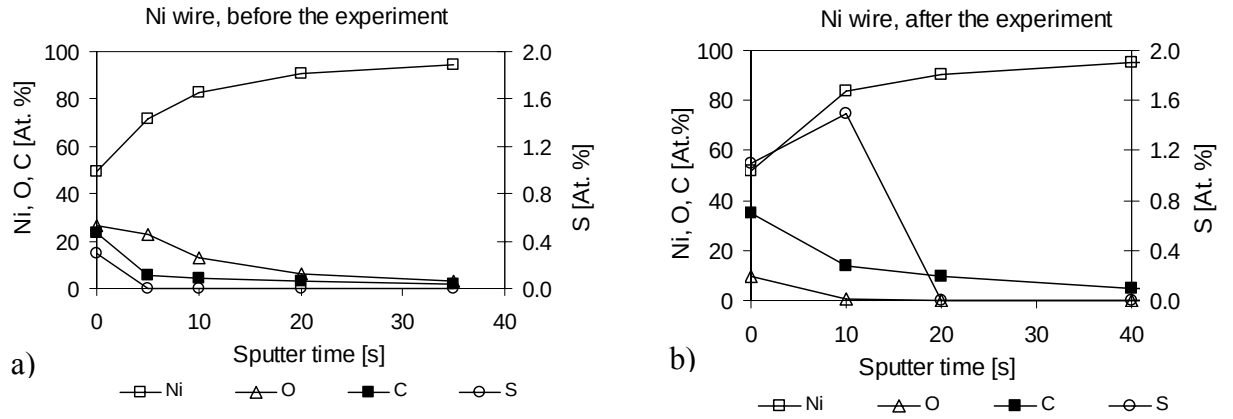

Figure 45. Depth profiling using AES. a) A Ni wire (reference sample) before the electrochemical experiment (annealed and electro polished) and b) The Ni wire after the electrochemical experiment outside the contact area. The Ni wire was placed on ZY10 during the electrochemical experiment. Sputtering was performed using 2 keV Ar^+ (45 $\mu A/cm^2$).

Two AES depth profiles were also performed in the Ni contact area on the Ni wire that was placed on ZY10 (not shown). One of the profiles showed up to 6 at. % Zr, but only 0.3 at. % S i.e. the same as the Ni wire before the electrochemical experiment. The other profile showed a thicker oxide scale and a sulfur profile similar to the one shown in Figure 45b.
TOF-SIMS images of the contact area of sample ZY13 after the electrochemical experiment are shown in Figure 46. The higher brightness the higher signal from the

respective element. The selected elements are showing that there in general is a higher impurity signal outside the contact area than inside the contact area. This corresponds with that the intensity for Zr and Y are higher in the contact area than outside the contact area. Ni, which is a cross over contamination from the Ni wire to the electrolyte, is also seen in the contact area. The tracks of Ni seen from the contact area are presumable from placing or removing the Ni wire, i.e. the Ni wire was drawn across the electrolyte.

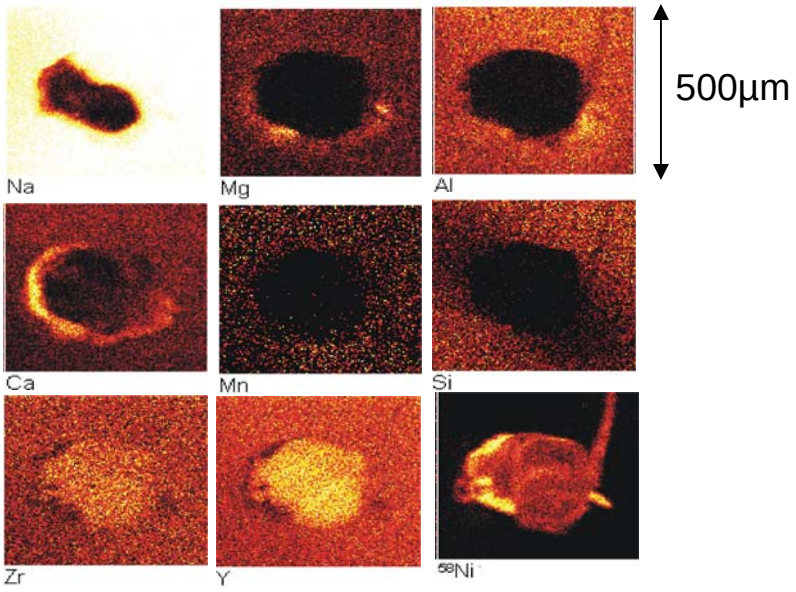

Figure 46. TOF-SIMS images of the contact area of ZY13 after the electrochemical experiment. The higher brightness the higher signal from the respective element.

A TOF-SIMS depth profile on ZY13 is shown in Figure 47a. The intensity within a profile varies. A general trend for all profiles is an initial steep increase followed by a steep decrease after which the intensity becomes relatively constant or decreases slightly. This trend is also seen in a previous study [27] and is explained by an establishment of a steady state of charging effects in the sputter process. For comparison the profiles were normalized by the intensity of $^{94}Zr^{+}$ as this is free of ZrH^{+} interference. Figure 47b shows the normalized Si signal for the measurement performed on ZY13 and the reference sample of ZY13. It is seen that the Si/^{94}Zr ratio outside the contact area (13-1 and 13-2) is higher than in the contact area and on the freshly polished reference sample (13R-1 and 13R-2). The maximum ratios from the contact area and the reference sample are 0.003 and 0.007 respectively, i.e. about 100 times lower than the peak value outside the contact area. All four electrochemically tested samples showed a lower normalized Si/^{94}Zr signal in the contact area than outside the contact area. The measurements on the reference samples showed a higher Si/^{94}Zr signal than that found in the contact area of ZY13. Comparison between the measurements outside the contact area and in the contact area shows that the elements Al, Mg, K, Cr, Mn and Fe have the same trend as Si i.e. higher normalized signal outside the contact area than in the contact area. In the case of Ni a higher normalized signal was found in the contact area than outside the contact area.

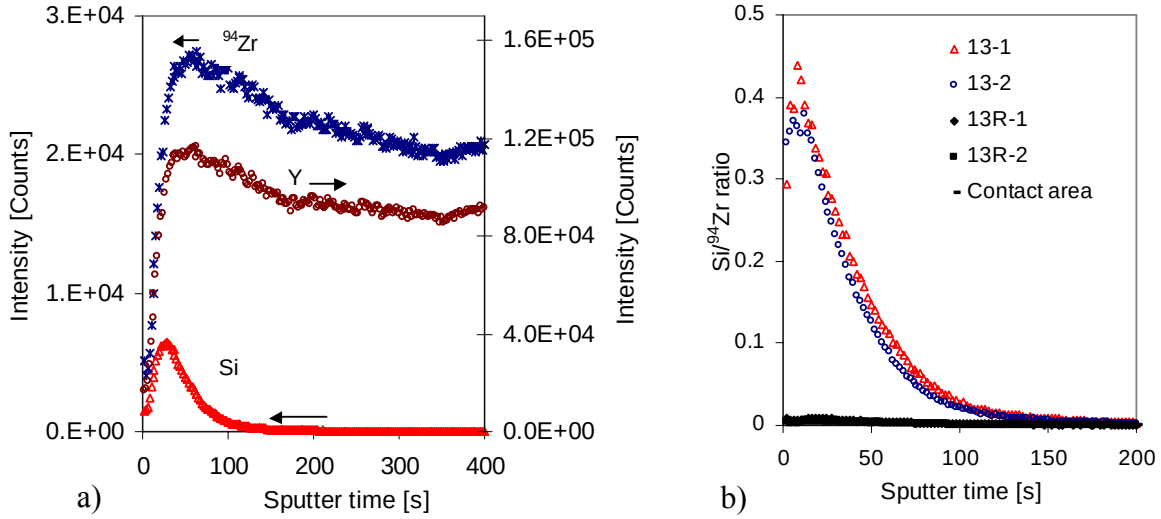

Figure 47. a) TOF-SIMS depth profile of ZY13. Raw intensity data for ^{94}Zr, Y and Si are shown. b) TOF-SIMS depth profile of Si/Zr for ZY13. The codes 13-1, 13-2 and "Contact area" are referring to positions on the electrochemically tested sample. 13-1 and 13-2 are outside the contact area. 13R-1 and 13R-2 are from the reference sample.

6.4.2 Electrochemistry

6.4.2.1 Impedance spectra

R_p and R_s were found from impedance spectroscopy. Two impedance spectra (2_034 and 2_037) are shown in Figure 48. The high frequency part from 10^4 – 10^5 Hz can be ascribed to the capacitance of the 3-electrode setup. Fluctuations in R_p occur, usually as a sudden drop followed by a steady increase. The impedance spectrum 2_034 is from a period where R_p was stable and spectrum 2_037 was performed after a sudden drop in R_p. From Figure 48b it can be a seen that R_s is the same in 2_034 and 2_037, which implies that the drop in R_p is not caused by a change in the size of the contact area.

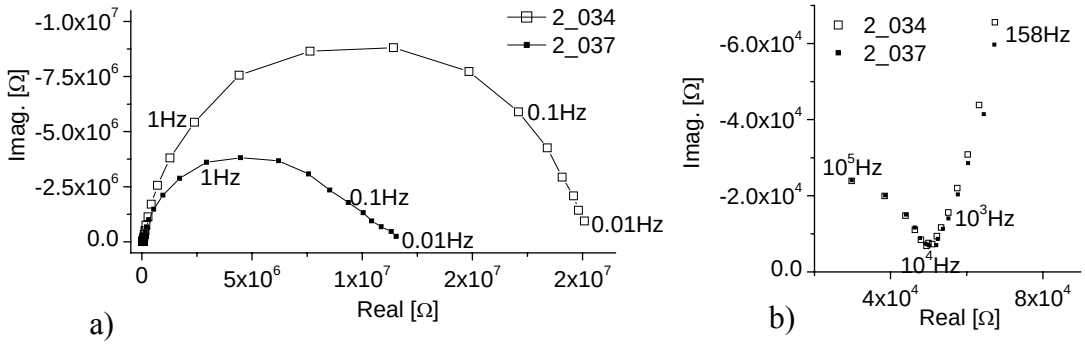

Figure 48. a) Impedance spectra for ZY10. Spectrum 2_034 shows a time independent measurement. In spectrum 2_034, R_p is increasing during the measurement, which causes a tail towards higher resistance. b) A close-up of the high frequency measurements showing that R_s is the same in the two spectra.

6.4.2.2 Contact area

The area specific resistance (ASR) is calculated (ASR≡ $R_p \cdot A_{contact}$) for comparison between measurements/samples with different contact area. As the contact area increases during the

electrochemical experiment the area (radius) was calculated from (19) [23] at each impedance measurement. In this relation an infinite thick electrolyte and a circular area is assumed. A relation [23] which matches our samples (not infinite thick and elliptic contact area) deviates less than 5 % from (19) and as 5 % is a small value in this context $\left(100 \cdot R_s < R_p\right)$ the simple approximation is used due to the ease of computation.

$$R_S = \frac{1}{4 \cdot \sigma \cdot r} \tag{19}$$

In (19) σ is the ionic conductivity and r is the radius of a circle. In this case the contact area is elliptic and an equivalent radius is used, i.e. $r = \sqrt{\alpha \cdot \beta}$, where 2α and 2β are the length of the long and short axis of the elliptic contact area. As seen from Figure 49b the area is fairly constant towards the end of the electrochemical experiment. Thus, the values calculated from (19) can be calibrated according to the contact area of the Ni wire determined by SEM (Figure 49a) after the electrochemical experiment. The behavior of R_s seen in Figure 49b was observed for all samples. In the following all ASR values will be based on the area calculated from (19). In all four cases the area increased by a factor of ~2 compared to the first measurement at 500°C, see Figure 49b. The SEM contact areas for ZY10, ZY13, ZY18 and ZSc6Y4 were 0.069, 0.059, 0.052 and 0.045 mm^2, respectively.
When point electrode experiments are conducted an initial annealing at higher temperature is required to stabilize the contact area. In this study one objective was to follow the degradation of the electrodes at 500°C hence it was not possible to use a higher initial temperature, as this would probably change the degradation profile. This is the reason why calculated areas are used for the ASR.

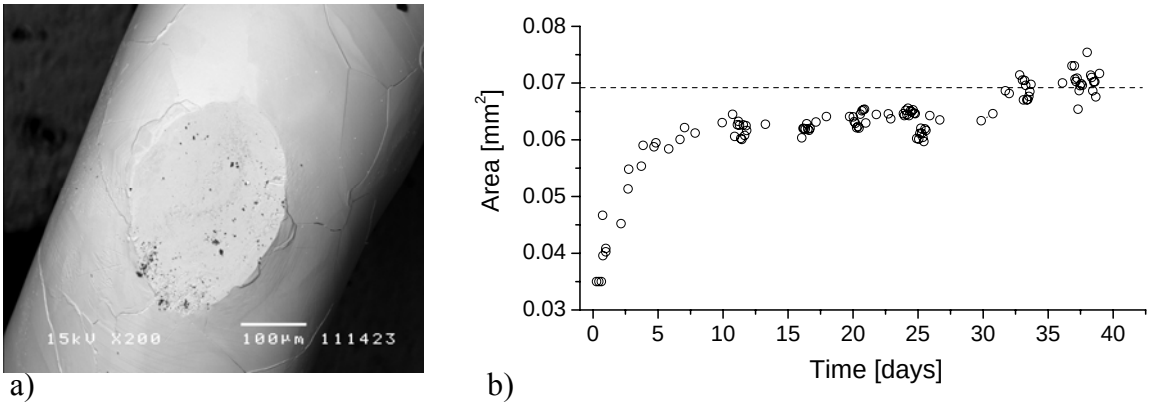

a) b)

Figure 49. a) SEM image of the contact area on a Ni wire after the electrochemical experiment. The Ni wire was pressed against ZY10. α=172 µm, β=128 µm, area=0.069 mm^2, perimeter=0.952 mm. b) Calculated area vs. time for ZY10 at 500°C. The dashed line represents the area measured with SEM (0.069 mm^2).

6.4.2.3 Temperature variation

The variation of R_s and ASR with temperature for ZY10 is shown in Figure 50. The activation energies were derived from the cooling run. The activation energies for R_s for ZY10, ZY13, ZY18 and ZSc6Y4 were 1.02, 1.28, 1.31 and 1.16 eV, respectively. The activation energies for ASR for ZY10, ZY13, ZY18 and ZSc6Y4 were 0.92, 0.49, 0.78 and 0.17 eV, respectively.

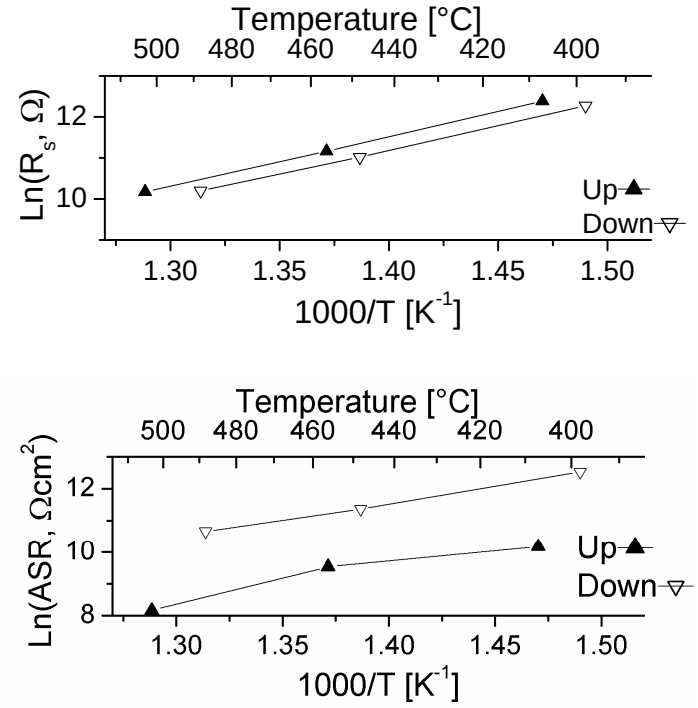

Figure 50. Temperature dependence on R_s and ASR for ZY10. The ASR values were based on calculated areas. The "Up" and "Down" notation corresponds to heating run and cooling run, respectively.

The trend of R_s and ASR from the heating run and cooling run for ZY13, ZY18 and ZSc6Y4 shows a behavior similar to ZY10 (Figure 50), hence only the graph for one sample is shown.

6.4.2.4 Long-term stability at 500°C

During the 500°C period the temperature fluctuated from 484-515°C and this caused noticeable changes in R_s and ASR. The resistance values were adjusted to 500°C using the E_a derived from the cooling run, except for the ASR in case of ZSc6Y4 where an average (E_a=0.7 eV) of the ASR for the others samples was used. This average was used as ZSc6Y4 experienced a high polarization before the cooling run, which dramatically lowered the ASR. The corrected ASR and R_s values versus time for the ZY10 are shown in Figure 51. The long-term stability of ZY13, ZY18 and ZSc6Y4 shows a dependence on R_s and ASR similar to ZY10 (Figure 51), hence only one sample is shown. The scatter within the decreasing tendency in R_s is not necessary an area effect but can be ascribed to the uncertainty in the determination. Initial and average ASR values were determined at 500°C in 3% H_2O/H_2, see Table 11. The average ASR values were calculated, as the initial increase seemed to level out e.g. in case of ZY10 (Figure 51) after day 20.

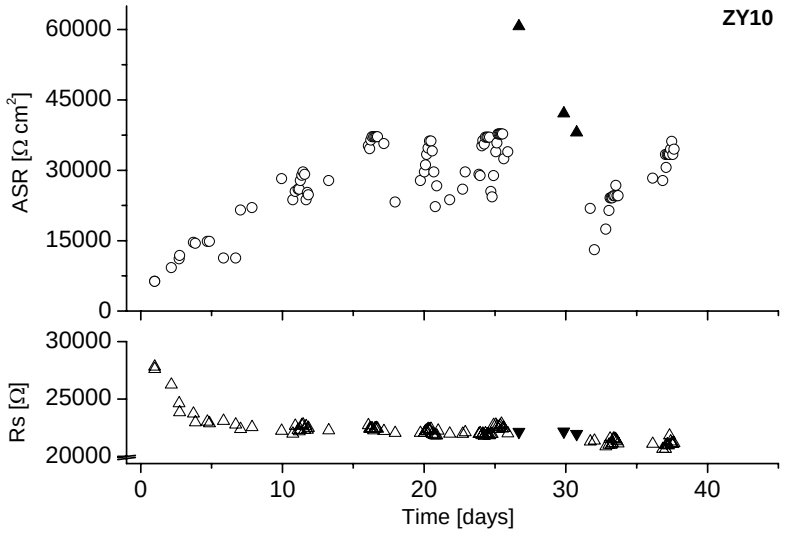

Figure 51. ASR and R_s versus time for ZY10. Measurements performed in 3% H_2O/H_2 and 0.7% H_2O/H_2 are depicted as open and filled symbols, respectively. The values were corrected to 500°C.

Table 11. Initial and average ASR values calculated at 500°C in 3% H_2O/H_2.

Sample	$ASR_{initial}$ [kΩ·cm^2]	$ASR_{average}$ [kΩ·cm^2]	Degradation factor $ASR_{average}/ASR_{initial}$
ZY10	3.7	29	7.8
ZY13	2.4	14	5.8
ZY18	3.4	28	8.2
ZSc6Y4	4.7	22	4.7

6.4.2.5 Strong polarization

During the 500°C period sample ZSc6Y4 experienced a high polarization of up to 30 V (~day 24) for a short period of 5-10 s. This polarization caused the ASR to decrease dramatically. It was not clear if the polarization was cathodic or anodic.

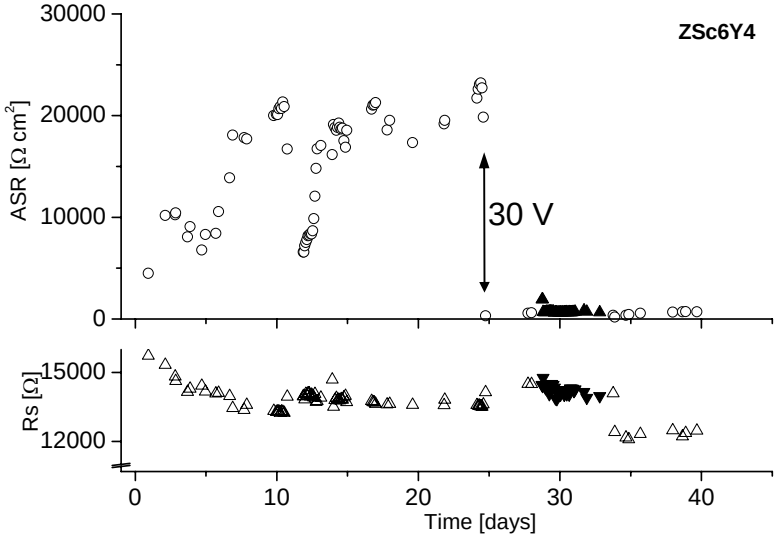

Figure 52. ASR and R_s versus time for ZSc6Y4. Measurements performed in 3% H_2O/H_2 and 0.7% H_2O/H_2 are depicted as open and filled symbols, respectively. The values were corrected to 500°C. At day ~24 the electrode was polarized with 30 V.

6.5 Discussion

6.5.1 Surface analysis

6.5.1.1 AES on the Ni wire

Prior to the electrochemical experiment only the expected impurity elements (oxygen, carbon and sulfur) could be detected on a heat treated and electro polished Ni wire (reference sample). These elements are always detected with AES when Ni has been exposed to the atmosphere due to adsorption. A small amount of sulfur (0.06 ppm, see Table 6) is present in the Ni wire but it is under the detection limit for the AES. A noteworthy difference is that the sulfur content outside the contact area is higher on the Ni wire after the electrochemical experiment i.e. sulfur is either segregating from the Ni or is present in the gas phase. A poising effect of sulfur is known to enhance the polarization resistance [1]. The two profiles performed in the contact area were different regarding the elemental distribution of sulfur and zirconia implying that the contact area of the Ni wire is inhomogeneous.

6.5.1.2 XPS on the electrolytes

On the polished electrolytes carbon was found as the only impurity. After the electrochemical experiment Si was detected on all electrolytes. From the literature [17,18] it is known that Si segregates from the bulk to the surface of yttria stabilized zirconia. The reason why no Si are detected on the surface of polished crystals is that the bulk concentration is too low (ppm level) to be detected by XPS.

6.5.1.3 TOF-SIMS on the electrolytes

The TOF-SIMS could detect some impurities on the reference samples but in general the impurity level was lower than on the electrochemically tested samples. A close up from Figure 47 of the first 100 s, shows that the Si signal peaks before the Y and ^{94}Zr signals. In

general all the impurities peak before the Zr and Y species (and Sc in case of ZSc6Y4). This indicates that the impurities are located in the outermost atomic layers. The signals from the impurities disappear at around 100-200 s, which corresponds to 1-20 Å if a sputter rate of 1-10 Å per 100 s is assumed [26]. In cases where a sputter current of 16 nA is used instead of 3 nA the impurity peaks disappear at 20-40 s, which corresponds well to a proportionality between the sputter rate and sputter current.

6.5.2 Electrochemistry

6.5.2.1 Temperature dependence

In the case of R_s (Figure 50) the ohmic resistance from the heating run are higher than the measurement from the cooling run due to creeping of the Ni wire (increasing contact area) during the electrochemical experiment. R_s measurements from the heating run are shown to confirm the R_s measurements from the cooling run.
The E_a for the ASR varies a lot (0.17-0.92 eV) indicating different rate limiting steps. The notable low activation energy on ASR (0.17 eV) for ZSc6Y4 is believed to be an effect of the high polarization. ASR values from the heating run do not show an Arrhenius dependence. An explanation to this could be decomposition of organic compounds adsorbed on the surfaces of Ni and SZ during heating. The trend in the Arrhenius plot is not believed to be caused by fluctuations in the ASR for the following reasons: 1) From the Arrhenius plot all four electrodes show the same trend for the heating run and all four electrodes show a straight line from the cooling run. 2) More than one measurement was performed at each temperature on each electrode, and the scatter between these measurements is negligible compared to the dependence on temperature. 3) From Figure 51 it can be seen that the no fluctuations observed in the start of the measurement. This is also true for ZY13, ZY18 and ZSc6Y4. An explanation to this can be that the impurities are causing the fluctuations i.e. no fluctuations in the start of the electrochemical experiment as the electrodes are "clean".

6.5.2.2 Long-term stability at 500°C

All four samples showed a general trend of increasing ASR with time. Fluctuations in ASR occur, usually as a sudden drop followed by a steady increase. Initial and average ASR values are calculated and their ratios (degradation factors) are listed in Table 11. The degradation of the electrodes is believed to be caused be the segregation of impurities.
For all four electrodes the polarization resistance increased when the water content was lowered from 3 to 0.7 %. Fluctuations occurs and it is difficult to give an exact increase, but a factor ~2 seems reasonable. The change was reversible. R_s were as expected not influenced by the water content as the conductivity of the electrolytes is stable over a wide range of oxygen partial pressures. Due to the uncertainty and fluctuations accompanied with the ASR no dependence of the electrolyte compositions is evident at 500°C in 0.7 or 3% H_2O/H_2.

6.5.2.3 Strong polarization

The strong polarization of ZSc6Y4 caused the ASR to drop from 19 kOhm·cm^2 to 0.3 kOhm·cm^2, i.e. it lowered by a factor of ~60. The R_s value did not change within the uncertainty, i.e. the lower ASR value is not an area effect. The ASR value increased after the strong polarization. After 15 days the ASR value reached 0.6 kOhm·cm^2. From strong anodic and cathodic polarizations experiments on Ni pattern electrodes an effect on ARS was only seen after the cathodic polarization. It is therefore believed that the 30 V polarization was cathodic.

6.6 Conclusion

After the electrochemical experiment a higher impurity level was seen on the electrode materials even though high purity materials were used at a relatively low temperature. A higher sulfur concentration was detected with AES on the Ni wire. Many elements were observed on the SZ single crystals with TOF-SIMS but only Si was detected with XPS indicating that Si is the main component segregating to the surface. The segregation outside the contact area is independent on the current applied to the electrode. From the TOF-SIMS imaging and depth profiles Ni was detected in the contact areas on the SZ single crystals. Also, a lower content of impurities was evident in the contact area.

Our findings do not suggest any dependence on the electrolyte composition for: $(ZrO_2)_{0.9}(Y_2O_3)_{0.1}$, $(ZrO_2)_{0.87}(Y_2O_3)_{0.13}$, $(ZrO_2)_{0.82}(Y_2O_3)_{0.1}$ and $(ZrO_2)_{0.9}(Y_2O_3)_{0.04}(Sc_2O_3)_{0.06}$ on the polarization resistance (OCV) at 500°C in 0.7-3% H_2O/H_2. Changing the atmosphere from 3% H_2O/H_2 to 0.7% H_2O/H_2 at 500°C increased the polarization resistance of all samples by a factor of ~2. All electrodes degraded by a factor of 5-8 over 10-20 days at 500°C in 3% H_2O/H_2. Segregation of impurities is believed to cause this degradation. The fluctuations in ASR are believed to be due to the nature of the electrode-electrolyte interface and not external actions such as vibrations. A high polarization of the ZSc6Y4 caused the ASR to drop by a factor of ~60. The polarization effect will be treated further in chapter 7.

7 Pure vs. impure SZ surfaces under strong cathodic polarization at the H_2/H_2O/Ni/SZ electrode

7.1 Abstract

Impedance measurements and potential sweeps were performed on a model system of the SOFC (solid oxide fuel cell) anode. The model system was made by pressing a bent Ni wire onto an electrolyte of stabilized zirconia (hereafter referred to as a point electrode). Four single crystals were used as electrolytes: two with the composition of $(ZrO_2)_{0.87}(Y_2O_3)_{0.13}$ and two with the composition of $(ZrO_2)_{0.9}(Sc_2O_3)_{0.06}(Y_2O_3)_{0.04}$. One crystal of each composition was heat treated prior to the electrochemical experiment so that an impurity film (Si, Al and Na) on the surface was formed by segregated impurities. It was found that the polarization resistance at OCV (open circuit voltage) was higher for the electrodes with impure electrolyte surface. The polarization resistance lowered considerably for all electrodes when a strong cathodic overpotential (~2000 mV vs. air) was applied.

7.2 Introduction

It is known that segregation of impurities to the interfaces and the three phase boundary (TPB) increases the polarization resistance of the H_2/H_2O/Ni/SZ electrode [5,6]. In chapter 6 it was shown that when using high purity materials at relatively low temperature (500°C) to prevent fast segregation the negative effect of impurities still appeared. In order to verify that the impurities at the electrolyte surface play an important role for the polarization resistance electrochemical measurements were performed with electrolytes that were polished (pure surface) and electrolytes that were heat treated (impure surface). A strong cathodic polarization of the metal/SZ electrodes is known to decrease the polarization resistance of the electrode [28]. This was also seen in chapter 6 for the Ni/SZ point electrode. In Nguyen and Mason [28] and references therein it was hypothesized that trapped electrons in the electrolyte surface (color center) lowered the polarization resistance due to a high catalytic activity. Also, the reduction of zirconia was observed. In this study it will be investigated which effect the strong cathodic polarization has on the impure and pure electrodes, respectively.

The reactions under investigation at the Ni/SZ electrode are the oxidation of hydrogen and the reduction of water, see (20) and (21) respectively.

$$H_{2(g)} + O^{2-}_{(SZ)} \rightarrow H_2O_{(g)} + 2e^-_{(Ni)} \qquad (Anodic\ \ current) \qquad (20)$$

$$H_2O_{(g)} + 2e^-_{(Ni)} \rightarrow H_{2(g)} + O^{2-}_{(SZ)} \qquad (Cathodic\ current) \qquad (21)$$

Reaction (20) and (21) dominate when the cell is operated as a fuel cell (SOFC) and as an electrolyzer cell (SOEC, solid oxide electrolyzer cell), respectively.

The real SOFC anode is a porous Ni/SZ composite in order to optimize mass transport and charge transfer near or at the three phase boundary (TPB) where the Ni, SZ and fuel gas (e.g. $H_{2(g)}$) meet. A point electrode is used here as a model system because: 1) It provides a well defined length of the TPB and 2) the easiness of investigating the Ni/SZ interface after an electrochemical experiment and 3) to obtain a more well defined electrode potential compared to the composite anode. In a cermet anode the reaction takes place over a distance of ~10 μm from the electrolyte. This causes a gradual potential drop through the cermet anode due to the resistance of the SZ network. This means that the reactions in (20)

and (21) take place at different potentials at the same time, which makes it more difficult to analyze kinetic data.

7.3 Experimental

7.3.1 Materials and sample preparation

A nickel wire (Ø=0.5 mm) from Alfa Aesar (Puratronic®) was used as working electrode. The stated purity was 99.999 % (metal basis). Prior to the electrochemical experiment the Ni wires were annealed in 3% H_2O/9% H_2/N_2 (1000°C, 7 days) and electro polished.
Four single crystals were used as electrolytes: Two with a composition of $(ZrO_2)_{0.87}(Y_2O_3)_{0.13}$ and two with a composition of $(ZrO_2)_{0.9}(Sc_2O_3)_{0.06}(Y_2O_3)_{0.04}$. The crystals $(ZrO_2)_{0.9}(Sc_2O_3)_{0.06}(Y_2O_3)_{0.04}$ were provided by Dr. Sergey Shkerin and professor Perfilliev, Institute of High-Temperature Electrochemistry, RAS, 20 S. Kovalevskaya Str., 620219 Ekaterinburg, Russia. The surface orientations of the samples are unknown. The $(ZrO_2)_{0.87}(Y_2O_3)_{0.13}$ electrolytes was purchased at MTI Corporation (www.mticrystal.com). The purity is stated as 99.99 % and the surface orientation is [100]. All electrolytes were polished with 6, 3, 1 and ¼ μm diamond suspension. For the final polishing an acidic suspension of alumina particles (0.02 μm, OP-AA suspension, Struers) was used. After polishing of both Ni wires and electrolytes they were cleaned in an ultrasonic bath with ethanol. One electrolyte of each composition was hereafter heat treated at 1450°C in order to produce at impurity film by segregated impurities on the surface. The exact procedure for the heat treatment is given in section 9.3. Finally, the electrodes were mounted while wearing gloves, mask and hairnet in a laminar air flow system. The electrodes with the pure electrolyte surface were coded ZY13 ($(ZrO_2)_{0.87}(Y_2O_3)_{0.13}$) and ZSc6Y4 ($(ZrO_2)_{0.9}(Sc_2O_3)_{0.06}(Y_2O_3)_{0.04}$), while the electrodes with the impure surfaces, which were heat treated (h) prior to the electrochemical, were coded ZY13_h and ZSc6Y4_h.
Platinum was used as counter and reference electrodes and was painted on the electrolyte using Pt paste (Degussa, 308A). As current collector for the counter and the reference electrodes Pt meshes were used in order to allow gas transport to the electrodes. A mesh consists of 0.1 mm Pt wires with a mask size of 0.5x0.5 mm, the thickness of the mesh is 0.3 mm.

7.3.2 Electrochemical measurements

A frequency response analyzer (Solartron 1255b) in combination with a potentiostat (Solartron 1287) was used to perform the impedance spectra and the potential sweeps in a 3-electrode setup (4-wires, one atmosphere). The impedance spectra were acquired using a 30 mV signal at OCV. Figure 53 shows a sketch of the 3-electrode setup and a photo of the electrodes used in this work. On top of the alumina tube a weight of copper (315 g) is arranged to press the Ni wire against the electrolyte. The electrodes were operated for ~33 days in 3% H_2O/H_2, except for two hours during the strong cathodic polarization where dry hydrogen was used. A YSZ (yttria stabilized zirconia) based oxygen sensor with atmospheric air as reference gas indicated oxygen pressures of $2\cdot10^{-31}$ atm (EMF=-1151 mV), $1\cdot10^{-27}$ atm (EMF=-1136 mV) and $2\cdot10^{-24}$ atm (EMF=-1117 mV) in 3% H_2O/H_2 at 500, 600 and 700°C, respectively. The oxygen pressure in dry hydrogen at 700°C was $2\cdot10^{-28}$ atm (EMF=-1310 mV), which corresponds to a gas mixture of 0.03% H_2O/H_2 [22]. This gas mixture will be referred to as dry hydrogen. The pressure in the system was 1 atm at all times.

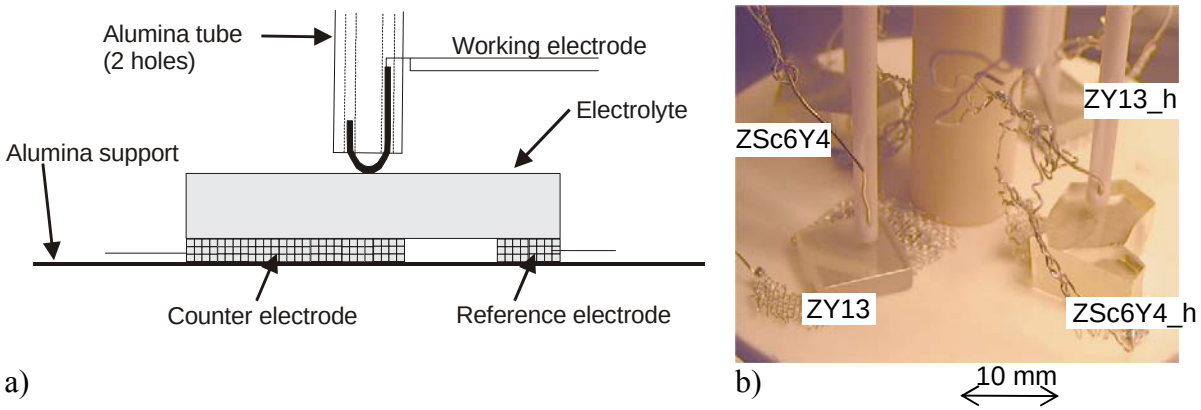

Figure 53. a) Sketch of the 3-electrode setup. Two leads are connected to the working electrode (Ni wire). Pt is used as counter and reference electrodes. Two Pt meshes collect the current and allow for gas transport to the electrodes. b) Photo of the electrodes used in this experiment and the electrode numbering.

The strong cathodic polarization was performed in dry hydrogen so that the amount of current, in coulombs, used for reduction of water would be negligible. Hence, the coulombs for reduction of other species (SZ and/or impurities) would be known. However, it turned out that the amount of coulombs for reduction of water was not negligible as the kinetics of the water reduction enhanced drastically during the strong cathodic polarization. In other words it is not known which fraction of the cathodic current that was used for reduction of water or reduction of other species (SZ and/or impurities). In order not to reduce a considerable amount of the SZ crystals the amount of coulombs for reducing the SZ in a distance of 2 µm directly beneath the Ni contact area was calculated. The calculation is based on pure zirconia and a contact area of 0.1 mm^2, see (22) and (23). The amount of coulombs was calculated to ~$4 \cdot 10^{-3}$ C.

$$n_{ZrO2} = \frac{d \cdot A \cdot \rho_{ZrO2}}{M_{ZrO2}} = \frac{2 \cdot 10^{-4}\, cm \cdot 10^{-3}\, cm^2 \cdot 5.6\, g/cm^3}{123\, g/mol} = 9.2 \cdot 10^{-9}\, mol \qquad (22)$$

$$\begin{aligned} n_{Coulomb} &= n_{ZrO2} \cdot n_{elektroner} \cdot F \\ &= 9.2 \cdot 10^{-9}\, mol \cdot 4 \cdot 96485\, C/mol \\ &= 3.6 \cdot 10^{-3}\, C \end{aligned} \qquad (23)$$

The strong cathodic polarizations were performed by potential sweep in dry hydrogen using a sweep rate of 20 mV/s. The sweeps were stopped when a charge of ~$4 \cdot 10^{-3}$ C was transferred. The potential sweeps and the sweeps corrected for R_s are shown in Figure 54 and Figure 55, respectively. The potential sweeps that has been corrected for the R_s value looks unusual as the electrode potential (E) begins to decrease with increasing current. This is explained by the strong activation of the electrode with respect to the reduction of water, which is seen at large electrode potentials. It is also seen that the two electrolyte compositions ($(ZrO_2)_{0.87}(Y_2O_3)_{0.13}$) and $(ZrO_2)_{0.9}(Sc_2O_3)_{0.06}(Y_2O_3)_{0.04}$ has a turning point

regarding to the activation at different electrode potential ~2000 mV vs. air and ~2100 mV vs. air respectively.

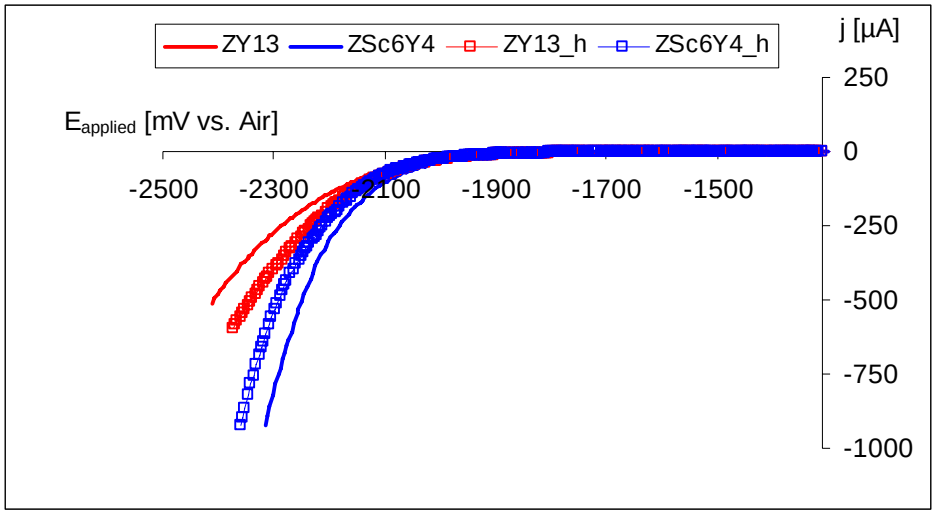

Figure 54. Potential sweeps (20 mV/s) for the electrodes in dry hydrogen (EMF=-1310 mV vs. air) at 700°C. The potential sweeps were interrupted when a charge of ~$4 \cdot 10^{-3}$ C was transferred.

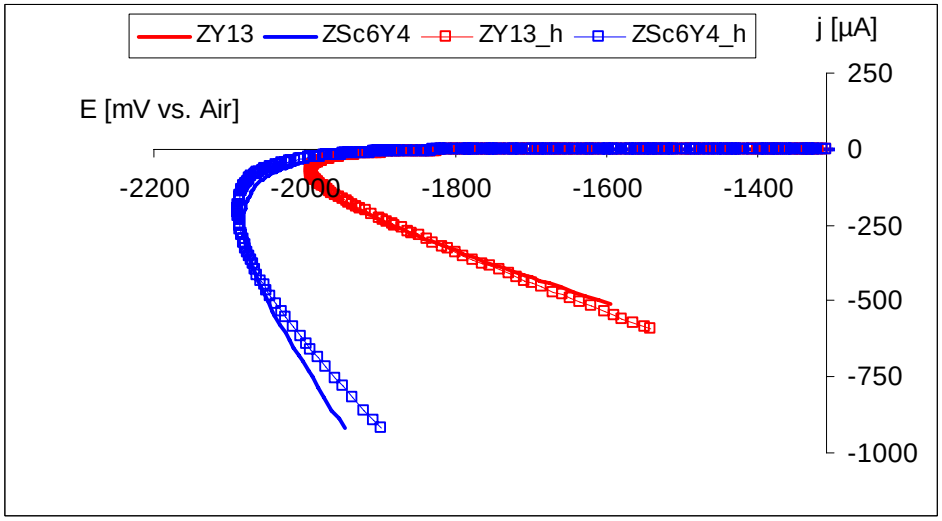

Figure 55. Potential sweeps (20 mV/s) for the electrodes in dry hydrogen (EMF=-1310 mV vs. air) at 700°C. The potential sweeps were corrected for the R_s value. The sweeps were interrupted when a charge of ~$4 \cdot 10^{-3}$ C was transferred.

The electrodes were heated from room temperature to 500°C and kept at this temperature for 12 h. Next, the temperature was increased to 600°C and kept at this temperature for 5 days. Finally, the temperature was increased to 700°C and kept at this temperature for 21 days before cooling down. Measurements were performed at 600 and 500°C before cooling to room temperature. The heating and cooling rates were 5°C/min. The time scales shown in the figures throughout this chapter begin when the temperature reached 500°C.

7.3.3 Surface characterization techniques

SEM (scanning electron microscopy) was performed using a Jeol JSM-5310LV. An SEM image was used to determine the Ni/SZ contact area from the Ni wire. Backscattered electrons were used to produce the images.

XPS (X-ray photoelectron spectroscopy) was performed using a Sage 100 from SPECS with a non-monochromated Mg-Kα X-ray source and a take-off angle of 90°. From the full spectrum elements in the sample were determined using a step size of 0.5 eV and a detector pass energy of 100 eV. Narrow scans with a step size 0.2 eV and a detector pass energy of 23 eV were performed to get a better resolution. An electron floodgun was used to limit charging. XPS was used for analysis of the electrolyte surface.
AFM (atomic force microscopy) was performed using a PSIA XE-150. The electrolyte surface was investigated to see topographic differences between the contact area where the Ni wire were placed and the electrolyte area outside the contact area.

7.4 Results

7.4.1 Surface analysis

The impurities detected with XPS on the surface of the four electrolytes before and after the electrochemical experiment are listed in Table 12. Carbon is also detected on the electrolytes before and after the electrochemical experiment. The carbon originates from organic species in the atmosphere that adsorbs to the surface when transporting the electrolytes to the XPS. No impurities could be detected on the polished crystals (ZY13 and ZSc6Y4) before the electrochemical experiment. Afterwards Si and Na were detected on the same crystals. The analysis of the heat treated crystals (ZY13_h and ZSc6Y4_h) showed the presence of Si, Al and Na. After the electrochemical experiment the amount of Si and Al were approximately the same while the Na had increased significantly.

Table 12. XPS of the electrolytes before (B) and after (A) the electrochemical experiment.

	ZY13	ZY13_h	ZSc6Y4	ZSc6Y4_h
Si/Zr, before	-	0.12	-	0.11
Si/Zr, after	0.07	0.13	0.06	0.13
Al/Zr, before	-	0.13	-	0.14
Al/Zr, after	-	0.11	-	0.14
Na/Zr, before	-	0.02	-	0.02
Na/Zr, after	0.24	0.18	0.23	0.24

A SEM image of the Ni wire used on ZSc6Y4 prior to
the electrochemical experiment is shown in Figure 56. This wire looked similar to the other Ni wires used.

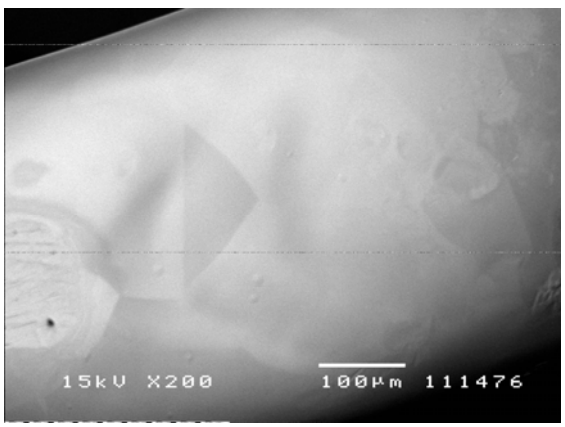

Figure 56. SEM image of the Ni wire before it was used as point electrode for sample ZSc6Y4.

SEM images of the elliptic contact area on the Ni wires after the electrochemical experiment are shown in Figure 57 - Figure 60. The size of the contact area (A), the perimeter (p) and the length of the long (2α) and short (2β) axis of the elliptic contact area are listed in the figure text. The Ni wire from electrode 3 fractured while dismounting it from the alumina tube (Figure 59). The contact area was broken up in two parts due to the fracture. The two parts are shown with dashed lines. A few holes, scratches and irregularities is seen in the contact area but in the general the contact areas are fairly smooth and provides a well defined length of the TPB.

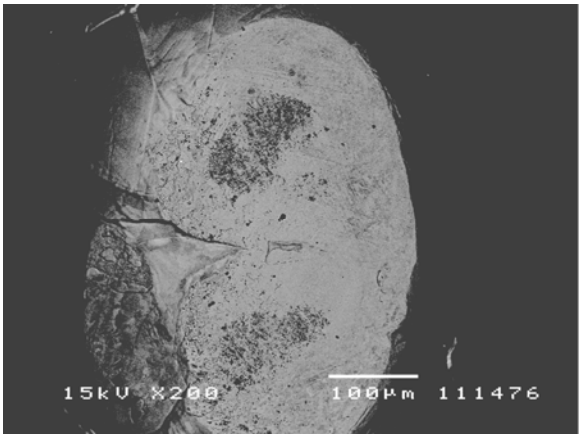

Figure 57. Ni wire from ZY13 after the electrochemical experiment. α=243 µm, β=135 µm, A=0.103 mm^2 and p=1.234 mm.

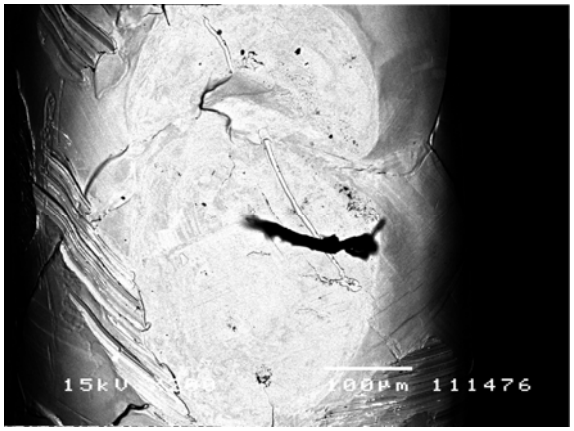

Figure 58. Ni wire from ZSc6Y4 after the electrochemical experiment. α=250 µm, β=128 µm, A=0.10 mm^2 and p=1.25 mm.

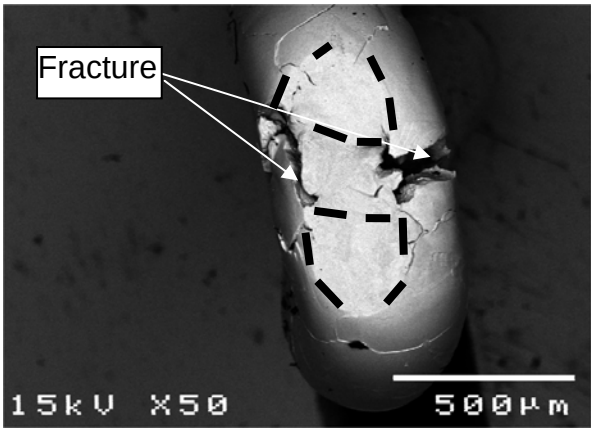

Figure 59. Ni wire from ZY13_h after the electrochemical experiment. The fracture originates from dismounting of the Ni wire from the alumina tube. α=225 µm, β=139 µm, A=0.098 mm^2 and p=1.17 mm.

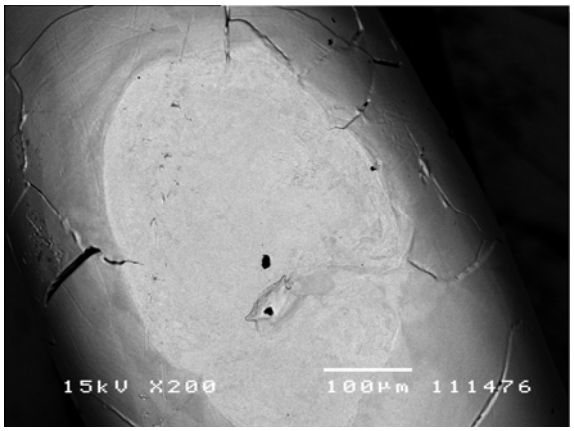

Figure 60. Ni wire from ZSc6Y4_h after the electrochemical experiment. α=227 µm, β=152 µm, A=0.11 mm^2 and p=1.21 mm.

AFM images were acquired for ZY13_h. Two scans were performed: one with 10x10 µm and one with 1x1 µm (see Figure 61 and Figure 62, respectively). Note that the ratio between the height and length axis's are not the same. The height axis has a minor division in order to bring out the structure. The highest region in the 10x10 µm scan are believed to be a particle that landed on the sample after the electrochemical experiment. The scans are performed partly in the contact area and partly outside the contact area. In contact area a coarse structure, which will be refered to as a "hill and valley" structure, is formed. In the borderline of the contact area a rim, that is higher than the surroundings, is seen. Outside of the contact area the surface appeared smooth compared to the hill and valley structure.

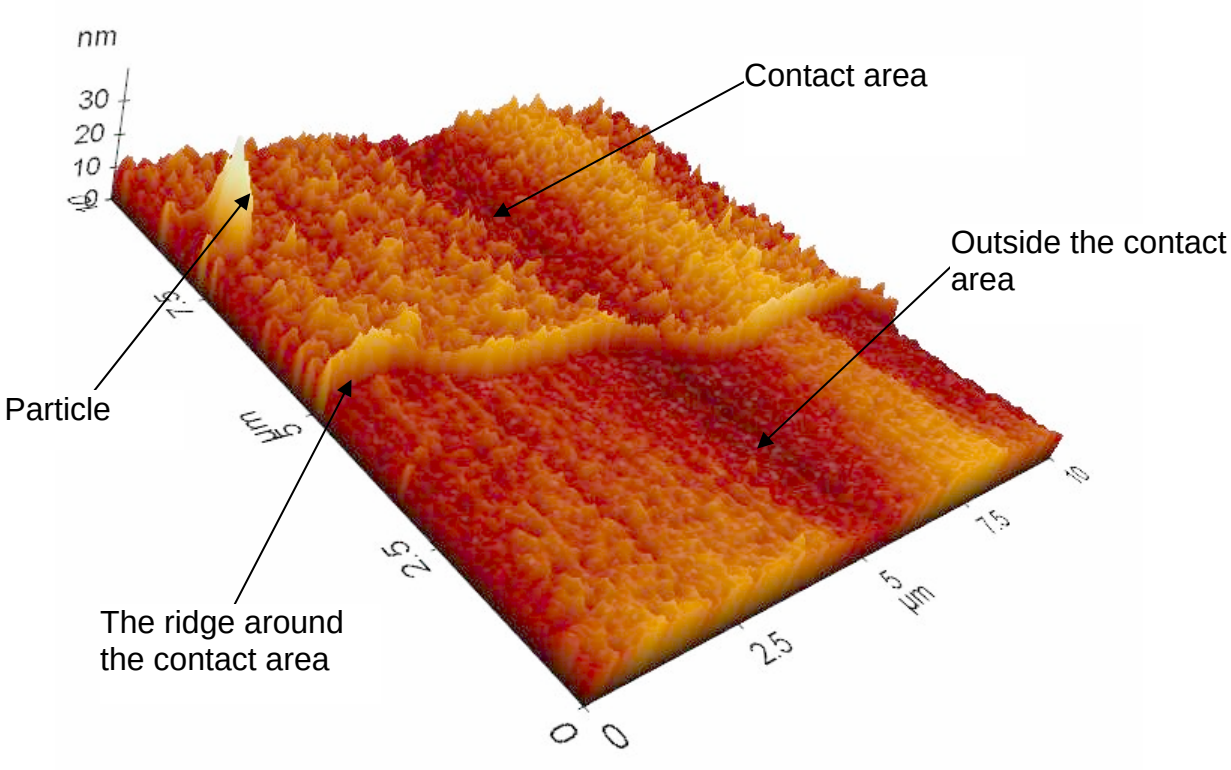

Figure 61. AFM image of ZY13_ h after the electrochemical experiment. The scanned area is 10x10 µm. The height axis has a minor division than the length axis's in order to bring out the structure.

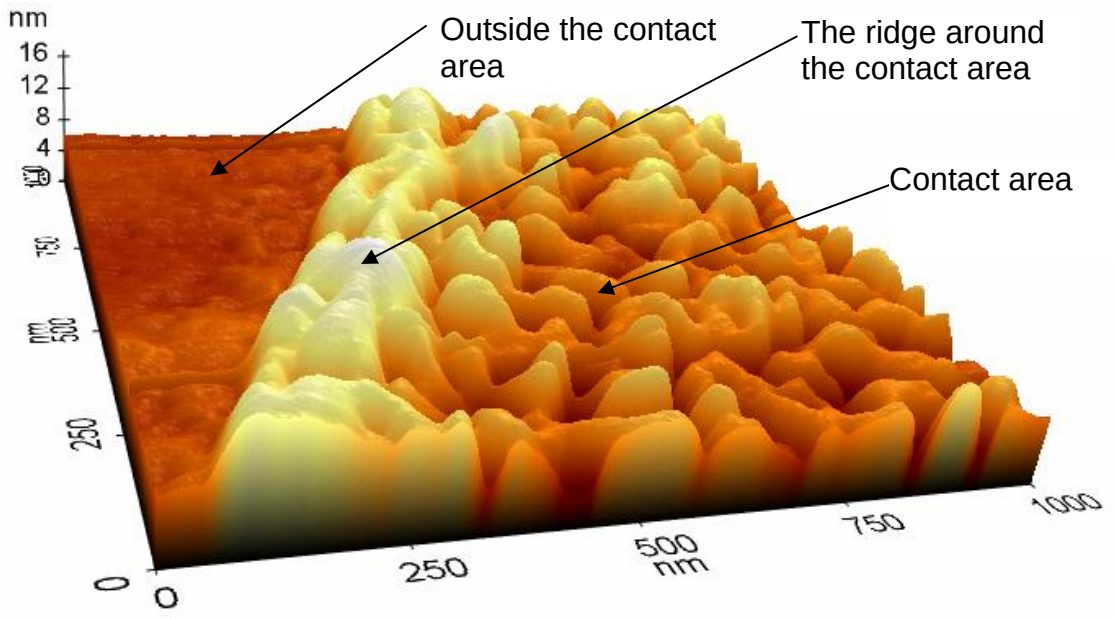

Figure 62. AFM image of ZY13_ h after the electrochemical experiment. The scanned area is 1x1 µm. The height axis has a minor division than the length axis's in order to bring out the structure.

7.4.2 Electrochemistry

7.4.2.1 Area specific resistance

The contact area between the Ni wire and SZ increases during the experiment due to creep of the Ni wire, this is seen as a decrease in the R_s value. The R_s value is related to the radius of the contact area through[4]

$$R_S = \frac{1}{4 \cdot \sigma \cdot r}, \tag{24}$$

where σ is the ionic conductivity and r is the radius of a circle. In this case the contact area is elliptic and an equivalent radius is used, i.e. $r = \sqrt{\alpha \cdot \beta}$, where 2α and 2β are the length of the long and short axis of the elliptic contact area. The contact areas are determined by SEM after the electrochemical experiment. As the contact area in the end of the experiment corresponds to the R_s value from the end of the experiment, the area throughout the experiment are calibrated according to this. The activation energies for R_s, which are used to calibrate between different temperatures were derived from the impedance measurements from the cooling run. The area specific resistance (ASR) is calculated ($ASR \equiv R_p \cdot A$) for comparison between the measurements and electrodes as the contact area (A) increases during the experiment and varies from electrode to electrode.

7.4.2.2 Impedance spectra

Figure 63 and Figure 64 show the first impedance spectra recorded at 500°C for the ZY13 and ZY13_h and ZSc6Y4 and ZSc6Y4_h, respectively. The figures shows that the ASR for the heat treated samples (ZY13_h and ZSc6Y4_h) are higher than for the polished samples (ZY13 and ZSc6Y4).

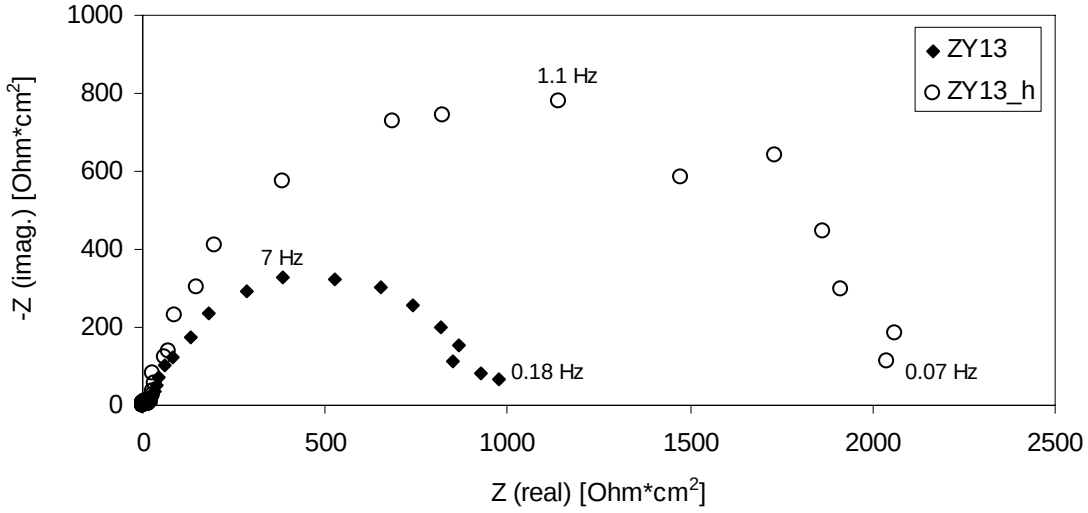

Figure 63. The first impedance spectra recorded for ZY13 and ZY13_h (500°C, 3% H_2O/H_2).

[4] In this relation an infinite thick electrolyte and a circular area is assumed. A relation [23] which matches our samples (not infinite thick and elliptic contact area) deviates less than 5 % from (24) and as 5 % is a small value in this context the simple approximation is used due to the ease of computation.

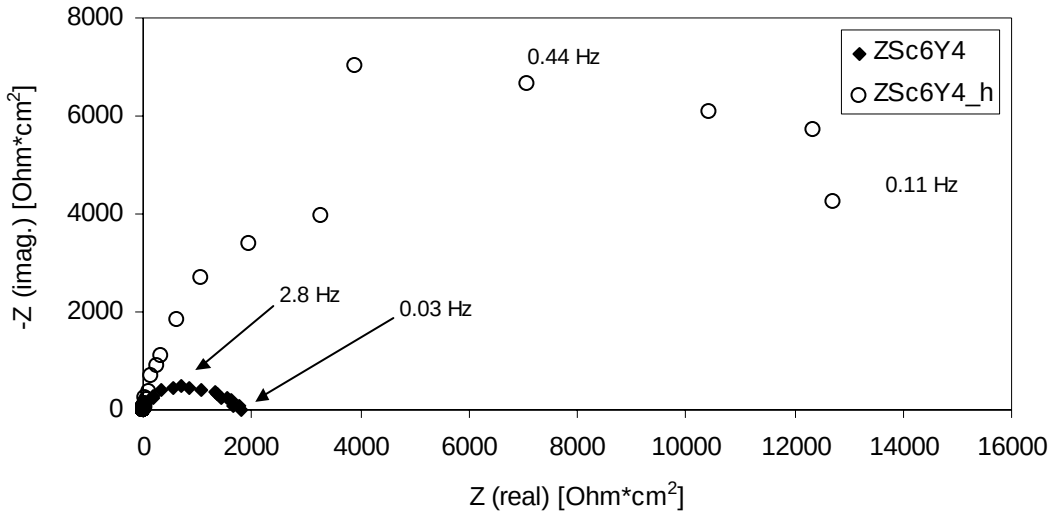

Figure 64. The first impedance spectra recorded for ZSc6Y4 and ZSc6Y4_h (500°C, 3% H_2O/H_2).

7.4.2.3 Time dependence at 500, 600 and 700°C

ASR as a function of time for the four electrodes at 500°C, 600°C and 700°C are shown in Figure 65 - Figure 67.

During the 500°C period the ASR values for all the electrodes increased and they did not reached a stable value before the temperature was increased to 600°C. The electrode that showed the largest relative increase (factor of 7.7) was ZY13_h, otherwise the relative increase was between 2.2 and 3.5, see Table 13.

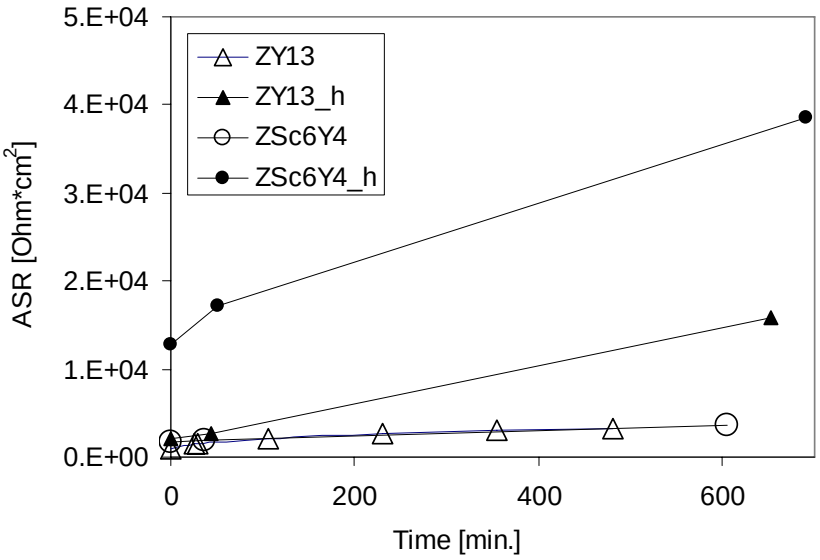

Figure 65. ASR as a function of time at 500°C (3% H_2O/H_2).

Table 13. Initial and final ASR values for the four electrodes at 500°C.

Electrode	$ASR_{initial}$ [Ohm·cm^2]	ASR_{final} [Ohm·cm^2]	$ASR_{final}\backslash ASR_{initial}$
ZY13	944	3320	3.5
ZY13_h	2050	15800	7.7
ZSc6Y4	1700	3660	2.2
ZSc6Y4_h	12700	38500	3.0

During the 600°C period an increase in ASR was also seen for the four electrodes. The scattered measurements are believed to be fluctuations and not erroneous measurement. The relative increase in ASR for the electrodes during this period was between 1.8 and 2.6, see Table 14. The measurement point for ZSc6Y4 that deviates a lot is disregarded in Table 14.

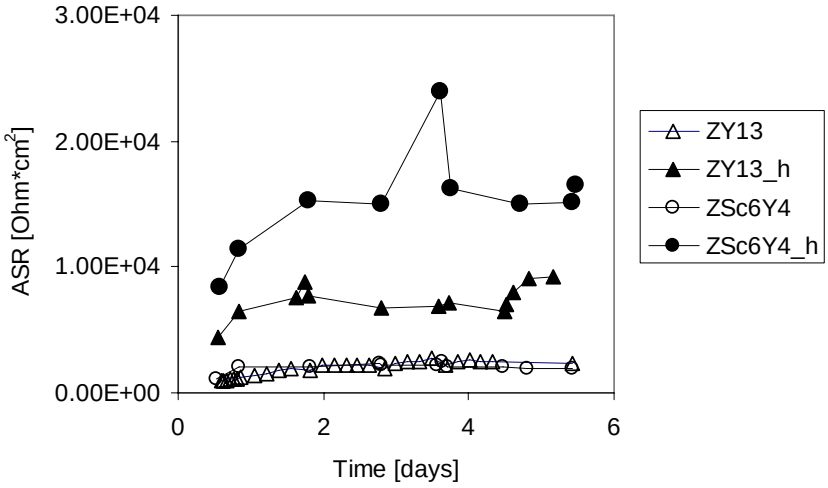

Figure 66. ASR as a function of time at 600°C (3% H_2O/H_2).

Table 14. Initial and final ASR values for the four electrodes at 600°C.

Electrode	$ASR_{initial}$ [Ohm·cm^2]	ASR_{final} [Ohm·cm^2]	$ASR_{final}\backslash ASR_{initial}$
ZY13	922	2370	2.6
ZY13_h	4380	9280	2.1
ZSc6Y4	1060	1960	1.8
ZSc6Y4_h	8400	16500	2.0

At the 700°C the period from day ~5.5 to ~6.5 only a minor increase in ASR for the four electrodes was evident. The relative increase was between 1.1 and 1.3, see Table 15.

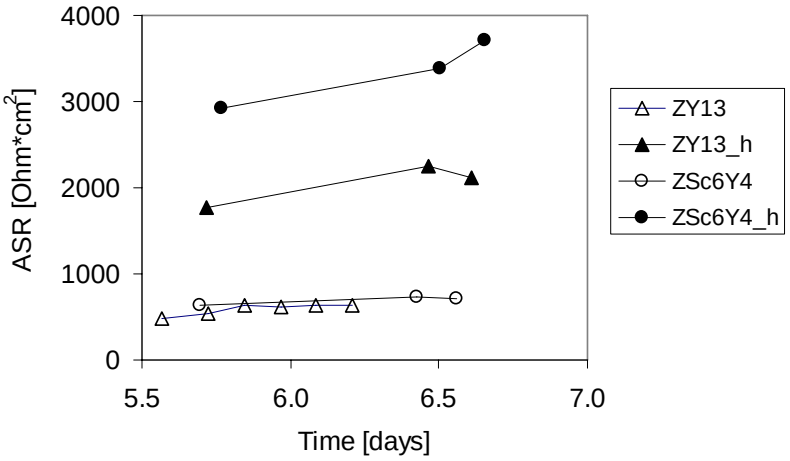

Figure 67. R_p as a function of time at 700°C (3% H_2O/H_2).

Table 15. Initial and final ASR values for the four electrodes at the 700°C period.

Electrode	$ASR_{initial}$ [Ohm·cm^2]	ASR_{final} [Ohm·cm^2]	$ASR_{final}\backslash ASR_{initial}$
ZY13	472	628	1.3
ZY13_h	1770	2110	1.2
ZSc6Y4	640	719	1.1
ZSc6Y4_h	2920	3710	1.3

7.4.2.4 Effect of strong cathodic polarization

After the electrodes became relatively stable at 700°C they were cathodically polarized in dry hydrogen (-1310 mV vs. air, 0.03% H_2O/H_2). Impedance spectra immediately before and after the strong cathodic polarization for the four electrodes in 3% H_2O/H_2 are shown in Figure 68 - Figure 71. The impedance spectra are shown here as log(|Z|) vs. log(frequency) and -Theta vs. log(frequency) in order to show the large change due to the strong cathodic polarization. Theta is the phase angle between the voltage and current. The letter "C" in the legend of the figures refers to the spectra performed after the strong cathodic polarization. The R_p+ R_s and the R_s values can be read at the low and high frequency, respectively (where the phase angle is zero). For the four electrodes the R_p values decrease considerable while no evident change is seen for the R_s value, i.e. the contact area is constant so the decrease in R_p is not an area effect. A single distribution around one frequency corresponds to a single semi circle in the Z(imag.) vs Z(real) impedance plot, which indicates that there may be only one significant rate determining step etc. Before the strong cathodic polarization a clear difference is seen between the heat treated electrolytes and the polished electrolytes. The heat treated electrolytes show two very distinct distributions at high and low frequency, while the polished electrolytes shows two distributions at low frequencies that are more or less overlapping. After the strong cathodic polarization only one distribution around a single frequency is seen for the four electrodes.

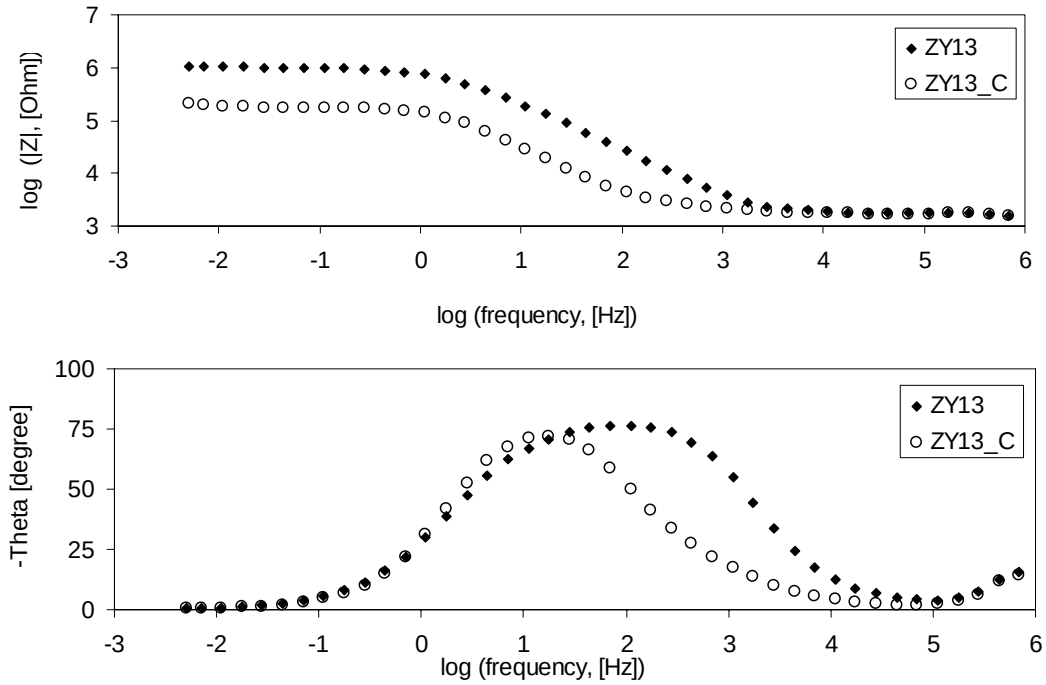

Figure 68. Impedance spectra for ZY13 immediately before (closed symbols) and after (open symbols) a strong cathodic polarization. The spectra are recorded at 700°C in 3%H_2/H_2O.

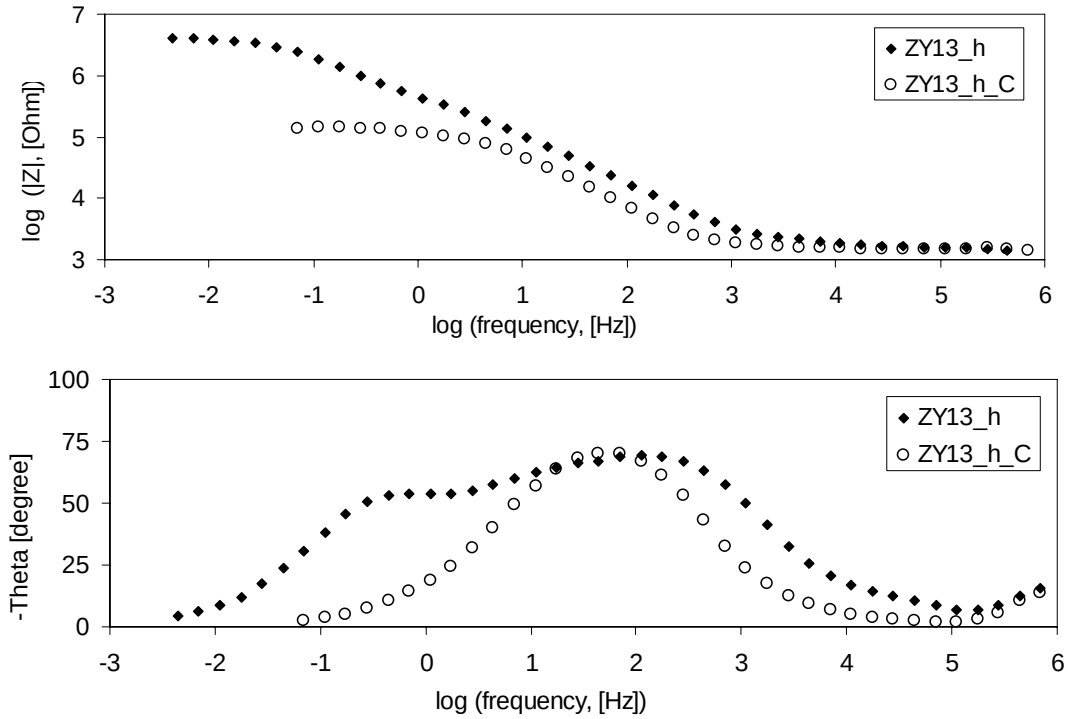

Figure 69. Impedance spectra for ZY13_h immediately before (closed symbols) and after (open symbols) a strong cathodic polarization. The spectra are recorded at 700°C in 3%H_2/H_2O.

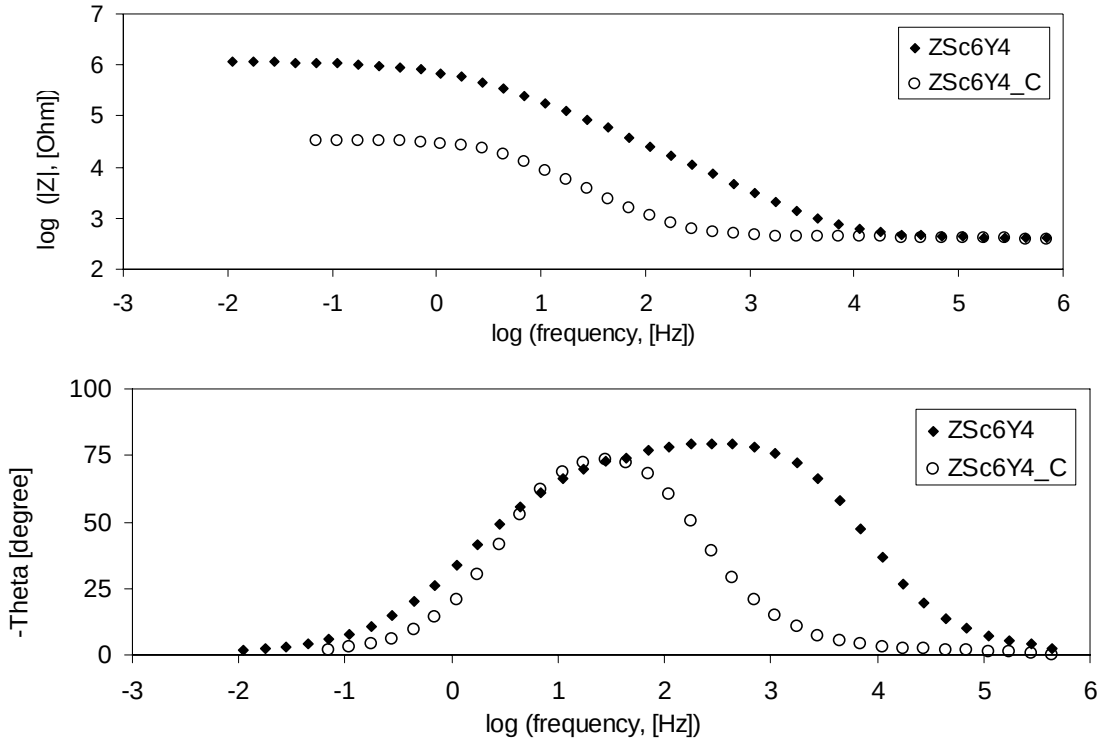

Figure 70. Impedance spectra for ZSc6Y4 immediately before (closed symbols) and after (open symbols) a strong cathodic polarization. The spectra are recorded at 700°C in 3%H_2/H_2O.

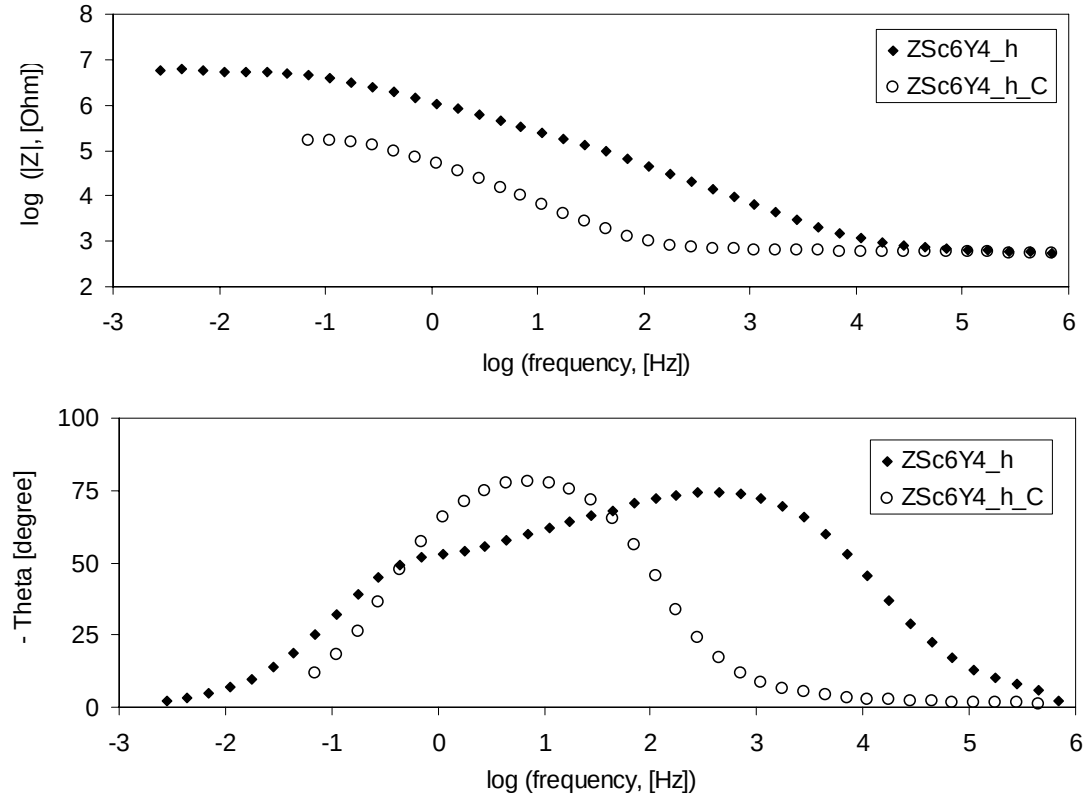

Figure 71. Impedance spectra for ZSc6Y4_h immediately before (closed symbols) and after (open symbols) a strong cathodic polarization. The spectra are recorded at 700°C in 3% H_2/H_2O.

7.4.2.5 Time dependence after the strong cathodic polarization

The ASR for ZY13 decreases from 849 to 156 Ohm·cm^2 due to the strong cathodic polarization, see Figure 72. It is seen that the ASR increases and reaches the same ASR value, after ~7 days, as before the strong cathodic polarization. Some fluctuations are seen after the increase, but the average value is around the same ASR value as before the strong cathodic polarization.

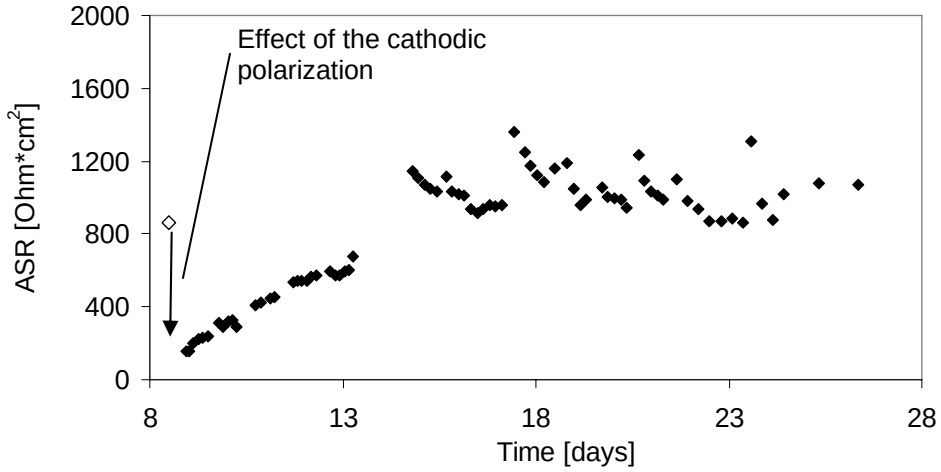

Figure 72. ASR for ZY13 as a function of time after the strong cathodic polarization at 700°C (3% H_2O/H_2). The open symbol represents the ASR value immediately before the strong cathodic polarization. The closed symbols show the ASR values after the strong cathodic polarization.

Figure 73 shows the time dependence of ZY13_h after the strong cathodic polarization. The ASR decreases from 2920 to 121 Ohm·cm^2 after the strong cathodic polarization. Hereafter it decreases until day ~20 where it becomes stable around an average value of about 200 Ohm·cm^2.

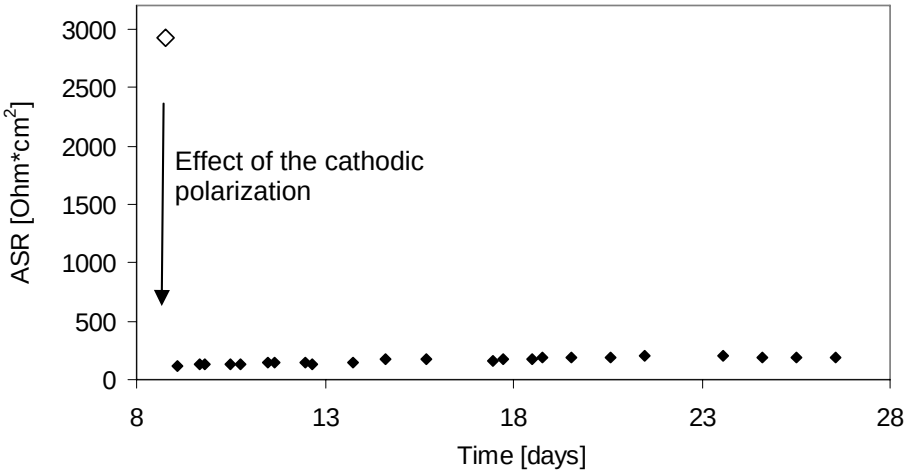

Figure 73. ASR for ZY13_h as a function of time after the strong cathodic polarization at 700°C (3% H_2O/H_2). The open symbol represents the ASR value immediately before the strong cathodic polarization. The closed symbols show the ASR values after the strong cathodic polarization.

After the strong cathodic polarization the ASR for ZSc6Y4 decreases from 1060 to 29 Ohm·cm^2 where after the ASR value increased (see Figure 74). Two linear degradations

profiles are seen: a steep increase from day 9 to day 15 and a less steep increase from day 15 to 27. The later increase do not seem to level out.

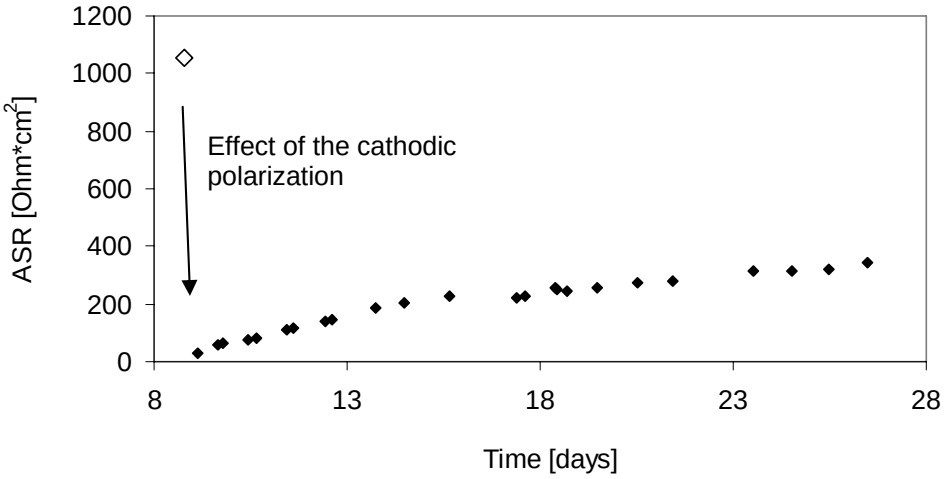

Figure 74. ASR for Zsc6Y4 as a function of time after the strong cathodic polarization at 700°C (3% H_2O/H_2). The open symbol represents the ASR value immediately before the strong cathodic polarization. The closed symbols show the ASR values after the strong cathodic polarization.

The response of ZSc6Y4_h after the strong cathodic polarization is shown in Figure 75. The ASR value decreased to ~130 Ohm·cm^2 after the strong cathodic polarization after which it increases and seems to level out at ~1000 Ohm·cm^2.

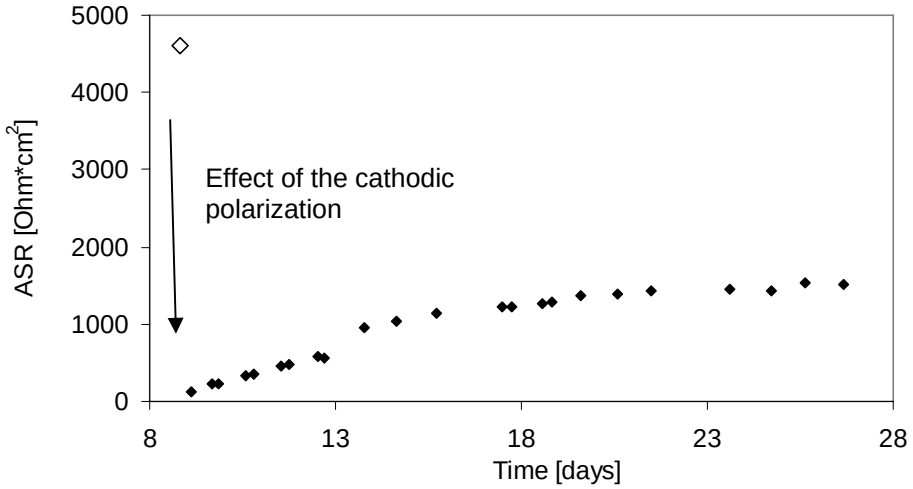

Figure 75. ASR for ZSc6Y4_h as a function of time after the strong cathodic polarization at 700°C (3% H_2O/H_2). The open symbol represents the ASR value immediately before the strong cathodic polarization. The closed symbols show the ASR values after the strong cathodic polarization.

The effect of strong cathodic polarization is summarized in Table 16 together with the activation energies on ASR derived from the cooling run and the amount of current, in coulombs per area, used for reduction. The electrode (ZY13) that showed the highest activation energy (1.1-1.3 eV) was the one that returned to the ASR value it had before the strong cathodic polarization. The other electrodes showed about the same activation energies (0.4-0.65 eV).

Table 16. The effect of strong cathodic polarization on ASR at 700°C together with derived activation energy from the cooling run (700 →500°C). All measurements are performed in 3% H_2O/H_2. ASR_{before}= immediately before the strong cathodic polarization. ASR_{after}= immediately after the strong cathodic polarization. ASR_{15}= 15 days after the strong cathodic polarization.

Electrode	ASR_{before}	ASR_{after}	ASR_{15}	(ASR_{after}/ ASR_{before})*100	(ASR_{15}/ ASR_{before})*100	Cathodic polarization [C/cm^2]	E_a for ASR [eV]
ZY13	849	156	1070	18	126	3.9	1.1-1.3
ZY13_h	2920	121	192	4.1	6.6	4.3	0.5-0.6
ZSc6Y4	1060	29	345	2.7	33	4.8	0.4-0.6
ZSc6Y4_h	4620	133	1520	2.9	33	4.6	0.55-0.65

7.4.2.6 Potential sweeps before and after the strong cathodic polarization

Potential sweeps were performed prior to the strong cathodic polarization and in the end of the 700°C period after the strong cathodic polarization (15 days after), see Figure 76 - Figure 79. An overpotential of η=±200 mV was used and the sweep direction was: OCV → cathodic overpotential → anodic overpotential → OCV. The sweep rate was 5 mV/s. Hysteresis are seen for all the four electrodes: at cathodic overpotentials a capacitive loop is seen and at anodic overpotentials an inductive loop is seen. Arrows are given in cases where the hysteresis can be seen on the graphs. A different characteristic in current is seen between anodic and cathodic overpotentials. At anodic overpotentials the current increases non-linearly, while there seems to be a limiting current at cathodic overpotentials.

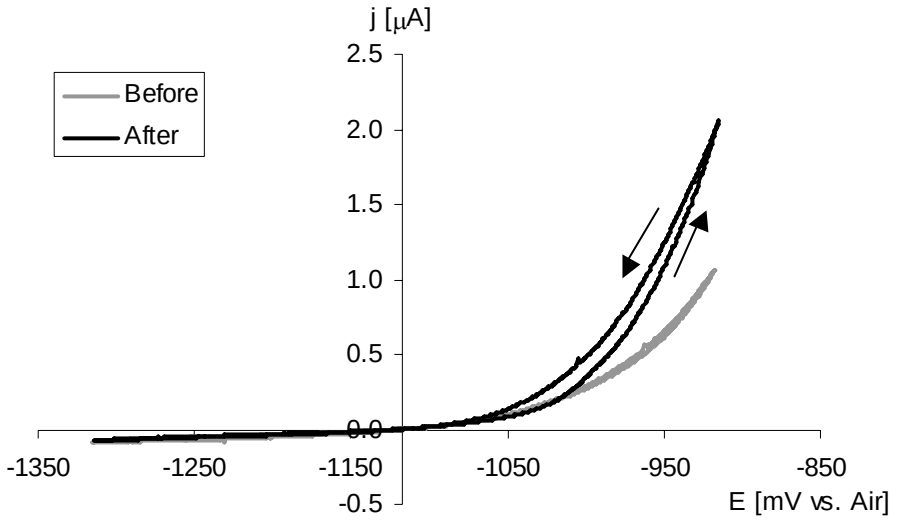

Figure 76. Potential sweep for ZY13 (5 mV/s) at 700°C in 3%H_2O/H_2. Before = Potential sweep before the strong cathodic polarization. After= Potential sweep 15 days after the strong cathodic polarization. Sweep direction: -1117 → -1317 → -917 → -1117 mV vs. air. EMF= -1117 mV vs. air.

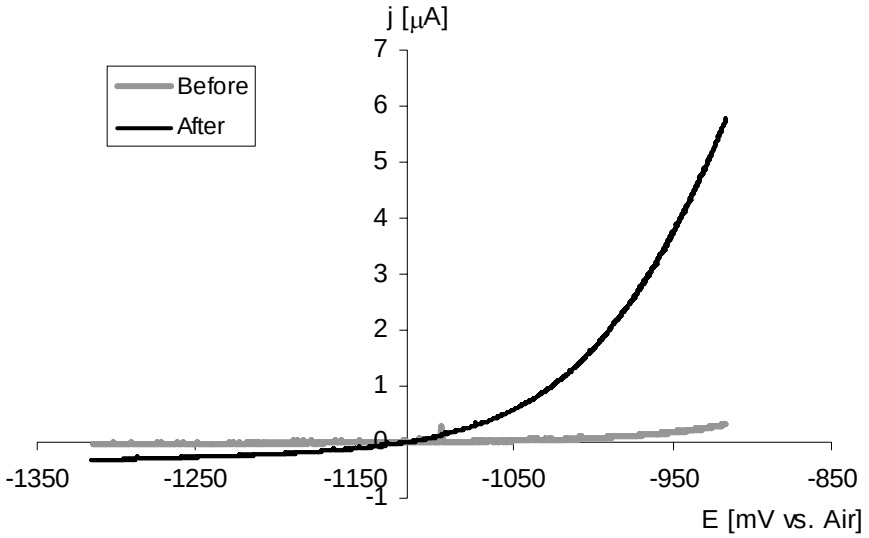

Figure 77. Potential sweep for ZY13_h (5 mV/s) at 700°C in 3%H_2O/H_2. Before = Potential sweep before the strong cathodic polarization. After= Potential sweep 15 days after the strong cathodic polarization. Sweep direction: -1117 → -1317 → -917 → -1117 mV vs. air. EMF= -1117 mV vs. air.

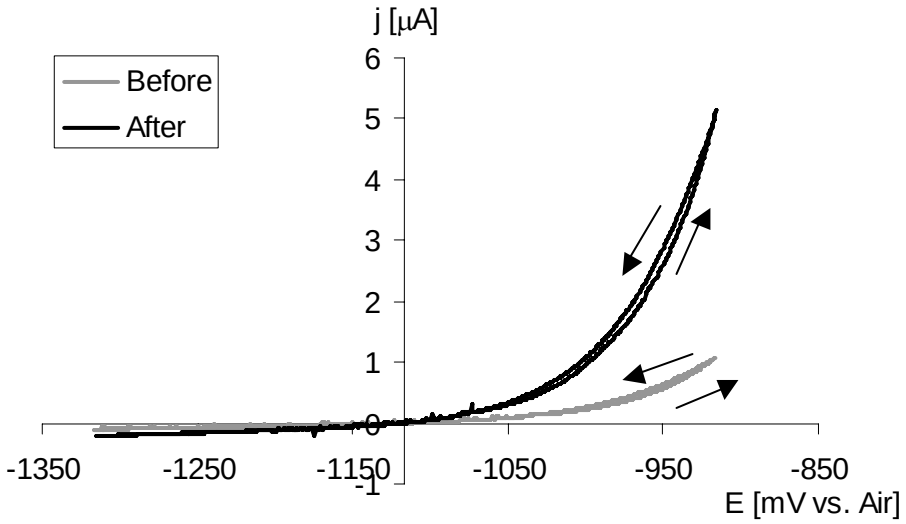

Figure 78. Potential sweep for ZSc6Y4 (5 mV/s) at 700°C in 3%H_2O/H_2. Before = Potential sweep before the strong cathodic polarization. After= Potential sweep 15 days after the strong cathodic polarization. Sweep direction: -1117 → -1317 → -917 → -1117 mV vs. air. EMF= -1117 mV vs. air.

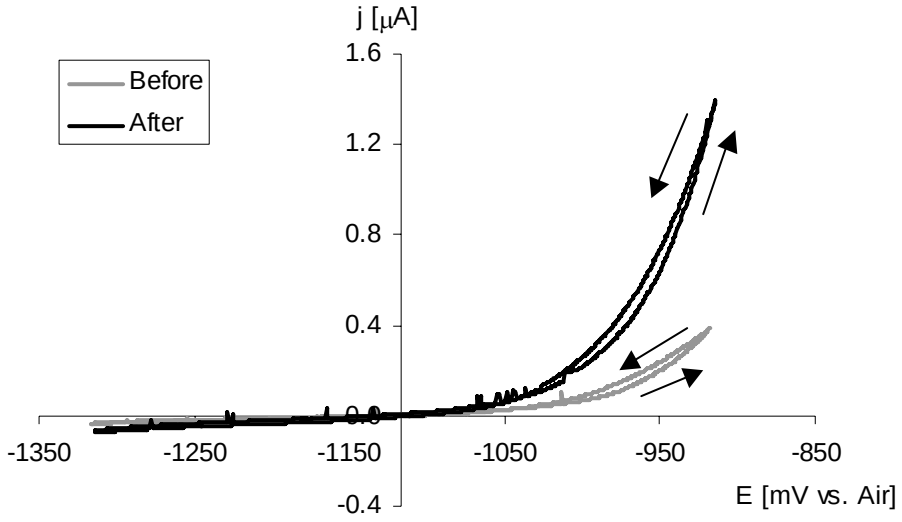

Figure 79. Potential sweep for ZSc6Y4_h (5 mV/s) at 700°C in 3%H_2O/H_2. Before = Potential sweep before the strong cathodic polarization. After= Potential sweep 15 days after the strong cathodic polarization. Sweep direction: -1117 → -1317 → -917 → -1117 mV vs. air. EMF= -1117 mV vs. air.

The current density at η=±200 mV and the ratios between the current densities before and after the strong cathodic polarization are listed in Table 17. Except for ZY13 is it seen that the current densities at η=±200 mV are notably higher after the strong cathodic polarization compared to before the strong cathodic polarization. For the ZY13 no remarkable difference is seen, which corresponds with that fact that the ASR value at OCV were about the same before the strong cathodic polarization and 15 days after the strong cathodic polarization. It is also seen that the current densities are lower for the heat treated samples than the polished samples, which is in agreement with the ASR value at OCV.

Table 17. Extracted data from the potential sweeps performed before the strong cathodic polarization and in the end of the 700°C period after the strong cathodic polarization (15 days after).

Electrode		j at η=200 mV vs. air [μA/cm^2]	j(After)/ j(Before) at η=200 mV	-j at η=-200 mV vs. air [μA/cm^2]	j(After)/ j(Before) at η=-200 mV
ZY13	Before	971	~2	78	~1
	After	1942		83	
ZY13_h	Before	310	~19	44	~7
	After	5750		320	
ZSc6Y4	Before	1020	~5	102	~2
	After	5204		214	
ZSc6Y4_h	Before	336	~4	30	~2
	After	1273		61	

7.5 Discussion

7.5.1 Surface analysis

The XPS result from the two pre heat treated electrolytes showed the presence of Si, Al and Na. No impurities were found on the polished electrolytes. After the electrochemical experiment the Ni wires were removed from the electrolytes and XPS was performed. The

XPS analyzes an area of ~1 cm^2. This means that the signals from the contact area (~0.1 mm^2) are negligible, i.e. the chemical composition outside the contact area is determined. The Si/Zr and Al/Zr ratios for ZY13_h were 0.12 and 0.13, respectively, before the electrochemical experiment and 0.13 and 0.11 afterwards; i.e., the ratios are about the same. For ZSc6Y4_h the Si/Zr and Al/Zr ratios were 0.11 and 0.14, respectively, before the electrochemical experiment and 0.13 and 0.14 afterwards; i.e., also here the ratios are about the same. The Na/Zr ratio for ZY13_h and ZSc6Y4_h were 0.02 and 0.02, respectively, before the electrochemical experiment and 0.18 and 0.24 afterwards; i.e., a significantly increase in the Na content is seen. The same amount of Si and Al, before and after the electrochemical experiment, were expected since the pre heat treatments were at 1450°C and the electrochemical experiment were at 700°C i.e. a higher temperature produces a higher impurity content on the surface [18]. It is believed that the lower Na content seen on ZY13_h and ZSc6Y4_h before the electrochemical experiment is due to evaporation of Na at 1450°C. The time difference between the pre heat treatment (7 days) and the electrochemical experiment (35 days) are not thought to influence the amount of impurities on the surface. Hughes [18] showed that the amount of segregated Si for YSZ single crystals were constant after 300 min at 900°C and as this time scale is much shorter than both 7 and 35 days the time is not believed to be an issue. No impurities were detected on the polished crystals (ZY13 and ZSc6Y4) before the electrochemical experiment. After the electrochemical experiment Si/Zr and Na/Zr ratios were 0.07 and 0.24 and 0.06 and 0.24 for ZY13 and ZSc6Y4 respectively. Again, a lower Si amount was expected for ZY13 and ZSc6Y4 than for ZY13_h and ZSc6Y4_h as they had only experienced a temperature of 700°C. The impurities detected on the electrolytes surfaces are known to segregate to the surface from the bulk of SZ [17,18].
The contact areas on the Ni side did not appear equally smooth after the electrochemical experiment. This is, however, not believed to influence the electrochemical measurement as it was shown in chapter 4 that the difference in appearance of the contact areas did not seem to influence the electrochemical measurement.
The structure, detected with AFM, on the ZY13_h surface after the electrochemical experiment was as expected from the work by Vels Jensen [10], i.e. formation of a hill and valley structure in the contact area and the formation of a ridge around the contact area. The ridge from the work of Vels Jensen's work consisted of impurities and it was concluded that a higher impurity content of the electrode materials produces a larger rim. It is therefore thought that the ridge from ZY13_h also consists of impurities, but this has not been confirmed. The ridge from ZY13_h is about 2-10 nm high and the purity of the Ni and YSZ is 99.99 % and 99.999 %, respectively. Vels Jensen used YSZ with a purity of 99.91-99.94 % and reported rims of 0.25 and 1.6 μm for a purity of the Ni of 99.995% and 99.8 %, respectively. This is in agreement with the fact that the higher impurity content produces a higher rim. The fact that Vels Jensen's electrode experiments were at 1000°C compared to 700°C used here might influence the size of the rim as a higher impurities content is seen at the surfaces as function of temperature. Also, the strong cathodic polarization may influence the size of the rim.
The hill and valley structure in the contact area is presumable formed due to the interaction between the Ni and SZ. The formation of the ridge is probably due a redistribution of impurities in order to lower the interfacial free energy as explained by Vels Jensen [10].

7.5.2 Electrochemistry

7.5.2.1 Initial impedance spectra at 500°C

The initial impedance spectra at 500°C are interesting as they provide information on the electrodes in the state where minimum degradation has occurred. The ASR values were

higher for the heat treated samples than for the polished samples. The ratio between the ASR values of ZY13 and ZY13_h was 2.2 and the ratio between ZSc6Y4 and ZSc6Y4_h 7.5. In chapter 6 it was shown that the electrolyte composition had no influence on the ASR. Hence, it could be expected that the ratios between the heat treated and polished samples were the same for the electrodes. However, it must be considered that the segregated impurities on the heat treated samples lies in a thin layer (1-20 Å, see chapter 6). This thin film might be brooked up while placing the Ni wire on the electrolytes. A broken impurity layer is not thought to impede the electrode process as much as a non broken layer. So if the film was broken on ZY13_h and not ZSc6Y4_h this could be an explanation to the different ratios of 2.2 and 7.7.

7.5.2.2 Time dependence at 500, 600 and 700°C

The ASR for the four electrodes increased a factor of 2.2 – 7.7 during the 500°C period, see Table 13. It was expected that the ASR for the polished samples (ZY13 and ZSc6Y4) would increase as this was seen in chapter 6 for similar electrodes. The increase is presumably due to segregation of impurities and the formation of a rim. An increase in the ASR for the heat treated samples was not expected as no further segregation is believed to take place at 500°C when the electrolytes (ZY13_h and ZSc6Y4_h) were heated at 1450°C for a week. However the formation of a ridge might be the explanation to the increase. An explanation could also be that the impurity film was broken up while placing the Ni wire onto the electrolyte and a subsequent reorganization of the impurities caused the increase. Even though the ASR values were not relaxed during the 500°C period the temperature was increased to 600°C. This was done because the resistance of the heat treated electrodes became large (~10^8 Ohm) and this resistance resulted in large scatter in the impedance spectra due to a low signal to noise ratio. During the 600°C period the ASR values for all the electrodes increased a factor 1.8 – 2.6 (see Table 14) and the temperature was raised to 700°C, again due to the high resistances. During the 700°C period the ASR values only increased by a factor 1.1 – 1.3 (see Table 15), which indicates that the ASR values are becoming stable. No evident difference in ASR between the different electrolytes (ZY13 and ZSc6Y4) is seen. This is in agreement with the conclusion from chapter 6 that ASR is independent of the electrolyte composition.

7.5.2.3 Effect of strong cathodic polarization

Immediately after the strong cathodic polarization was performed the ASR values decreased while the R_s values remained unchanged for all the electrodes, see Figure 68 - Figure 71. Also, some characteristic changes were seen in the phase angle (theta) as a function of the frequency. After the strong cathodic polarization all the electrodes shows only one distribution around one frequency. Before the strong cathodic polarization there seems to be a distribution around two overlapping frequencies at high frequency for the samples that were initially pure on the surface (ZY13 and ZSc6Y4). For the heat treated samples (ZY13_h and ZSc6Y4_h) two characteristic distributions were also seen; one at high frequency and one at low frequency. A single distribution around one frequency indicates that there may be only one significant rate determining step. This means that the number of rate determining steps decreases due to the strong cathodic polarization.

7.5.2.4 Time dependence after the strong cathodic polarization

The ASR's 15 days after the strong cathodic polarization resistance were: 1) ZY13 had approximately the same ASR as before the strong cathodic polarization, 2) ZY13_h remained almost unchanged after the strong cathodic polarization and 3) ZSc6Y4 and ZSc6Y4_h regained ~1/3 of the ASR after the strong cathodic polarization. Note that in the case of ZY13 and ZY13_h the final ASR value for ZY13_h was lower than for the ZY13

i.e. now the impure electrode shows the lowest ASR. Also, the activation energy for ASR was considerably higher for ZY13 probably because it had recovered its ASR value (see Table 16). As seen from Table 16 ZY13, which recovered its original ASR value, was polarized with 3.9 C/cm^2. The three other electrodes were polarized with 4.3-4.8 C/cm^2. This could indicate that ~3.9 C/cm^2 is a critical amount for if an electrode is to recover to its original ASR value after a strong cathodic polarization under the given conditions.

7.5.2.5 Potential sweeps

The current density at $\eta=\pm200$ mV was used as a characteristic value to compare the potential sweeps. Prior to the strong cathodic polarization both the current density at cathodic and anodic overpotentials were higher for the polished electrolytes than for the heat treated electrolytes, which is in agreement with the ASR values at OCV. Except for the ZY13 at $\eta=+200$ mV, the ratios between the current densities before and 15 days after the strong cathodic polarization show the same trend as the corresponding ASR values, i.e. the current densities had increased and the ASR (OCV) had lowered. For ZY13 at $\eta=+200$ mV the current density is ~2 times as larger than compared to the value before the strong cathodic polarization, see Table 17. A similar value would be expected when comparing to the ASR value at OCV, see Table 16. However, a factor of ~2 is low compared to the ratio of the three other samples, which is 4-19, so it is not sought as an significant difference. Also, the ASR (OCV) values fluctuates so the difference in current densities seen at $\eta=+200$ mV might be due to fluctuations. Comparing the current densities at $\eta=\pm200$ mV with the ASR value at OCV one find that they show the same trend i.e. a larger ASR value goes with a smaller current density (see Table 16 and Table 17). This indicates that the ASR value at OCV is a characteristic parameter for both the anodic and cathodic current densities. This means that only measurements at OCV for different electrodes are necessary to determine which electrode that shows the highest current density at anodic and cathodic polarization. The non linear increase in the cathodic current at cathodic overpotentials seen at below -1200 mV vs. air at 700°C in chapter 5 was not seen for any of the electrodes here. However, it is believed that the increase would appear if a slightly (~100 mV) higher cathodic potential than -1317 mV vs. air at 700°C was applied.

7.6 Conclusion

The electrolytes that were pre heated treated at 1450°C showed the same amount of Si and Al on the surface before and after the electrochemical experiment, while the amount of Na had increased significantly. The lower Na content on the heat treated electrolytes are probably due to Na evaporation at 1450°C. The initially pure electrolyte showed Si and Na on the electrolyte surface after the electrochemical experiment. Si, Al and Na are all known to segregate from the bulk to the surface of SZ. The electrolyte surface developed a hill and valley in the contact area, i.e. the Ni/SZ interface is dynamic. A ridge around the contact area was also seen.

The ASR value for the electrodes increased significantly during the 500 and 600°C period. At the 700°C period only a minor increase was evident. For the pure electrodes the increase is ascribed to segregation of impurities to the surface and the built up of a ridge near or at the TPB. For the impure electrodes the increase is ascribed to a reorganizing of the segregated impurities and the built up of a ridge near or at the TBP. The electrodes with the impure surfaces showed a higher ASR than the electrodes with the pure surface. This indicates that the impurities on the electrolyte surface are an important factor for the polarization resistance. The strong cathodic polarization decreased the ASR at OCV (700°C, 3% H_2/H_2O) to 3-18 % of the ASR value before the strong cathodic polarization. No consensus about the long time stability of the strong cathodic polarization effect was

observed: ZY13 recovered its original ASR value, ZY13_h remained almost constant after the polarization and ZSc6Y4 and ZSc6Y4_h recovered to ~1/3 of their original ASR value. The ASR value at OCV was found to be a characteristic parameter for the anodic and cathodic current densities. This means that only measurements at OCV for different electrodes are necessary to determine which electrode that shows the highest current density at anodic and cathodic polarization.

8 Surface analysis of YSZ and the Ni wire

In this chapter collected surface analyses from the Ni wires and YSZ are shown. It will be shown that the impurities seen on the YSZ surface presumably originates from the bulk and that a recurring segregation takes place after removal of the impurities. Also, the difficulties with determining Ca from XPS will be discussed. The amount of Si and Na on the surface as a function of heat treatment temperature is commented. Analyses of the sulfur content on the Ni wire as a function of the temperature are shown and discussed.
The analyses of the Ni wires and YSZ crystals are partly from the electrodes used and partly from other heat treatments. The analysis shown from the Ni wire and YSZ used as point electrodes are from outside the contact area. In that way the segregation of impurities should not be influenced by the electrochemically experiment and can be interpreted as heat treatments.
The XPS and AES apparatus used for the following analysis are described in chapter 6.

8.1 Surface analysis of YSZ

8.1.1 Recurring segregation and impurities from the surroundings

The following experiment was performed in order to investigate if an YSZ crystal wrapped in Pt foil (not sealed) and heat treated would shown the same amount of impurities on the surface as a crystal that was directly exposed to the surroundings (not wrapped in Pt foil). The later corresponds to the electrolytes in an electrode experiment. Also, it was tested if the impurities on the surface after a heat treatment would reoccur after being removed by polishing and heat treated again. The experiment was performed using a $(ZrO_2)_{0.87}(Y_2O_3)_{0.13}$ single crystal (ZY13). The experimental procedure and the detected impurities is listed below:

Step no.	Action	Si/Zr
1	Polishing of the crystal	
2	XPS	0
3	Heat treatment (1000°C, 3% H_2O/H_2, 7 days)	
4	XPS	0.19
5	Polishing of the crystal	
6	XPS	0
7	Heat treatment of the crystal wrapped in Pt foil (1000°C, 3% H_2O/H_2, 7 days)	
8	XPS	0.19

After polishing of the crystal no impurities was detected on the surface, except from carbon that originates from adsorbed organic species in the atmosphere. Trace amount of Na and Al were detected in step no. 4. Otherwise Si was the only impurity seen. The amount of Si (Si/Zr=0.19) was the same whether the crystal was wrapped in Pt foil or not. This indicates that the Si is segregating from the bulk YSZ. If the Si was a contaminant from the surroundings a lower Si content would be expected from the crystal wrapped in Pt foil. Furthermore no Si was detected on the Pt foil used for wrapping the crystal, both the inner and outer side was analyzed. Additionally no Si was found on the Ni wires that were heat treated in the same furnace used for heat treatments of the YSZ crystals. The two above observations confirms that the Si is not coming from the surroundings but is segregation from bulk of YSZ. No Pt was detected on the YSZ crystal that was wrapped in Pt foil.

The experiment also shows that Si keeps segregating to the surface after being removed by polishing. This recurring segregation is also seen by de Ridder *et al.* [17].

8.1.2 Difficulties in determine Ca with XPS

Ca was not quantified with XPS as the electron binding energies for the major lines falls close together with Zr (see Table 18). Indications of the Ca Auger peak LMM at 964 eV (Mg anode) were seen in some XPS spectra. For the crystal that was heat treated with the Pt foil the Ca/Zr ratio was determined with AES to 0.1. Ca was also detected by TOF-SIMS on the electrolytes described in chapter 5. From this it seems plausible that Ca is present on surface of heat treated YSZ crystals even though it is not evident from the XPS spectra. Note that a step size of 0.5 eV was used in the XPS spectra were the major lines of Ca and Zr were seen to overlap (not shown). It would be desirable to perform a high resolution scan (narrow scan) to see if the major lines could be separated.

Table 18. Binding energy for the major lines for Ca that fall close together with the lines for Zr [29].

	Binding energy [eV]		Binding energy [eV]
Ca $2p_{3/2}$	347	Zr $3p_{3/2}$	330
Ca $2p_{1/2}$	351	Zr $3p_{1/2}$	343
Ca 2s	440	Zr 3s	430

8.1.3 Temperature dependence of Si and Na

The Si/Zr and Na/Zr ratios were collected for the ZY13 single crystals after various heat treatments, see Figure 80 and Figure 81. The crystals were polished before each heat treatment in that way a clean surface was the starting point for all the heat treatments. Different atmospheres were used for the heat treatments, which make the comparison more difficult. It is however believed that the major factor influencing the segregation behavior is the amount of water and the temperature. The uncertainty in determination of the amount of impurities with XPS is investigated on electrolyte ZY18 in chapter 6. Here the relative low Si/Zr ratio of 0.02 was found. This sample was chosen to get an upper limit of the uncertainty as higher uncertainty is expected from a low amount of impurities. The sample was measured four times with the XPS. These measurements was analyzed and it was found that the results deviated by ±12 %, hence this uncertainty is assumed in all measurements. There seems to be a maximum Si/Zr ratio between 0.15-0.20 that is reached at around 700°C. The relative large difference in Si/Zr ratio at 700°C is difficult to explain as the other surface contamination is Na and this ratio is about the same in the two cases. Also, the indication of the Ca Auger peak LMM was very weak in both cases. The lower Si/Zr ratio at 1000°C is probably due the higher water content, which causes Al to appear on the surface. This is seen to lower the Si/Zr ratio in section 9.3. The Na/Zr ratio peaks at 700°C and is presumably not stable on the surface at 1000 and 1450°C, hence the lower ratios.

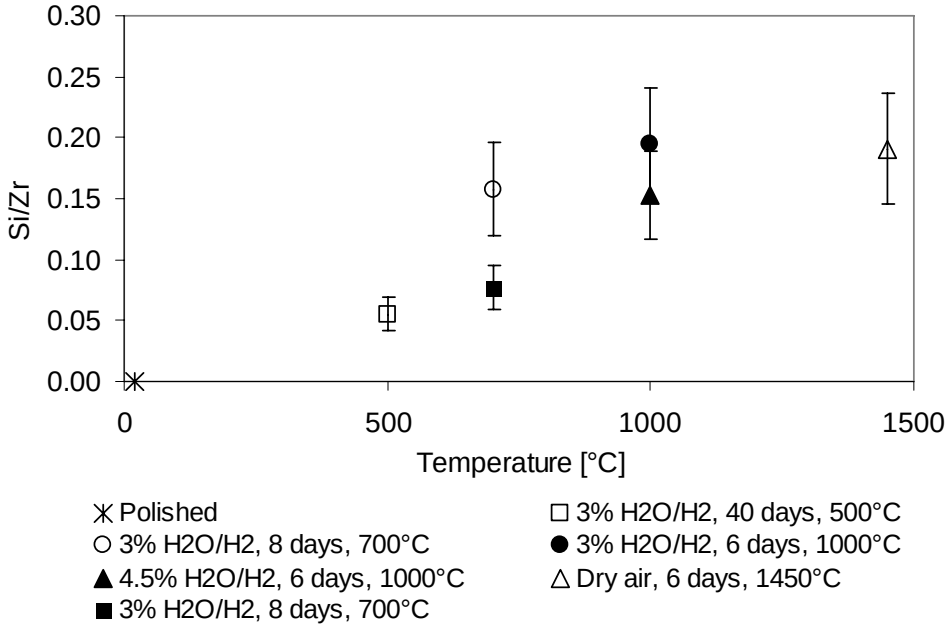

Figure 80. Si/Zr ratio as a function of heat treatment temperature for $(ZrO_2)_{0.87}(Y_2O_3)_{0.13}$ single crystal. The different atmospheres and heat treatment time is indicated by symbols. The error bars are ±12 %.

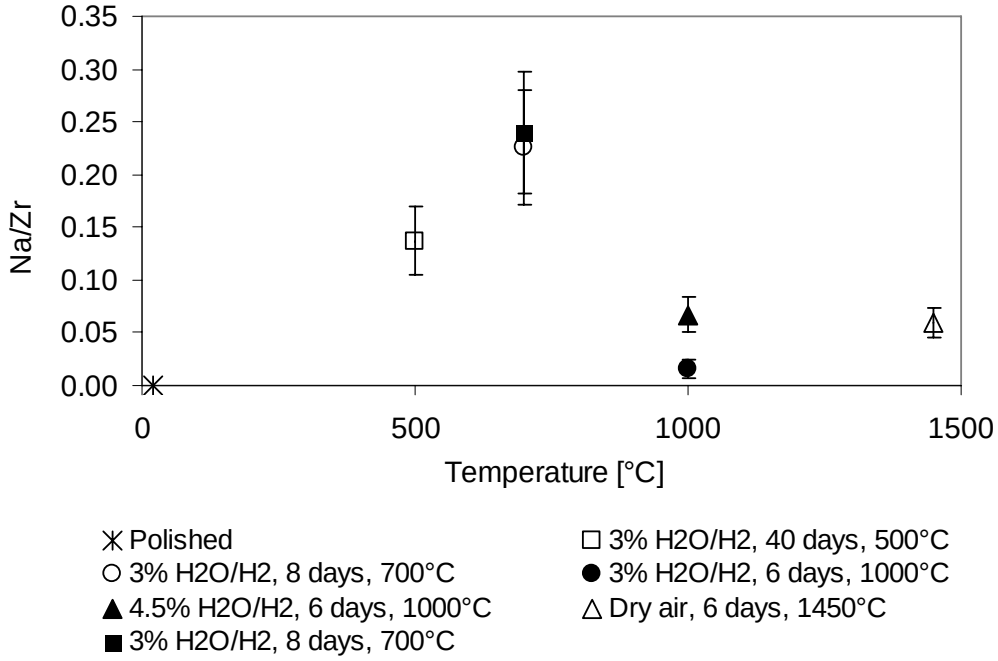

Figure 81. Na/Zr ratio as a function of heat treatment temperature and atmosphere for $(ZrO_2)_{0.87}(Y_2O_3)_{0.13}$ single crystal . The different atmospheres and heat treatment time is indicated by symbols. The error bars are ±12 %.

No evident yttria segregation was seen for the ZY13 single crystal. This might be due to the relatively high yttrium content. No yttria segregation was seen for the ZY10 and ZY18 single crystals from chapter 6, but it had experienced at maximum temperature of 500°C only. In the case of the ZSc6Y4 single crystal used in chapter 6 and section 9.3 no yttria or

scandia segregation were evident. Yttria segregation was seen for the ZY8 polycrystalline sample from section 9.3 only.

8.2 Surface analysis of the Ni wire

The element of most interest detected on the Ni wire, with AES, is sulfur as this is known to increase the polarization resistance of the H_2/H_2O/Ni/YSZ electrode reaction [1,24]. AES depth profiles of the sulfur content for Ni wires heat treated at various temperatures are shown in Figure 82. The depth profiles were performed using an ion gun with 2 keV Ar^+ and a current of 45 $\mu A/cm^2$. The point at 0 s for the 1000°C are not easily explained. Also, it is not completely understood why sulfur is detected after 40 s sputtering for the Ni wire heat treated at 700°C as there seems to be less sulfur than on the 1000°C. As seen in Figure 45, oxygen and carbon is also detected on the Ni wire as the Ni wires are exposed to the atmosphere before the AES measurement. These impurities are found in about the same amount on the Ni wires shown in Figure 82. So the oxygen and carbon cannot explain the difference in appearance of the sulfur. The sulfur detected on the electro polished Ni wire is also believed to originate from the atmosphere. Also, the small amount of sulfur (0.06 ppm, see Table 6) that is present in the Ni wire is under the detection limit for the AES. Overall the figure is interpreted as: a higher temperature produces a higher sulfur content and the sulfur signal disappears at around 30 s.

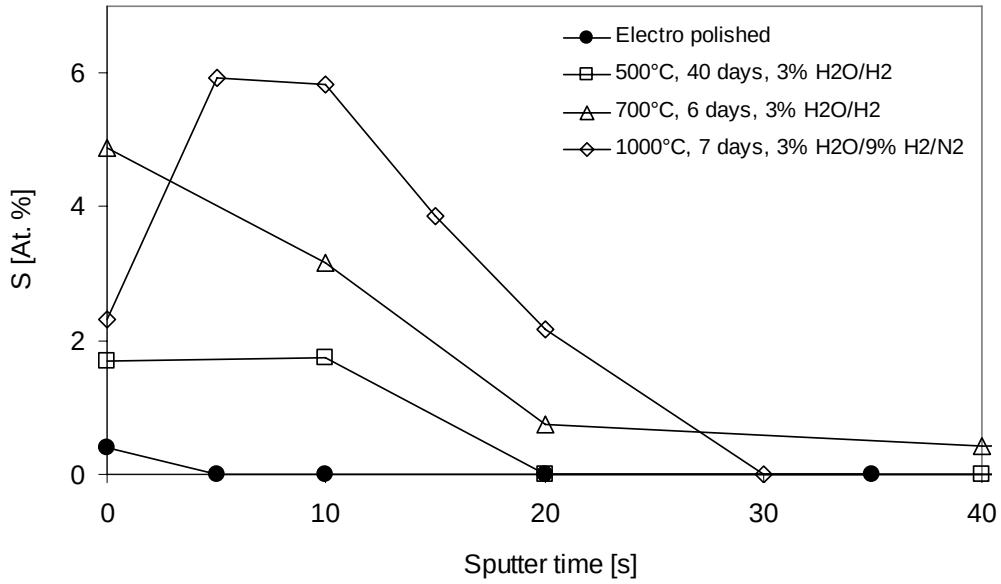

Figure 82. Sulfur content as a function of sputter time for heat treated Ni wires. The depth profiling was performed using 2 keV Ar^+ and a current of 45 $\mu A/cm^2$.

If the sulfur segregates to the surface the concentration of sulfur will increase on the surface and be detectable with AES, i.e. the same phenomenon as Si in SZ. A first analysis of Figure 82 would be that a higher temperature produces a higher sulfur concentration on the surface of Ni similar to Si in SZ. However, according to thermodynamics [30] the NiS should react with H_2 to form volatile H_2S at ≤ 300°C even at a relative high content of H_2S on 0.1 vol.%. The gasses used in the setup were H_2 (>99.9 %) but there was no certificate on the sulfur content. The supplier informed that the impurities mainly were N_2 (700 ppm), O_2 (10 ppm) and H_2O (15 ppm). For the nitrogen the purity was 99.8 % and the supplier informed that the sulfur content was on the ppb level. This indicates that the H_2S content would be far below 0.1 vol.%, hence according to thermodynamics there should be no S

present at the surface at ≤ 300°C. From this one would expect a Ni wire free of sulfur during a heat treatment. However, it should be kept in mind that the thermodynamic data are from bulk material and the surface is presumably more reactive. So it is not straightforward to interpret Figure 82, i.e. it is not clear whether the sulfur is segregating from the bulk of the Ni wire or is coming from the surroundings i.e. gas, gas tube system, electrochemical setup etc. The explanation to the higher sulfur content on the surface if sulfur is coming from the surroundings could be that there is a source of sulfur in the system that evaporates at high temperature.
The following calculations deal with the surface coverage of sulfur on the Ni wire. If the sputter yield (Y) is set to 3 (as for pure Ni [31]) the sputter time can be converted to a depth using (25)[19].

$$\frac{dz}{dt} = \frac{I \cdot M \cdot Y}{e \cdot A \cdot \rho \cdot N_A}$$

$$= \frac{1.8 \cdot 10^{-6}\ A \cdot 58.7\ g/mol \cdot 3\ atoms/Ar_{ion}}{1.6 \cdot 10^{-19} C \cdot 0.04\ cm^2 \cdot 8.9\ g/cm^3 \cdot 6.022 \cdot 10^{23}\ atoms/mol} = 0.9\ Å/sek \qquad (25)$$

In equation (25) I is the sputter current, M is the molar mass of Ni, e is the charge of an electron, A is the sputter area, ρ is the density of Ni and N_A is the Avogadro constant. If a monolayer of Ni is set to ~2.2 Å it would take 2.5 s to remove one monolayer of Ni. This indicates that several layer of NiS are present on the heat treated Ni wires.
Another way of analyzing the results is to calculate the time it takes for every Ni surface atom to collide with an Ar ion. The number of Ni surface ions is calculated from

$$Ni_{surface} = \left(\frac{\rho \cdot N_A}{M}\right)^{2/3} = \left(\frac{8.9\ g/cm^3 \cdot 6.022 \cdot 10^{23}\ atoms/mol}{58.7\ g/mol}\right)^{2/3} = 2 \cdot 10^{15}\ Ni/cm^2 \qquad (26)$$

The density of Ar ions is $2.8 \cdot 10^{14}$ Ar/(cm^2·s) i.e. every surface Ni atom would collide with a Ar ion after ~7 s. As the sputter process is random it must be expected that it take longer time for all the Ni surface atoms to collide with an Ar ion. If it take four times as long time, which seems realistic, all of the surface Ni atoms would be hit after 28 s. This is about the time that the S signal disappears for the heat treated Ni wires. Except for the Ni wire heat treated at 1000°C, this indicates that the S are not fully covering the whole Ni surface. The small amount of sulfur seen on the electro polished Ni wire is expected when the sample has been exposed to the atmosphere.

8.3 Conclusion

The Si detected on the surface of YSZ is presumable segregated from the bulk. The Si on the surface could be removed by polishing. After removal of the Si and a subsequent heat treatment Si was detected again. A higher heat treatment temperature produces a higher Si/Zr ratio.
The origin of S on the Ni wire is unknown. It is also unknown if the S is fully or partly covering the Ni wire.

9 Removal of trace impurities from YSZ

9.1 Abstract

In chapter 6 it was sought to perform electrochemical measurements at a relative low temperature (500°C) to avoid segregation impurities. However Si was still detected on the surface of the stabilized zirconia single crystals used. It is tedious to perform point electrode measurements at lower temperature due to the low signal to noise ratio and the long time required to perform an impedance spectra. A long time is needed because the resistance is high and this means that the relaxation time of the electrode is long, i.e. a long time is needed to obtain the low frequency intercept with the real axis. Another way of avoiding the impurities is to remove them totally. Trace amount of impurities are always present in YSZ and observation of segregated impurities to the surface for the purest YSZ materials available have been reported by de Ridder *et al.* [17]. An experiment was also performed by de Ridder *et al.* where an YSZ sample (99.922%, 780 ppm of impurities) was heat treated 13 times at above 1000°C and after each treatment the segregated impurities were removed by sputtering. After each heat treatment the surface composition of Si, Na, Ca and O was the same. It was estimated that 4 ppm of impurities was removed. This means that if the sample should be totally cleaned by this method approximately 2500 heat treatments with subsequent cleaning would be needed. Even if a 99.99 % clean sample was used (same dimensions) it would demand 325 heat treatments with subsequent cleaning. A route where the impurities are continuously removed at high temperature seems necessary to avoid a large amount of repetitions. Two different routes of removing the trace impurities from the YSZ were investigated: 1) Continuously removal by sputtering on a heated YSZ sample in a vacuum chamber and 2) Reaction with H_2O at high temperature to form volatile Si compounds.

9.2 Removal of trace impurities by sputtering

9.2.1 Introduction

From fundamental catalysis studies of metals in vacuum chambers it is well known that impurities are segregating to the surface when heat treatments are performed. A common routine before using a metal for investigations is to clean it by sputtering at high temperature. A metal sample is easy to heat (> 1000°C) by sending current through. YSZ is an electronic insulator and the same route cannot be used for heating. Several heating methods were discussed: 1) Heating on a plate, 2) heating by light and 3) heating by AC using the oxygen ion conductivity. It should be noted that one side of the heated YSZ sample must be free so that sputtering can be performed. The aim was to heat the sample to above 1000°C in order to get a high segregation rate so that the cleaning could be performed within a reasonable time scale (a week). A heating plate of metal seems problematic because it has to be warmer than the YSZ sample and that would produce a vapor pressure of the metal, which might contaminate the YSZ sample. Heating by light might also be problematic as the crystal is transparent so other parts of the vacuum chamber might be heated considerable. Heating with AC was therefore chosen as this would heat the YSZ directly and therefore have the minimum heat transfer to the vacuum chamber in which sensitive equipment is located e.g. X-ray gun, electron gun, electron analyzer, sputter gun.

9.2.2 Experimental and results

Initial heating experiments were conducted in a test vacuum chamber with no sputter or analysis equipment, to test if it would be possible to heat a YSZ sample with AC. The YSZ sample is a poor oxygen ion conductor at room temperature and it is therefore necessary to preheat the sample to ~300°C. The preheat treatment was performed with a filament located ~3 mm from the YSZ sample, i.e. the YSZ sample was preheated by radiation. An alumina sheet was used to cover the filament in order to limit cross contamination from the filament to the sample, see Figure 83. The reason that AC is used instead of DC is that the experiment is conducted in vacuum, i.e. there is no oxygen to react at the electrodes and be conducted through the sample. The frequency of the AC must be high enough to avoid electrode reactions e.g. reduction of YSZ. The frequency was set to 10 kHz.

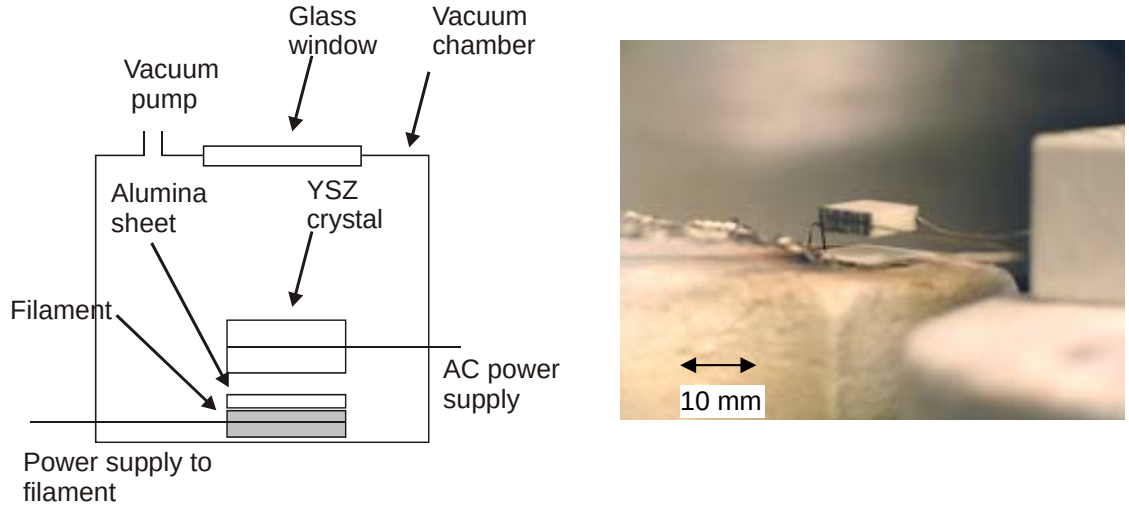

Figure 83. A) A schematic of the heating setup for heating a YSZ sample with AC in a vacuum chamber. B) Picture of the YSZ sample with electrodes on each side. A heating filament for pre heating is placed below the YSZ sample. An alumina sheet is covering the filament in order to limit direct evaporation of the filament to the YSZ sample.

The pressure in the chamber was measured to 1-2 mmHg by a Pirani-probe. The vacuum was achieved by using a Trivac-pump from Leybold-Heraeus. The preheating filament was connected to a standard power supply. The AC voltage was generated from a Toellner (TOE 7402) frequency generator and amplified with an PA1000 from LD-systems, which can supply maximum of 140 V. A transformer (Torid, model TA500/30, 2x30 V to 2x115 V) was used to achieve an even higher voltage, i.e. the available voltage was $\left(140\,V \cdot \frac{115\,V}{30\,V}\right)$ 540 V. An oscilloscope (Philips PM3384) was used to monitor the phase angle between the voltage and the current. A schematic of the electrical system is shown in Figure 84.

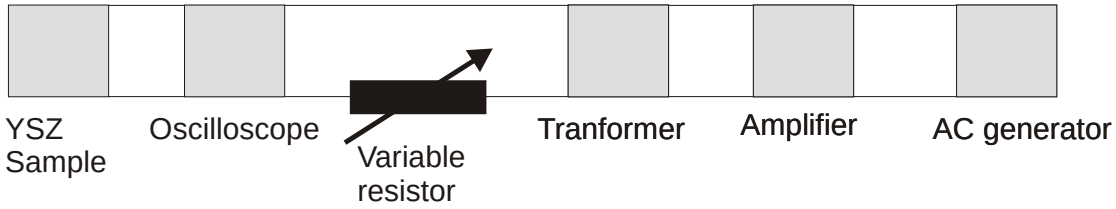

Figure 84. Schematic of the electrical system used to heat the YSZ sample.

It was first tried to heat a polycrystalline $(ZrO_2)_{0.97}(Y_2O_3)_{0.03}$ (10x10x3 mm), in order not to damage a single crystal. Grooves of 10x0.5 mm were made on each side on two of the parallel 10x3 mm sides. Platinum paste was painted in the grooves and platinum wires (Ø=0.5 mm) were inserted. Finally, platinum paste was painted all over the two 10x3 mm sides and it was fired at 1300°C (2 h, 150°C/min).
The heat transfer from the sample to the surroundings at a given temperature of the sample is equal to the power needed to keep the sample at this temperature, i.e. the number of watts that should be supplied. In the following it is sought to calculate the number of watts needed as a function of the temperature of the YSZ sample. The heat transfer can take place through the Pt wires and via radiation. The heat conduction through the two Pt wires is calculated from the following formula [32]

$$Q_{Pt\,wires} = k \cdot \frac{A}{l} \cdot \Delta T\,, \tag{27}$$

where k is the thermal conductivity, A is the area of the terminal surface and l is the length of the Pt wire and ΔT is the temperature gradient. A mean value for the thermal conductivity, in the temperature span (800-1400°C), of Pt was chosen, 0.87 W/(cm·K) [33]. The thermal radiation was calculated using the following formula [32]

$$Q_{thermal\,emmision} = \varepsilon \cdot \sigma \cdot A \cdot \left(T_1^4 - T_2^4\right), \tag{28}$$

where ε is the emission factor, σ is the Stefan-Boltzmann constant ($5.67 \cdot 10^{-8}$ W/(m^2·K^4)), A is the surface area of the YSZ sample and T_1 and T_2 are the temperature of the sample and surroundings respectively. The emission factor for zirconia is 0.18-0.43 [33] and is strongly dependent on the surface roughness. In general a rough surface produces a higher emissivity. The emissivity is here set to 0.43 to get the upper limit for the watts needed. Figure 85 shows the number of watts that are transferred from the sample to the surroundings as a function of temperature. The temperature of the surroundings were ~20°C. It is seen that the thermal conduction through the Pt wires is negligible compared to the emission at above ~400°C.

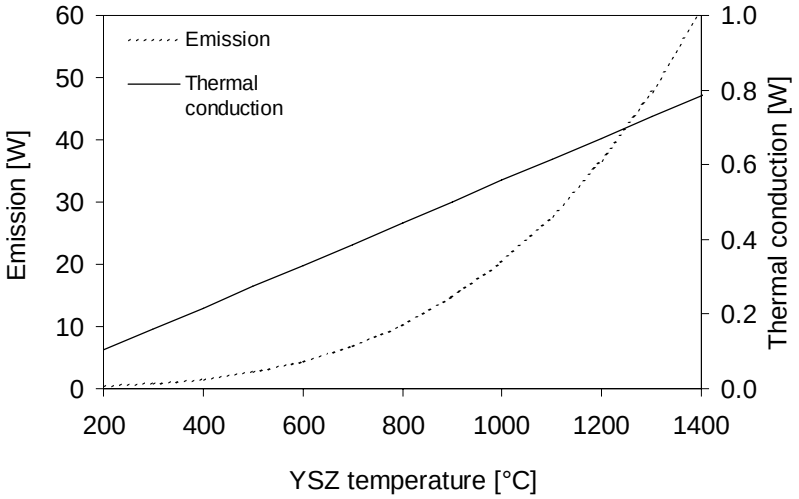

Figure 85. Heat conduction from a heated YSZ sample. The thermal conductivity and emission are calculated from equation (27) and (28) respectively. The temperature of the surroundings was 20°C.

The voltage needed across the YSZ sample can be calculated by the watts needed to keep the YSZ sample at a certain temperature and the ionic conductivity (resistance) of the YSZ sample [34], see (29). The needed voltage and the resulting current are shown in Figure 86.

$$\sigma_{3YSZ} = 39.98 \frac{S}{cm} \cdot exp\left(\frac{-68.97 \frac{kJ}{mol}}{8.1345 \frac{J}{mol \cdot K} \cdot T} \right). \tag{29}$$

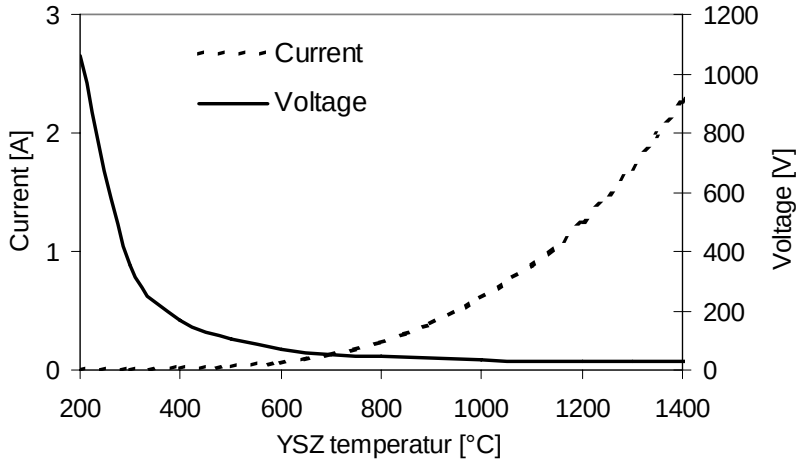

Figure 86. The voltage across the polycrystalline $(ZrO_2)_{0.97}(Y_2O_3)_{0.03}$ (10x10x3 mm) sample and the resulting current as function of the temperature.

As seen from Figure 86 the voltage changes three orders of magnitude. This requires high demand of the voltage source. It is therefore desirable to preheat the sample as this lowers the initial voltages needed. The voltage needed decreases exponential with increasing temperature. As the voltage across the sample is controlled manually there is a risk for current "run away", i.e. very rapid heating because the resistance of the sample lowers and the voltage is kept constant. This rapid heating is sought to avoid, as it most likely will

cause the YSZ sample to crack due to mechanical stress (thermal shock). To limit the risk of "run away" a variable resistor (0-100 Ω) was inserted in series with the YSZ sample.
The procedure for heating the sample was first to put a high AC voltage over the YSZ sample and then preheat it with the filament until the AC had an effect, i.e. until the sample was warm enough for ion conduction to take place. In the beginning when the sample was cold no ion conduction occurs as the displacement between current and voltage was 90°, i.e. the AC had no effect. As the sample were preheated the displacement changed towards 0° and heating by AC was initiated. Corona discharge was observed when applying higher than ~300 V (10 kHz). This was seen as a blue/violet light. The Corona discharge was sought to avoid as it was not possible to distinguish between the current used to heat the YSZ sample and the current for the corona discharge. That is to say there would be no control over the number of watts there is supplied to the sample when corona discharge occurs. The corona discharge may not be a problem when a better vacuum than 1-2 mmHg is available. The heating procedure for the polycrystalline $(ZrO_2)_{0.97}(Y_2O_3)_{0.03}$ is pointed out below:

1. 270 V (10 kHz) was applied across the sample. The voltage and current was monitored with the oscilloscope. The voltage and current was displaced 90°, i.e. no effect was put in to the sample.
2. When the preheating filament was supplied with 20 W a decreasing of the phase angle (displacement) towards 0° was initiated i.e. heat was disposed in the YSZ sample from the AC. While the temperature of the YSZ sample increased (i.e. lowering of the resistance) the voltage was manually lowered to 180 V and the preheating filament was turned off.

The temperature of the sample was determined from the conductivity of the sample (the setup is in principle a conductivity measurement just with a high voltage). From the conductivity the temperature was derived using (29). The temperature determined from the conductivity and the temperature determination from the radiation are in good agreement, see Figure 87.

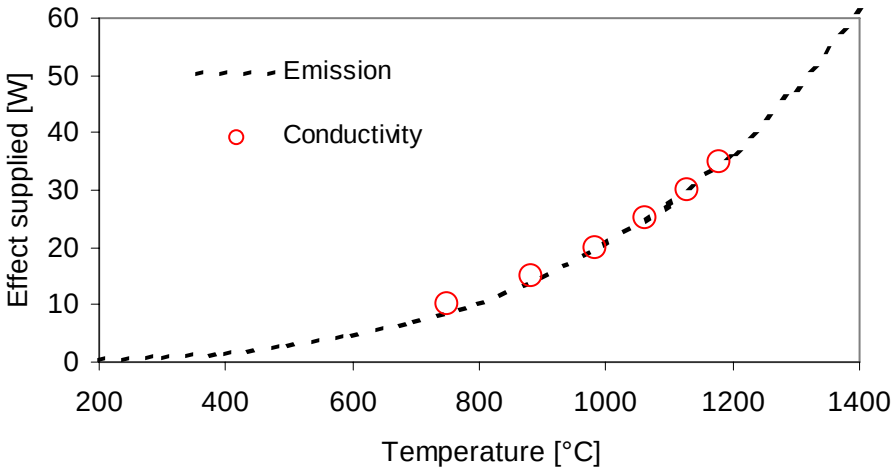

Figure 87. The temperature determined from the conductivity plotted together with the emission curve (ε=0.43).

A photo of the $(ZrO_2)_{0.97}(Y_2O_3)_{0.03}$ (10x10x3 mm) sample when 35 W is applied is shown in Figure 88. It was no problem to maintain a stable temperature of the sample as the resistance in series worked as a voltage divider. If the temperature of the sample should

suddenly drop the resistance would increase and a larger voltage drop over the sample would occur making the situation stable again. The long term stability was tested by keeping the sample heated for two hours. This test proceed satisfactory.

Figure 88. Photo of the $(ZrO_2)_{0.97}(Y_2O_3)_{0.03}$ (10x10x3 mm) sample when heated with AC (10 kHz, 35 W).

The $(ZrO_2)_{0.97}(Y_2O_3)_{0.03}$ sample shown in Figure 88 was quenched due to power failure and then heated again. The sample did not crack during the quenching.

The above experiment was also carried out with a single crystal of $(ZrO_2)_{0.87}(Y_2O_3)_{0.13}$ (10x10x3 mm). Even though the same procedure was used the crystal cracked during heating. Also, when the crystal was quenched an additional crack was formed (see Figure 89).

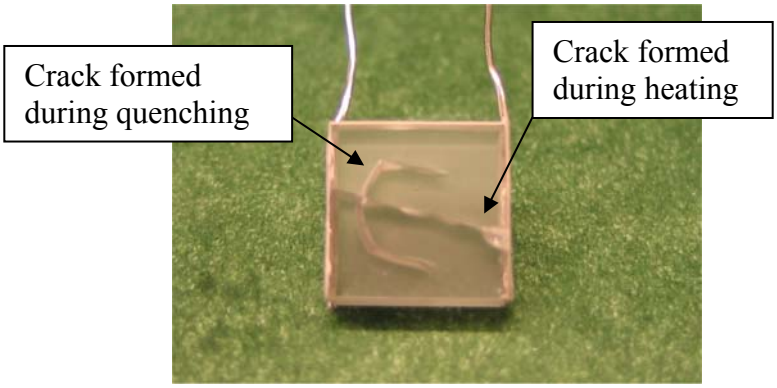

Figure 89. Cracks in the $(ZrO_2)_{0.87}(Y_2O_3)_{0.13}$ (10x10x3 mm) after an AC heating experiment.

It is believed that the single crystal cracked because it is less mechanically robust than the polycrystalline $(ZrO_2)_{0.97}(Y_2O_3)_{0.03}$. It is also believed that the crack is formed in a stationary situation (thermal stress) as the crystal was heated slowly, i.e. no thermal shock. The order of magnitude calculation below shows that the temperature gradient in the sample in the stationary situation can cause the sample to crack, due to thermal stress. The calculation is based on formula (30) [35], which determines the maximum temperature difference before a flat plate cracks. In the derivation of the formula it is assumed that the ends of the flat plate is constrained. This situation is similar to the problem for the AC heating as the surface has a lower temperature than the center, hence the surface is constrained by the lower temperature compared to that of the center. In order to get the maximum allowable temperature one needs maximum strength, minimum Poisson ratio, minimum thermal expansion and a minimum elastic modulus. In equation (30) ΔT_{max} is the maximum temperature difference before fracture, σ_f is the strength, ν is Poisson's ratio, α is the thermal expansion coefficient and E it the modulus of elasticity.

$$\Delta T_{max} = \frac{\sigma_f \cdot (1 - \nu)}{\alpha \cdot E}, \tag{30}$$

The thermal expansion coefficient for a $(ZrO_2)_{0.97}(Y_2O_3)_{0.03}$ polycrystalline and a $(ZrO_2)_{0.87}(Y_2O_3)_{0.13}$ single crystal are $10.5 \cdot 10^{-6}$ K^{-1} and $10.23 \cdot 10^{-6}$ K^{-1}, respectively [24], i.e. this makes no difference for this order of magnitude calculation. The Poisson ratio was set to 0.22 for both the single crystal and the polycrystalline sample. The σ_f and E for a partially stabilized zirconia (~$(ZrO_2)_{0.97}(Y_2O_3)_{0.03}$) are 698-980 MPa and 210-238 GPa and for a $(ZrO_2)_{0.88}(Y_2O_3)_{0.12}$ single crystal they are 346 MPa and 233 GPa [35]. This gives a maximum temperature difference for the single crystal and the polycrystalline sample of ~110°C and ~220-350°C. As this is a realistic temperature difference this might be the explanation for fracture. Other explanations could be flaws in the single crystal or thermal shock.

Other experience gained with heating of $(ZrO_2)_{0.92}(Y_2O_3)_{0.08}$ polycrystalline (ZY8-poly) samples is listed below:

1. When using 200 Hz in stead of 10 kHz the YSZ is reduced. This was clearly seen as a blackening of the YSZ at the Pt electrodes. It was possible to reoxidize the YSZ by heating to 1300°C (2 h) in air, hence it became white again.
2. Temperature measurement with a thermo couple placed directly on the YSZ sample caused it to crack. The thermocouple was made of Pt and 10% Rh/Pt with diameters of 0.3 mm and melted to a spot. The YSZ sample probably cracked because the thermo couple functioned as a cold spot and caused thermal stress.
3. A ZY8-poly sample was placed directly on the preheating filament and heated solely by the filament. It succeeded to heat the sample so it started to glow (~1000°C). After two hours the sample became colder and it stopped glowing. The reason for this was that Pt from the filament had evaporated to the YSZ surface (the surface facing the filament) and functioned as a radiation shield. This meant that less heat was conducted from the filament to the YSZ sample. Note that the main heat transfer at high temperatures is dominated by emission. Furthermore the sample cracked. The crack was probably caused by thermal stress.

9.2.3 Discussion and conclusion

A successfully stable heating of a polycrystalline $(ZrO_2)_{0.97}(Y_2O_3)_{0.03}$ with AC in vacuum was performed. Also, the sample was mechanically stable to thermal stress and thermal shock. When heating a single crystal of $(ZrO_2)_{0.87}(Y_2O_3)_{0.13}$ in a similar manner it cracked. Also, a quenching of the single crystal caused an additional crack. This implies that the single crystal was not stable to thermal stress and thermal chock. The experiment was not preceded into the vacuum chamber with the sputter equipment due to the fact that the single crystal was too fragile.
Another heating method must be considered in order to minimize thermal stress e.g. additional heating with light.

9.3 Removal of impurities by reaction with water at high temperature

9.3.1 Introduction

It is known that SiO_2 reacts with water and form volatile Si-O-H species at high temperatures [36] e.g.

$$SiO_{2(s)} + 2H_2O_{(g)} \rightarrow Si(OH)_{4(g)}. \quad (31)$$

The Si that is detected on the surfaces of SZ is most likely in the form of SiO_2, but it will be refered to as Si. In this experiment it is investigated if the Si on the surface of SZ would be removed by heating in a humid atmosphere at high temperature. The XPS apparatus used for the following analysis is described in chapter 6.

9.3.2 Experimental and results

Three samples were used in the experiment: 1) A single crystal of $(ZrO_2)_{0.87}(Y_2O_3)_{0.13}$ (ZY13), 2) A single crystal of $(ZrO_2)_{0.9}(Y_2O_3)_{0.04}(Sc_2O_3)_{0.06}$ (ZSc6Y4) and 3) A polycrystalline $(ZrO_2)_{0.92}(Y_2O_3)_{0.08}$ (ZY8-poly). To test if the Si would be removed from the surface of the samples by the reaction with water the following experimental series was carried out (XPS measurements were performed on each sample after each step):

1. The crystals were polished to obtain a surface free of impurities.
2. The samples were heat treated in dry air at 1450°C (150 h, 150°C/h) in order to produce Si on the surface.
3. Hereafter a heat treatment at 1450°C (150°C/h) was performed in order to remove the Si. The first atmosphere used in the heat treatment was 8% H_2O/9% H_2/N_2 (240 h, 1450°C). This humid atmosphere should continuously remove the Si as it segregates to the surface. The humid atmosphere was replaced by dry air (26 h) while the temperature was at 1450°C. The dry air was used to control if the Si were totally removed from the samples. If there were any Si left if should show on the surface after the heat treatment in dry air. This heat treatment will in the following be refered to as: 8% H_2O/9% H_2/N_2+dry air.
4. It turned out that the Si was not removed from the surface after the previous step. Additionally Al were also detected after the previous step. In order to see if a surface free of Si could be obtained by a heat treatment solely in a humid atmosphere (8% H_2O/9% H_2/N_2, 200 h, 1450°C) was performed. The heating rate was 150°C/h. The samples were quenched from 1450°C over a period of 2 h. The samples were quenched in order to limit the possibility that Si would segregate during a slow cooling, i.e. the segregation of Si is presumably faster than the removal of Si by water at low temperature.
5. The previous step did not provide a Si or Al clean surface. Finally a heat treatment was performed in dry air at (150 h, 1450°C, 150°C/h) in order to test if the original surface (after step 1) could be reproduced, i.e. if Al would disappear.

The heat treatments were performed in a alumina tube with an inner diameter of 4 cm. The gas flow was 1000 ml/min (20°C, 1 atm), which corresponds to a gas velocity of ~4 m/min at 1450°C and 1 atm.
The XPS spectra of the Si and Al region after each of the above steps for the three samples are shown in Figure 90 - Figure 92. Also, the spectra for the polished samples are shown. The spectrum for the polished polycrystalline $(ZrO_2)_{0.92}(Y_2O_3)_{0.08}$ was provided by Vels Hansen. The Si/Zr and Al/Zr ratios were determined from narrow scans and not the part of the wide scan shown the in figures. The intensity is normalized to the largest signal from the wide scans. The chronology of the spectra in the figures is from below and up. Note that the surface was not polished between the steps.

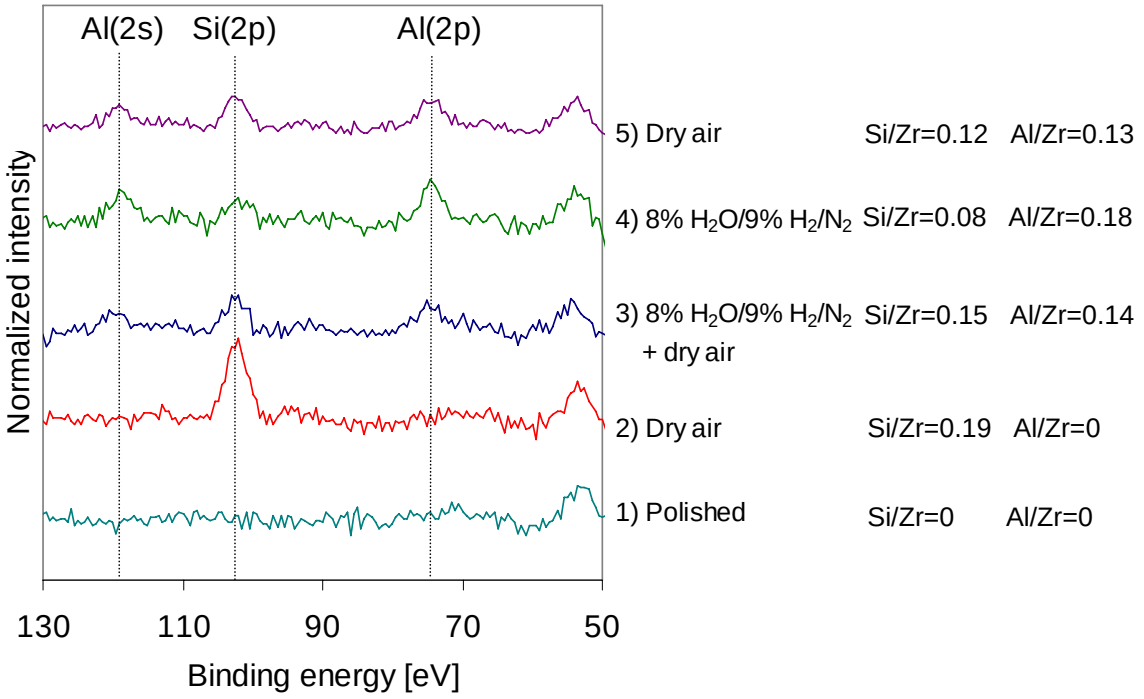

Figure 90. Region of the XPS spectra for the $(ZrO_2)_{0.87}(Y_2O_3)_{0.13}$ single crystal. The intensity is normalized to the largest signal in the wide scan (1100-0 eV). The heat treatments were at 1450°C.

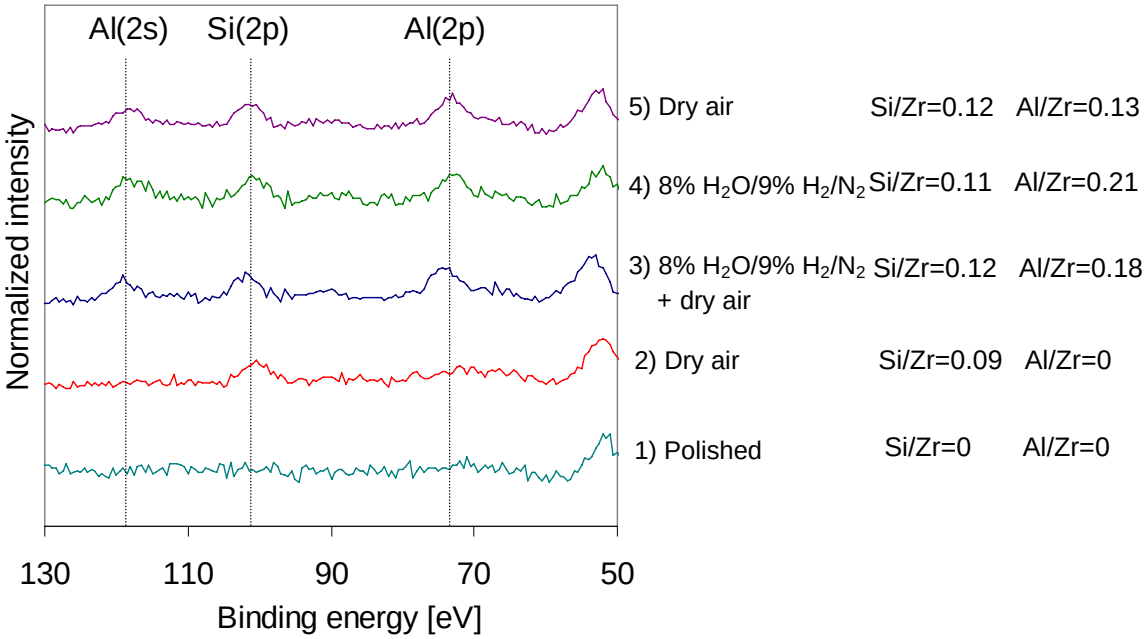

Figure 91. Region of the XPS spectra for the $(ZrO_2)_{0.9}(Y_2O_3)_{0.04}(Sc_2O_3)_{0.06}$ single crystal. The intensity is normalized to the largest signal in the wide scan (1100-0 eV). The heat treatments were at 1450°C.

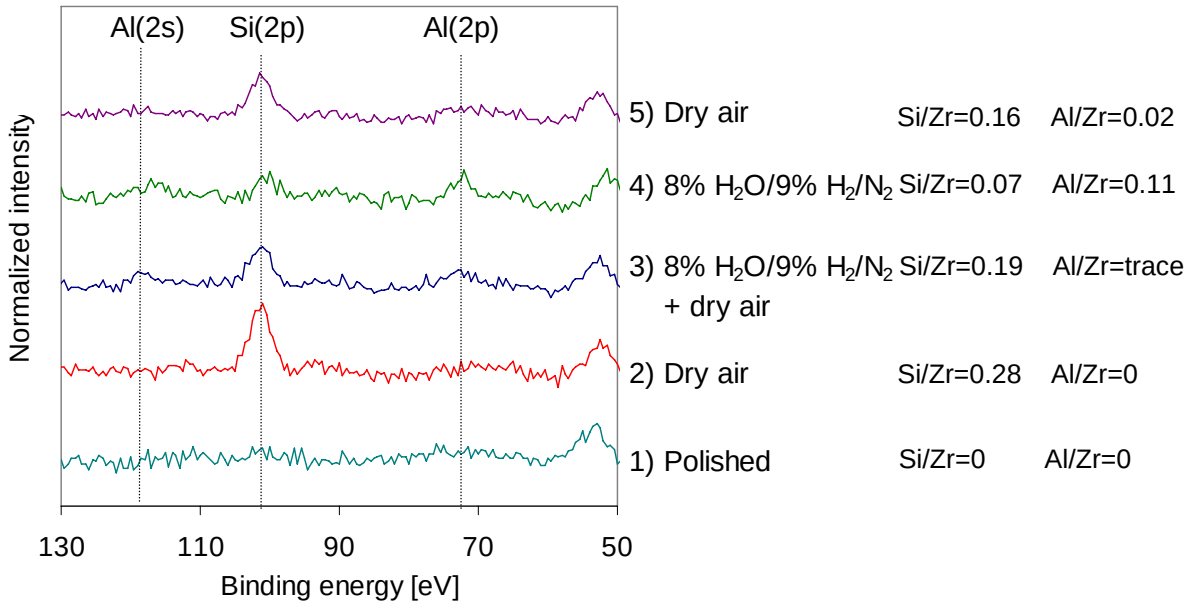

Figure 92. Region of the XPS spectra for the polycrystalline $(ZrO_2)_{0.92}(Y_2O_3)_{0.08}$. The intensity is normalized to the largest signal in the wide scan (1100-0 eV). The heat treatments were at 1450°C.

The Si/Zr, Al/Zr and Na/Zr ratios after each heat treatment for the three samples are summarized in Table 19. The uncertainty of the impurity ratios is assumed to be ±12 % as accounted for in section 8.1.3.

Table 19. Impurities detected with XPS on heat treated electrolytes. ZY13=$(ZrO_2)_{0.87}(Y_2O_3)_{0.13}$, ZSc6Y4=$(ZrO_2)_{0.9}(Y_2O_3)_{0.04}(Sc_2O_3)_{0.06}$, ZY8-poly=$(ZrO_2)_{0.92}(Y_2O_3)_{0.08}$.

Step	Ratio	ZY13	ZSc6Y4	ZY8-poly
1) Dry air	Si/Zr	0.19	0.09	0.28
	Al/Zr	0	0	0
	Na/Zr	0.06	0.05	0.06
2) 8% H_2O/9% H_2/N_2 + Dry air	Si/Zr	0.15	0.12	0.19
	Al/Zr	0.14	0.18	trace
	Na/Zr	0.02	0.01	0.06
3) 8% H_2O/9% H_2/N_2	Si/Zr	0.08	0.11	0.07
	Al/Zr	0.18	0.21	0.11
	Na/Zr	0.02	0.02	0.03
4) Dry air	Si/Zr	0.12	0.11	0.16
	Al/Zr	0.13	0.14	0.02
	Na/Zr	0.02	0.02	0.05

9.3.3 Discussion and conclusion

After the heat treatment in dry air Si was detected on all the samples. After the following heat treatment first in wet hydrogen and then in dry air both Al and Si were detected. The conclusion after the second heat treatment was that the Si was not removed from the samples and that Al is detected after a heat treatment in a relative humid atmosphere (8 %),

i.e. the trace impurities were not removed. Except for the ZSc6Y4 the Si/Zr ratio was lower after the second heat treatment. After the third heat treatment in wet hydrogen Al and Si were still seen. For all the samples there was a trend of a lower Si amount and a higher Al amount. This indicates that the surface is not free of Si at 1450°C in 8 % H_2O, unless the quenching was too slow so that the Si was able to segregate in this period. A trend of a increasing Si/Zr ratio and an decreasing Al/Zr ratio was seen after the fourth and last heat treatment. No obvious trend was found for Na contamination. The trends observed were all more pronounced for the polycrystalline ZY8-poly. It can be concluded that Al is seen when a heat treatment is performed in 8% H_2O/9% H_2/N_2 at 1450°C. It cannot be concluded that Si is removed by reaction with water or if it just suppressed by Al. Hereby meaning that Si is becoming less surface near if Al is located on top of the Si, i.e. in the outer most surface layer. In the same way it cannot be concluded that Al is removed in the last heat treatment as Al and Si might exchange location.
Al is also known to react with water and form volatile compounds at high temperatures [36]. Maybe it would be worth while to perform the heat treatment with optimized parameter for Si and Al removal, i.e. higher temperature, higher water content and higher gas velocity [36].

10 Discussion

In this overall discussion it is sought to draw connections between the individual chapters and to summarize the important observations throughout the project. Also, a more detailed discussion for certain observations is given here as compared to the individual chapters.

10.1 Surface analysis

The surface analysis of the electrode materials (Ni and SZ) after an electrochemical experiment resulted in a sketch of the electrode as shown in Figure 93. The sulfur on the Ni wire was detected with AES. It is not certain whether sulfur is segregating from the Ni or is coming from the surroundings or if it is partly or completely covering the Ni surface. TOF-SIMS images and depth profiles of the SZ crystals indicate that the impurity level is higher outside the contact area than inside the contact area. One AES analysis of the Ni contact area showed traces of Si (chapter 4) so it cannot be ruled out that the impurities stick to the Ni side when removing the Ni wire from the SZ after an electrochemical experiment. Also, the impurity level in the contact area is similar to that of a freshly polished SZ crystal. A homogeneous distribution of the impurities outside the contact area was seen. Many elements are detected with TOF-SIMS but only Si, Na, Ca and Al were detected with XPS and AES indicating that these are the most abundant elements. Al was only detected in the electrode experiment (chapter 5) where the crystal had experienced an atmosphere with above 3% H_2O. This corresponds well with the observations in section 9.3 that Al is detected after a heat treatment in humid atmosphere (8% H_2O/ 9% H_2/N_2) and not in a dry atmosphere (dry air). The thickness of the impurity film produced at 500°C was determined from TOF-SIMS depth profiling to 1-20 Å (chapter 5). The ridge and the hill and valley structure are detected with an AFM. No chemical analysis of the ridge was performed but is it presumably formed by impurities as reported by Vels Hansen [10].

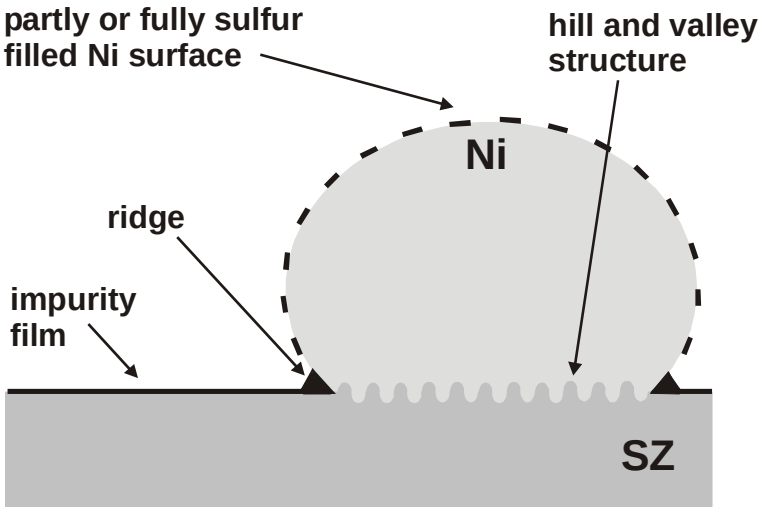

Figure 93. Schematic of the Ni/SZ electrodes that has been studied in this work.

The removal of trace impurities from YSZ samples by reaction with water or sputtering was not successful. In chapter 9 suggestions for further work to remove the trace impurities are given.

10.2 Electrochemistry

The ratio between the maximum and minimum ASR at OCV between four similar Ni/YSZ electrodes, in the same experiment, was found to be 2.6 (chapter 4). Two similar electrodes (one from chapter 5 and one from chapter 7) can be compared to the electrodes investigated in chapter 4. The comparison shows that the ratio between the maximum and minimum ASR at OCV found for the six electrodes was 14. This indicates that it is more difficult to reproduce measurement between experiments than between electrodes in the same experiment. However, the ratio is still lower than the one found by Vels Jensen [10], which was about 200. As concluded in chapter 4, the low variation may be due to the efforts on controlling the impurities, surface roughness, atmosphere and history of polarization. The fact that single crystals were used instead of polycrystalline samples may be important. Finally it should be mentioned that the maximum variation between the ASR values on the same electrode in the same atmosphere was a factor of 2.5.

In chapter 5 it was concluded that the polarization resistance at OCV decreases with increasing water content in the range from ~0.1-3% H_2O. At anodic overpotentials the polarization resistance decreased with increasing water content in the whole range tested (0.1-20% H_2O). The polarization resistance at cathodic overpotentials was found to be independent of the water content. When looking at Figure 94 it is seen that no matter how the water is formed or consumed species (intermediates, reactants, products) must be transported through the ridge, impurity film, Ni and/or the Ni/ridge interface. These transport ways will from now on be refered to as barriers.

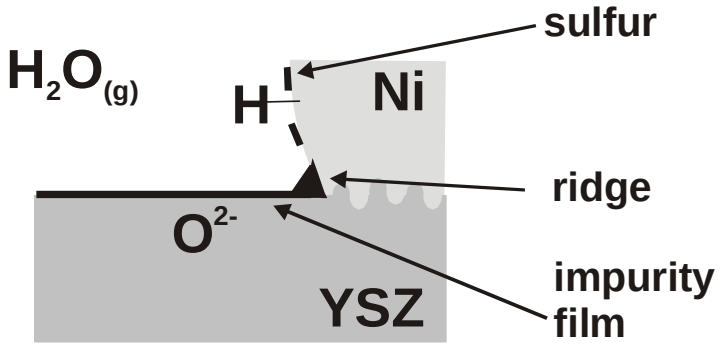

Figure 94. Schematic of the Ni/SZ electrodes that have been studied in this work. For the hydrogen (H) and oxide ions (O^{2-}) to combine, species must be transported through the ridge, impurity film, Ni and/or the Ni/ridge interface.

It is believed that the water promotes the transport of species through the barriers, and this lowers the polarization resistance. The effect of water can also be used to explain the hysteresis in most of the potential sweeps shown in this thesis. At increasing anodic overpotentials the current increases non-linearly. This may be due to the fact that water is formed and probably promotes the transport through the barriers. At cathodic overpotentials there seems to be a limiting current independent of the water content. An explanation could be that water in/at the barriers are consumed during the cathodic reaction, hence the difficulty for the transport of species is greater. An explanation to why water promotes the transport through the barriers may be that the water reacts with the impurities. This could change the properties for transporting of species through the barriers. If this explanation is true, it will explain why the classical electrodes restrictions (charge transfer and mass transfer) described in the introduction are not observed.

The explanation that the impurity film is hindering the electrode reaction is in good agreement with the $^{16}O/^{18}O$ surface exchange experiment performed by de Ridder *et al.* [17]. The experiment showed that a higher impurity content at the surface lowers the exchange rate between ^{16}O and ^{18}O. Though de Ridder *et al.* is referring to a hindering at the cathode this may also be related to the anode as O^{2-} (or a combination of O^{2-} and hydrogen) has to be transferred through the barriers e.g. the impurity layer.

The degradation factor is defined as the ratio between the initial ASR and the final ASR after the degradation. An average value is used for the final ASR as the measurements fluctuate. The ASR values described in the following is at OCV in 3% H_2O/H_2. The degradation of the electrodes at 500°C is seen both in chapter 6 and 7. The degradation factor from chapter 6 was found to be 5-8 and the degradation times were 10-20 days. From the ZY13 electrode (chapter 7) a degradation factor can also be derived as the electrode returned to its original ASR value after the strong cathodic polarization. In this case the degradation factor is calculated from the first measurement at 500°C and the measurement at 500°C after the crystal had been heated to a maximum temperature of 700°C. The degradation factor was 19. The higher degradation factor can be explained by the fact that the crystal had been at 700°C, hence a higher Si and S content are expected on the electrolyte and the Ni wire respectively (see Figure 80 and Figure 82). Also, the fact that the electrodes from chapter 6 were heated to 300 and 400°C before reaching 500°C compared to the sample from chapter 7 which were directly heated to 500°C may play a role. The degradation is very fast in the beginning, hence it is expected that some initial degradation occur at 300 and 400°C. This means that larger degradation factors would be expected if the samples were heated directly to 500°C. This initial degradation was also seen in a Ni pattern experiment (see appendix D). The degradation factor here was ~3 at 400°C and the degradation time were about 8 days. The lower degradation factor in the pattern experiment can be explained by the lower temperature, hence less impurities are expected. Also, the time before reaching 400°C might be important as the degradation is fast in the beginning. Literature about segregation rates for YSZ at low temperature (500°C) are limited. de Ridder *et al.* [17] showed that already after 1 h at 500°C (O_2, 1.5 bar) 74 % of the surface was covered with impurities. A YSZ single crystal was used in the this experiment, and the impurities were detected with LEIS (low energy ion scattering). This fast segregation time does not agree with the degradation time of the electrodes at 500°C, which is 10-20 days. One would expect a faster degradation time for the electrodes based on the LEIS experiment. Other factors than the segregation rate to the surface must then be considered in order to explain the difference in time scale. Factors that also could influence the degradation are: 1) The built up of a ridge around the contact area and 2) The sulfur adsorption on the Ni wire. Also, the development of a hill and valley structure in the contact area occurs during an electrode experiment, but it does not seem likely that this will influence the electrochemical reaction. For the experiments performed at 700°C no initial degradation was seen. This is probably because the degradation at this temperature is so fast that the degradation process already had occurred before the first measurement. Finally, it should be mentioned that this initial degradation might not be seen at real Ni/YSZ composite anodes, as they have already been heat treated at high temperature before they are used as electrodes.
No evident dependence on the polarization resistance was found (chapter 6 and 7) using the different electrolyte compositions: $(ZrO_2)_{0.9}(Y_2O_3)_{0.1}$, $(ZrO_2)_{0.87}(Y_2O_3)_{0.13}$, $(ZrO_2)_{0.82}(Y_2O_3)_{0.18}$ and $(ZrO_2)_{0.9}(Y_2O_3)_{0.04}(Sc_2O_3)_{0.06}$. This may be due to the fact that impurities are segregating to the surface, hence the electrolytes are alike on the surface where the reaction take place.

The effect of the strong cathodic polarization (<-2000 mV vs. air at 700°C) seen in chapter 6 and 7 are hypothesized by Nguyen and Mason [28] and references therein to be caused by trapped electrons in the electrolyte surface (color center), which lowers the polarization resistance due to a high catalytic activity. As impurities are shown to cause a higher polarization resistance, another hypothesis seems likely: reduction of the impurities during a strong cathodic polarization. This will cause the impurities to be metallic and hence be able to conduct electrons. Hereby the barriers that are influenced by the impurities will be changed and promote the electrode reaction.

In the introduction it was mentioned that an extrapolation (Mogensen *et al*. [8]) showed that the polarization resistance of the hydrogen electrode in an aqueous electrolyte was 10-100 times lower than the Ni/YSZ electrode at 1000°C. It was also implied that a part of this difference could be due to impurities. The degradation factor, which is ascribed to impurities, was found to be a factor 5-19. The lowering of ASR by strong cathodic polarization, which also was hypothesized to be an effect of impurities, was found to be a factor 5-60. None of the comparisons are straightforward but it indicates that the Ni/YSZ electrode has the potential of being improved by a factor of 10-100 if the effects of impurities were avoided.

11 Conclusion

- In spite of the efforts of making electrochemical measurements in a very clean system, impurities were still found on the surface of the electrode materials after an electrochemical experiment. The impurities found on the electrolyte materials are believed to segregate from the bulk to the surface. The origin of sulfur on the Ni wires is still unclear.

- The Ni/YSZ interface was found to develop a hill and valley structure at 700°C in humidified hydrogen. Also, a ridge around the contact area was found.

- No evident dependence on the polarization resistance was seen using the different electrolyte compositions: $(ZrO_2)_{0.9}(Y_2O_3)_{0.1}$, $(ZrO_2)_{0.87}(Y_2O_3)_{0.13}$, $(ZrO_2)_{0.82}(Y_2O_3)_{0.1}$ and $(ZrO_2)_{0.9}(Y_2O_3)_{0.04}(Sc_2O_3)_{0.06}$.

- It is hypothesized that water promotes the transport of intermediates/ reactants/products through the barriers that are influenced by impurities. Hence a higher water content in/at the impurity phase enhances the rate of the electrode reaction.

- The ASR at OCV was found to degrade by a factor of 5-19 compared to its original value at 500°C (3% H_2O/H_2). The degradation is believed to be caused by: 1) Segregated impurities, 2) The built up of a ridge around the contact area and 3) The sulfur adsorption on the Ni wire.

- After a strong cathodic polarization (<-2000 mV vs. air at 700°C) the ASR was seen to decrease by a factor of 5-60 compared to the ASR value immediately before the strong cathodic polarization. It is hypothesized that the reason for the much better performance after the strong cathodic polarization is due to reduction of impurities from oxide to metal.

12 Outlook

In order to confirm that the impurities take part in the degradation of the electrode it would be valuable to:

- Remove the trace amounts of impurities from the electrolyte material.
- Remove the sulfur contamination.

The hypothesis that water promotes the electrode reaction due to a change in transport properties of the impurities would make it interesting to:

- Add material that promotes the transport properties of the impurities, i.e. makes it conductive for the reactants and products of the electrode reaction.

The effect of strong cathodic polarization should be studied further by:

- Changing the parameters: 1) Potential used for the reduction and 2) the amount of material (impurities/stabilized zirconia) reduced.
- Performing the strong cathodic polarization on a real Ni/YSZ composite anode.

Even though no work on the SOFC cathode has been performed in this project some relations may be drawn, e.g. the negative effects of impurities was showed by de Ridder *et al.* [17] in a $^{16}O/^{18}O$ surface exchange experiment. Therefore, the above suggestions for improving the anode could apply for the cathode as well, i.e.:

- Removal of trace impurities from the electrode materials.
- Test if water had an effect on the cathodic reaction.
- Adding material that changes the transport properties of the impurities. Vervoort *et al.* [37] showed by a $^{16}O/^{18}O$ surface exchange experiment that implementation of V and W in the surface of YSZ in certain cases enhanced the oxygen exchange rate. It would be interesting to perform an electrochemical experiment where V and W had been added to the cathode material.
- Reduction of impurities at the cathode similarly to the strong cathodic polarization of the anode.

References

[1] Primdahl, S., Ph.D. Thesis: Nickel/yttria-stabilised zirconia cermet anodes for solid oxide fuel cell, ISBN 9036513375, Risø National Laboratory, Denmark, 1999.

[2] Atkins, P. W., Physical Chemistry, ISBN 0198501021, Oxford University Press, 1999.

[3] Bard, J. A. and Faulkner, R. L., Electrochemical methods, ISBN 0471055425, John Wiley & Sons, 1980.

[4] Vetter, J. K., Electrochemical Kinetics, Academic Press Inc., New York, 1967.

[5] Jensen, K.V., Wallenberg, R., Chorkendorff, I., Mogensen, M., Effect of impurities on structural and electrochemical properties of the Ni-YSZ interface, Solid State Ionics 160 (2003) 27-37.

[6] Liu, Y.L., Primdahl, S., Mogensen, M., Effects of impurities on microstructure in Ni/YSZ-YSZ half-cells for SOFC, Solid State Ionics 161 (2003) 1-10.

[7] Mogensen, M., Jensen, K.V., Jorgensen, M.J., Primdahl, S., Progress in understanding SOFC electrodes, Solid State Ionics 150 (2002) 123-129.

[8] Mogensen, M., Primdahl, S., and Sunde, S., SOFC anode kinetics, High temperature electrochemistry: Ceramics and Metals, Editores: Poulsen, F.W., Bonanos,N., Linderoth,S. Mogensen, M. and Zachau-Christiansen,B., Risø National Laboratory, Denmark, 1996.

[9] Liu, Y.L. , Jiao, C.G., Microstructure degradation of an anode/electrolyte interface in SOFC studied by transmission electron microscopy, Solid State Ionics 176 (2005) 435-442.

[10] Jensen, K. V., Ph.D thesis: The nickel-YSZ interface, ISBN 8755030424, Risø National Laboratory, Denmark, 2002.

[11] Bay, L., Ph.D. thesis: Electrode kinetics in high temperature fuel cells, DTU/DTV, 1998.

[12] Stoneham, A.M., Ceramic Surfaces - Theoretical-Studies, Journal of the American Ceramic Society 64 (1981) 54-60.

[13] Primdahl, S., Mogensen, M., Limitations in the hydrogen oxidation rate on Ni/YSZ anodes, Proceedings of the Sixth International Symposium on Solid Oxide Fuel Cells 99-19 (2005) 530-537.

[14] Koch, S., Hansen, K.V., Johansen, B.S., Risø National Laboratory, Denmark, Elchemea (2005)

[15] Z-plot and Z-view for Windows, Scribner Associates, Inc. (1998)

[16] Bieberle, A., Meier, L.P., Gauckler, L.J., The electrochemistry of Ni pattern anodes used as solid oxide fuel cell model electrodes, Journal of the Electrochemical Society 148 (2001) A646-A656.

[17] de Ridder, M., Vervoort, A.G.J., van Welzenis, R.G., Brongersma, H.H., The limiting factor for oxygen exchange at the surface of fuel cell electrolytes, Solid State Ionics 156 (2003) 255-262.

[18] Hughes, A.E., Segregation in single-crystal fully stabilized yttria-zirconia, Journal of the American Ceramic Society 78 (1995) 369-378.

[19] Chorkendorff, I., Experimental surface physics, Technical University of Denmark, 2003.

[20] Mizusaki, J., Tagawa, H., Saito, T., Kamitani, K., Yamamura, T., Hirano, K., Ehara, S., Takagi, T., Hikita, T., Ippommatsu, M., Nakagawa, S., Hashimoto, K., Preparation of nickel pattern electrodes on ysz and Their Electrochemical Properties in H2-H2O Atmospheres, Journal of the Electrochemical Society 141 (1994) 2129-2134.

[21] Brigeman , Aldrich, Vapor pressure of water, http://webbook.nist.gov/chemistry, 1964.

[22] Hartung, R., Möbius, H.H., Potentiometrische Bestimmung des Wasserdampf-dissoziationsgleichgewichtes zwischen 1000 und 1300K mit einer Festelektroytzelle, Chemie-Ing. - Tech. 40, 1968.

[23] Holm, R., Stationary contacts, Springer-Verlag, 1967.

[24] Minh, Q. N. and Takahashi, T., Science and technology of ceramics fuel cells, Elsevier,1995.

[25] Casselton, W.E.R., Blackening in yttria stabilized zirconia due to cathodic processes at solid platinium electrodes, Journal of Applied Electrochemistry 4 (1973) 25-48.

[26] Hansen, K.V., Norrman, K., Mogensen, M., TOF-SIMS studies of impurity segregation in yttria-stabilised zirconia, accepted.

[27] Hansen, V.K., Norrman, K., Høgh, J., Mogensen, M., Yttria and impurity segregation in yttria-stabilised zirconia in air and wet 9%H2/N2, Internal report, Risø National Laboratory fuel cell program, Denmark, 2004.

[28] Nguyen, C.B., Mason, M.D., Mechanisms of catalytic oxidation of hydrocarbons in a solid-electrolyte fuel cell, Proceedings of the conference on high temperature solid oxide electrolytes anions conductors 1, 1983.

[29] Moulder, F. J, Stickle, F. W., Sobol, E. P., and Bomben, D. K., Handbook of X-ray pohtoelectron spectroscopy, Physical Electronics, Inc., United States of America, 1995.

[30] Bale, C.W., Pelton, A.D., Thomson, W.T., Eriksson, G., Hack, K., Chartrand, P., Decterov, S., Melancon, J., Petersen, S., FactSage 5.3.1 (2004)

[31] Ziegler, J.F. , Biersack, J.P., The stopping and range of Ions in matter (SRIM) (2003)

[32] Callister, D. W., Materials science and engineering an introduction, John Wiley & Sons, inc., 1997.

[33] Handbook of Chemistry and Physics, CRC Press, 76th edition, 1995.

[34] Bonanos, N., BC 378, Internal report, Risø National Laboratory fuel cell program, 2004.

[35] Wachman, B. J., Mechanical properties of ceramics, John Wiley & Sons, inc., United States of America, 1996.

[36] Opila, E. J., Oxidation and Volatilization of Silica Formers in Water Vapor, Journal of American Ceramic Society, 86 [8], 1238-48, 2003.

[37] Vervoort, A.G.J., Scanlon, P.J., de Ridder, M., Brongersma, H.H., van Welzenis, R.G., Surface modification of a fuel cell material by ion implantation, Nuclear Instruments & Methods in Physics Research Section B-Beam Interactions with Materials and Atoms 190, 813-816, 2002.

Appendices A-C

Appendix A: High impedance of the reference electrode

When measuring potentials it is important that the input impedance of the measurement equipment is much larger than the impedance of the potential probe (in this case the reference electrode). Impedance measurements were therefore performed on the reference electrode to test if this was a problem. The impedance of the reference electrode was hereafter compared to the input impedance of the measurement equipment (Solartron 1260 and Solartron 1255b+1287) by an equivalent circuit analysis.

The reference electrode with the highest impedance was chosen in order to study a worst case situation. The impedance of the reference electrode can be described by an RQ-circuit with an *n* value of 0.5. For simplicity the summit frequency was used to calculate the capacitance. From this capacitance an RC-circuit, with the values 10^5 Ohm and 24 nF, was used to describe the reference electrode. The measurements on the reference electrode were performed in 2-electrode mode using the reference electrode and the counter electrode. The counter electrode is larger than the reference electrode so the main impedance is expected to originate from the reference electrode.

The input impedance (RC-circuit) of the Solartron 1255b+1287 is 10^{10} Ohm and 50 pF and the input impedance of the Solartron 1260 is 10^6 Ohm and 35 pF. Note that for the Solartron 1260 a capacity of 100 pF was added to the 35 pF because of the leads connecting the junction box with the Solartron 1260. This is not relevant for the 1287 because the shields of these leads are kept at the same potential as the core (driven shields).

The test voltage that the measurement equipment should determine if the influence of the reference electrode is negligible was set to 1 V with a phase angle of 0°. The deviation from this voltage and phase angle is representing the error that the reference electrode introduces. The equivalent circuit and result of the analysis for the Solartron 1255b+1287 is shown in Figure 1A and Figure 2A respectively. The software used for modeling was DesignLab version 8.0. The voltage and phase angle the measurement equipment are monitoring are probed at “V” and “Vp”, see Figure 1A.

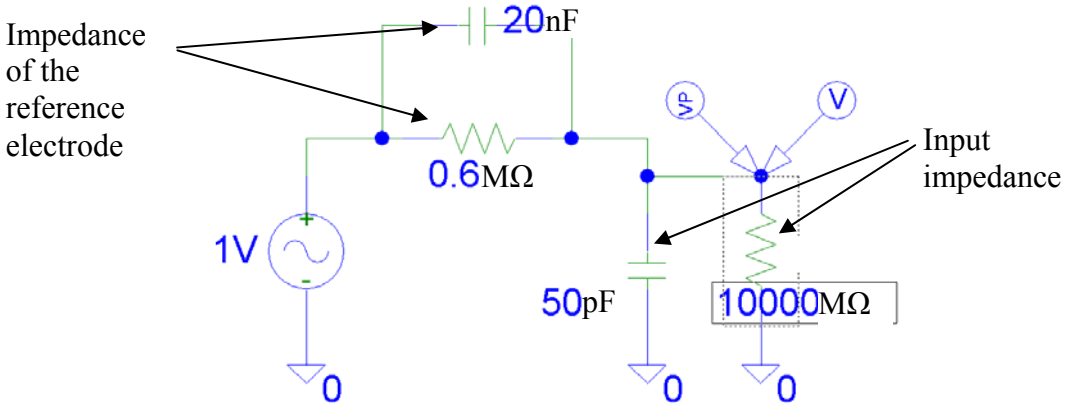

Figure 1A. Equivalent circuit of the reference electrode and the input impedance of the Solartron 1255b+1287. The reference electrode has an impedance of $6 \cdot 10^5$ Ohm and 20 nF. The input impedance of the Solartron 1255b+1287 is 10^{10} Ohm and 50 pF. A test voltage of 1 V with a phase angle of 0° is used in the circuit analysis. The deviation of the voltage and phase angle from the test voltage is shown in Figure 2.

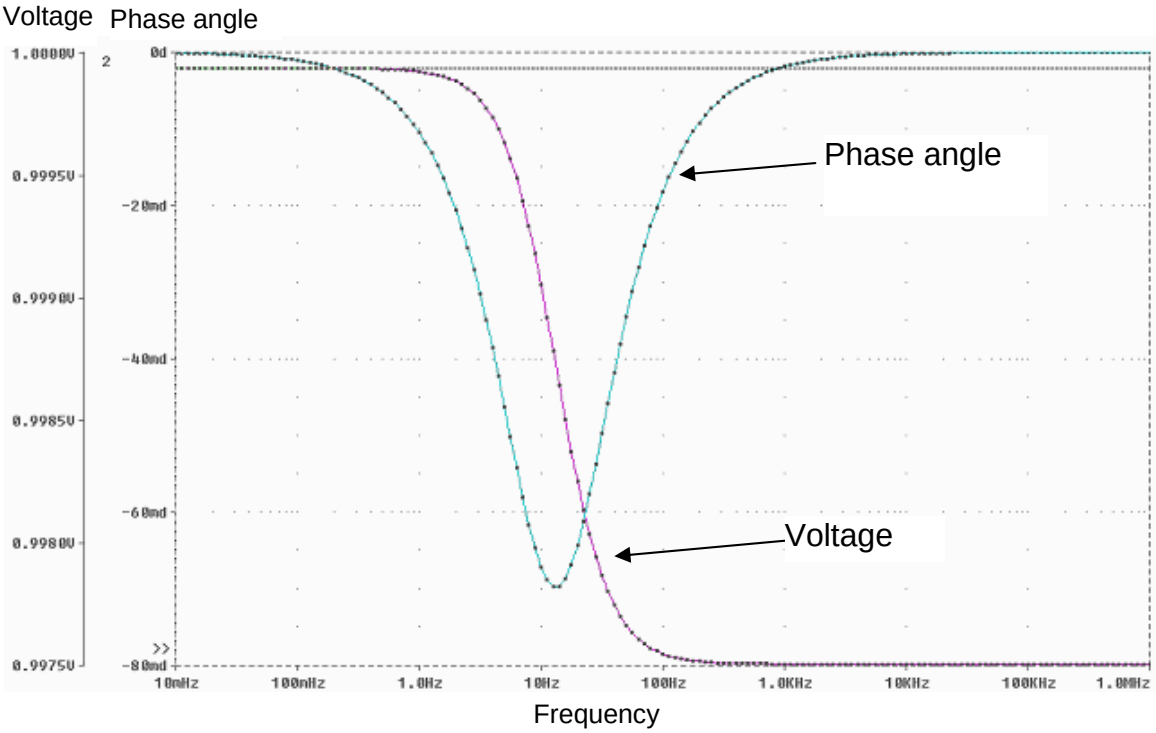

Figure 2A. The voltage and phase angle that the Solartron 1255b+1287 monitors of a test voltage for 1 V with a phase angle of 0°. The ideal situation is where the voltage and phase angle are monitored to 1 V and 0° phase angle.

The equivalent circuit and result of the analysis for the Solartron 1260 is shown in Figure 3A and Figure 4A. Again, the test voltage that the measurement equipment should determine was set to 1 V with a phase angle of 0°.

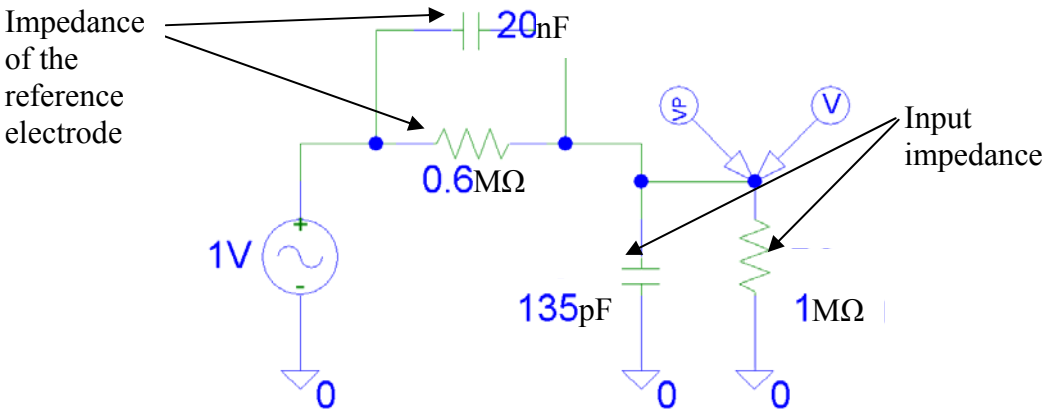

Figure 3A. Equivalent circuit of the reference electrode and the input impedance of the Solartron 1260. The reference electrode has an impedance $6 \cdot 10^5$ Ohm and 20 nF. The input impedance of the Solartron 1260 is 1 MOhm and 35 pF. A capacity of 100 pF was added to the 35 pF because of the leads connecting the junction box with the Solartron 1260. A test voltage of 1 V with a phase angle of 0° is used in the circuit analysis. The deviation of the voltage and phase angle from the test voltage is shown in Figure 2.

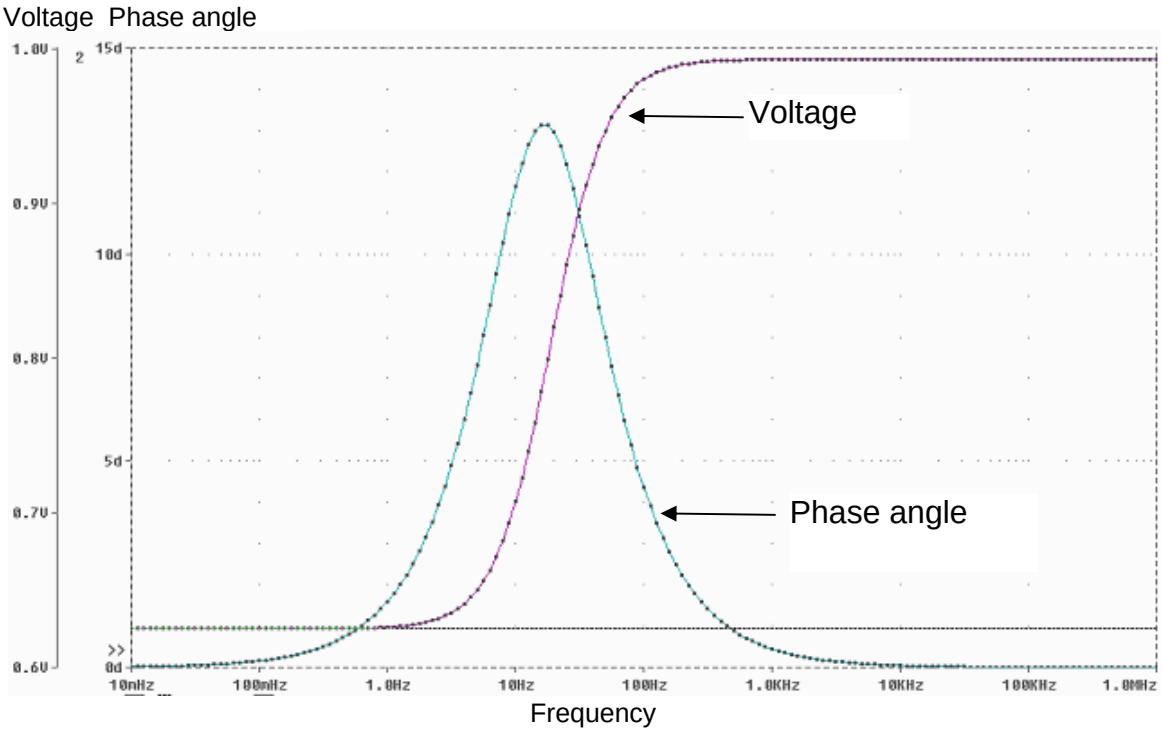

Figure 4A. The voltage and phase angle that the Solartron 1260 monitors for a test voltage for 1 V with a phase angle of 0°. The ideal situation is were the voltage and phase angle are monitored to 1 V and 0° phase angle.

The maximum error in determining the voltage and phase angle of the test voltage with the Solartron 1255b+1287 are 0.9975 V and –0.08° i.e. the errors are negligible.

The maximum error in determining the voltage and phase angle of the test voltage for Solartron 1260 are 0.625 V and 13° i.e. the errors are large an unacceptable[5].

The conclusion for the analysis in this appendix is that the impedance of the reference electrodes does not influence the measurement on the electrode when using Solartron 1255b+1287. In cases where the Solartron 1260 was used it was found necessary to determine the impedance of the reference electrode in order to analyze if it would create erroneous measurements for the electrode.

[5] Measurements that were performed on a dummy cell showed that the errors could be corrected, as the input impedance of the apparatus is known. These corrections are not performed for any of the impedance spectra in this thesis.

Appendix B: Impedance spectra and potential sweeps from a dummy cell

A preliminary electrode experiment showed a large noise in the impedance spectra of a high impedance sample (~MΩ). This was also seen when the measurement were performed in 2-electrode mode i.e. the problem with high impedance at the reference electrode is avoided. A dummy cell with high impedance was made in order to test the validity of the measurement equipment i.e. Solartron 1260 and Solartron 1255b+1287.

Figure 1B shows a schematic of the dummy cell connected to the Solartron 1255b+1287. The problem with high impedance at the potential probe is treated in appendix A so the dummy is here connected in 2-electrode mode in order to avoid this problem.

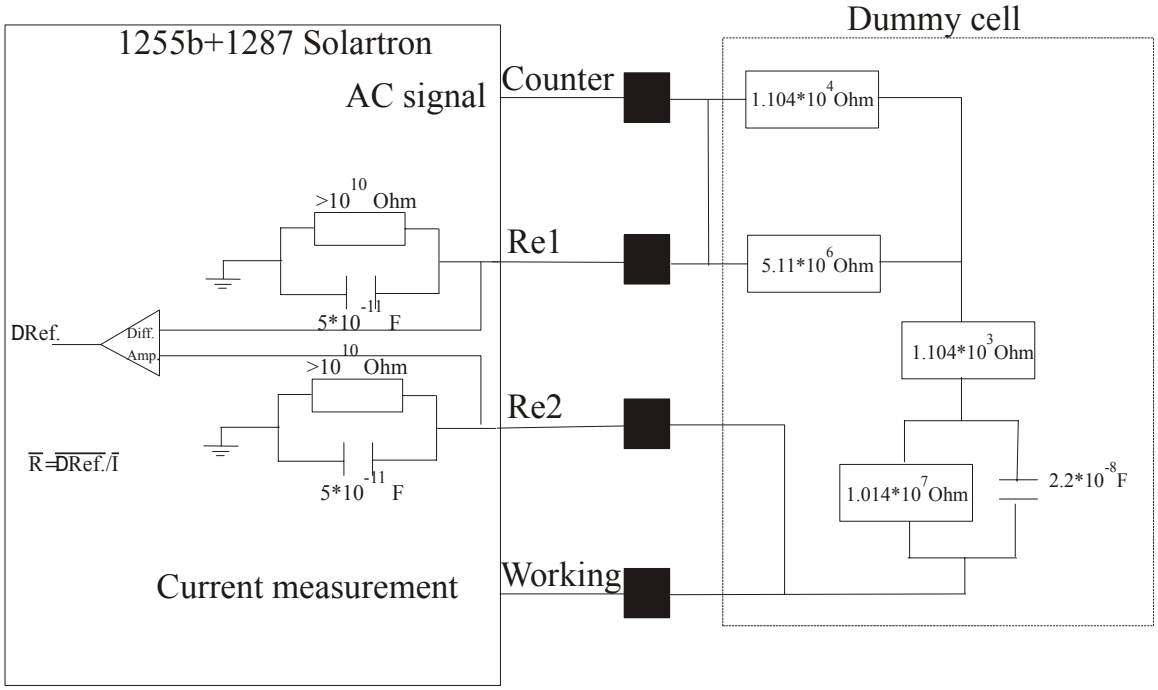

Figure 1B. Schematic of Solartron 1255b +1287 connected to a dummy cell. The dummy cell is here connected in 2-electrode mode.

The R_s (series resistance) value of the dummy cell in two electrode mode is $1.2 \cdot 10^4$ Ohm ($1.104 \cdot 10^4 + 1.104 \cdot 10^3$ Ohm) and the R_p (polarization resistance) is $1.014 \cdot 10^7$ Ohm.

Impedance measurements were performed on the dummy cell in 2-electrode mode using the Solartron 1260 (see Figure 2B - Figure 4B) and the Solartron 1255b+1287 (see Figure 5B), respectively. The number of cycles and the voltage amplitude used for the impedance spectra are specified in the figure text. The number of cycles is the number of voltage cycles that the Solartron performs at each frequency. An increase of the voltage amplitude and/or an increase in the number of cycles make the measurement less sensitive for noise.

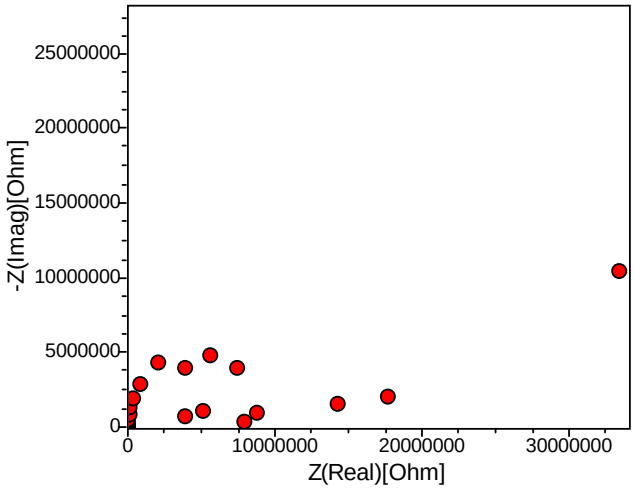

Figure 2B. Impedance measurement on the dummy cell in 2-electrode mode using the Solartron 1260. A voltage of 30 mV and 1 cycle were used.

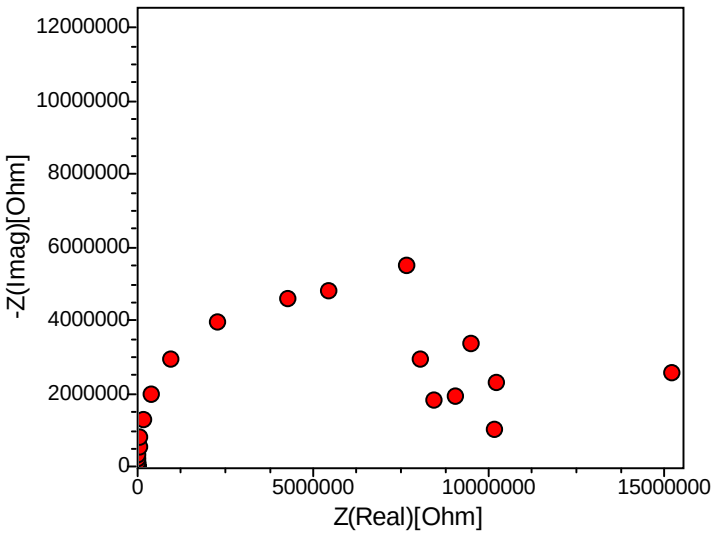

Figure 3B. Impedance measurement on the dummy cell in 2-electrode mode using the Solartron 1260. A voltage of 30 mV and 10 cycles were used.

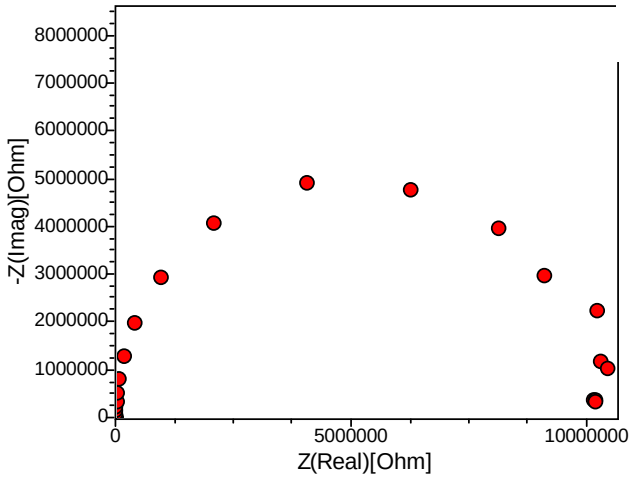

Figure 4B. Impedance measurement on the dummy cell in 2-electrode mode using the Solartron 1260. A voltage of 30 mV and 500 cycles were used. This spectrum took 24 h to collect.

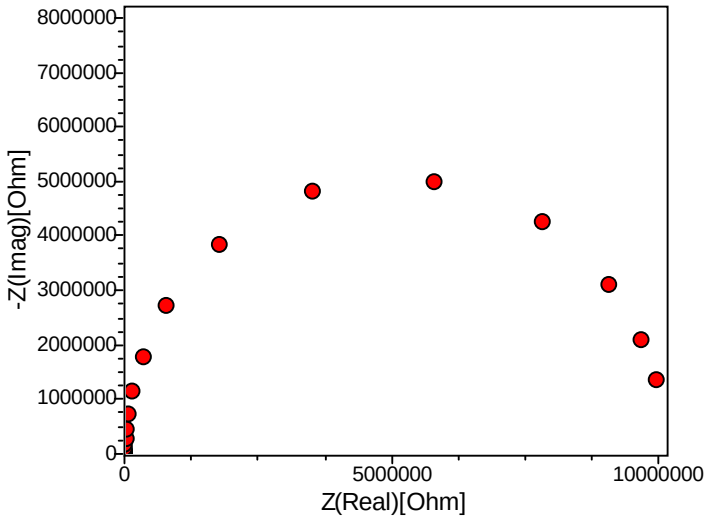

Figure 5B. Impedance measurement on the dummy cell in 2-electrode mode using the Solartron 1255b+1287. A voltage of 2 mV and 1 cycle were used.

The R_s value of the dummy cell where in all cases determined satisfactory. In order to achieve a satisfactory determination of R_p using the Solartron 1260 a 30 mV signal and 500 cycles was needed. Using a large number of cycles prolongs the time to perform a impedance measurement. In this case it took 24 h to acquire the impedance spectra using 500 cycles. This time is unacceptable as the Ni/YSZ electrode can change considerable during 24 h.
Using the Solartron 1255b+1287 a satisfactory R_p value was obtained by a 2 mV signal and 1 cycle. The time used for this spectrum was ~10 min.
The conclusion is that the Solartron 1255b+1287 is better than the Solartron 1260 in performing high impedance measurements i.e. it is better at measuring small currents. The Solartron 1255b+1287 are therefore predominantly used as most electrodes show high impedance.

Potential sweeps were performed with the Solartron 1255b+1287 on the dummy cell in order to test this analysis method. Figure 6B show a potential sweep performed on the dummy cell. The sweep is performed in following direction 0 – (-0.1) – 0.1 – 0 V with a sweep rate of 1 mV/s.

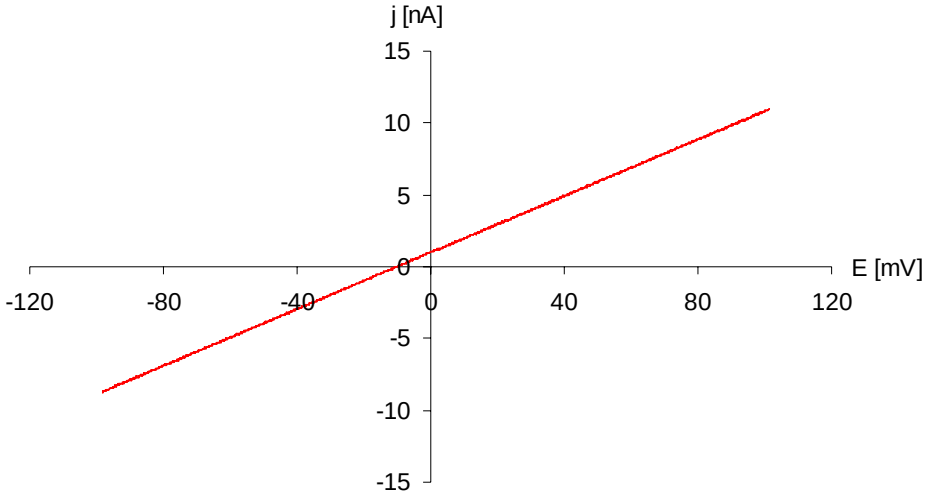

Figure 6B. Potential sweep for the dummy cell in 2-electrode. Sweep direction 0 – (-0.1) – 0.1 – 0 V. Sweep rate 1 mV/s.

The slope corresponds to the resistance of the dummy cell. The sweep shows an offset of a few nano amperes at zero voltage. Also, the outer potential limits were –98 and 101 mV when the settings were –100 and 100 mV.

The potential sweeps can be performed in either analog or stepped mode. Figure 7B shows a section of two potential sweeps that are performed in these modes.

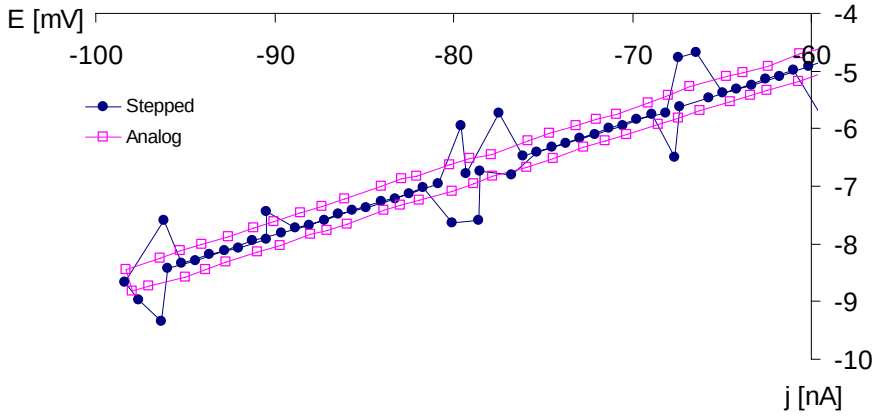

Figure 7B. Sweeps for the dummy cell in stepped and analog mode (0 – (-0.1) – 0.1 – 0 V with 10 mV/S)

Figure 7B shows that when using stepped mode noise occurs. In analog mode the noise is reduced but a small step in the current is seen when the potential sweep changes direction. When the sweep rate is reduced from 10 to 1 mV/s the step in current disappears. Based on the above observation it was decided to use the analog mode.

The conclusion on the potential sweeps performed on the dummy cell is: 1) An offset in current is seen at zero potential and 2) A step in current can be expected when the sweep direction is changed. The offset at zero voltage is corrected in the potential sweeps shown in this report. The step in current when changing sweep direction did not play an important role in the analysis of any of the potential sweeps so this feature is disregarded.

Appendix C: High purity H_2/H_2O/Ni/stabilized zirconia electrodes at 500°C

Published as:
High purity H_2/H_2O/nickel/stabilized zirconia electrodes at 500°C
J. Høgh, K. Vels Hansen, I. Chorkendorff, T. Jacobsen, K. Norrman and M. Mogensen.
Proceedings of the 29th International Conference on advanced Ceramics and Composites, The American Ceramic Society, Jan 2005.

HIGH PURITY H_2/H_2O/NICKEL/STABILIZED ZIRCONIA ELECTRODES AT 500°C

J. Høgh
Materials Research Department, Risø National Laboratory, DK-4000 Roskilde, Denmark, jens.hoegh@risoe.dk

K. Vels Hansen
Materials Research Department, Risø National Laboratory, DK-4000 Roskilde, Denmark

I. Chorkendorff
ICAT, Department of Physics and Department of Chemical Engineering, Technical University of Denmark, DK-2800 Kgs. Lyngby, Denmark

T. Jacobsen
Department of Chemistry, Technical University of Denmark, DK-2800 Kgs. Lyngby, Denmark

K. Norrman
Danish Polymer Center, Risø National Laboratory, DK-4000 Roskilde, Denmark

M. Mogensen
Materials Research Department, Risø National Laboratory, DK-4000 Roskilde, Denmark

Abstract

Segregated impurities seem to be detrimental for the performance of a SOFC (solid oxide fuel cell) anode. In this study the performance of a model system of the SOCF anode was measured. It is sought to minimize the segregation of impurities by using high purity materials at relatively low temperature to prevent fast segregation. Bent Ni wires (99.999 %) were pressed against polished single crystals of stabilized zirconia (SZ), thereby forming point electrodes. Four single crystals stabilized with: 10, 13 and 18 mol% yttria and one stabilized with 6 mol% scandia and 4 mol% yttria were used as electrolytes. The polarization resistances (R_p) at OCV (open circuit voltage) of the electrodes were measured from 400-500°C in mixtures of H_2/H_2O over 46 days. The R_p for all electrodes increased significantly during the first 10-20 days at 500°C after which they became relatively constant. An effect on the R_p of the different electrolytes was not evident. The Ni wires and single crystals were analyzed before and after the electrochemical experiment using SEM (scanning electron microscopy) to study morphology, and surface sensitive techniques for determination of composition and distribution of elements. After the electrochemical experiment the analysis showed segregation of impurities to the surfaces/interfaces, which means that a pure model system was not achieved even though high purity materials were used at a relatively low temperature. These impurities are believed to impede the electrode processes and hence to cause the increase in R_p.

Introduction

Recently it was shown that segregation of impurities to the interfaces has a negative influence on the kinetics of the $H_{2(g)}/H_2O_{(g)}/Ni_{(s)}/SZ_{(s)}$ electrode, resulting in a more ineffective electrode [1,2]. Also, segregated impurities at the interface may be the reason for the disagreements about the kinetics in literature, which has been accounted for elsewhere[3].

The purpose of our study is to perform electrochemical measurements in a very clean system to avoid the effects of impurities. This is attempted by using high purity materials, lowering the operation temperature to prevent fast segregation of impurities, and by limiting impurities from the environment.

The reactions under investigation at the Ni/SZ electrode are the oxidation of hydrogen and the reduction of water, see (1) and (2) respectively.

$$H_{2(g)} + O^{2-}_{(SZ)} \rightarrow H_2O_{(g)} + 2e^-_{(Ni)} \qquad \text{(Anodic current)} \qquad (1)$$

$$H_2O_{(g)} + 2e^-_{(Ni)} \rightarrow H_{2(g)} + O^{2-}_{(SZ)} \qquad \text{(Cathodic current)} \qquad (2)$$

Reaction (8) and (9) dominate when the cell is operated as a fuel cell (SOFC) and as an electrolyzer cell (SOEC, solid oxide electrolyzer cell), respectively.

The real SOFC anode is a porous Ni/SZ composite in order to optimize mass transport and charge transfer near or at the three phase boundary (TPB) where the Ni, SZ and fuel gas meet. A point electrode is used here as a model system because: 1) It provides a well defined length of the TPB and 2) the easiness of investigating the Ni/SZ interface after an electrochemical experiment.

Experimental

Materials and sample preparation

As the working electrodes a nickel wire (Ø=0.5 mm) from Alfa Aesar (Puratronic®) was used. The stated purity was 99.999 % (metal basis). Prior to the electrochemical experiment the Ni wires were annealed in 3% H_2O/9% H_2/N_2 (1000°C, 7 days) and electro polished.

Four different electrolyte compositions of single crystals were used: $(ZrO_2)_{0.9}(Y_2O_3)_{0.1}$, $(ZrO_2)_{0.87}(Y_2O_3)_{0.13}$, $(ZrO_2)_{0.82}(Y_2O_3)_{0.18}$ and $(ZrO_2)_{0.9}(Sc_2O_3)_{0.06}(Y_2O_3)_{0.04}$. They were coded ZY10, ZY13, ZY18 and ZSc6Y4, respectively. The crystals ZY10, ZY18 and ZSc6Y4 were provided by Dr. Sergey Shkerin and professor Perfilliev, Institute of High-Temperature Electrochemistry, RAS, 20 S. Kovalevskaya Str., 620219 Ekaterinburg, Russia. The surface orientations of the samples are unknown. The ZY13 electrolyte was purchased at MTI Corporation (www.mticrystal.com). The purity is stated as 99.99 % and the surface orientation is [100]. All electrolytes were polished with 6, 3, 1 and ¼ μm diamond suspension. For the final polishing an acidic suspension of alumina particles (0.02 μm, OP-AA suspension, Struers) was used. After polishing and cleaning of both electrodes and electrolytes in an ultrasonic bath with ethanol, they were handled with gloves using mask and hairnet in a laminar air flow system.

Platinum was used as counter and reference electrodes and were painted on the electrolyte using Pt-paste (Degussa, 308A). As current collector for the counter and the reference electrodes Pt meshes were used in order to allow gas transport to the electrodes (Figure 1). A mesh consists of 0.1 mm Pt wires with a mask size of 0.5x0.5 mm, the thickness of the mesh is 0.3 mm.

Electrochemical set-up

A 3-electrode set-up (4-wires, one atmosphere) and impedance spectroscopy were used to measure R_p at OCV using a 30 mV signal. A frequency response analyzer (Solartron 1255b) in combination with a potentiostat (Solartron 1287) were used for the electrochemical measurements. Two gas compositions ~3% H_2O/H_2 and ~0.7% H_2O/H_2 were used and a YSZ based oxygen sensor with atmospheric air as the reference gas indicated oxygen pressures of $1.5 \cdot 10^{-31}$ atm (EMF=-1156 mV) and $9.5 \cdot 10^{-33}$ atm (EMF=-1202 mV) at 500°C, respectively. Figure 1 shows a sketch of the electrochemical 3-electrode set-up. On top of the alumina tube a weight of copper (315 g) is arranged to press the Ni wire against the electrolyte. Prior to the electrochemical experiment the set-up, which consists mainly of alumina, was heat treated twice to remove volatile material; first in air (technical air, 21 mol% O_2 and 79 mol% N_2) and then in humidified hydrogen (3% H_2O/H_2). The heat treatments were conducted at 1000°C for 7 days.

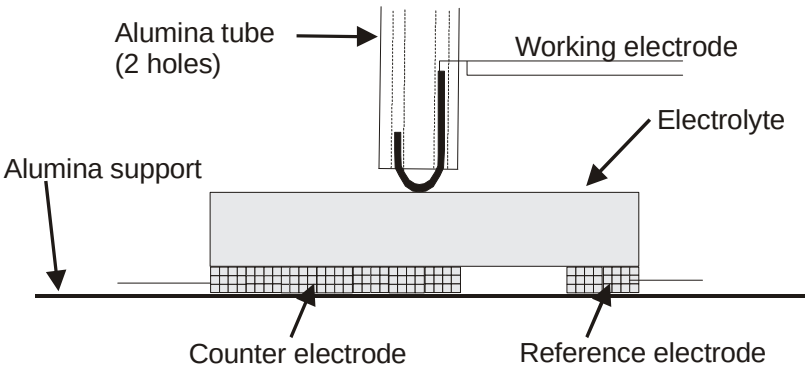

Figure 1. Sketch of the 3-electrode set-up. Two leads are connected to the working electrode (Ni wire). Pt is used as counter and reference electrodes. Two Pt meshes collect the current and allow for gas transport to the electrodes.

It was found that 2-electrode measurements had a higher signal to noise ratio compared to 3-electrode measurements, hence fewer cycles (less time) were necessary for each impedance measurement using the 2-electrode mode. The area of the counter electrode is around 1000 times larger than the area of the working electrode (Ni wire), hence a negligible contribution from the counter electrode is expected on the total R_p. Also, the series resistance (R_s) should not be affected, as this resistance mainly originates from the current constriction at the point electrode. 3-electrode measurements were performed to confirm the results from 2-electrode measurements and they were in good agreement.

The four electrodes were operated for 46 days. The samples were heated from room temperature to 400°C over 4 h and kept at this temperature for 15 h. Next the temperature was increased to 450°C over 30 min and kept at this temperature for 7 h. Finally, the temperature was increased to 500°C over 30 min and kept at this temperature for 38 days before cooling down. Measurements were performed at 450 and 400°C before cooling to room temperature. The heating and cooling sequences will be referred to as the heating run and the cooling run.

Surface characterization techniques

Several surface techniques were used to characterize the Ni wires and the single crystals before and after the electrochemical measurements.

SEM (scanning electron microscopy) was performed using a Jeol JSM-5310LV. SEM images were used to determine the Ni/SZ contact areas from the Ni wires. Elemental

analysis was performed using energy dispersive X-ray spectroscopy (EDS, Noran). EDS probes a volume of ~1 μm^3. EDS was used to verify the bulk composition of the electrolytes.

XPS (X-ray photoelectron spectroscopy) was performed using a Sage 100 from SPECS with a non-monochromated Mg-Kα X-ray source and a take-off angle of 90°. From the full spectrum elements in the sample and the atomic concentrations were determined using a step size of 0.5 eV and a detector pass energy of 100 eV. Narrow scans with a step size 0.2 eV and a detector pass energy of 23 eV were performed to get a better resolution. An electron floodgun was used to limit charging. XPS was used for analysis of the electrolyte surfaces.

AES (Auger electron spectroscopy) was performed using a model Phi 550/590 spectrometer from Perkin Elmer. The electron gun was set to 5 keV and a take-off angle of 48° was used. The step size was 1 eV. Depth profiling was performed using an ion gun with 2 keV Ar^+ and a current of 45 $\mu A/cm^2$. AES was used for elemental surface analysis after the electrochemical experiment of the Ni wire placed on ZY10. An AES analysis was also performed on a Ni wire (reference sample) that were annealed in 3% H_2O/9% H_2/N_2 (1000°C, 7 days) and electro polished. XPS and AES probe a depth of 10-40 Å.

TOF-SIMS (Time of flight secondary ion mass spectrometry) was performed on the electrolytes with a TOF-SIMS IV from ION-TOF GmbH. At first scans were performed to produce images of the elemental distribution. Depth profiles were subsequently performed. Xe^+ (3 keV, 3-16 nA) was used as coarse sputtering and Ga^+ (25 keV, 1 pA, 300x300 μm^2) was used for analysis. The total sputter time was 250-1000 s. The procedure for the depth profiling was: 0.5-2 s sputter → 0.5-1 s pause → ~1 s analysis (1/20kHz). The pause was inserted to limit charging even though an electron floodgun was used. The sputter rate on similar materials (ZY8, polycrystalline) was estimated elsewhere[4] to 1-10 Å per 100 s using Xe^+ (3 keV, 3 nA, 100x100 μm^2). TOF-SIMS images and depth profiling of all samples were performed after the electrochemical measurements. In the case of ZY13 and ZSc6Y4, two polished reference samples (not heat treated) were additionally examined. For each sample two depth profiles were performed outside the contact area and one inside the contact area. Two depth profiles were performed on each of the reference samples.

Results

Surface analysis

XPS measurements showed only carbon as an impurity on the polished electrolytes. When the samples have been exposed to the atmosphere carbon is always seen due adsorption of organic species. After the electrochemical experiment, Si/Zr ratios of 0.06, 0.05, 0.02 and 0.07 were observed on ZY10, ZY13, ZY18 and ZSc6Y4, respectively. Note that the Zr content is not the same in the crystals.

AES depth profiles of the Ni wire before and after the electrochemical experiment are shown in Figure 2.

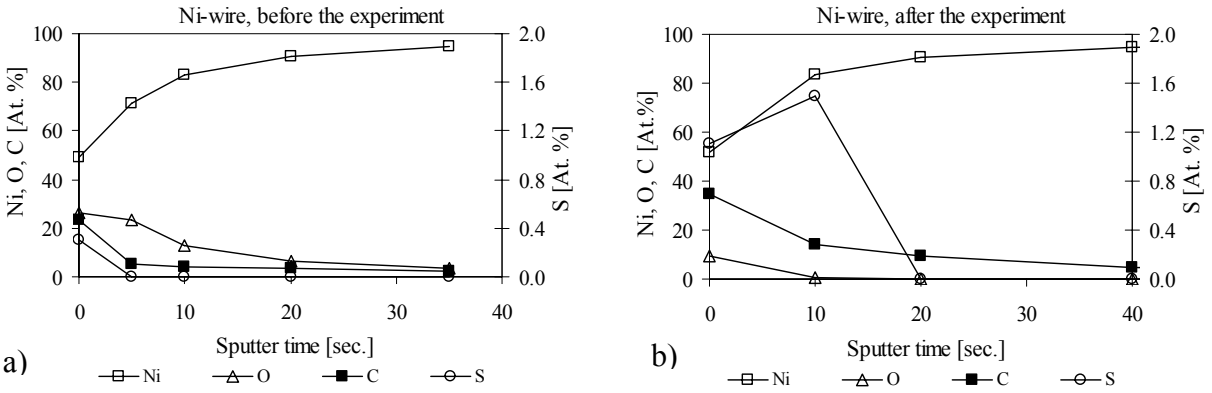

Figure 2. Depth profiling using AES. a) A Ni wire (reference sample) before the electrochemical experiment (annealed and electro polished) and b) The Ni wire after the electrochemical experiment outside the contact area. The Ni wire was placed on ZY10 during the electrochemical experiment.

Two AES depth profiles were also performed in the Ni contact area on the Ni wire that was placed on ZY10 (not shown). One of the profiles showed up to 6 at. % Zr, but only 0.3 at. % S i.e. the same as the Ni wire before the electrochemical experiment. The other profile showed a thicker oxide scale and a sulfur profile similar to the one shown in Figure 2b.

A TOF-SIMS depth profile on ZY13 is shown in Figure 3a. The intensity within a profile varies. A general trend for all profiles is an initial steep increase followed by a steep decrease after which the intensity becomes relatively constant or decreases slightly. This trend is also seen in a previous study[4] and is explained by an establishment of a steady state of charging effects in the sputter process. For comparison the profiles were normalized by the intensity of $^{94}Zr^{+}$ as this is free of ZrH^{+} interference. Figure 3b shows the normalized Si signal for the measurement performed on ZY13 and the reference sample of ZY13.

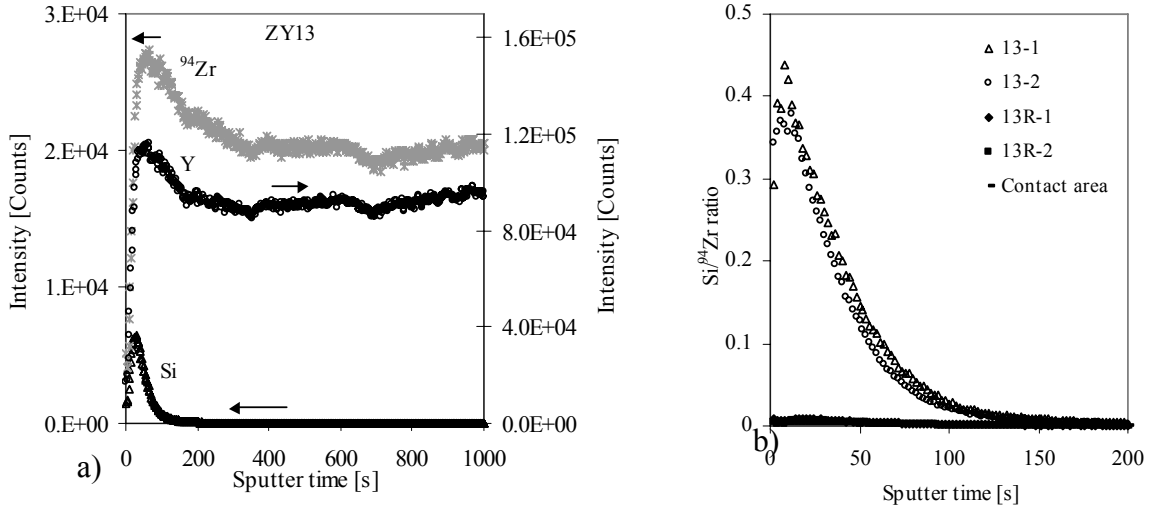

Figure 3. a) TOF-SIMS depth profile of ZY13. Raw intensity data for ^{94}Zr, Y and Si are shown. b) TOF-SIMS depth profile of Si/Zr for ZY13. The codes 13-1, 13-2 and "Contact area" are referring to positions on the electrochemically tested sample. 13-1 and 13-2 are outside the contact area. 13R-1 and 13R-2 are from the reference sample.

Figure 3b shows that the Si/^{94}Zr ratio outside the contact area (13-1 and 13-2) is higher than in the contact area and on the freshly polished reference sample (13R-1 and 13R-2). The maximum ratios from the contact area and the reference sample are 0.003 and 0.007 respectively, i.e. about 100 times lower than the peak value outside the contact area. All

four electrochemically tested samples showed a lower normalized Si/^{94}Zr signal in the contact area than outside the contact area. The measurements on the reference samples showed a higher Si/^{94}Zr signal than that found in the contact area of ZY13. Comparison between the measurements outside the contact area and in the contact area shows that the elements Al, Mg, K, Cr, Mn and Fe have the same trend as Si i.e. higher normalized signal outside the contact area than in the contact area. In the case of Ni a higher normalized signal was found in the contact area than outside the contact area.

Electrochemistry

Impedance spectra: R_p and R_s were found from impedance spectroscopy. Two impedance spectra (2_034 and 2_037) are shown in Figure 4. The high frequency part from $10^4 - 10^5$ Hz can be ascribed to the capacitance of the 3-electrode set-up. Fluctuations in R_p occur, usually as a sudden drop followed by a steady increase. The impedance spectrum 2_034 is from a period where R_p was stable and spectrum 2_037 was performed after a sudden drop in R_p. From Figure 4b it can be a seen that R_s is the same in 2_034 and 2_037, which implies that the drop in R_p is not caused by a change in the size of the contact area.

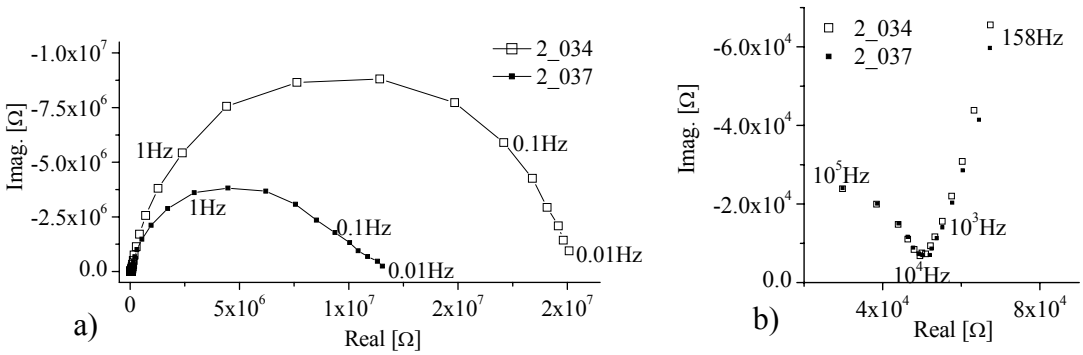

Figure 4. a) Impedance spectra for ZY10. Spectrum 2_034 shows a time independent measurement. In spectrum 2_034, R_p is increasing during the measurement, which causes a tail towards higher resistance. b) A close-up of the high frequency measurements showing that R_s is the same in the two spectra.

Contact area: The area specific resistance (ASR) is calculated ($ASR \equiv R_p \cdot A_{contact}$) for comparison between measurements/samples with different contact area. As the contact area increases during the electrochemical experiment the area (radius) was calculated from (19)[5] at each impedance measurement. In this relation an infinite thick electrolyte and a circular area is assumed. A relation[5] which matches our samples (not infinite thick and elliptic contact area) deviates less than 5 % from (19) and as 5 % is a small value in this context $\left(100 \cdot R_s < R_p\right)$ the simple approximation is used due to the ease of computation.

$$R_S = \frac{1}{4 \cdot \sigma \cdot r} \tag{3}$$

In (3) r is the radius of a circle. In our case the contact area is elliptic and a equivalent radius is used, i.e. $r = \sqrt{\alpha \cdot \beta}$, where 2α and 2β are the length of the long and short axis of the elliptic contact area. σ is the ionic conductivity. As seen from Figure 5b the area is fairly constant towards the end of the electrochemical experiment. Thus, the values calculated from (19) can be calibrated according to the contact area of the Ni wire determined by SEM (Figure 5a) after the electrochemical experiment. The behavior of R_s

seen in Figure 5b was observed for all samples. In the following all ASR values will be based on the area calculated from (3). In all four cases the area increased by a factor of ~2 compared to the first measurement at 500°C, see Figure 5b. The SEM contact areas for ZY10, ZY13, ZY18 and ZSc6Y4 were 0.069, 0.059, 0.052 and 0.045 mm^2, respectively.

When point electrode experiments are conducted an initial annealing at higher temperature is required to stabilize the contact area. In this study one objective was to follow the degradation of the electrodes at 500°C hence it was not possible to use a higher initial temperature, as this would probably change the degradation profile. This is the reason why calculated areas are used for the ASR.

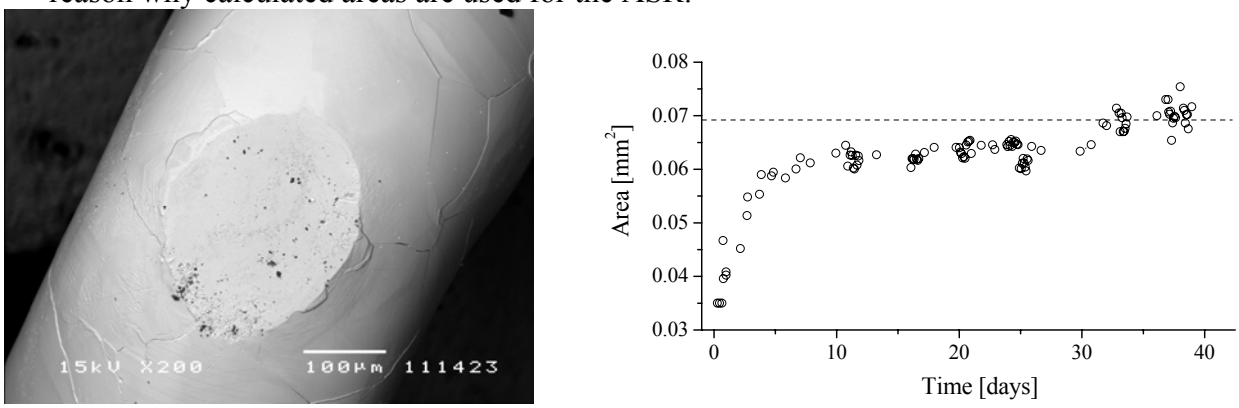

a) b)

Figure 5. a) SEM image of the contact area on a Ni wire after the electrochemical experiment. The Ni wire was pressed against ZY10. α=172 µm, β=128 µm, area=0.069 mm^2, perimeter=0.952 mm. b) Calculated area vs. time for ZY10 at 500°C. The dashed line represents the area measured with SEM (0.069 mm^2).

Temperature variation: The variation of R_s and ASR with temperature for ZY10 is shown in Figure 6. The activation energies were derived from the cooling run. The activation energies for R_s for ZY10, ZY13, ZY18 and ZSc6Y4 were 1.02, 1.28, 1.31 and 1.16 eV, respectively. The activation energies for ASR for ZY10, ZY13 and ZY18 were 0.92, 0.49 and 0.78 eV, respectively.

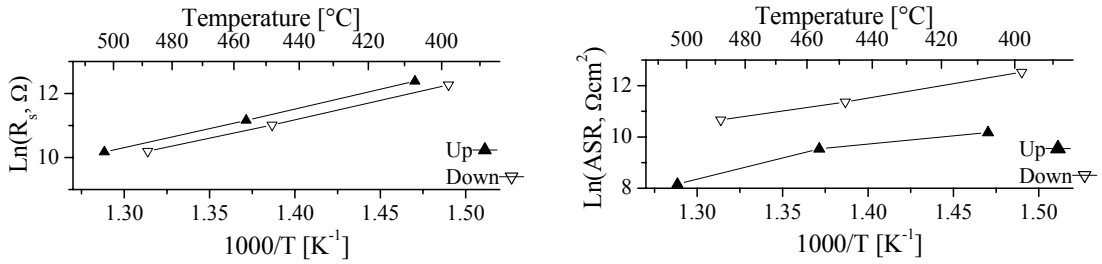

Figure 6. Temperature dependence on R_s and ASR for ZY10. The ASR values were based on calculated areas. The "Up" and "Down" notation corresponds to heating run and cooling run, respectively.

The trend of R_s and ASR from the heating run and cooling run for ZY13, ZY18 and ZSc6Y4 shows a behavior similar to ZY10 (Figure 6), hence only the graph for one sample is shown.

Long-term stability at 500°C: During the 500°C period the temperature fluctuated from 484-515°C and this caused noticeable changes in R_s and ASR. The resistance values were adjusted to 500°C using the E_a derived from the cooling run, except for the ASR in case of

ZSc6Y4 where an average (E_a=0.7 eV) of the ASR for the others samples was used. The corrected ASR and R_s values versus time for the ZY10 are shown in Figure 7.

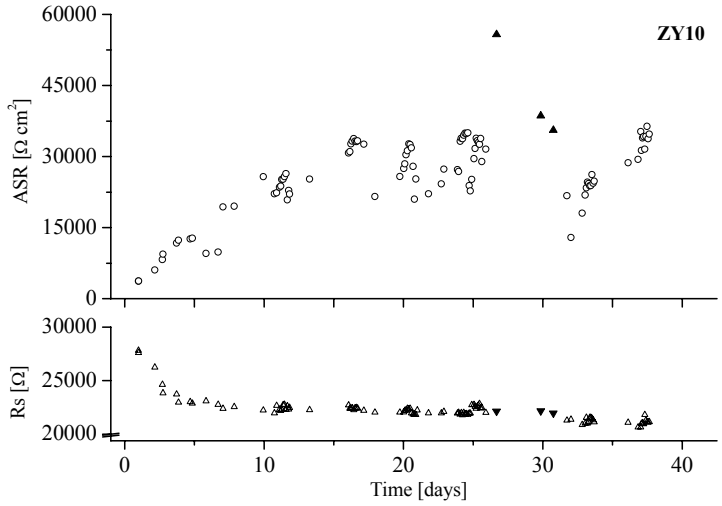

Figure 7. ASR and R_s versus time for ZY10. Measurements performed in 3% H_2O/H_2 and 0.7% H_2O/H_2 are depicted as open and filled symbols, respectively. The values were corrected to 500°C.

The long-term stability of ZY13, ZY18 and ZSc6Y4 shows a dependence on R_s and ASR similar to ZY10 (Figure 7), hence only one sample is shown. The scatter within the decreasing tendency in R_s is not necessary an area effect but can be ascribed to the uncertainty in the determination.

Initial and average ASR values were determined at 500°C in 3% H_2O/H_2, see Table 1. The average ASR values were calculated, as the initial increase seemed to level out e.g. in case of ZY10 (Figure 7) after day 20.

Table 1. Initial and average ASR values calculated at 500°C in 3% H_2O/H_2.

Sample	$ASR_{initial}$ [kΩ·cm^2]	$ASR_{average}$ [kΩ·cm^2]	Degradation factor $ASR_{average}/ASR_{initial}$
ZY10	3.7	29	7.8
ZY13	2.4	14	5.8
ZY18	3.4	28	8.2
ZSc6Y4	4.7	22	4.7

Discussion

Surface analysis

AES on the Ni wire: Prior to the electrochemical experiment only the expected impurity elements (oxygen, carbon and sulfur) could be detected on a heat treated and electro polished Ni wire (reference sample). These elements are always detected with AES when Ni has been exposed to the atmosphere due to adsorption. A noteworthy difference is that the sulfur content outside the contact area is higher on the Ni wire after the electrochemical experiment i.e. sulfur is either segregating from the Ni or is present in the gas phase. A poising effect of sulfur is known to enhance the polarization resistance.[6] The two profiles performed in the contact area were different regarding the elemental distribution of sulfur and zirconia implying that the contact area of the Ni wire is inhomogeneous.

XPS on the electrolytes: On the polished electrolytes carbon was found as the only impurity. After the electrochemical experiment Si was detected on all electrolytes. From the literature[6,7] it is known that Si segregates from the bulk to the surface of yttria stabilized zirconia. The reason why no Si are detected on the surface of polished crystals is that the bulk concentration is too low (ppm level) to be detected by XPS.

TOF-SIMS on the electrolytes: The TOF-SIMS could detect some impurities on the reference samples but in general the impurity level was lower than on the electrochemically tested samples. A close up from Figure 3 of the first 100 s, shows that the Si signal peaks before the Y and ^{94}Zr signals. In general all the impurities peak before the Zr and Y species (and Sc in case of ZSc6Y4). This indicates that the impurities are located in the outermost atomic layers. The signals from the impurities disappear at around 100-200 s, which corresponds to 1-20 Å if the sputter rate of 1-10 Å per 100 s is assumed[4]. In cases where a sputter current of 16 nA is used instead of 3 nA the impurity peaks disappear at 20-40 s, which corresponds well to the proportionality between the sputter rate and sputter current.

Electrochemistry

Temperature dependence: In the case of R_s (Figure 6) the measurements from the heating run are higher than the measurement from the cooling run due to creeping of the Ni wire (increasing contact area) during the electrochemical experiment. R_s measurements from the heating run are shown to confirm the R_s measurements from the cooling run.

The E_a for the ASR varies a lot (0.49-0.92 eV) indicating different rate limiting steps. ASR values from the heating run do not show an Arrhenius dependence. An explanation to this could be decomposition of organic compounds adsorbed on the surfaces of Ni and SZ during heating. The trend in the Arrhenius plot is not believed to be caused by fluctuations in the ASR for the following reasons: 1) From the Arrhenius plot all four electrodes show the same trend for the heating run and all four electrodes show a straight line from the cooling run. 2) More than one measurement was performed at each temperature on each electrode, and the scatter between these measurements is negligible compared to the dependence on temperature. 3) From Figure 7 it can be seen that not much scatter is observed in the start of the measurement. This is also true for ZY13, ZY18 and ZSc6Y4. An explanation to this can be that the impurities are causing the scatter i.e. no scatter is seen in the start of the electrochemical experiment as the electrodes are “clean”.

Long-term stability at 500°C: All four samples showed a general trend of increasing ASR with time. Fluctuations in ASR occur, usually as a sudden drop followed by a steady increase. Initial and average ASR values are calculated and their ratios (degradation factors) are listed in Table 1. The degradation of the electrodes is believed to be caused be the segregation of impurities.

For all four electrodes the polarization resistance increased when the water content was lowered from 3 to 0.7 %. Scatter occurs and it is difficult to give an exact increase, but a factor ~2 seems reasonable. The change was reversible. R_s were as expected not influenced by the water content as the conductivity of the electrolytes is stable over a wide range of oxygen partial pressures. Due to the uncertainty and scatter accompanied with the ASR no dependence of the electrolyte compositions is evident at 500°C in 0.7 or 3% H_2O/H_2.

Conclusion

After the electrochemical experiment a higher impurity level was seen on the electrode materials even though high purity materials were used at a relatively low temperature. A higher sulfur concentration was detected with AES on the Ni wire. Many elements were observed on the SZ single crystals with TOF-SIMS but only Si was detected with XPS

indicating that Si is the main component segregating to the surface. The segregation outside the contact area is independent on the current applied to the electrode. From the TOF-SIMS imaging and depth profiles Ni was detected in the contact areas on the SZ single crystals. Also, a lower content of impurities was evident in the contact area.

Our findings do not suggest any dependence on the electrolyte composition for: $(ZrO_2)_{0.9}(Y_2O_3)_{0.1}$, $(ZrO_2)_{0.87}(Y_2O_3)_{0.13}$, $(ZrO_2)_{0.82}(Y_2O_3)_{0.18}$ and $(ZrO_2)_{0.9}(Y_2O_3)_{0.04}(Sc_2O_3)_{0.06}$ on the polarization resistance (OCV) at 500°C in 0.7-3% H_2O/H_2. Changing the atmosphere from 3% H_2O/H_2 to 0.7% H_2O/H_2 at 500°C increased the polarization resistance of all samples by a factor of ~2. All electrodes degraded by a factor of 5-8 over 10-20 days at 500°C in 3% H_2O/H_2. Segregation of impurities is believed to cause this degradation. The fluctuations in ASR are believed to be due to the nature of the electrode-electrolyte interface and not external actions such as vibrations.

Acknowledgements

This work is a part of Jens Høgh´s Ph.D.-project and is sponsored by the Danish Technical Research Council (STVF).

REFERENCE LIST

1 Jensen K.V., Wallenberg R., Chorkendorff I. and Mogensen M., "Effect of impurities on structural and electrochemical properties of the Ni-YSZ interface", *Solid State Ionics*, **160** [1-2] 27-37 (2003).

2 Liu Y.L., Primdahl S. and Mogensen M., "Effects of impurities on microstructure in Ni/YSZ-YSZ half-cells for SOFC", *Solid State Ionics*, **161** [1-2] 1-10 (2003).

3 Mogensen M., Primdahl S. and Sunde S., "SOFC Anode Kinetics", *High Temperature Electrochemistry: Ceramics and Metals, Editors: Poulsen F. W, Bonanos N. , Linderoth S. , Mogensen M. and Zachau-Christiansen B. 17th Risø International Symposium on Materials Science 1996*, 77 (1996).

4 Hansen K.V., Mogensen M. and Norrman K., "TOF-SIMS studies of yttria-stabilised zirconia", *In preparation*.

5 Holm R. "Electric contacts", *Stationary contacts*, **4th edition** (1967).

6 Primdahl S. and Mogensen M., "Limitations in the hydrogen oxidation rate on Ni/YSZ anodes", *Proceedings of the sixth international symposium, solid oxide fuel cells*, 530-540 (1999).

7 de Ridder M., Vervoort A.G.J., van Welzenis R.G. and Brongersma H.H., "The limiting factor for oxygen exchange at the surface of fuel cell electrolytes", *Solid State Ionics*, **156** [3] 255-262 (2003).

8 Hughes A.E. "Segregation in single-crystal fully stabilized yttria-zirconia", *Journal of the American Ceramic Society*, **78** [2] 369-378 (1995).

Appendix D: Electrochemical measurements made in dry CO/CO_2 and H_2/H_2O atmospheres on single crystal YSZ using pattern electrodes

To be published as:
Electrochemical measurements made in dry CO/CO_2 and H_2/H_2O atmospheres on single crystal YSZ using pattern electrodes

Andreas Ehn*, Jens Høgh**, Mariusz Graczyk***, Kion Norrman**, Lars Montelius***, Mark Linne* and Mogens Mogensen**.

* Combustion Physics, LTH, Sweden
** Risø National Laboratory, Denmark
*** Solid States Physics, LTH, Sweden

26th Risø International Symposium on Materials Science, Solid State Electrochemistry, Sep 2005

Electrochemical measurements made in dry CO/CO_2 and H_2/H_2O atmospheres on single crystal YSZ using pattern electrodes

Andreas Ehn*, Jens Høgh**, Mariusz Graczyk***, Kion Norrman**, Lars Montelius***, Mark Linne* and Mogens Mogensen**.

* Combustion Physics, LTH in Sweden
** Risø National Laboratory, in Denmark
*** Solid States Physics, LTH in Sweden

Abstract

Oxidation/reduction of H_2/H_2O and CO/CO_2 atmospheres on Ni/YSZ pattern electrodes was electrochemically investigated in the temperature range 500 °C – 700 °C. Two different samples were tested with 0.5 and 1 μm thick nickel pattern electrodes. The controlled triple phase boundary length was 41 cm for both the samples. The pattern electrodes were made on a 5 mm thick single crystal of YSZ with a surface area of 10x10 mm^2. Contact mask UV-lithography with spin-coated resist was used to construct the electrodes. The structure of the pattern electrodes was built on a system with lines. The line width was 50 μm. Electrochemical measurements were performed in a single-atmosphere setup, using a moisture meter to monitor the vapour pressure of the exhaust gas. In order to

relate the CO/CO_2 results to earlier nickel pattern electrode results, the cell was also characterized by impedance spectroscopy in H_2/H_2O atmosphere.

Introduction

Natural gas (which consists mainly of methane) is the preferred fuel for solid oxide fuel cells (SOFC). Using the present SOFC technology the natural gas has to be reformed, i.e. reacted with steam to form H_2 and CO, which are both considered fuels for SOFC. Insight regarding the kinetics of the electrochemical oxidation process of both H_2 and CO is thus of current interest. To collect electrochemical data on electrodes in these atmospheres nickel pattern, cermet and point electrodes have been used, see e.g. [1-12]. Electrochemical data for the separate CO/CO_2 atmospheres, where CO is oxidized into CO_2 using nickel point electrodes [4,5] and using Ni-YSZ cermet electrodes [11,12] has been published, but the results are very much in disagreement. The drawback of point electrodes is that the triple phase boundary length, Ltpb, is hard to vary in a controllable manner, and it is by nature very short. The composite Ni-yttria stabilised zirconia (YSZ) cermet has the drawback of a potential distribution inside the electrode, and it is difficult to determine Ltpb, making the interpretation of the kinetic data troublesome. Electrochemical measurements were thus performed in CO/CO_2 atmospheres and H_2/H_2O using nickel pattern electrodes. Here, some preliminary results are reported.

Experimental

A single crystal of YSZ cut along the (100) direction with a surface of 10x10 mm^2 was used as the electrolyte. The thickness of the electrolyte used was 5 mm. The composition of the crystal was investigated with EDS and was determined to 13 mol% yttrium content.

Cleaning of the YSZ surface was an initial step in the electrode construction process. It was done in four steps, using trichloroethylene, isopropanol, acetone and deionised water. Each cleaning step was performed in an ultrasonic bath for 5 minutes. After the chemical cleaning oxygen plasma (5 mbar) for 1 minute was used to remove remains of organic species. Next, the nickel layer was deposited by evaporation in a chamber that was initially at about $4 \cdot 10^{-7}$ mbar. Before etching photolithographic process was performed. The nickel layer was spin coated with resist S1813 at 3000 rpm for 30 s. Soft baking was done in a convection oven at 90 °C for 30 minutes. Resist was exposed in the contact mask aligner Karl Süss MJB3 for 5sec. The pattern was developed for 70 seconds in the developer MF319 followed by hard baking in convection oven at 120 °C for 30 min. A mixture of HNO_3:H_2O (1:19) was used to etch away Ni. The etching times were 10 and 19 minutes due to different thickness of the nickel layers. Resist was then removed in the 1165 remover at 50 °C for 5 minutes and finally samples were cleaned in an RCA1 process. The two different samples had different nickel layer thickness as well as nickel purity. The data for the two samples used in the measurements are listed in table 1.

A three-electrode set-up was used. The reference electrode is put around the YSZ as a belt. A groove was cut out around the crystal to fixate the reference electrode. To increase the contact area the groove was painted using platinum paste. Platinum paste was also used for the creation of the counter electrode. The Ni pattern is the working electrode.

The electrochemical measurements were performed in a furnace at temperatures between 350°C-700°C. The temperature was controlled within a few degrees accuracy. Impedance spectroscopy and potentiostatic measurements were performed using a frequency response analyzer (Solartron 1255b) in combination with a potentiostat (Solartron 1287). This equipment was controlled using the software Zplot. Flow controllers monitored the gas flow to the cell. A portion of the hydrogen flow was split off and passed through a water bottle to introduce water to the flow. The temperature of the water bottle was stabilized and a rotameter was used to adjust the water content and a moist meter was put in the exhaust

line to control the vapour pressure of the gas. The water bubbler was excluded when using CO/CO_2 gases. A pO_2-sensor was built into the setup to control the partial pressure of oxygen.

Results

The results presented here are based on the two different samples, A and B, described in table 1. In table 2 measurement data for these samples are presented to make the discussion clearer. The results focus on the real-part parameters of the impedance, Rs and Rp. Here Rp is the polarisation resistance, which is the resistance at lower frequencies minus Rs, the serial or ohmic resistance of the cell, which is the resistance at which the impedance curve comes down to the x-axis at high frequencies. Rs is determined from impedance spectra. Potentiodynamic, potentiostatic and impedance spectroscopy measurements gives the values of Rs + Rp. Electrochemical measurements were performed in two different atmospheres, H_2/H_2O and CO/CO_2. Typical impedance spectra of sample A can be seen both in H_2/H_2O (fig.1a) and CO/CO_2 (fig.1b) atmospheres. The impedance spectrum in fig.1a at 500 °C in 3% water/hydrogen atmosphere shows one arc with good symmetry, which is in good agreement with earlier reports [5-10]. The shape of the impedance spectrum is unaffected when the H_2/H_2O ratio is shifted. In 10 % CO/CO_2 at 600 °C two overlapping arcs are observed, which indicates that at least two processes are rate limiting. At lower CO/CO_2 ratios the spectrum changes character and one of the arcs becomes dominating with a relaxation frequency close to the low frequency arc in figure 1b. This two-arc behaviour is not seen for sample B in CO/CO_2.

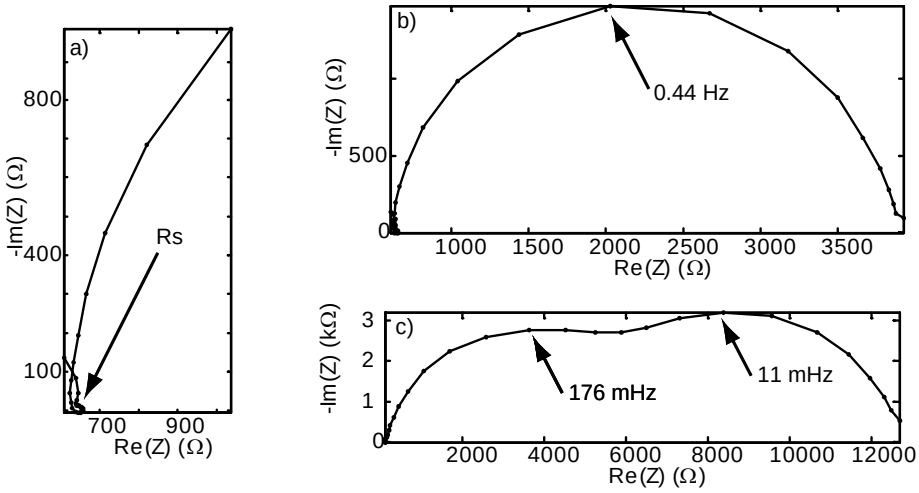

Fig. 8 a) High-frequency part blow-up of spectra in b) to see Rs. b) Impedance spectrum measured at 500 °C in 97 % H_2 + 3 % H_2O. c) Impedance spectrum in a 10 % CO + 90 % CO_2 atmosphere at 600 °C. All spectra are from sample A.

Results presented by Mizusaki [6] show unstable behaviour of nickel pattern electrodes at an early stage in the experiment. The stabilisation behaviour of Rp at 400°C is seen for sample B in figure 2. In the beginning of the experiment Rp rapidly increased. After about ten hours this behaviour stopped abruptly, Rp dropped below its starting value, and then it displayed moderate growth. Rs showed stable behaviour at various temperatures and achieved good agreement for the two samples in both atmospheres. The activation energy of Rs was calculated and the mean value was found to be 1.0 eV with a standard deviation of 0.07 eV. When the gas atmosphere was shifted between H_2/H_2O and CO/CO_2 the value of Rs for sample B was not affected but sample A was lowered by 12% at 500°C in CO/CO_2. The value of Rs in CO/CO_2 for sample A is in good agreement with the initial

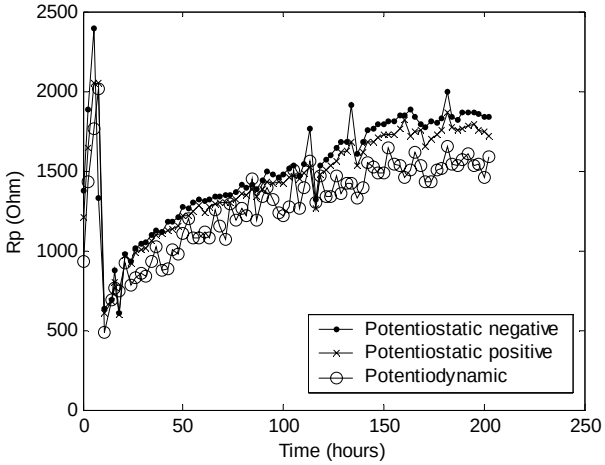

Fig. 9. Initial stabilisation behaviour of Rp over time for sample B at 400°C in H_2/3 % H_2O. The data points were collected by combing impedance spectra with potentio-dynamic and potentiostatic measurements. The amplitude of the impedance spectra was 25 mV. In the potentiostatic measurement the potential was held at 25 and -25 mV in 1 hour. The potentiodynamic measurement was scanned as (0→ -25 → 25 → 0) mV.

value of Rs in hydrogen water for sample B. The mean value of the activation energy of Rs in CO/CO_2 was 0.97 eV with the standard deviation 0.04 eV. No value of Rs could be determined for sample A at 700°C due to signal noise problem in CO/CO_2 atmosphere.

The difference between the samples was severe regarding Rp, and displayed a dependence on the gradient of the temperature (hysteresis) in the experiment. With increasing temperatures, the apparent activation energy of Rp was lower than the case with decreasing temperature. Increasing temperature in the H_2/3 % H_2O mixture produced value of 0.88 eV and 0.42 eV for A and B respectively. Decreasing temperature in the same atmosphere gave sample B a value of 1.0 eV. As in H_2/H_2O, differences are seen in CO/CO_2 depending on the direction of the temperature change. Values for increasing temperature were 0.75 and 0.74 eV for sample A and B, respectively, and for decreasing temperature 1.1 eV was calculated for sample A. In table 2 values of Rp in the different atmospheres are presented at different temperatures and atmospheres. Here the samples show very different behaviour with large differences in Rp for the two atmospheres. Sample A shows a much higher Rp value in CO/CO_2 than in H_2/H_2O, up to about 50 times higher. Sample B on the other hand shows less difference in the Rp values for the two atmospheres. Rp is about six times larger for sample B in H_2/H_2O, and in CO/CO_2 it is

Table 1 Different resistances in the two atmospheres where the H_2/H_2O atmosphere consequently contained 97 % H_2 + 3 % H_2O. In the last column ΔRs is the percentage of change in Rs.

Sample	Temp (°C)	CO-content	Rp_{H2} (Ω)	Rp_{CO} (Ω)	$Rp(H_2)/Rp(CO)$	Gas Switch	ΔRs (H_2-CO)
A	500	0.5 %	3850	205000	0.019	H-CO	- 12 %
A	700	2.5 %	330	6500	0.051	CO-H	-*
B	500	3 %	24880	19890	1.25	H-CO	3 %
B	650	5 %	4260	10143	0.42	CO-H	0

* Signal noise problems

about one tenth compared with sample A.

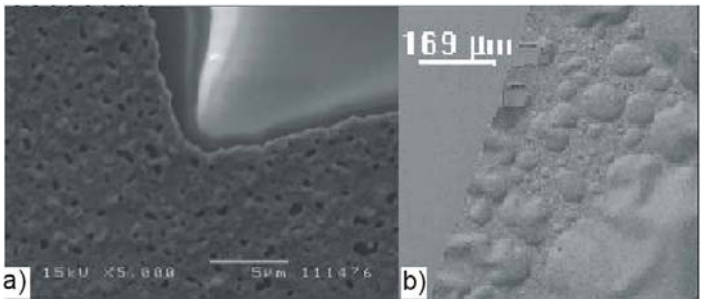

Fig. 10. SEM pictures of sample A (a) and B (b). Sample A had holes in the nickel layer al the way down to the YSZ. This was not the case for sample B where bubbles were formed underneath the Ni layer.

After the electrochemical measurements the microstructure of the nickel layer was investigated. Figure 3a and 3b show SEM pictures of the samples after testing i.e. heating to 700°C. The optical microscope showed holes all the way through the nickel layer down to the YSZ for sample A. For sample B bubbles were formed under the nickel layer. No holes were introduced in this thick nickel layer. To get surface information of sample B, EDS, TOF-SIMS and XPS were performed on nominally equal samples. They show that prior to testing, the samples were contaminated with a silicone layer of the type SiC_3H_9. After heating the YSZ is heavily contaminated with silica. Also on sample B both the YSZ and the Ni show a strong signal from sodium.

Discussion

Previous results [1, 2] report an increase of Rp very similar to the behaviour shown in figure 2. The increase in Rp is believed to be due to impurity segregation to the triple phase boundary. XPS and TOF-SIMS results show that sample B was covered with a thin layer of silicone prior to heating, which probably is from processing of the electrodes. This might be the reason for the initial fast increase of Rp that could be seen in figure 2. When the silicone is oxidized totally, crystalline SiO_2 may be formed and this process sets the tpb free again. Thereafter, segregation of silica and sodium from the YSZ and the Ni may slowly form a glassy barrier at the TPB.

In H_2/H_2O the large difference in activation energy of Rp seems to be connected to prior thermal history of the samples during testing. The reason for the apparent activation energy to be higher after heat treatment might be due to impurity segregation.

The shift in atmosphere gives different results for the two samples. Firstly, Rs of sample A shifted to a lower value when the atmosphere is shifted to CO/CO_2.This Rs value is in agreement with the initial Rs value for sample B in hydrogen/water at the same temperature. This points to an increase in the working electrode contact area of sample A during the time of gas change. The reason for this is unknown.

Secondly, Rp in hydrogen is a factor of six lower for sample A than for sample B. This may be due to the formation of the holes in the Ni-layer on sample A as these causes a considerable longer TPB line.

Thirdly, when the atmosphere is shifted from H_2/H_2O to CO/CO_2 the increase of Rp for sample A is much bigger than for sample B. This points to important differences in the TPB properties of the samples. This could possibly be related to the formation of TPB in holes and/or the difference in thickness of the Ni on the two samples.

Earlier results where H_2/H_2O and CO/CO_2 where compared using nickel-YSZ-cermet electrodes state that there are no major difference in Rp for the two different atmospheres [11]. Without any information on Rs during the measurements no conclusions can be made from this, especially since a cermet electrode is reminiscent of sample A's pattern electrodes with the distribution of holes.

Conclusion

Electrochemical measurements in H_2/H_2O and CO/CO_2 atmospheres using Ni pattern electrodes on YSZ indicate that the rates of the H_2/H_2O electrode reaction and the CO/CO_2 electrode reaction are in the same order of magnitude. However, it was not possible to fabricate pure TPBs, and the electrode reactions seem to be grossly effected by the various impurities. Difficulties in obtaining well-defined Ltpb were encountered.

References

1. K. Vels Jensen, PhD Thesis, Risø National Laboratory, Roskilde, Denmark (2002).
2. K. Vels Hansen, K. Norrman and M. Mogensen, J. Electrochem. Soc. **151**, A1436 (2004).
3. J. Høgh, K. Vels Hansen, I. Chorkendorff, T. Jacobsen, K. Norrman and M. Mogensen, High Purity H2/H2O/Nickel/Stabilized Zirconia Electrodes at 500°C, Proceedings of the 29th International Conference on Advanced Ceramics and Composites, The American Ceramic Society, Jan 2005.4. G. Ø. Lauvstad, S. Sunde, and R. Tunold, J. Electrochem. Soc. **149**, E497 (2002).
5. G. Ø. Lauvstad, S. Sunde, and R. Tunold, J. Electrochem. Soc. **149**, E506 (2002).
5. J. Mizusaki, H. Tagawa, T. Saito, T. Yamamura, K. Kamitani, K. Hirano, S. Ehara, T. Takagi, T. Hikita, M. Ippommatsu, S. Nakagawa and K. Hashimoto, Solid State Ionics, 70/71 ,52 (1994).
6. J. Mizusaki, H. Tagawa, T. Saito, K. Kamitani, T. Yamamura, K. Hirano, S. Ehara, T. Takagi, T. Hikita, M. Ippommatsu, S. Nakagawa and K. Hashimoto, J. Electrochem. Soc., **141**, 2129 (1994).
7. J. Mizusaki, T. Yamamura, N. Mori, H. Tagawa, K. Hirano, S. Ehara, T. Takagi, M. Hishinuma, H. Sasaki, T. Sogi, Y. Nakamura, K. Hashimoto, Proc. 17th Risø Intern. Symp. On Mat. Sci.: High Temperature Electrochemistry: Ceramics and Metals, Eds.: F. W. Poulsen et al. Risø National Laboratory, Roskilde, Denmark, p. 363 (1996).
8. A. Bieberle, PhD Thesis, Swiss Federal Institute of Technology, Zürich.
9. A. Bieberle, L. P. Meier and L. J. Gauckler, J. Electrochem. Soc. 148, A646 (2001).
10. B. de Boer, Ph.D. Thesis, University of Twente, Twente, The Netherlands (1998).
11. R.J. Aaberg, R. Tunold, Proc. 17th Risø Intern. Symp. On Mat. Sci.: High Temperature Electrochemistry: Ceramics and Metals, Eds.: F. W. Poulsen et al. Risø National Laboratory, Roskilde, Denmark, p. 511 (1996).
12. P. Holtappels, L.G.J. de Haart, M. Mogensen, U. Stimming, I.C. Vinke, J. Appl. Elecrochem. (1999) **29**, 561-568

Risø's research is aimed at solving concrete problems in the society.

Research targets are set through continuous dialogue with business, the political system and researchers.

The effects of our research are sustainable energy supply and new technology for the health sector.